1991 Research & Technology

Goddard Space Flight Center

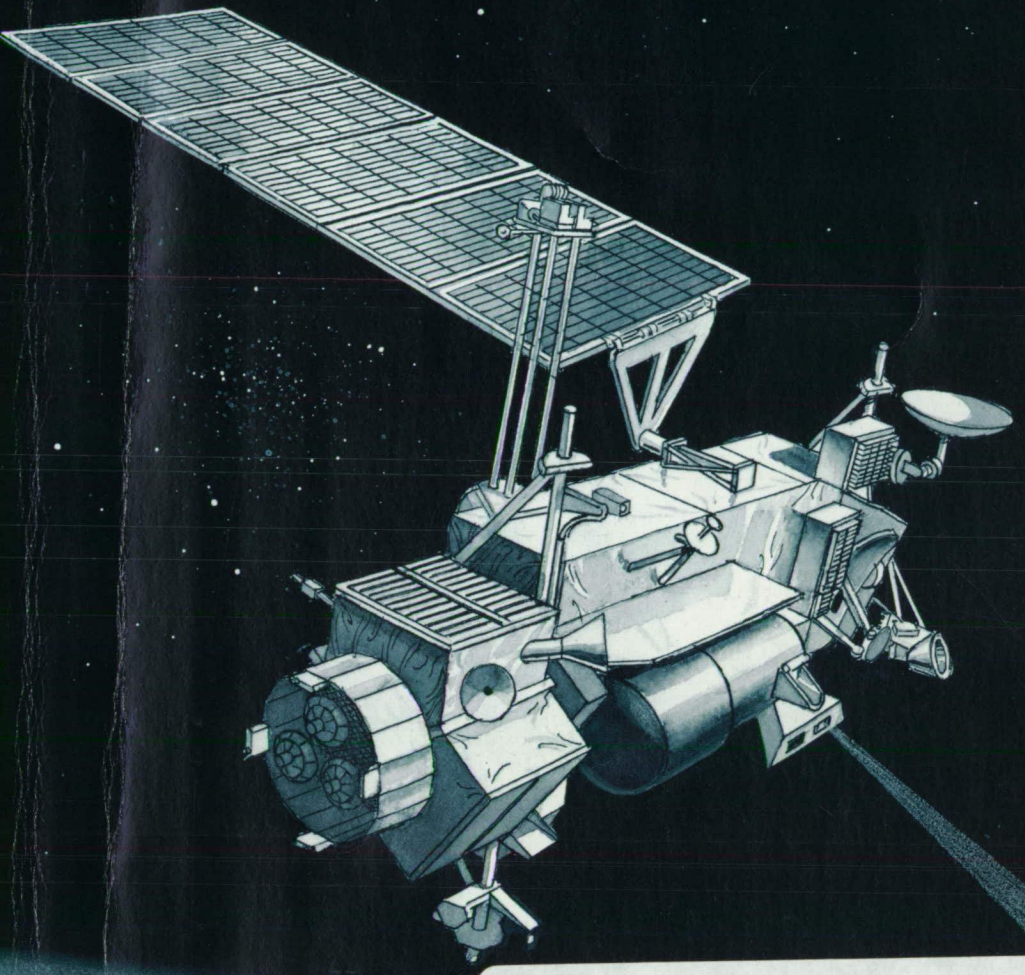

NASA

Nineteen ninety-one has been busy and exceptionally productive at Goddard Space Flight Center. We launched numerous payloads, made important scientific discoveries, developed several new programs, and deployed the fifth Tracking and Data Relay Satellite (TDRS-E).

As depicted on the front cover, the Upper Atmosphere Research Satellite (UARS), launched in September 1991, is an important new National Aeronautics and Space Administration program aimed at improving our knowledge of the stratosphere, mesosphere, and lower thermosphere, emphasizing those levels that are known to be particularly susceptible to change by external agents. Using a combination of measurements and theoretical studies, UARS will provide a focus for resolving scientific questions about the chemistry, dynamics, and overall energy balance of the upper atmosphere.

RESEARCH AND TECHNOLOGY

1991 R&T REPORT

GODDARD SPACE FLIGHT CENTER

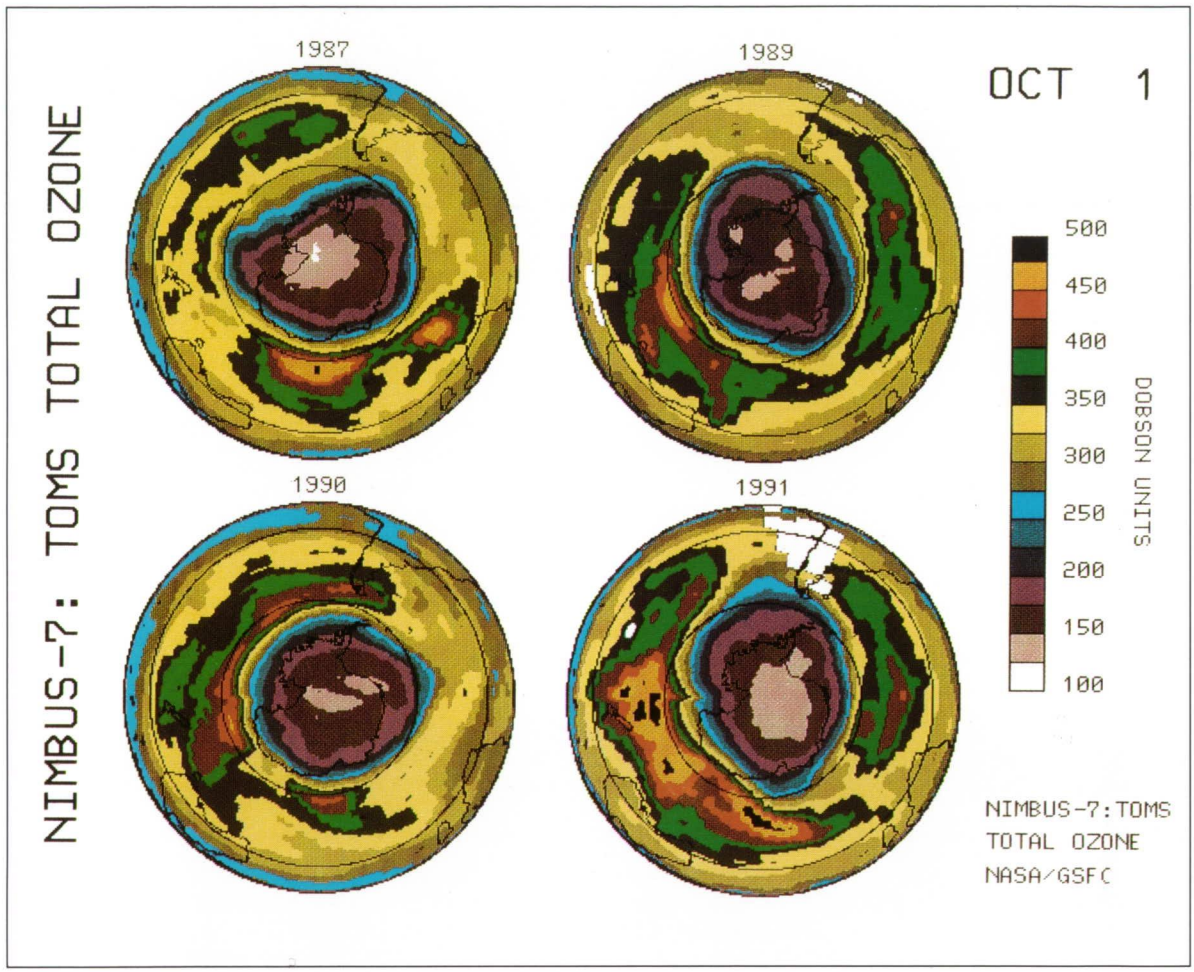

Nimbus-7/TOMS Ozone

The photo displays four Nimbus-7/Total Ozone Mapping Spectrometer (TOMS) false color images, comparing the ozone holes on October 1 in 1987, 1989, 1990, and 1991. The color scale on the right shows the total ozone values (missing data are white). The ozone hole is seen as pink, with the purple colors indicating extremely low ozone values. The area of all four holes is nearly equal.

Since its launch aboard NASA's Nimbus-7 polar-orbiting satellite in 1978, TOMS has provided reliable, high-resolution mapping of global ozone levels on a daily basis. TOMS is managed by NASA's Goddard Space Flight Center, Greenbelt, MD.

Foreword

Nineteen ninety-one has been busy and exceptionally productive at Goddard Space Flight Center. We launched numerous payloads, made important scientific discoveries, developed several new programs, and deployed the fifth Tracking and Data Relay Satellite (TDRS-E).

Our science instruments have been working extremely well. Data received from the Compton Gamma Ray Observatory, launched in April, has changed our view of the cosmos. Goddard's own Energetic Gamma Ray Experiment Telescope instrument on board Compton detected the most distant and most luminous gamma-ray source ever seen. In August, we flew the SSBUV-3 on Atlantis. The Cosmic Background Explorer (COBE) team received the prestigious National Air and Space Museum Award for its measurements of the spatial and spectral distribution of the cosmic background radiation left over from the "Big Bang."

The Hubble Space Telescope (HST) continues to gather science unobtainable with any other telescope. HST provided data that accurately measured the distance to our neighboring galaxy, the Large Magellanic Cloud; made images of a storm in progress on Saturn; and surprised astronomers by discovering hydrogen clouds throughout the universe. Our software experts, using restoration techniques, reconstructed many of the blurred images.

Of particular note in this era of growing concern about the Earth are the missions, experiments, and data that will help us understand our environment and the effects of anthropogenic activities on it. We launched a Total Ozone Mapping Spectrometer (TOMS) instrument on board a Soviet Cyclone, the first significant U.S. payload ever flown on a Soviet rocket. In October, data from the venerable TOMS instrument aboard Nimbus-7 showed the deepest ozone hole to date located over the Antarctic. The Upper Atmosphere Research Satellite (UARS), launched in September, returned data that confirmed the link between the presence and distribution of chlorine monoxide in the upper atmosphere and the depletion of ozone. UARS data also provided pictures of the sulfur dioxide cloud from Mount Pinatubo, which may contribute to global cooling over the coming years. With these activities, we can truly say that 1991 was the beginning of the Mission to Planet Earth. Goddard Space Flight Center's activities will form the centerpiece of NASA's involvement in this all-important venture.

Another Mission to Planet Earth milestone was the groundbreaking ceremony for the EOSDIS facility, planned to be in full operation by 1997. Senator Barbara Mikulski was the keynote speaker.

Through other Goddard projects we examined the solar eclipse, the Antarctic ice cap, glaciers, deserts and oceans. We flew the first Hitchhiker payload in five years, and we sent up a Get Away Special Bridge with 12 experiments on board Columbia.

We were visited by the President of Argentina, Carlos Menem, with whom we have formed a partnership in solar exploration through the Goddard co-sponsored SAC-B project, Argentina's first satellite, scheduled to launch in 1994.

All this adds up to a rich output for 1991, all made possible by an outstanding science/engineering team.

John M. Klineberg
Director

Contents

EARTH SCIENCES

Upper Atmosphere

Lower Atmosphere

Contents

Oceans

Hydrology

Contents

Global

SPACE SCIENCES

Solar

Contents

Planetary

Astro-I

Contents

Gamma Ray Investigations

Astrophysics

Contents

FLIGHT PROJECTS

ENGINEERING

Robotics

Mechanical

Contents

Electronics

Imaging and Optics

Contents

Contents

TDRSS

Mission Planning and Scheduling

Contents

Software Development and Test

Earth Sciences

As we prepare for Mission to Planet Earth, *a 15-year coordinated effort to study and understand the intricate interrelationships that contribute to global change, our scientists are developing effective strategies of coordinated measurements and observations. They are utilizing these measurements and observations for the development and application of predictive Earth system models.*

EARTH SCIENCES

Upper Atmosphere

UPPER ATMOSPHERE RESEARCH SATELLITE (UARS)

In 1976, the United States Congress issued a mandate to NASA: "*...carry out a comprehensive program of research, technology and monitoring of the upper atmosphere so as to provide for an understanding of and to maintain the chemical and physical integrity of the upper atmosphere.*" One of NASA's main responses is the Upper Atmosphere Research Satellite (UARS). UARS, launched on September 12, 1991, by Space Shuttle Discovery, is the centerpiece of a long-term, national program of space research into global atmospheric change, and the first observatory in NASA's Mission to Planet Earth. During its 18-month mission (which may extend as long as 9 years), UARS will carry out the first systematic, comprehensive study of the Earth's stratosphere and mesosphere.

The UARS program focuses on the Earth's upper atmosphere and its three altitude regions: the stratosphere, mesosphere, and thermosphere. The stratosphere begins ~15 km above the Earth's surface, is characterized by temperature increasing with altitude, and contains most of the atmospheric ozone. It is this ozone layer that protects life on Earth from the Sun's harmful ultraviolet (UV) rays, and which is the primary focus of the UARS mission. The mesosphere starts at ~55 km and is distinguished by decreasing temperature with altitude. The thermosphere begins near 80 km; in this region the temperature again increases with altitude. The objectives of the UARS mission are to study the physical and chemical processes in these atmospheric regions to:

- Understand the coupled chemistry, dynamics, and energy inputs that control upper atmosphere structure;
- Understand the response of the upper atmosphere to natural perturbations (such as volcanos) and man-made perturbations (such as chlorofluorocarbons or CFCs); and,
- Define the role of the upper atmosphere in climate and long-term climate change.

To meet these objectives, UARS addresses several areas of scientific study, including energy input and loss, photochemistry, dynamics and transport,

◂*The mounting evidence of environmental change affecting the whole Earth as a self-contained ecological system mandates study of the Earth as a planet. This study requires the global perspective of space observations: NASA's* Mission to Planet Earth. *UARS addresses the problem of stratospheric changes linked to human activities that lead to ozone depletion and is the leading element of that Mission.*

coupling among processes, and coupling between the upper atmosphere and the lower atmosphere. The need to study the upper atmosphere as a tightly coupled system, using highly coordinated and complementary data, has led to the concept of the UARS observatory as the instrument, with the individual sensors providing portions of the data required. Four of the sensors combine to measure the altitude profiles of 15 chemical species and temperature; two determine atmospheric winds (the first time that stratospheric winds have been measured from a satellite); and four measure energy inputs from the Sun, including UV radiation and high-energy particles.

The UARS observatory mounts 10 sensors on a mission-unique instrument module built and integrated by General Electric Astro-Space Division (Valley Forge, PA and East Windsor, NJ). The housekeeping functions for the UARS observatory are provided by the Multimission Modular Spacecraft (MMS), built by the Fairchild Space Company (Germantown, MD) under contract to GSFC's Satellite Servicing Project. The modules of the MMS provide propulsion, attitude control, communications and data handling, and power regulation systems for the observatory. One of the UARS MMS modules was previously flown on the Solar Maximum Mission, was retrieved from space, and has been refurbished for use.

UARS is in a near-circular 585-km orbit inclined 57° to the Equator. From this vantage point, its atmospheric sensors can see to 80° latitude, north and south, and provide near-global coverage. In addition, precession of the orbit plane allows these sensors to detect changes in the atmosphere related to local time of day. This precession, along with thermal and power considerations, dictates a 180° yaw maneuver approximately every 36 days during the mission, with the spacecraft alternately flying forward and backward. Every 72 days there is an orbit-adjust maneuver, using the on-board propulsion system to raise the orbit and compensate for atmospheric drag.

The data system is comprised of a dedicated Central Data Handling Facility (CDHF) located at GSFC, minicomputer-based Remote Analysis Computers (RACs) at the investigators' sites, and a high-speed electronic communications system to connect the RACs with the CDHF. Tape-recorded data are telemetered from the observatory through the Tracking and Data Relay Satellite System (TDRSS) to GSFC, where they are delivered to the CDHF daily. Here, computer programs, developed by the Instrument Investigators at their RACs and transferred to the CDHF, convert the telemetry data to several levels of processed data. The CDHF is used for production processing of the scientific data received from the spacecraft and for maintenance of the UARS data base. These data are stored on-line to facilitate quick access by users. A catalog of data is maintained in a data base management system which permits searches based on characteristics such as measurement parameter, time, instrument, and data level. The RACs at the investigators' sites are used to access data in the CDHF for geophysical analysis and in some cases for linking with larger computers for more computer-intensive scientific analyses. For the instrument investigators, the RACs are also used to develop and maintain the software for processing data to levels 1, 2, and 3 in the CDHF. The high-speed communication between the CDHF and the RACs creates, in effect, a distributed data system for UARS and facilitates connection with other scientific data networks.

The UARS program, from its earliest planning phase, has included active participation by theoretical and analytical scientists representing all aspects of the study of the stratosphere and the mesosphere. Specialists in radiative transfer, atmospheric dynamics, and photochemistry lead theoretical groups as Principal Investigators on the UARS Science Team. In addition, many of the experimental investigations also bring theoretical Co-Investigators to the Team. These scientists provide important scientific support and will contribute significantly to the scientific interpretation of the measurements.

An extensive program of correlative measurements supports the UARS mission. In addition to data needed for independent evaluation and validation of UARS instrument data, these correlative measurements provide information to augment UARS data for theoretical and analytical studies. Examples

of this information include parameters not measured by UARS, different perspectives of temperature or ozone fields from operational spacecraft, and ground- or balloon-based measurements producing extended temporal data at one location.

Activation of instruments began within a few days of the spacecraft being released from the shuttle. Many instruments required several weeks of outgassing before they turned on high voltages or opened doors, but a few were able to commence scientific data acquisition earlier. By 2 months after launch, most of the instruments were processing some level of data in the CDHF, and several were in a relatively routine processing mode. For example, the Particle Environment Monitor (PEM) and the Solar-Stellar Irradiance Comparison Experiment (SOLSTICE) have provided processed data on energy inputs; the Microwave Limb Sounder (MLS) data have shown the distributions of ozone, water vapor, and chlorine monoxide in and around the Antarctic ozone hole and elevated sulfur dioxide amounts related to recent volcanic events; and the Improved Stratospheric and Mesospheric Sounder (ISAMS) has provided initial near-global data products for ozone, water vapor, and key nitrogen compounds.

These data and the rest of the information derived from UARS will be used in the formulation of environmental policies. Of equal importance, the answers that the UARS mission provides will encourage more questions and will lead to a greater awareness of the upper atmosphere and its role in maintaining life on Earth.

Contact: Charles E. Trevathan (Code 430)
(301) 286-8536

Carl A. Reber (Code 910)
(301) 286-6534

Sponsor: Office of Space Science and Applications

Charles E. Trevathan received his BS in Electrical Engineering from North Carolina State University. He has served as the Project Manager of the UARS Project since May 1991. He had served as Deputy Project Manager from the start of the UARS system definition phase in early 1980 until his most recent assignment. Earlier in his GSFC career, which began in May 1965, Mr. Trevathan served as design engineer and engineering manager responsible for development of spacecraft communications, data handling, and computer subsystems. During that period, he authored several related articles and papers for a number of technical publications and professional conferences.

Dr. Carl A. Reber, UARS Project Scientist in the Laboratory for Atmospheres, is responsible for the scientific integrity and usefulness of the mission. Among his achievements, Dr. Reber made the first direct measurements of upper atmospheric composition from a satellite on Explorer-17. He has also won several Special Achievement Awards and earned a PhD in Atmospheric and Oceanic Sciences from the University of Michigan. Dr. Reber has 32 years of experience at GSFC.

IMPROVED LIDAR FOR THE MEASUREMENT OF STRATOSPHERIC OZONE AND TEMPERATURE

Over the past several years, a mobile laser radar (lidar) has been developed at GSFC which is capable of measuring ozone and temperature in the stratosphere. As a result of data obtained in several intercomparison campaigns, a number of improvements have been added to the instrument in the past year. The most important change in the system has been the introduction of a rotating, mechanical shutter in the optical detection train.

Simply speaking, a lidar instrument consists of a laser transmitter that emits a beam of light into the atmosphere, a telescope to collect light backscattered by the atmosphere, and a detection system to sense and quantitatively measure the backscattered light. The GSFC lidar uses photomultiplier tubes (PMTs) as the sensors. Because powerful lasers are used in this lidar system, the detection system encounters signals that vary by as much as 10 orders of magnitude. This large dynamic range exceeds the range over

which the photomultiplier tube exhibits linear behavior.

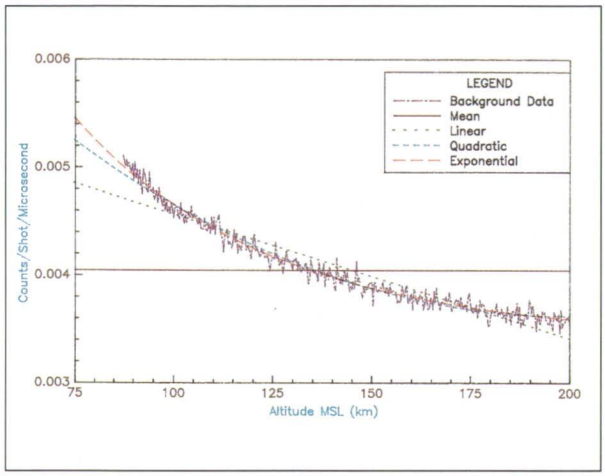

An illustration of curved background and mathematical fits to the data to estimate the background.

Previous data have indicated that the large pulse of light, incident on the PMT as the laser beam first enters the field-of-view of the telescope, introduces a spurious long-lived decay on the output of the PMT which is evident at low light levels (i.e., signals from 40 km and above). This decay, superimposed on the lidar signal and which is evident in the background region of the signal, makes it impossible to determine accurately the signal, which is due solely to atmospheric scattering of the transmitted laser light. This decay is illustrated in the first figure along with several mathematical fits to the data in an effort to estimate the background. In this case, background means not only the skylight unrelated to the transmitted laser pulse, but also the spurious decay induced by the very large signal from low altitudes. The fit that most closely follows the data is a nonlinear exponential expression which we have used to extrapolate to lower altitudes for background subtraction. This expression is very sensitive to the altitude at which the fit is begun and so the background determination becomes somewhat subjective when this signal-induced decay is present. Ozone profiles measured with the GSFC lidar have, on average, tended to measure artificially low values above 39 to 40 km. The starting altitude for this background fit can be adjusted so that the retrieved

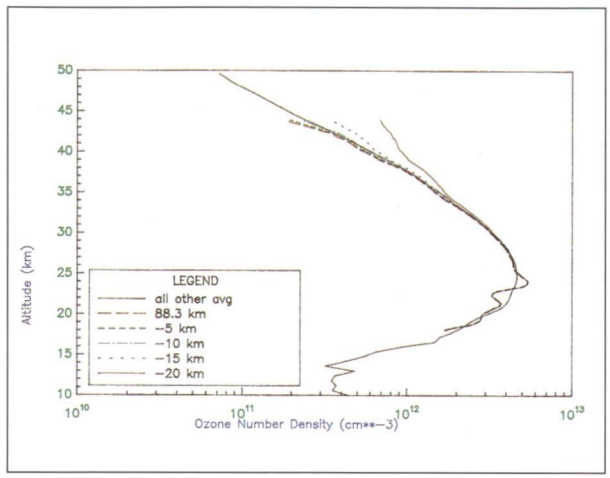

Ozone comparison of how variations in high starting altitude change the ozone profile.

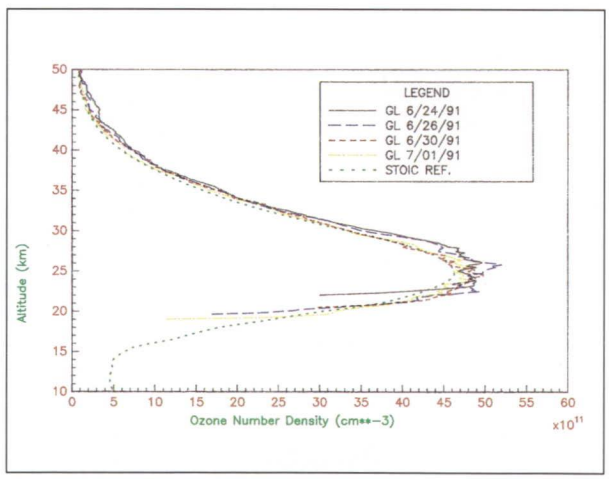

Ozone comparison with the 1989 STOIC reference.

ozone profile more nearly matches the expected profile, as seen in the second figure. This, however, is scientifically unacceptable.

Our approach to the problem has been to design and implement a mechanical shutter capable of blocking the photomultiplier tubes from the intense, early lidar return, and still open fast enough so that a useful ozone measurement can be made starting at ~20 km. This design was recently tested at the JPL Table Mountain Facility (TMF) in the San Gabriel Mountains east of Los Angeles. Data collected during this testing period indicate that the signal-

induced decay is greatly reduced when the PMTs are completely blocked until the laser pulse is ~12 to 14 km above the trailer. This limits the ozone profiles to a minimum altitude of ~19 to 20 km.

The major improvement comes at the high end of the profile, however. Using the shutter, the PMTs appear to be in a linear regime; the background is flat and can be calculated as a mean. Profiles measured in this way now appear to be reliable above 45 km. There is no sensitivity to the starting altitude for the mean background calculation, which removes the subjectivity inherent in our previous analysis. The third figure plots several ozone profiles recorded at TMF during the engineering tests of the system. Also plotted is a reference profile measured during a major intercomparison at TMF in July 1989. Each of the recent profiles appears to be good up to ~50 km.

Contact: Thomas J. McGee (Code 917)
(301) 286-5645

Sponsor: Office of Space Science and Applications

Dr. Thomas J. McGee received a PhD in Chemistry from the University of Notre Dame in 1970. Since joining GSFC in 1980, he has pursued his research interests in optical measurements of atmospheric constituents and in the spectroscopy of small molecules.

GLOBAL TRACKING OF THE JUNE 1991 ERUPTION CLOUD OF MOUNT PINATUBO WITH THE TOTAL OZONE MAPPING SPECTROMETER INSTRUMENT

The Nimbus-7 satellite, launched in late 1978, crosses the Equator every 26° (2900 km) of longitude at local noon, observing the entire Earth once a day (13.7 orbits/day). The Total Ozone Mapping Spectrometer (TOMS) instrument, on board the Nimbus-7 satellite, provides global sulfur dioxide (SO_2) and ozone data by measuring the UV albedo, the ratio of backscattered Earth radiance to incoming solar irradiance. As a monitor of volcanism, the TOMS instrument is best used to detect and track SO_2 outputs from the explosive phases of eruptions. The TOMS observes SO_2 in both the atmosphere and stratosphere; its lower detection limit of a given eruption cloud is ~5 kilotons of SO_2. The major advantages of the TOMS instrument are its capability to detect explosive eruptions virtually anywhere on the sunlit Earth within 24 hours and its ability to measure the complete spatial extent of large, explosive eruptions.

Injection of SO_2 into the stratosphere from volcanic eruptions results in absorption of incoming solar radiation, which should produce a net cooling of the Earth's surface. Our long-range research objectives are to increase our knowledge of the role of volcanic SO_2 in modifying regional and global climate. We are continuously monitoring volcanic activity in an effort to quantify the volcanic contribution of SO_2 to the atmosphere, and to examine possible petrologic and tectonic factors that cause variation in volcanic SO_2 production. All eruptions with a potential for measurable amounts of erupted SO_2 are routinely examined. Thus, our research group at GSFC was well prepared when, on June 15, 1991, Mount Pinatubo erupted in one of the largest volcanic events in this century.

Mount Pinatubo is an andesitic island arc volcano, located on southern Luzon Island, Philippines. The most recent documented eruption occurred ~635 years ago, but Pinatubo has not been studied in great detail and there may have been more recent, undocumented activity. Minor eruptive activity began on June 9 and was first observed by the TOMS instrument on June 12. Between the 12th and the 15th, several small clouds (on the order of 100 kilotons of SO_2) were observed drifting westward.

The cataclysmic eruption on June 15 lasted 15 hours, until early the following morning. The TOMS image on June 16 showed that the center of the SO_2 cloud had already drifted 1000 km to the west-southwest (WSW) as a discrete mass. The column SO_2 values were so high at the center of the cloud that they saturated the sensor's column detection limits.

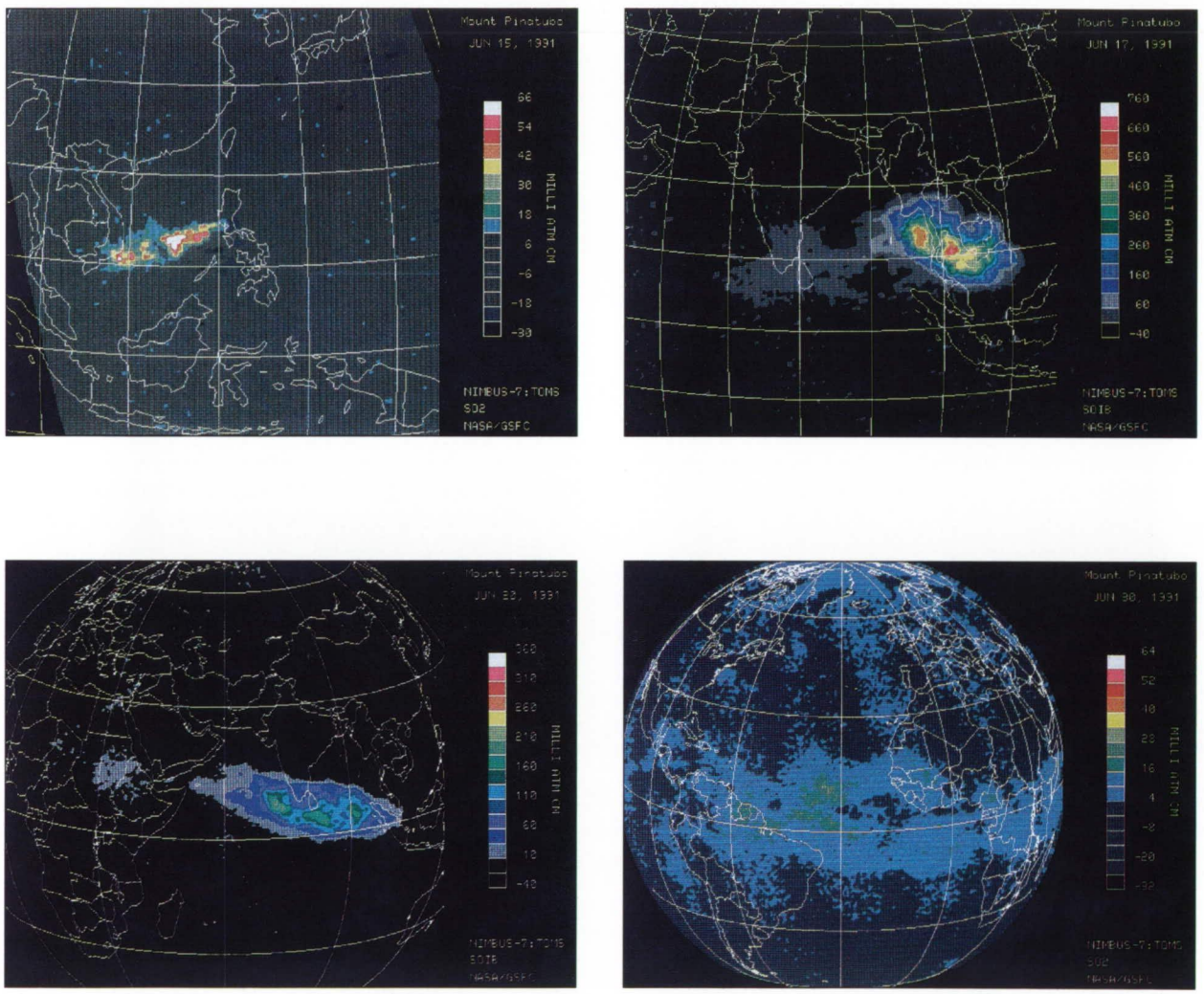

A TOMS chronology of the erupted SO_2 clouds from Mount Pinatubo in June 1991 is depicted in the above four figures. The total column amounts of SO_2 are in milli atm cm, which can be converted to a mass (tons) over the integrated cloud area. The scales vary to depict the clouds in greater detail. The top left figure, June 15 image, shows the results of several minor explosive events the previous day. These clouds total ~500 kilotons of SO_2. The depressed values over the island were caused by cloud reflectance in a typhoon that had just struck the Philippines. The top right figure, June 17 image, gives the first accurate measurement of the cataclysmic eruption cloud: 18,500 kilotons of SO_2, and nearly 5 million km^2 in area. The bottom left figure, June 20 image, shows the westward drifting main body, and a small leading cloud. The bottom right figure, 2 weeks after the main eruption, shows that the dispersing cloud straddles the Equator and now covers more than 50 million km^2.

The June 17 image indicated a gradual expansion of the horizontal SO_2 cloud boundaries. The cloud center had drifted another 1200 km to the WSW, over the Gulf of Siam. The leading edge of the cloud, however, was shearing away from the main portion and was located over the southern tip of India. This leading edge had traveled 5500 km in 36 hours at an average velocity of over 40 m/s. The cloud velocity in the early posteruption days suggested altitudes of 25 to 30 km, based on typical stratospheric wind speeds. The SO_2 cloud as a whole had now dispersed enough so that individual column values could be measured, and yielded a total SO_2 tonnage of 18,500 kilotons. The horizontal extent of the observable SO_2 cloud was ~5 million km^2.

The TOMS image of June 20 (4½ days after the eruption) showed a broadening main cloudmass, and a leading cloud separate from the main body. The trailing edge of the cloud remained over Sumatra ~2000 km from the Pinatubo volcano. The main cloud portion covered from the Equator to ~15°N in latitude, and was centered in longitude over the tip of India. The leading cloud had reached central Africa, and corresponded to a much lower speed of just over 23 m/s.

The physical configuration of the SO_2 cloud then began to form a fairly homogeneous unit, and no longer consisted of a main concentrated mass and a leading lobe or leading cloud. On June 30, 2 weeks after the main eruption, the SO_2 cloud spread over 16,000 km in length, and reached from 10°S to 20°N. The cloud area extended over 50 million km^2. The leading edges of the visible cloud reached the longitude of California, while the trailing edge remained over Indonesia. This cloud measured 12,000 kilotons of SO_2. After 14 days, the Pinatubo cloud still contained roughly 2/3 of its original SO_2. On July 7, 22 days after the main eruption, the TOMS-observed SO_2 cloud completed its trip around the world.

The eruption cloud from Pinatubo is by far the largest that we have observed with the TOMS instrument. Using the June 17 measurement and accounting for cloud dispersion, we estimate that the June 15 eruption of Mt. Pinatubo emitted ~20 million tons of SO_2. By comparison, we measured 7 million tons of SO_2 from the El Chichón, Mexico eruption of 1982. The El Chichón SO_2 cloud remained mostly in the Northern Hemisphere. The SO_2 emitted by El Chichón produced a measurable climate signal, but the magnitude of that effect is less certain. Observational and theoretical estimates place the surface cooling effect in the year following the El Chichón eruption between 0.2 and 0.5°C for the Northern Hemisphere.

Thus, the eruption of Mount Pinatubo offers the exciting prospect to observe and study potentially large climatic responses. The Pinatubo eruption injected nearly three times as much SO_2 into the stratosphere as did El Chichón. Pinatubo should have a significant influence on the global climate, but it remains to be seen whether this influence will represent a linear increase (e.g., a tripling) in the magnitude and longevity of cooling effects of El Chichón or produce a whole new climate signal. The next few years should provide an interesting test of both observational and theoretical efforts.

The TOMS instrument has lasted far beyond its expected operational lifetime and continues to provide useful and timely data. However, the instrument has shown signs of aging in decreased performance. To ensure continued daily measurements of ozone and SO_2, researchers planned the launch of several new TOMS instruments. On August 15, in the first joint U.S./U.S.S.R. space venture, a new TOMS was launched on board a Soviet Meteor-3 spacecraft.

We would like to acknowledge Dr. Charles Schnetzler (Code 921), Dr. Arlin Krueger (Code 916), and Mr. Scott Doiron (Hughes STX) who are the other contributing authors.

Contact: Louis Walter (Code 920)
(301) 286-2538

Gregg Bluth (Code 921)
(301) 286-2754

Sponsor: Office of Space Science and Applications

Dr. Louis S. Walter performs research on gaseous emissions from volcanoes in the Laboratory for Terrestrial Physics. Currently, he is writing a book on the use of space technology in disaster management. He has published analyses of the first lunar samples. Dr. Walter has 28 years of experience at GSFC and holds a PhD from the Pennsylvania State University.

Dr. Gregg J. S. Bluth is a Visiting Scientist from the Universities Space Research Association. He received an AB in Geology from the University of California and a PhD in Geochemistry from the Pennsylvania State University. He is currently researching connections among physical and geochemical characteristics of volcanoes and volcanic SO_2 emissions. He has been working at GSFC since October 1990.

REAL-TIME METEOROLOGICAL SUPPORT OF THE ARCTIC AIRBORNE STRATOSPHERIC EXPEDITION

Concern for the welfare of the ozone layer has increased because of reported stratospheric ozone losses, and the resultant increases of solar UV radiation at the Earth's surface. These reports began in 1985 with the discovery of large losses of ozone over Antarctica, as derived from surface station measurements. These Antarctic losses, now widely described as the Antarctic ozone hole, were confirmed and extended via the use of TOMS on board the Nimbus-7 satellite. Calculations of total ozone trends over the globe using the TOMS data also revealed large downward trends in the northern mid-latitudes between January and April, in addition to the large Antarctic ozone losses.

Poor understanding of lower stratospheric ozone losses led to two stratospheric airborne campaigns: the Airborne Antarctic Ozone Experiment (AAOE), conducted during August and September 1987 from Punta Arenas, Chile, and the Airborne Arctic Stratospheric Experiment (AASE), conducted in January and February 1989 from Stavanger, Norway. The AAOE mission revealed that heterogeneous chemical processes were releasing chlorine from its reservoir state (HCl and chlorine nitrate) into reactive forms that destroyed ozone. AASE revealed that the Arctic polar vortex contained concentrations of chlorine monoxide in amounts similar to those found over the Antarctic during AAOE, but with small ozone losses occurring within the polar vortex. However, AASE did not determine the cause of the ozone losses in the northern mid-latitudes. To determine the cause of these losses, the second Airborne Arctic Stratospheric Experiment (AASE II) will be conducted from Bangor, Maine between October 1991 and March 1992.

The AASE II goals are to: (1) determine the cause of the negative Northern Hemisphere ozone trend reported from the TOMS observations; (2) determine if an obvious Northern Hemisphere ozone hole will form; (3) determine the present chemical state of the lower stratosphere, primarily focusing on an understanding of the gas phase and heterogeneous photochemistry; and (4) determine the future chemical state of the stratosphere as abundances of trace gases and environmental conditions change. The AASE II mission will be conducted using the two aircraft used for AASE I and AAOE—the high-altitude NASA ER-2 and the long-range NASA DC-8. In addition to the aircraft, supplementary data will be provided by a variety of groups and instruments (e.g., total ozone from the TOMS instrument, chemical constituent measurements from the European Arctic Stratospheric Ozone Experiment, and ozonesondes from the Canadian Atmospheric and Environmental Service).

To profitably employ the NASA aircraft and their instruments, it is necessary to guide the aircraft into air which has possibly undergone ozone loss. This air is found within the polar vortex and has been exposed to temperatures below 195 K. Polar vortex air is identified by low values of nitrous oxide. AAOE and AASE-I results showed that the boundary between polar and mid-latitude air, as defined by nitrous oxide levels, was extremely sharp. During one AASE-I flight at 68,000 ft, a 20-percent nitrous oxide reduction occurred over a horizontal distance of 3 km as the ER-2 penetrated the polar air mass.

Gradients of other stratospheric trace gases showed similar sharpness. However, forecasts of stratospheric nitrous oxide measurements are not available. In addition to sharp gradients of trace gases, it was discovered that concentrations of various trace gases in air, that had encountered temperatures below 195 K, were highly perturbed. In particular, total odd nitrogen was depressed and chlorine monoxide was elevated. Hence, it is important to forecast temperatures, and to determine the thermal history of air masses. In short, the history of an air mass and accurate assessment of the polar vortex position is crucial for planning aircraft flight tracks.

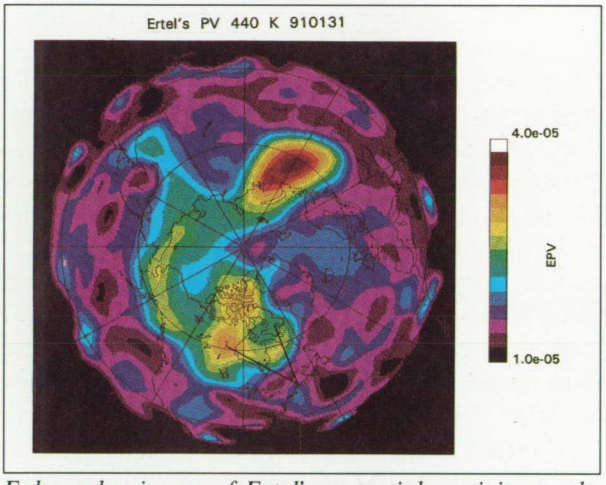

False-color image of Ertel's potential vorticity on the 440-K isentropic surface for January 31, 1991. Orange-red colors indicate polar air and blue-purple colors indicate mid-latitude air.

The figure is a color image of the polar vortex on January 31, 1991. The image represents Ertel's potential vorticity (PV) on the 440-K isentropic surface. PV is highly anticorrelated with nitrous oxide, and is crucial for the identification of both polar and mid-latitude air. January 31 closely followed a major stratospheric warming, which seriously distorted the shape of the vortex. The polar air (i.e., the vortex) is indicated by the higher PV values (yellow-orange-red), while low PV indicates mid-latitude air (blue-purple). Most of the polar air material is concentrated in two lobes, the first located over the northern portion of Russia (60°N, 60°E), while the second is located over northern Canada. (Latitude-longitude lines are at 30° increments.) If the ER-2 had been flying on January 31, several possible flight paths would have been available. Two of these possible flight tracks originating at Bangor (45°N, 68°W) are superimposed on the image as dark lines. The first flight track is a straight north run towards the pole, grazing the forward edge of the vortex lobe. The second track angles towards the northwest and would have penetrated to the center of the northern Canada polar air. Clearly, the northwestern angled flight track would have been more valuable than the direct north flight. Definition of these tracks is only possible by use of timely and accurate stratospheric global forecast data.

Both AASE-I and AAOE relied on the facsimile transfer of plots from the United Kingdom's Meteorological Office (UKMO) to the remote sites for planning ER-2 flight trajectories. This procedure inhibited flight planning because tuning and re-analysis of the meteorological information required a retransmission of a complete set of plots after communicating new requirements to the UKMO. At GSFC, we have developed software for automatically transferring meteorological data from the National Meteorological Center (NMC) to the remote field site in Bangor, Maine (via the cooperation of the NMC/Climate Analysis Center. Hence, meteorological data are directly accessible by the mission personnel in the hangar with the aircraft, rather than accessible only by facsimile transmission. The system utilizes the NASA Science Internet to remotely access the data on the NMC computers and to transmit the data electronically to a Unix-based computer workstation in the hangar with the ER-2. In the hangar, the data will be processed into machine-readable form and additional products will be generated. Data to be transmitted include surface weather observations, balloon observations, commercial aircraft observations, temperature retrievals derived from the TIROS operational vertical sounder, conventional meteorological analyses, and forecast analyses extending from the surface to the upper stratosphere. This is the first stratospheric mission in which the meteorological data will be electronically available in real-time for planning and analysis purposes.

In addition to the transferred products, we have developed software for producing PV from NMC geopotential heights and temperatures, calculating the trajectories of air masses using winds derived from our balanced wind algorithm, and for using the one-dimensional aircraft trace gas data to produce a three-dimensional picture of the trace gases. These tools can be used with both NMC forecasts and the NMC analyses, and are invaluable for developing flight plans and for analyzing the data after the completion of a flight. All data will be provided to the instrument investigators on the ER-2 and DC-8 as ancillary measurements for interpreting their data. The availability in the field of these data will lead to a mission that can rapidly respond to atmospheric variability, and can re-adjust its goals as the data are analyzed in the field. The real-time meteorological data will maximize the efficiency of each flight, allow for the achievement of the mission goals without worrying about the cooperation of the vortex when flying blindly, and produce a maximum yield of information about the ozone losses in the stratosphere.

Contact: Paul A. Newman (Code 916)
(301) 286-3806

Sponsor: Office of Space Science and Applications

Dr. Paul A. Newman is a Stratospheric Physicist studying the dynamics of the stratosphere, with particular emphasis on the mixing and transport of stratospheric trace gases. He has a PhD in Physics from Iowa State University.

THREE-DIMENSIONAL STRUCTURE OF THE PLANETARY BOUNDARY LAYER AS REVEALED BY A SCANNING AIRBORNE LIDAR

Airborne probing of the planetary boundary layer (PBL) using lidar has contributed significantly to our understanding of the processes that occur in the lowest layer of the atmosphere. Since the early 1980s, GSFC has played an active role in PBL research using the Boundary Layer Lidar System (BLLS) that has flown a number of times on the NASA Electra. Data acquired with the BLLS have helped to advance our knowledge of convective processes, convective structure, heat and moisture fluxes, convectively produced gravity waves, and air-mass modification of cold-air outbreaks by interaction with the Gulf Stream. In addition, the lidar data have been used to verify and test the performance of boundary-layer models in an effort to further our understanding of the governing physical processes and to increase their accuracy.

One of the limitations imposed on remote sensing of the atmosphere by airborne lidar to date has been two-dimensionality—most, if not all airborne lidars are restricted to the nadir along-track plane. The new Large Aperture Scanning Airborne Lidar (LASAL) system was designed to overcome this limitation. LASAL was a GSFC Director's Discretionary Fund (DDF) proposal that was funded for fiscal years 1988 to 1991. The main goal of the project was the creation of the first next-generation airborne lidar system that had both across-track scanning and along-track volume tracking abilities. The across-track scanning capabilities of LASAL enable the three-dimensional rendering of atmospheric aerosol structure below the plane. The volume-tracking capability of LASAL is also unique; it can be used to perform atmospheric tomography and to compute the aerosol extinction cross-section in the region from below the plane to the tracking height.

The LASAL system incorporates a large (36- x 24-in) scanning mirror which has two axes of movement—parallel and perpendicular to the plane's path—using two separate programmable motors. LASAL utilizes a Nd:YAG laser (532-nm) firing at 16 pulses per second (16 Hz) and a 22-in Cassegrain telescope. The scanning mirror and telescope are mounted in the bomb-bay section of the NASA P-3. The data system, which includes a real-time color display, laser and associated optics, is housed in the passenger section of the aircraft.

LASAL was flown for the first time in December 1990, over the ocean east of the Wallops Flight Facility, VA. During this test flight, excellent data

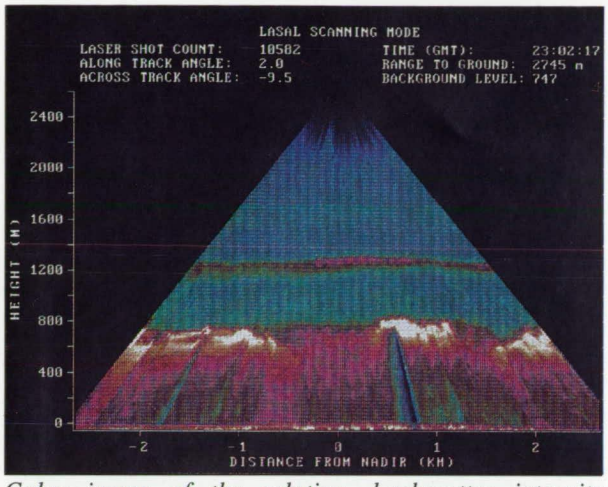

Color image of the relative backscatter intensity received by the LASAL instrument for one scanning sequence. The top of the PBL can be seen at about 800 meters.

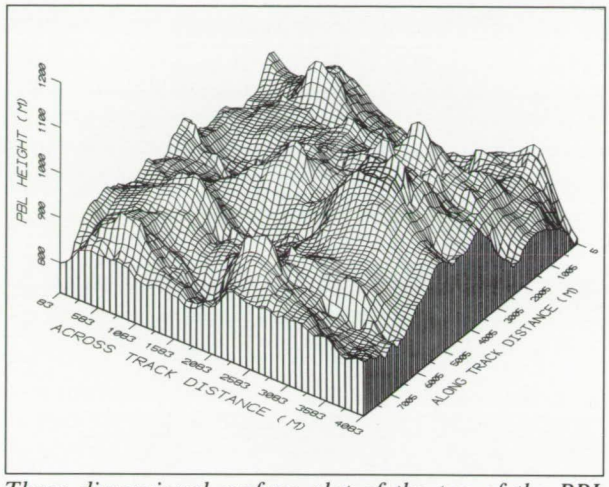

Three dimensional surface plot of the top of the PBL derived from LASAL data. The heights range from about 800 to 1100 meters.

were acquired in both modes of operation. In the interest of brevity, only the scanning mode data will be presented here. The first figure shows an example of one across-track scan displayed in a color-coded image format, where the largest signal is shown as white. The signal decreases through the browns, purples and greens, to the lowest signal presented in light blue. The mirror was scanning at 10°/s; each laser shot is separated by ~0.625° of arc. At this scan rate the across-track, horizontal resolution is ~30 m at the ground for an aircraft altitude of 3 km. The vertical resolution was 15 m.

The top of the boundary layer can be clearly seen at ~800 m and is associated with a very sharp gradient of aerosol scattering. By computing the height of the top of the PBL using lidar data from many such scans, it is possible to derive a three-dimensional surface representation of the instantaneous height of the PBL along the flight path.

The second figure represents the shape of the top of the PBL for a data segment 4 km wide by ~8 km long. The heights shown in the figure range from ~800 to 1100 m. This type of display is valuable for determining the actual physical shape of the convective cells as well as their orientation, and is a major advance in the utility of airborne aerosol lidar as compared to a nadir-pointing-only lidar system.

Contact: Dr. S. H. Melfi (Code 917)
(301) 286-6348

Steve Palm (SSAI)
(301) 286-4277

Dave L. Carter (Code 924)
(301) 286-6319

Sponsor: Office of Space Science and Applications

Dr. Melfi is Head of the Laboratory for Atmospheres' Environmental Sensors Branch. He actively participates in lidar remote sensing of the atmosphere and has developed systems to measure atmospheric water vapor using Raman scattering. Dr. Melfi also conducts research on the atmospheric boundary layer using airborne lidar systems and has developed methods for applying the data to difficult research areas. Dr. Melfi earned his MS and PhD in Physics from the College of William and Mary.

Mr. Palm earned a BS in Physical Science and an MS in Meteorology from the University of Maryland. Mr. Palm began working at GSFC in 1979 and has since been responsible for the development and operation of a number of airborne lidar systems designed to remotely probe the atmospheric boundary layer. Mr. Palm developed a number of analysis

methods that use lidar data to ascertain various boundary layer parameters.

Mr. Dave L. Carter is the Project Manager and Lead Mechanical Engineer responsible for the development, design and integration of the LASAL hardware components. Mr. Carter began work at GSFC in 1984 and earned a BS in Mechanical Engineering from the University of Maryland in 1987. He earned an MS in Engineering Management from George Washington University in 1991.

SATELLITE MEASUREMENTS OF THE GREENHOUSE EFFECT BY UPPER AIR WATER VAPOR

Water vapor is a potent greenhouse gas. In the upper troposphere, water vapor blocks the upwelling thermal radiation between 5 and 8 μm, on the midwave side of the peak in the Earth's outgoing flux near 11 μm. Carbon dioxide has a similar, and more famous, greenhouse effect between 13 and 18 μm, on the longwave side of the peak. (Visible solar radiation is called shortwave by climatologists.) If persistent convective processes can increase the number of water vapor molecules above 500 mb, there will be a significant blanketing effect on the lower tropospheric and surface temperatures.

Despite its importance, the effect of upper air water vapor on the Earth's radiation budget has received relatively little systematic attention until recently. Water vapor injection and removal processes are numerically complicated and are poorly understood, and it is still common for numerical weather models to fail to estimate observed water vapor concentrations by a factor of 2. From basic principles, it is not obvious what happens to the water vapor that is injected into the upper air by great convective episodes like the annual monsoons and the occasional El Niño/Southern Oscillation (ENSO) events. Does the moisture remain there and warm the Earth, or does enhanced nearby subsidence dry the upper air and cool the Earth, or do the two effects cancel?

We must turn to satellite observations to discover how the upper air moisture actually varies on global, regional, seasonal, and interannual scales. Fortunately, sensors with infrared channels designed to sound the upper air moisture have been flown on the operational NOAA polar-orbiting weather satellites since 1978.

NOAA has archived the water vapor brightness observations from the 6.7- and 7.2-μm bands in a relatively compact format that includes useful corrections for viewing angle and cloud cover. We have regridded these data, combining the two water vapor channels into a single value that represents the brightness temperature at 6.5 μm as observed by the TIROS Operational Vertical Sounder (TOVS). The brightness corresponds to the atmospheric temperature in the top few millimeters of water vapor. The result is a climatological database of the outgoing midwave radiation for nearly every day from 1979 to 1989.

The figure presents the first systematic measurement of the monthly climatology of the radiation losses controlled by upper air water vapor. Dark regions delineate cold, radiation-trapping regions above vigorous convection, such as the monsoons of India, Indonesia, Africa and Amazonia. Bright regions in the upper air water vapor band delineate upper air dry regions where heat is escaping from lower levels. The bright bands apparently represent the descending branch of the large convective cells, returning air to lower levels that was carried up from nearby, persistently rainy regions.

During northern summer from June to September, a bright dry slot dominates, surrounding most of the Earth at 15°S. During the Indian summer monsoon, the upper troposphere over the Middle East and the South Indian Ocean subsides and releases radiation, compensating for heat trapped north of the Equator. The weaker summer monsoons over Central America and over sub-Saharan Africa also develop corresponding bright dry slots in the water vapor patterns; these occur over the oceans southwest of the land-based convection. By far, the highest intensity radiation losses in the water vapor band occur over the Middle East during July and August.

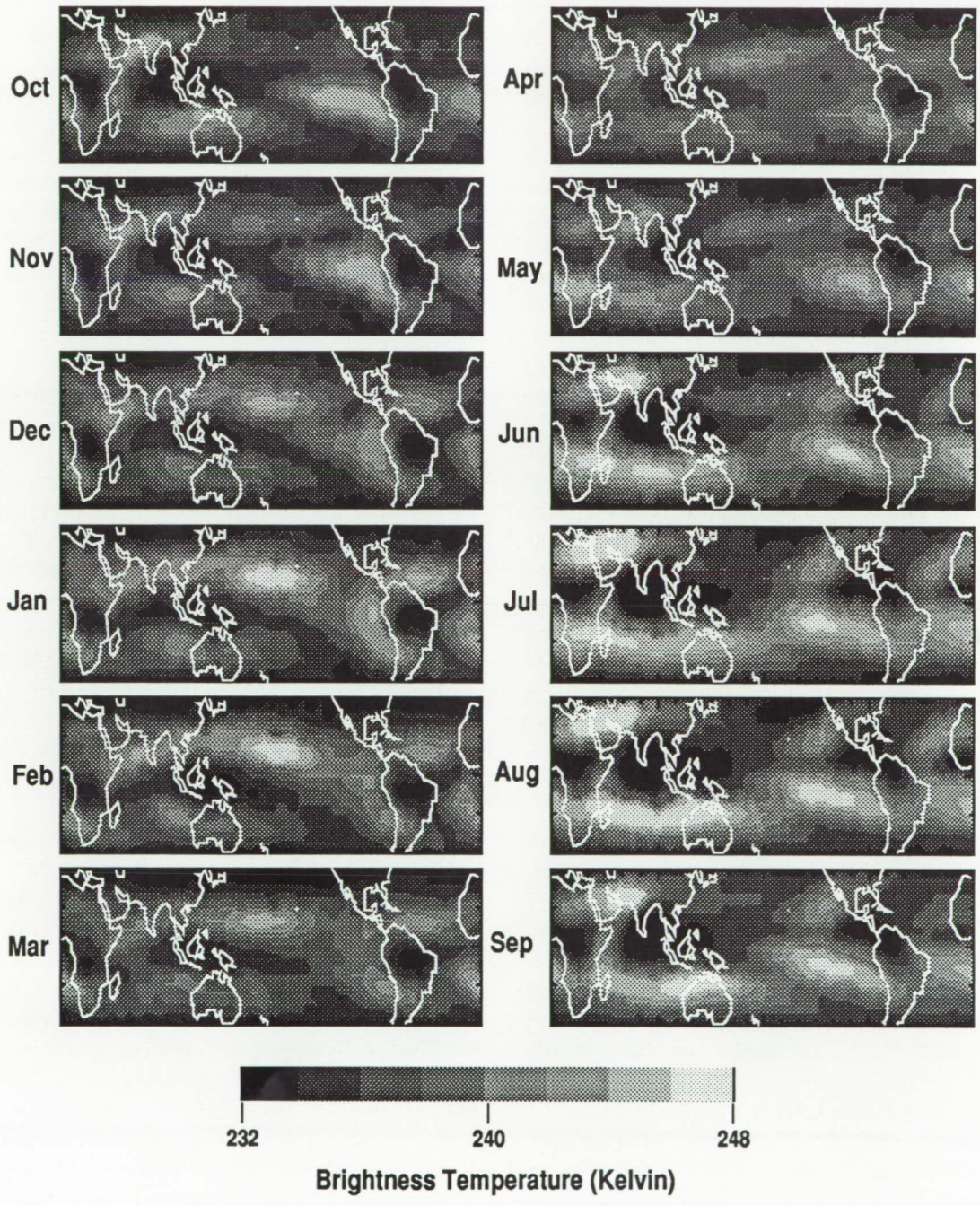

The first systematic measurement of the monthly climatology of the radiation losses controlled by upper air water vapor.

During the autumn and winter months in the Northern Hemisphere, the dry band surrounding the Earth at 15°N is unexpectedly much less intense than the corresponding slot at 15°S in the other half of the year. During January and February, only the region over the central Pacific southwest of Hawaii develops an intense dry slot. This mid-Pacific dry slot is unexpectedly remote from the weak winter monsoon over northern Indonesia, and remains to be explained in terms of upper air dynamics. During January, a weak horseshoe-shaped region forms in the upper air water vapor north, west, and south of the monsoon over Amazonia.

These satellite observations indicate that the upper troposphere surrounding the seasonal convective outbreaks is bright and much less saturated with water vapor, so that there is surprisingly little net variation in the average outgoing radiation in the 5- to 8-μm band on a global scale, despite large regional and seasonal variations. The decade-long TOVS database of moisture-controlled radiance provides material for several climatological research studies. For instance, it will be interesting to discover the underlying cause for the profound difference in the global appearance between northern hemispheric winter (October to March) and southern winter (April to September), and whether the midwave radiation budget was perturbed during the unusually large ENSO event of 1982-1983.

Contact: Dennis Chesters (Code 913)
(301) 286-9007

Sponsor: Office of Space Science and Applications

Dr. Dennis Chesters is a Physical Scientist in the Climate and Radiation Branch of the Laboratory for Atmospheres. He specializes in remote sensing of the atmosphere using thermal infrared data from weather satellites. He is particularly interested in the problems of detecting and visualizing complex multidimensional atmospheric phenomena embedded within satellite data. Dr. Chesters has been at GSFC for 12 years, and is currently the GOES Project Scientist.

NLC-91: AN INTERNATIONAL COLLABORATION TO STUDY THE SUMMER POLAR MESOSPHERE

Noctilucent clouds (NLC) (see first figure) are the highest clouds in our atmosphere. They occur at the cold mesopause near 83-km altitude during the polar summer, and can only be observed from the Earth's surface under unique viewing conditions requiring a negative solar declination. Although discovered more than 100 years ago in 1885, they are still an intriguing puzzle about which we know surprisingly little. Cloud characteristics as fundamental as particulate composition, size, shape, and origin still remain a mystery.

We suspect that NLC's are composed of ice particulates, possibly nucleated by metallic ions and dust of meteoric origin, and that they occur near the extremely cold summer mesopause which can reach temperatures as low as 110 K. They are thought to be related to polar mesospheric clouds (PMC) which blanket the polar cap above 80° latitude in summer, and gradually thin out at latitudes as low as 50°. New interest in these clouds revolves around recent speculations that their water content originates via methane from the troposphere and is of anthropogenic origin, and that they contain particulates sufficiently large to damage space shuttle tiles during re-entry.

The recent discovery of polar mesospheric summer radar echoes (PMSE), in conjunction with the paucity of information about NLCs, forms the basis for some fascinating problems regarding mesospheric chemistry, dynamics, and turbulence. PMSEs are coherent radar echoes in the polar summer mesosphere (~80 to 90 km) first observed by the MST radar in Alaska, but now observed on a fairly regular basis by other 50-MHz radars such as SOUSY and CUPRI. EISCAT has also observed these echoes at 224 MHz and at even higher frequencies, which is unexpected when one considers the scattering coefficients for electrons in this region.

A photo of noctilucent clouds, the highest clouds in our atmosphere.

How do such echoes occur? Are they related to local turbulence? Can aerosol chemistry alter the local scattering coefficients to permit such echoes to occur? These are all questions that have brought the summer mesopause to the forefront as an exciting topic for study.

Rockets are the only viable platform for in-situ studies of NLCs, since the region is too high for aircraft and balloons and too low for satellites. NLC-91 was developed as a coordinated international rocket/radar campaign to study many of the questions alluded to above, and has already been recognized as a project in the international Solar Terrestrial Energy Program (STEP). It was conducted between July 24 and August 10, 1991 from ESRANGE (Kiruna, Sweden), with Soviet rocket flights from Heiss Island during the same period. Twenty-one rocket flights were launched from ESRANGE, and another 10 from Heiss Island. The ESRANGE rocket launches carried instrumentation provided by scientists from Sweden, Norway, Germany, Austria, Switzerland, United Kingdom, U.S.S.R., and the U.S., which emphasizes the international interest in this scientific area. In addition, the EISCAT radar observatory (Tromsø, Norway) and the CUPRI radar (Cornell University, located at ESRANGE) provided data throughout the campaign.

The primary objective was to study the physical and chemical characteristics of NLCs and to determine their possible relationship to the PMSEs. To achieve these goals, the European collaborators provided four Nike Orion payloads, two each of DECIMALS and TURBO, which concentrated on ion composition, particulate structure, and mesospheric turbulence. The U.S. collaborators provided seven assorted payloads to concentrate on the electrodynamic properties of the atmosphere in the vicinity of NLCs and PMSEs. These included two Black Brant

mother/daughter payloads (E-Field) to measure vector electric fields and energy deposition, two Nike Orion Payloads (PEP) to study ion mobility, concentration and conductivity as well as mesospheric turbulence, and three Super Arcas payloads (MISTI) to study ion conductivity with two alternative techniques. All payloads with the exception of MISTI carried photometric devices to detect the presence of NLCs. In addition, eight meteorological payloads (Viper Dart), using the falling-sphere technique, and two using the chaff-ejection technique were coordinated with the rocket launch sequences. Finally, the 10 Soviet rockets (MK-100B) planned for Heiss Island were used to measure chemical and electrodynamical properties of the mesosphere in the polar cap during the ESRANGE salvo periods. The second figure provides a schematic depicting the organizational structure of the NLC-91 Campaign.

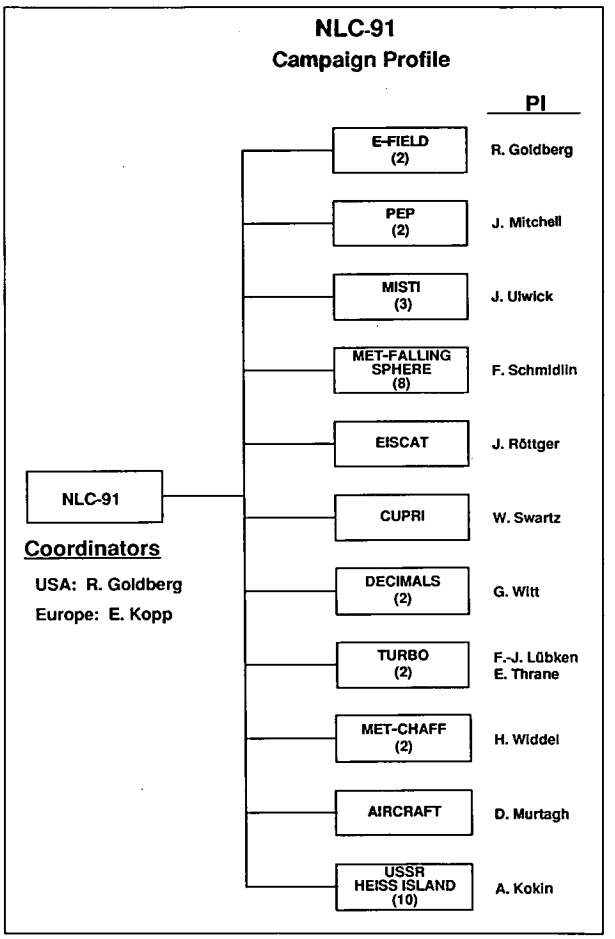

A schematic depicting the organizational structure of the NLC-91 campaign.

The campaign strategy was to launch one sequence of payloads into a strong NLC display, with or without the presence of NLCs (SALVO-A), and a second sequence into a multilayered PMSE condition, with or without the presence of NLCs (SALVO-B). A third mini-sequence, composed of one MISTI and one MET payload (SALVO-C), was to be launched into a PMSE condition different than that of SALVO-B. In this manner, we would be able to compare the various features associated with each phenomenon. To ascertain the presence of NLCs, Sweden and Germany provided aircraft with spotters ~500 km south of ESRANGE. This site was selected as ideal for observing NLCs that might cover the ESRANGE region; the aircraft were needed to permit observation on nights when lower cloud cover might obscure viewing from ground sites, which is an important asset considering the infrequent occurrence of blanketing NLCs at the latitudes of ESRANGE.

In spite of winds that often negated launch for several of the U.S. payloads, thunderstorms that flooded the launch area and wiped out power for two nights, and a lack of NLCs, we were able to successfully conduct the program as planned. SALVO-A was launched into a PMSE condition exhibiting two strong scattering layers between 80 and 90 km at both radar sites on the early morning of August 1, 1991. The layers began to fade, but still remained as two distinct layers during the latter part of the sequence. No NLCs were observed during this sequence, which included one each of MISTI, TURBO, E-FIELD, PEP, three falling spheres, and one chaff. SALVO-C was launched into a single-layered and weaker PMSE on August 5. Finally, on the night of August 9/10, 3 days before the close of the window (based on NLC observing conditions), we launched SALVO-B into an NLC display that blanketed ESRANGE. CUPRI also reported a weak scattering layer near 85 km during the launch sequence, which included two DECIMALS, one each of MISTI, TURBO, E-FIELD, and PEP, four falling spheres, and one chaff.

Preliminary evaluation of the results indicates that most payloads performed well with nearly all

instruments functioning successfully. We anticipate that this campaign will produce important results and improve our understanding of these poorly understood phenomena.

Contact: Richard A. Goldberg (Code 696)
(301) 286-8603

Robert F. Pfaff, Jr. (Code 696)
(301) 286-6328

Sponsor: Office of Space Science and Applications

Dr. Richard Goldberg is a Senior Staff Scientist in the Laboratory for Extraterrestrial Physics. Dr. Goldberg served as Program Director for the Solar Terrestrial Research Program at the National Science Foundation from 1989 to 1991. His study emphasizes middle atmospheric electrodynamics and coupling processes. He also has been Principal Investigator for more than 70 rocket payloads. Dr. Goldberg, who holds a PhD from Pennsylvania State University, has received several achievement awards. He has 28 years of experience at GSFC.

Dr. Robert Pfaff, Jr., has 6 years of experience in GSFC's Laboratory for Extraterrestrial Physics. He holds an AB from Brown University, a DES from the University of Paris, and a PhD from Cornell University. He was a Co-Investigator on the Polar Electric Field Instrument project. His research interests include electric-field instrumentation on rockets and satellites, as well as plasma wave instabilities and turbulence.

NONLOCAL THERMODYNAMIC EFFECTS IN THE UPPER ATMOSPHERE—PRODUCTION OF VIBRATIONALLY EXCITED NO FROM THE REACTION OF O WITH NO_2

UARS, which was launched in September 1991, carries two instruments (the Cryogenic Limb Array Etalon Spectrometer (CLAES) and the Improved Stratospheric and Mesospheric Sounder (ISAMS)) that will measure the infrared emissions of a number of trace gas constituents. These emissions arise from transitions between vibrational levels, typically in the ground electronic state. Radiance data for these emissions are used to infer species concentrations. It is usually assumed that the vibrational-level populations follow a Boltzmann distribution, i.e., the ratio of the population of the emitting level to the population of the lower level is $\sim e^{-\Delta E/kT}$, where ΔE is the energy difference between the two vibrational levels, k is the Boltzmann constant, and T is the gas temperature. In this case the gas is considered to be in local thermodynamic equilibrium (LTE). Molecular dynamical processes, such as photodissociation and chemical reactions, can produce level populations that are not in LTE and under some atmospheric conditions this can be manifested in the retrieved emission intensities. These non-LTE effects can result in erroneous estimations of the trace constituent concentration, if they are not included in the retrieval algorithms.

Nitric oxide (NO) is one example of a stratospheric molecule that will be measured by UARS. Recently developed photochemical models of the upper atmosphere have predicted that the NO infrared emission will not be in LTE. Estimated values for several chemical/physical parameters were used in the model calculations, since the required laboratory data were not available. One estimated quantity was the population distribution among vibrational levels produced in the reaction

$$O+NO_2 \rightarrow NO(v)+O_2.$$

There is sufficient energy available in this reaction that if all of the available energy were deposited in the vibration of the NO product, that molecule would be highly excited. By comparison, calculations using LTE considerations predict that at room temperature, 99.99% of the NO molecules would be in the lowest possible vibrational state.

Because model calculations are sensitive to the chemical and physical parameters that they incorporate, we have initiated a program to supply needed laboratory data on these fundamental processes. For our first contribution we have

measured the relative population distribution ratio for the vibrational levels of NO formed by the above reaction. A fast-flow system and low total gas pressure (<2 torr) were used for these experiments to eliminate quenching of the vibrationally excited states of NO by the gases present in the apparatus. Atomic oxygen was generated by microwave discharge dissociation of molecular oxygen (O_2); argon was used as an inert carrier gas, and nitrogen dioxide (NO_2) was injected into the gas stream just before the observation area. The NO product was detected using a laser-based technique. The molecule is excited by UV radiation from the laser and then emits photons that are monitored by a sensitive detector. This type of detection scheme is commonly referred to as laser-induced fluorescence (LIF). Because the laser can be tuned, it is possible to monitor the population in various vibrational levels of the NO molecule. Our results indicated that this reaction produces ~87 percent of the NO molecules in the lowest vibrational level and ~13 percent in the next higher vibrational level. No excitation of extremely high vibrational levels was observed which suggests that the O_2 product may carry some of the available energy.

This project was funded by the Director's Discretionary Fund and subsequently supported by the Upper Atmosphere Research Program (UARP). The project benefitted from participation by Dr. C. M. Moralejo whose tenure at GSFC as an NAS/NRC Resident Research Associate was supported by the UARP.

Contact: John E. Allen, Jr. (Code 691)
(301) 286-5896

Regina J. Cody (Code 691)
(301) 286-3782

Sponsor: Director's Discretionary Fund
Office of Space Science and Applications

Dr. John E. Allen, Jr. works in the Laboratory for Extraterrestrial Physics. He received a BS and an MS in Applied Physics and a PhD in Physics from the University of Florida. John has 13 years of experience at GSFC.

Dr. Regina J. Cody has 17 years of experience at GSFC. She currently works in the Astrochemistry Branch of the Laboratory for Extraterrestrial Physics. Dr. Cody holds a BS in Chemistry from West Liberty State College in West Virginia and a PhD in Physical Chemistry from the University of Pittsburgh.

THERMOSPHERE-IONOSPHERE-MESOSPHERE ENERGETICS AND DYNAMICS MISSION

The Thermosphere-Ionosphere-Mesosphere Energetics and Dynamics (TIMED) mission will obtain global measurements of geophysical parameters of the lower thermosphere, ionosphere, and mesosphere and will be used to determine the seasonal and diurnal variations of these regions. This mission will consist of two spacecraft, one in a near-polar orbit of ~95° inclination, and the other in a 49° inclination orbit.

The TIMED-H and -L spacecraft are planned for launch in mid-1998. Each spacecraft will carry up to 14 instruments. Each spacecraft will be launched by a Delta-II launch vehicle and will have a design lifetime of 4 years. Each spacecraft will have an onboard propulsion system to allow the orbits to be adjusted to achieve the scientific objectives during the entire mission.

The TIMED spacecraft will consist of aerodynamically clean cylinders with minimal protrusions into the atmosphere. The dual-spin spacecraft with a spin capability of one revolution per orbit (rpo) will be provided to permit several instruments to look forward (ram direction) along the velocity vector for high spatial resolution along the orbit and to permit other instruments to look in the zenith, wake, nadir, or limb directions. In addition, a spin-mode of operation (selectable up to 10 rpm) with the spin axis normal to the orbit plane will permit the instruments to sweep through all angles of attack within each spin period. This will enable the instruments to examine background levels, to evaluate attitude

TIMED-H and -L Mission Instruments and Measurements	
Instruments	Measurements
Fabry-Perot Interferometer	DE-2; UARS
Neutral Mass Spectrometer/Wind and Temperature	AE-1,2,3,4,5; DE-2; San Marco D/L
Ion Mass Spectrometer	ISIS-2; DE-1; AE-3,4,5
Langmuir Probe	AE-1,2,3,4,5; DE-2; PVO
Ion Drift Meter/Retarding Potential Analyzer	AE-3,4,5; DE-2; OGO-6; PVO
UV Spectrometer	OGO-4,5,6; AE-3,4 GAL; MAR-6,7,9; PION-12; SME
Imaging Photometer	AE-3,4,5
Satellite Electrostatic Triaxial Accelerometer	AE-3,4,5; S85-1; S3-1,3; SEATA-1,2,3
Energetic Particles Analyzer	ISIS-1,2; OGO-4,6; AE-3,4; DE-1,2
Global UV Airglow Imager	POLAR BEAR; HILAT; DELTA 180-181
Solar EUV Spectrometer/XUV Photometer	AE-3,4,5; OSO-4; San Marco
Vector Magnetometer	DE-1,2; ISEE-1,2
Near Infrared Spectrometer	SME
Electric Field Detector/Plasma Wave Experiment	DE-1,2; ISEE-1,2; CRRES
Infrared Limb Sounder	Nimbus-6,7; UARS

sensitivities of the measurements, or to obtain information on particle pitch angle distributions. A flat surface will be incorporated on the forward ram surface of the spacecraft (in the one-rpo mode) to provide an unobstructed 2π-steradian field of view for the forward-facing instruments.

The spacecraft will provide a pointing accuracy of 1°. A despun solar-pointing platform will be provided on the TIMED-H spacecraft to permit the Solar Extreme Ultraviolet Spectrometer to point at the center of the Sun with an accuracy of 10 arcmin for measuring solar flux.

A remote command and data storage capability will be provided on board the spacecraft to permit instrument operation during any portion of an orbit. The Tracking and Data Relay Satellite System (TDRSS) support of the science data is precluded by the low-perigee passes, because a high-gain antenna is not feasible. However, housekeeping telemetry, commanding, and ranging can be accomplished using the S-band single access system of the TDRSS. Science data can be stored and dumped to the Wallops ground station.

The instrument complements for the TIMED-H and -L pre-phase-A study consist of 14 and 9 instruments, respectively (see the table). Eight of the 14 instruments will be on board the high-inclination spacecraft and the low-inclination spacecraft as well, to make correlative measurements. The near-polar spacecraft (TIMED-H) will be placed in a highly elliptical (150- x 6000-km) orbit initially. During the

first 2 years of operation (Phase 1), the spacecraft perigee will be lowered into the lower thermosphere and ionosphere (between 120 and 150 km). After the first year, the apogee altitude will be lowered to 3000 km by aerodynamic drag. After 2 years, the spacecraft orbit will be changed to 250 and 300 km circular (Phase 2). The duration of each circular orbit will be about 1 year.

The 49° inclination spacecraft (TIMED-L) will be placed initially into a 400-km circular orbit. Phase 1 will last for about 1½ years, and the orbit altitude will range from 300 to 400 km. During Phase 2 of TIMED-L, the spacecraft orbit will be changed to an elliptical orbit with a 1,500-km apogee and a 150-km perigee. During this phase, spacecraft perigee will be lowered to the 120- to 130-km region. The spacecraft orbit will be circularized at 300 km after ~3 years into the mission (Phase 3).

After the design mission lifetime of 4 years, the remaining propellant will be used to place each spacecraft in a circular orbit with the highest possible altitude for the remainder of the extended mission.

Contact: John J. O'Brien (Code 402)
(301) 286-9434

Sponsor: Office of Space Science and Applications

Mr. John O'Brien, Study Manager for TIMED, has worked at GSFC for 25 years and has received several achievement awards. He holds a BS in Physics.

Lower Atmosphere

SIMULATED ANNEALING APPLIED TO THE ATMOSPHERIC TEMPERATURE AND WATER VAPOR INVERSION PROBLEM

An important component of NASA's research efforts in the atmospheric sciences involves the use of satellite measurements of Earth-emitted thermal radiation to infer the vertical distribution of temperature and gaseous constituents such as water vapor and ozone on a global and time-continuous basis. These inferences are possible due to well-established radiative transfer equations (RTEs) relating the frequency-dependent radiative emission of a medium and some particular physical aspect of the medium. Because desired quantities appear as unknowns under the integral sign, the equation must be inverted through an appropriate numerical method to retrieve the physical state of the Earth-atmosphere system corresponding to the observed spectral signature. Passive remote-sensing measurements of naturally emitted radiation in the infrared (600 to 2700 cm^{-1}) and microwave (50 to 60 GHz) spectral regions are routinely processed in this fashion for the purpose of monitoring the thermodynamic state and composition of the Earth-atmosphere system.

The current generation of operational atmospheric sounding instruments, specifically the HIRS/2 and MSU sensors on board the NOAA TIROS-N series of satellites, utilize 20 spectral channels to provide daily three-dimensional global temperature and humidity fields with a horizontal spatial resolution of ~50 km. These fields have provided invaluable information for radiation budget studies, global monitoring of trends in atmospheric temperature and composition, and improved initialization of numerical weather forecasting and general circulation models. However, the mean vertical temperature profile accuracies, as determined by differences between collocated radiosonde reports and satellite-derived temperatures, remain in the neighborhood of ~2°C. Similarly, the accuracies for a highly variable gaseous constituent such as water vapor are estimated at no better than 30 percent when integrated over 3-km-thick layers. However, recent theoretical and experimental results have indicated that significantly enhanced sounding capability is attainable by employing sensors with thousands of high-resolution spectral channels, optimally located to maximize the information content of the radiance measurements and to minimize the effects of instrumental noise on the derived quantities.

Researchers at GSFC have conducted simulated retrievals of atmospheric temperature and water vapor

profiles using the 4,000-channel high-resolution Atmospheric Infrared Sounder (AIRS) to be flown aboard EOS platforms in the late 1990s. The advantages inherent in a system with increased spectral resolving power are shown in the first figure, which compares the theoretical weighting functions for the HIRS/2 channels with a small subset of AIRS temperature sounding channels. The latter clearly span the solution space more fully and possess narrower halfwidths than the HIRS/2 channels, providing better vertical resolution and increased retrieval accuracies, especially in the stratosphere. However, increasing the number of sounding channels by two orders of magnitude may pose special convergence or stability problems for the traditional numerical techniques when solving the nonlinear RTE. Therefore, experiments have been undertaken with a class of optimization techniques referred to as simulated annealing methods which avoid the numerical instabilities associated with these methods.

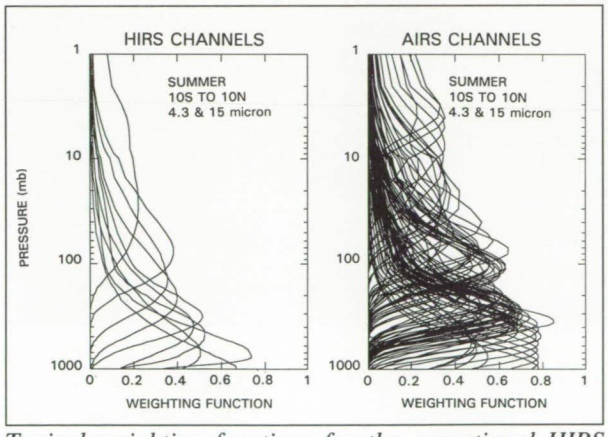

Typical weighting functions for the operational HIRS and the next-generation AIRS instruments.

The method simulates the thermodynamic processes involved in the slow annealing of physical systems to a ground state, whereby local increases in the system energy are occasionally allowed to avoid trapping in nonoptimal local minima (e.g., as in the crystallization process). If the atmospheric temperature-humidity retrieval problem is cast as an optimization problem characterized by an energy function to be minimized, then the connection to statistical mechanics becomes clear. The unknown parameters

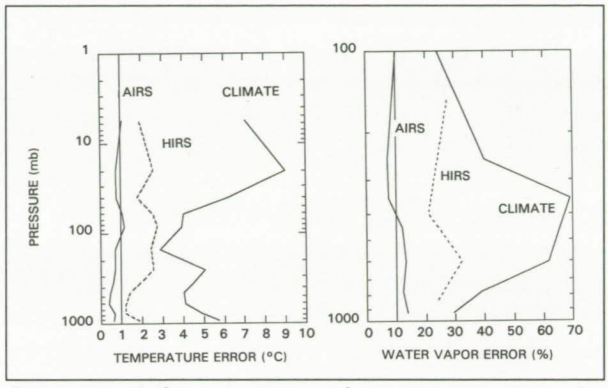

Comparison of temperature and water vapor accuracies using HIRS channels and a select subset of 90 AIRS channels by the method of simulated annealing.

such as level temperatures relate to the molecular positions, the energy or cost function to the internal energy, and the optimal profile or solution configuration to the ground state of the thermodynamic system. The method is simply implemented as a sequence of forward calculations using trial configurations of the atmospheric parameters, subject to a probabilistic acceptance criterion. The process is repeated until the differences between the observed and computed radiances reach a predetermined noise level (i.e., the energy function is minimized).

We have applied simulated annealing to the retrieval of atmospheric parameters by generating synthetic radiance spectra for each of 400 globally distributed profiles of temperature and water vapor derived from observed radiosonde data. For comparison purposes, results were obtained for a subset of 1,000 AIRS channels located in the CO_2 and H_2O absorption bands, as well as for a set of 15 HIRS channels. Root-mean-square (RMS) errors for temperature at 13 levels and integrated water vapor amounts in 7 layers are shown in the second figure for both instruments. The corresponding RMS differences with climatology are also shown for reference. The significant improvement seen in the temperature and humidity retrievals for the AIRS channels is testimony both to the advantages of high spectral resolution as well as to the successful application of optimization techniques such as simulated annealing to complex problems in atmospheric remote sensing. Such

dramatic improvements will undoubtedly play a significant role not only in the quality of forecasts derived from numerical weather prediction models, but also in the monitoring and understanding of long-term global climate change.

Future studies will explore the implementation of computational algorithms such as simulated annealing and neural networks on massively parallel processor architecture as part of the recently approved high-performance computing initiative. This will be necessary to ensure efficient processing of the high spectral- and spatial-resolution data originating from future EOS instruments such as AIRS.

Contact: George Serafino (Code 936)
(301) 286-3021

Sponsor: Office of Space Science and Applications

Mr. George Serafino works in the Space Data and Computing Division and has performed research in the areas of atmospheric remote-sensing techniques, data analysis and instrument characterization for the Nimbus-7 and NOAA TIROS-N series of satellites. He has 8 years of experience at GSFC. He holds a BS in Physics from Trinity College, Hartford, CT, and an MS in Meteorology from the University of Maryland, College Park.

REGIONAL WIND ANALYSIS

During the 6-month interval from October 1, 1990 to April 1, 1991, NASA and the Office of Naval Research (ONR) conducted the Surface Wave Dynamic Experiment (SWADE). The purpose of this experiment was to develop a better understanding of the physical processes that lead to the growth and decay of oceanic surface waves. Numerical modeling will play an important role in the analysis of the data; this work, in turn, may lead to better modeling of oceanic waves. Because oceanic waves are forced by surface winds, an accurate wind analysis is crucial to the success of the experiment.

Wind analyses done at weather centers around the globe, with the best resolutions being on the order of 1° x 1°, are much coarser than the details of wave data. Furthermore, observations over the sea are often poor in quality and coverage. As an example, the first figure shows the surface operational wind analysis from the National Meteorological Center (NMC) for 18Z, October 26, 1990. At this time, a major, explosive cyclone was developing along the eastern coast of the U.S. The shape of the system is fairly well-captured, but the maximum winds were considerably underestimated and the fine structure is missing. For these reasons we have developed at the Global Modeling and Simulation Branch (GMSB) a superior regional, fine-mesh (resolution of 50 km) wind analysis for our SWADE work.

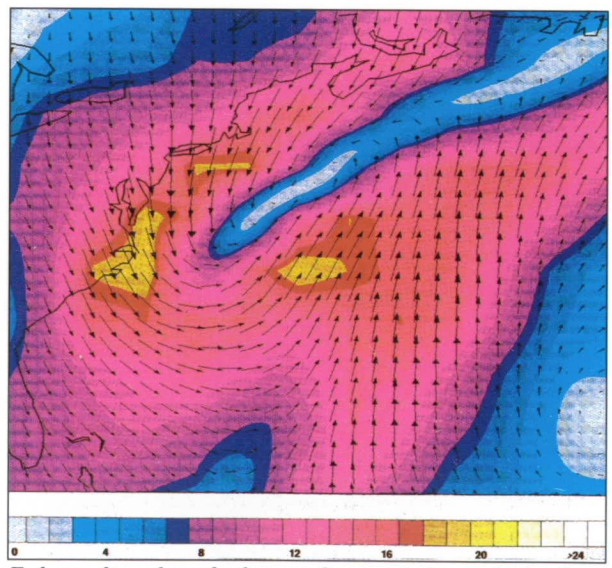

False-color plot of the surface wind analysis from 18Z, October 26, 1990 from the operational NMC global analysis.

The analysis requires a first-guess field, which may be taken from a coarse-mesh analysis or a numerical prediction model. After using gross error and nearest neighbor checks to verify the quality of the data, we use the successive correction method (SCM) for the actual analysis. We have not used a more sophisticated scheme, such as optimum interpolation (OI), because we lack the proper error statistics and correlations for this mesoscale analysis. Another advantage that we enjoy over the operational analysis

is the additional observations given by a number of meteorological buoys placed off the eastern coast just for this experiment.

The second figure shows the improved analyses achieved by our system, portraying the same time period as the first figure. Note the strengthening of the wind maxima, particularly near the Delmarva Peninsula. In addition, our analysis contains a great deal more detail. Subsequent verification of our analysis against observational data showed excellent agreement.

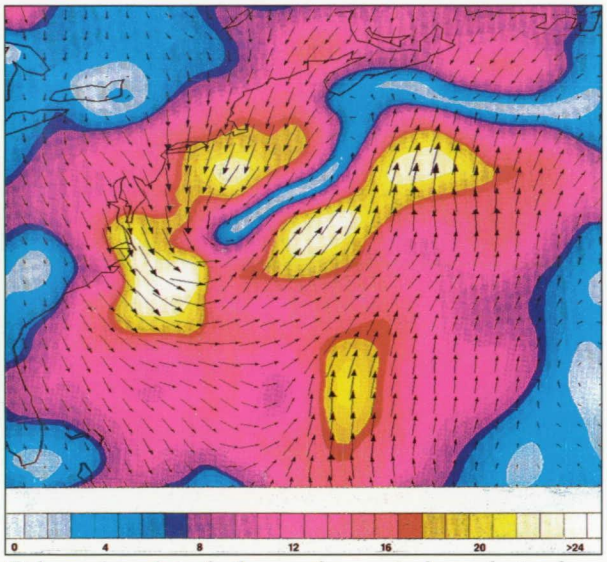

False-color plot of the surface wind analysis from 18Z, October 26, 1990 from the SWADE regional wind analysis.

At present, our analysis requires a coarse-mesh, first-guess field which is currently available every 6 hours. This makes the temporal resolution of the analysis much poorer than the spatial resolution. Because we have data at every hour, we are developing an assimilation system that uses a fine-mesh regional model to give the first guess at every hour. An additional bonus is that we will produce a three-dimensionally consistent atmospheric analysis.

Contact: Dean G. Duffy (Code 911)
(301) 286-9543

Sponsor: Office of Space Science and Applications

Dr. Dean G. Duffy received his ScD from MIT in 1975 and has been a research meteorologist with GSFC since 1980. His areas of interest are in the areas of applied mathematics, dynamic meteorology and computer (wave) modeling.

DISCOVERY OF AN EQUATORIAL TEMPERATURE AND WIND ANOMALY

A well-known phenomenon in the equatorial ionosphere is the Equatorial Ionization Anomaly (EIA), also known as the Appleton-Burkard anomaly. During daytime, two ionization-density crests develop near 20° magnetic latitude at altitudes above 150 km. The two crests, with a trough in between, intensify during the day, usually reach a maximum in the evening, and then decay sometime during the night. This effect is known to be caused by electromagnetic drift in a narrow latitudinal belt around the Equator, which is upward during the day and downward during the night. The electric fields causing the effect are of planetary scale and are generated by tidal winds in the atmospheric dynamo region between 80 to 120 km; they are communicated to higher altitudes along the Earth's magnetic field lines.

Many years ago, an effect similar in morphology had also been seen in the neutral atmosphere. Measurements of N_2 and O densities by the neutral mass spectrometer on board the OGO-6 satellite showed two peaks at ±20° in latitude on either side of the magnetic equator and not the geographic equator, as one would have expected. Based on these observations, it was predicted that the two ion-density crests of EIA would offer increased resistance to the flow of neutrals from the hot day side to the cold night side. As a result, the neutral winds would be reduced in the latitude regions of the crests and enhanced in the narrow belt around the ionization trough. Because the winds are significantly involved in the redistribution of energy, their modulation

would modulate also the temperature and density. We have now been able to verify these predictions.

The Dynamic Explorer-2 (DE-2) satellite, launched and operated between 1981 and 1983, was in a polar orbit with its perigee at 286 km and apogee at about 1,000 km. The wind and temperature spectrometer (WATS) and the Langmuir Probe (LP) were two of several experiments on board DE-2. WATS measured the gas temperature, and the zonal and vertical wind components, while LP measured the electron and ion densities. Data obtained close to the Equator provided an opportunity to examine the coupling effects of the EIA with the neutral atmosphere.

The analysis of these data shows clear evidence of anomalous latitudinal variations in the zonal winds and temperature at low latitudes, as seen in the figure. The zonal winds exhibit a maximum centered around the dip equator flanked by minima on either side around 25°, while the temperature exhibits a pronounced bowl-shaped minimum at the magnetic equator flanked by maxima on either side. The two minima in the zonal winds and the corresponding maxima in temperature are collocated with the crests of the EIA. The maximum in zonal winds and the minimum in gas temperature are collocated with the trough of the EIA. The observed differences between maxima and minima in temperature and zonal winds, on many occasions, are observed to exceed 100 K and 100 m/s, respectively.

The equatorial temperature and wind anomaly (ETWA) discussed here has so far been observed only during high levels of solar activity; it is not known whether the effect is also present during periods of lower level activity. Understanding this distinction is an important point that requires clarification; it may explain ultimately why the ETWA phenomenon has eluded present-day empirical models.

Contact: R. Raghavarao (Code 914)
(301) 286-6253

L. E. Wharton (Code 914)
(301) 286-3486

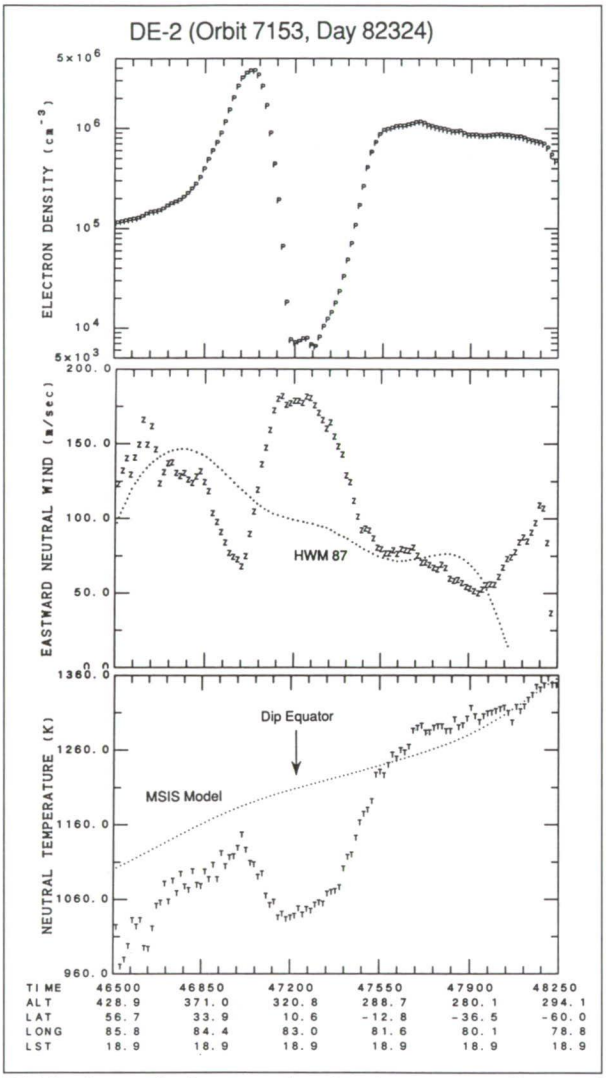

DE-2 data of electron density (upper panel), zonal winds (middle panel) and neutral temperature (lower panel) for November 20, 1982, at 18.9 local solar time, plotted versus latitude.

Hans G. Mayr (Code 914)
(301) 286-7505

Sponsor: Office of Space Science and Applications

Dr. R. Raghavarao received a PhD from the Andhra University, and is a Senior Professor at the Physical Research Laboratory, Ahmedabad, both in India. He holds a Senior Resident Research Associateship from the U.S. National Research Council.

Dr. Lawrence E. Wharton received a PhD from the University of Maryland. He is a Physicist with 13 years of service at GSFC.

Dr. Hans G. Mayr received a PhD from the University of Graz, Austria. He is an Atmospheric Scientist with the Dynamics Explorer and Pioneer Venus projects, and has 23 years of experience at GSFC.

SATELLITE AND AIRCRAFT STUDIES OF THE KUWAIT OIL FIRE SMOKE

Between May 16 and June 12, 1991, a Gulf Oil Fire Smoke Experiment was conducted in the Persian Gulf region, with coordinated data acquisition using the Landsat Thematic Mapper (TM). This experiment was an airborne campaign involving two U.S. and one German research aircraft. The purpose was to examine the physical, radiative, and chemical properties of the optically dense smoke plumes that arose from the 732 oil wells initially set ablaze in Kuwait during the 1991 Gulf War. Of this number, some 550 wells were still burning in mid-May. As of November 1991, all fires have been extinguished. To those who participated in the field experiment, the sight of hundreds of burning oil wells and palls of black, white, and grey smoke were unforgettable. In addition to the oil fire smoke studies, there were many opportunities to study the desert dust aerosol that is a common and persistent feature of the Middle East. Since the Saudi Arabian desert is often used to calibrate satellite sensors, the opportunity was taken to obtain useful spectral and angular reflectance measurements of the desert, and to make in-situ measurements of the size distribution and optical properties of the desert aerosol. These additional datasets will likely prove invaluable to future NASA missions.

A mosaic of two TM images of the Persian Gulf region acquired on May 30 is shown in the first figure, where band 7 (2.2 μm) was assigned to red, band 4 (0.83 μm) to green, and band 2 (0.56 μm) to blue. Kuwait City, at the northern point of land just south of the Gulf of Kuwait, is partially obscured by smoke flowing over the Gulf of Kuwait from the Raudhatain and Sabriyah oil fields, located off the northwest corner of the image. Somewhat lighter smoke can be seen coming from the Minagish oil field just west of the Greater Burgan oil field.

The combined plume, which extended south along the Persian Gulf coast into Saudi Arabia, consisted of ~30 percent salt, 15 to 20 percent soot, 8 percent sulfate, and clouds of dust stirred up by the hot eddy currents generated by the fires. The enlargement of the Greater Burgan field shown in the second figure clearly reveals sources of both dark and light smoke, as does the inset photograph taken from the NCAR Electra research aircraft during overflights of Kuwait on May 23. Along much of the coast, the smoke plume remained confined to a strip ~25 km in width near the fires, widening to ~60 km and thinning out as it moved off the Arabian Peninsula towards the Gulf of Oman and India. As it moved with the wind from day to day, its effects could be felt well away from the coast over potentially vulnerable desert regions. In addition to being confined to a horizontal band tens of kilometers in width that can wander over a much wider area depending on wind direction and speed, the smoke plume was also restricted in the vertical dimension, presenting a well-defined base and top. It was generally capped by a strong temperature inversion, usually between 3 and 4 km, which may, in part, have been self-generated by solar heating at the top of the dark plume. Its base was located at an altitude of 0.5 km and was also quite flat after the layer had stabilized 200 km downwind of the burning oil fields.

The primary tools used to examine the properties of the smoke plumes in the field experiment were the research aircraft of the National Center for Atmospheric Research (Lockheed Electra) and the University of Washington (Convair C-131A). The C-131A contained a multiwavelength scanning radiometer developed at GSFC for the purpose of measuring the angular distribution of scattered radiation deep within a cloud layer. Both aircraft were based in Bahrain and flew a combined total of ~200 research hours in the Persian Gulf region. Previous efforts to predict how even more widespread

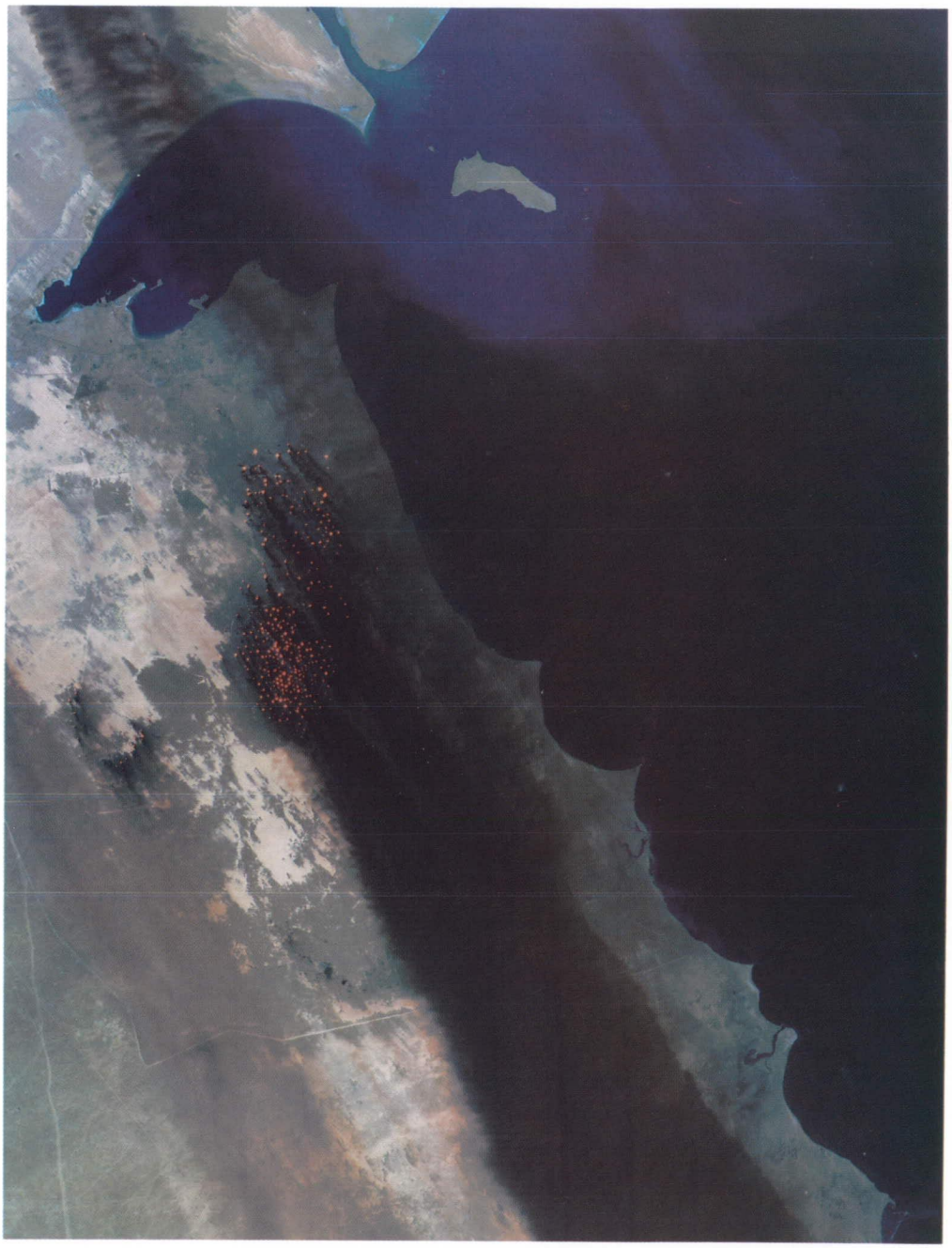

Mosaic of two Landsat-4 TM scenes of Kuwait acquired on May 30, 1991. In processing this image, band 7 (2.2 μm) was assigned to red, band 4 (0.83 μm) to green, and band 2 (0.56 μm) to blue. Kuwait City is located on the southern shore of the Gulf of Kuwait, which opens into the Persian Gulf in the northwest corner of the image. The smoke generated by the fires burning in the Greater Burgan oil field south of Kuwait City is readily apparent, as is the smoke generated by the Raudhatain and Sabriyah oil fields north of Kuwait City and the Minagish oil field just west of Greater Burgan.

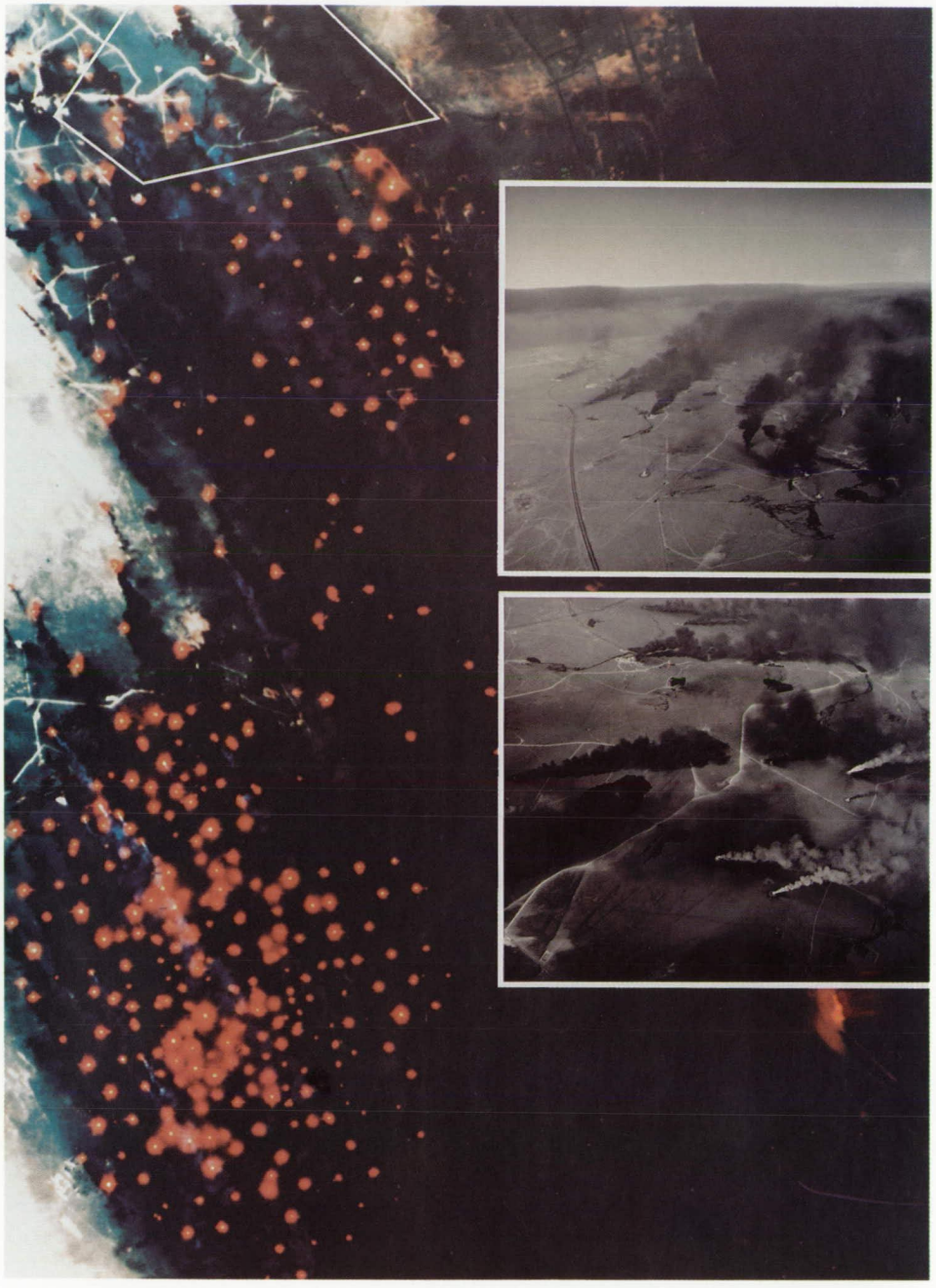

Enlargement of the Landsat-4 TM image of the Greater Burgan oil field showing both white and black smoke plumes. The inset photograph of the white and black smoke plumes and some of the burning oil wells was obtained from the NCAR Electra aircraft on May 23, 1991.

smoke would affect global climate have been thwarted by poor knowledge of how much smoke would be produced and how such smoke would be scavenged in clouds. Hydrophobic particles might remain in the atmosphere for months, and may even self-loft to the stratosphere via absorption of solar radiation, whereas hygroscopic particles would be scavenged much more rapidly by clouds. Climatic effects from the Kuwaiti fires are expected to be confined to the Gulf region, but observations of the character of the smoke were expected to help determine how more widespread fires might affect global climate. In addition, because the expected changes in radiation, cloud microstructure, and air chemistry were so large, observations in Kuwait can help to bypass years of study directed at detecting weaker effects of current anthropogenic emissions on the global climate. The in-situ study clarified a number of points:

- Based on the total emission rates of various materials from the Kuwait oil fires, ~4.6 million barrels of oil were being burned each day, which amounts to slightly less than the U.S. daily import of oil.

- There was considerable SO_2 in the smoke (up to 1,000 ppbv), amounting to ~57 percent of that from electric utilities in the U.S.; the CO_2 emission rate (up to 130 ppmv) was ~2 percent of world-wide emissions from fossil fuel and biomass burning.

- Particle size distributions were bimodal, with maximum concentrations of ~100,000 particles cm^{-3} (clear air ~100 cm^{-3}). The mass loading of particles often exceeded 100 $\mu g\ m^{-3}$.

- Smoke was diverse in appearance and optical properties.

- White smoke scattered sunlight very efficiently and was composed of cubic salt crystals.

- Black smoke was highly absorbing in the visible and was probably pure soot.

- Smoke reflectance was somewhat greater than Persian Gulf reflectance.

- The optical thickness of the composite smoke plume 100 km downwind of the fires was 2 to 3 in the visible wavelength region.

- 75 to 80 percent of the incident solar radiation was absorbed in the thickest portions of the smoke, with 10 percent transmitted and the rest reflected.

- The absorption of solar radiation by the smoke produced an instantaneous heating rate of the smoke that, near noon, was ~25°C per day.

- Smoke exhibited backscattering (glory) and rainbow features in the visible and near-infrared, features characteristic of spherical particles (oil drizzle droplets formed from condensation within the first 100 km of the fires).

- Particles in the black smoke quickly formed chain aggregates.

- ~70 percent of the smoke particles can serve as cloud condensation nuclei downwind of the fires at a supersaturation of 1 percent.

Many of the aircraft data are still being processed and analyzed, and will undoubtedly reveal further properties of the smoke which will provide input into model computations of the effects of the dark plumes on the regional climate. The effects of the various particulates on the ecosystem, and on the physical well-being of the people in the region, will also need to undergo continuing scrutiny, both during the period that the fires were being gradually extinguished and afterwards as the region slowly recovers in the aftermath of these devastating fires.

Contact: Robert F. Cahalan (Code 913)
(301) 286-4276

Michael D. King (Code 913)
(301) 286-5909

Sponsor: Office of Space Science and Applications

Dr. Robert F. Cahalan is a Senior Research Scientist in the Climate and Radiation Branch of the Laboratory for Atmospheres. He earned his PhD in

Theoretical Physics from the University of Illinois. His current research includes empirical and theoretical studies of cloud fractal properties and large-scale sea-ice variations associated with atmospheric forcing. He has won a Senior Fellow Award from the National Center for Atmospheric Research and a NASA Quality Increase Award. He has 11 years of experience with GSFC.

Dr. Michael D. King holds a PhD in Atmospheric Sciences from the University of Arizona, and is responsible for the development and application of algorithms for the remote sensing of cloud and aerosol properties from airborne and satellite multispectral radiometers. He has been a visiting professor at the University of Washington, with whom he participated in the month-long airborne field experiment of the Kuwait oil fires in the Persian Gulf. Dr. King is a Fellow of the American Meteorological Society, and has received several Goddard and Langley Special Achievement Awards and the NASA Exceptional Service Medal. He has been with GSFC for 14 years.

SHUTTLE IMAGING RADAR C SOIL MOISTURE MEASUREMENTS

The Shuttle Imaging Radar C (SIR-C) is scheduled for flights in 1993 and 1994. It is probably the last of the SIR series of experiments before a planned Synthetic Aperture Radar (SAR) satellite is made available. The earlier missions (SIR-A and SIR-B) were limited to a single frequency (L-band) and horizontal polarization. SIR-C will be comprised of three units at frequencies in the L-, C-, and X-bands. The two lower frequency units (L- and C-bands) are implemented with quad polarization. In the SIR-B experiment (October 1984), it was demonstrated that radar backscatter depends on soil moisture, but that other surface parameters, like vegetation and roughness also affect the radar signature. The SIR-C approach of multiple frequencies and polarizations provides the means to unravel these surface parameters.

The fine resolution offered by SIR-C is essential in a number of hydrological and agricultural applications. Before the SIR-C launch, research activity will be limited to measurements provided by the Jet Propulsion Laboratory's airborne SAR and analysis of the acquired data. During July 1990, an experiment was conducted over a central Pennsylvania test site (Mahantango Creek) with the SAR aboard the NASA DC-8 aircraft. The test site is hilly and largely divided into small fields covered with a variety of crops. The hilly landscape and the smallness of the fields will make the task of data analysis very difficult and challenging.

The airborne SAR has three frequencies (P-, L-, and C-bands) and quad polarization, and covers a wide range of incidence angles (15° to 50°). The wide range of incidence angles is required for the airborne SAR to give decent ground coverage. The radar backscatter, however, depends strongly on the incidence angle. This complicates the analysis of SAR data. The quick-look data from the flights over Mahantango Creek appear quite promising. Detailed analysis of the processed data has already begun. The digital elevation model of the test site is currently being integrated with the SAR images to facilitate the study of microwave backscatter dependence on surface roughness, soil moisture and vegetation cover.

Contact: James R. Wang (Code 975)
(301) 286-8949

Sponsor: Office of Space Science and Applications

Dr. James R. Wang is with the Microwave Sensors and Data Communication Branch, Laboratory for Hydrospheric Processes. His research interest is in the application of passive and active microwave techniques for remote sensing of geophysical parameters such as soil moisture, vegetation, water vapor, and precipitation.

USE OF MULTISPECTRAL SATELLITE DATA FOR DETERMINATION OF LAND SURFACE WATER BALANCE

The global hydrologic cycle is perhaps the most important of all the biogeochemical cycles. The intimate relationship between soil, vegetation, and climate has been long recognized. The diversity of natural vegetation is mainly a consequence of climatic factors of heat and moisture. The world water balance, particularly the water balance of land masses, has been studied for nearly a century. Significant work by a dedicated group of Soviet scientists has resulted in the following estimates of the land surface water balance: precipitation 800 mm; evaporation 485 mm; and runoff 315 mm. However, these are only estimates; there are many uncertainties with respect to both data and modeling of the processes which must be resolved to account for regional and interannual variations. Modeling and satellite data analyses, currently underway, recognize the intimate link between the water, heat, and the carbon balance of the land surface. The goal is to quantify regional and interannual variations of evaporation and soil moisture of different continents. The initial emphasis of these studies is on arid regions of Africa and Australia for the 11-year period from 1979 to 1989.

The plant communities of arid lands have adapted to shortages of water and its high year-to-year variability. These communities are stable and resilient without human intervention. The arid lands of Africa and Australia, like other arid lands of the world, have been undergoing transition due to anthropogenic pressures. Additionally, there is evidence that rainfall over sub-Saharan Africa is not in a steady-state condition (i.e., the long-term mean is not very well defined). Thus, the estimates of evaporation over the arid lands of Africa and Australia, based upon long-term mean rainfall, may not be appropriate for the period 1979 to 1989 because of changes in land surface and rainfall. Multispectral satellite data are being compiled to quantify land surface changes. For any quantitative analysis of land surface change, these satellite data must be corrected for atmospheric effects, for changes of sensor performance and characteristics, and for time of observations, particularly for observations by the Advanced Very High Resolution Radiometer (AVHRR) on board the NOAA satellites. These multispectral data are being supplemented by surface synoptic observations, determination of soil hydraulic properties, surface topography, and plant rooting characteristics. Much remains to be done to validate these data. In addition, runoff data for different rivers must be collected.

Evaporation is one of the most difficult processes to estimate. It directly links the land surface water balance to the heat balance, and to biosphere functioning. Transpiration, the major component of total evaporation, is a consequence of a plant's need for atmospheric carbon dioxide for maintenance and growth. Transpiration occurs as plants open their leaf stomata to take in atmospheric carbon dioxide, and water vapor within the leaf diffuses out into the atmosphere. A rather bold theory has recently been proposed which states that plants control their stomata through biochemical processes so that the carbon gained is optimized in relation to transpiration water loss. To examine this theory, visible reflectance can be used to provide information about fractional green vegetation or chlorophyll content of leaves. The near-infrared reflectance might be useful for analysis of a leaf's internal structure, and the clustering of leaves and woody components. Observations in the microwave region can provide information about vegetation water content. Synergism between these observations is being examined to determine their potential for quantifying changes of fractional vegetation cover and turgidity. An example of the synergism being studied is illustrated in the figure. It shows the observed relation between visible reflectance from AVHRR and the difference of vertically and horizontally polarized brightness temperature (polarization difference) at the 37-GHz frequency of the Scanning Multichannel Microwave Radiometer (SMMR) on board the Nimbus-7 satellite. The data presented are for March and September of 1982. The observed high correlation between these two satellite observations could stem from the correlation of the basic mechanisms governing these observations,

namely absorption of visible radiation by chlorophyll, and microwave radiation by the water content of vegetation. Infrared temperature observations can be a useful indicator of the surface heat balance, and thus can be used to corroborate changes of vegetation cover.

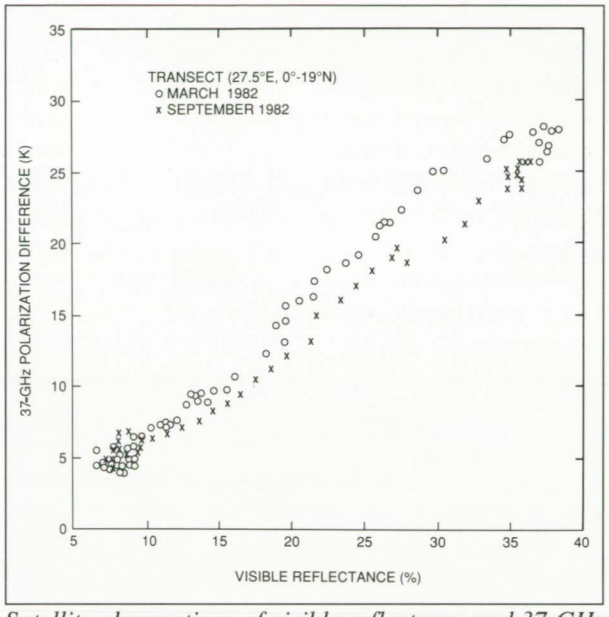

Satellite observations of visible reflectance and 37-GHz polarization difference along a transect in northern Africa, going from desert to rain forest.

Microwave observations at low frequencies from the Nimbus-7 satellite are being studied for estimating surface soil moisture. Other satellite data are being compiled for the surface air temperature, vapor pressure, radiation balance, and estimates of rainfall.

Contact: Bhaskar Choudhury (Code 974)
(301) 286-5155

Sponsor: Office of Space Science and Applications

Dr. Bhaskar Choudhury works on radiative transfer, heat and water balance modeling, and analysis of multispectral observations acquired from ground, aircraft and satellite platforms. He has worked at GSFC for 10 years. He received a PhD in Physics from the American University.

Oceans

GLOBAL OCEAN CIRCULATION MODELING

A major thrust of the NASA Mission to Planet Earth and of Earth science in general is the study of long-term climate change, its variability, and man's impact on it. To develop a fuller understanding of these changes, it is necessary to identify the coupled modes of response of the ocean-atmosphere-land systems and to identify their dominant patterns of variability, their relevant timescales, and the stability of these patterns with respect to perturbations. The coupled problem is of particular interest because over the past few years we have identified new modes that can only exist in a coupled system, but that have dominating effects on the climate. Such an example is the El Niño/ Southern Oscillation (ENSO) phenomenon, which manifests itself as variability in tropical sea-surface temperature with a timescale of 3 to 5 years, but has global climatic effects. While ENSO has been identified, it is a rather special case in which only the tropical upper ocean plays a role, and for which rather simple ocean models may suffice to capture the important physics. In general, the coupling between ocean and atmosphere is not as simple, and involves deeper water and connections between low and mid- or high latitudes, and can span ocean basins.

It is our objective over the next few years to undertake coupled ocean-atmosphere-land modeling studies of long-term climate variability. A pre-requisite is a high-resolution global ocean circulation model which can be run for the extended integrations needed to study interannual and interdecadal variability. Such a model has been developed and is being used for ocean circulation studies in the Oceans and Ice Branch at GSFC (see the figure).

The model utilizes a hybrid-layered vertical structure and a regular horizontal finite difference grid. Although the resolution of the model may be set for

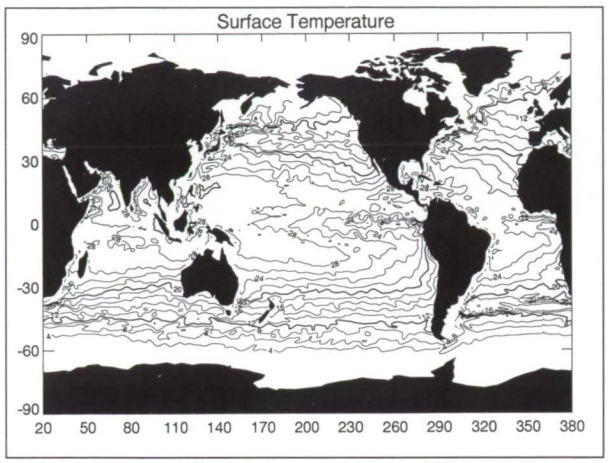

Sea surface temperature as simulated for July 1 of the 19th year of integration using climatological winds and atmospheric conditions.

each experiment, the most often used configuration has been a 7-layer version, with 1.25° resolution in the zonal direction and 2/3° resolution in the meridional. This resolution was chosen for its ability to capture the important physics of the tropical region, while providing a relatively fast computational speed. The global model requires ~1 hour to simulate 1 year on a single-processor Cray YMP.

The vertical layer structure is divided into three regions: the surface mixed layer, a deep region where the layers are isopycnal (having constant potential density) and a matching region which interpolates between the base of the mixed layer and the shallowest isopycnal layer.

The surface mixed layer has important effects, altering the way in which heat and momentum enter the ocean and how their effects are communicated with depth. Under conditions of strong heating and weak winds, the mixed layer becomes shallow, and the surface temperature rises rapidly, while under conditions of strong cooling and/or strong winds, the mixed layer deepens, providing a slow response in temperature and currents. In one view, it can be argued that the mixed layer behavior is the most important part of the ocean response in mid-latitudes. This is because the changes in mixed layer depth can be so great, while the ocean dynamics have such slow timescales that, for short-term (annual scales) changes, the currents can be assumed to be nearly steady. While this may or may not be the case, it is certainly true that the mixed layer deepening and shallowing is an important part of the ocean response to atmospheric forcing.

The surface layer is determined by using bulk turbulent energy budgets and by balancing the generation of turbulence by the wind stress against changes in mean potential and kinetic energy caused by deepening of the mixed layer. Provision is made to include the effects of penetrating solar radiation, which introduces heating at depth and provides a source of potential energy for mixing. This factor can be dominant in low latitudes, where solar radiation is strong and winds are weak.

In the deep ocean, the currents are removed from the stirring effects of the surface winds, and the flow is much more conservative. The relatively strong influence of stratification means that water tends to remain along surfaces of constant potential density. While lateral mixing along these surfaces can occur without doing work on the water parcel, mixing across isopycnal surfaces does require work, and is, therefore, greatly suppressed. A numerical scheme that treats the problem along these surfaces better represents the absence of cross-isopycnal mixing, allowing for better simulation of thermocline structure and the transport of heat and vorticity by the subsurface currents. In the common ocean circulation models used today, a depth coordinate is used in the vertical. The difficulty with depth coordinate models is that diffusivity is artificially introduced by numerical techniques for solving the finite difference equations, and when the coordinate system is not along the isopycnal surface, too much mixing occurs.

Our model has been run with climatological atmospheric conditions and integrated for 25 years, with a number of different parameterizations for the surface flux and other physical parameters. A key feature of the model is its modularity, enabling it to run with a wide variety of external conditions ranging from annual mean boundary conditions to a coupled mode with an atmospheric general

circulation model. ANSI Fortran source codes, on-line manual pages, and a user's guide are available for outside users who desire to use the model in other contexts.

Contact: Paul Schopf (Code 971)
(301) 286-7428

Sponsor: Office of Space Science and Applications

Dr. Schopf received his ScB from Brown University, and his PhD from Princeton University's Geophysical Fluid Dynamics Program. Since 1978, he has undertaken numerical and analytical studies of the ocean circulation at GSFC's Oceans and Ice Branch, with emphasis on ocean-climate interactions.

UPDATES TO THE AIR-SEA INTERACTION RESEARCH FACILITY

The Air-Sea Interaction Facility, located at the Wallops Flight Facility, has been utilized by government and university researchers since 1975. Its unique capabilities allow control over simulated wind, waves, and currents for a variety of experimental conditions important for remote-sensing theory and applications. Recently, extensive updates to the facility have begun that will enhance present capability and add exciting new possibilities.

The first of these, now complete, was replacement of the main motor controls for wind and current generation. The new electronic controls allow for the precise control and repetition of any motor speed (and thus wind and current velocity) in either direction by a PC. Previously, both motors ran at full speed requiring some of the output to be fed back to the input to control the flow through the test facility. The new controls allow for smoother flow at low speeds, as well as fully automated experiments. Using the PC, experimental conditions can be changed so that experiments can be run 24 hours a day if needed for more rapid data collection and processing. Full PC control also allows for repetition of transient phenomena. Because of the exact timing afforded by the PC, each transient case can be ensemble-averaged over a large number of exact repetitions to provide the statistics needed to study transient processes.

The second addition to the facility is an extensive false bottom, to allow further study of a new mechanism recently observed for generating high-frequency surface roughness in the absence of wind. The false bottom will provide a large area for both current shear and higher current flows, which can trap incoming waves, while shifting them to higher and higher frequencies, all without breaking. This has important implications for remote sensing, and may facilitate measurement of bottom topography in areas of current flow, even though the active radars cannot penetrate the ocean surface.

The third modification involves the wave tank itself. Both end sections are being expanded and improved to increase the generation of smooth winds and currents without turbulence. The modification will require moving the water pump, removing the bypass plumbing and valves (which are no longer needed with the electronic controls), and re-plumbing the current flow after the larger end sections are in place.

These updates will allow the facility to maintain its uniquely equipped position for the detailed study of air-sea interaction phenomena.

Contact: Steven R. Long (Code 972)
(804) 824-1034

Sponsor: Office of Space Science and Applications

Dr. Steven Long received a BS and an MS in Physics and a PhD in Physical Oceanography from North Carolina State University. Dr. Long came to GSFC's Wallops Flight Facility in 1975 as a National Research Council Resident Research Associate. Steve began his civil service in 1977, continuing the work he helped organize. Since that time, the NASA Air-Sea Interaction Research Facility has been host to joint experiments with universities, foundations, and government agency research groups from the U.S. and several foreign countries, as well as to in-house experiments.

ASYMMETRY OF THE TRENDS IN THE ARCTIC AND ANTARCTIC SEA-ICE COVERS FROM 1978 TO 1987

Sea ice is an important part of the global climate system. The two key aspects of the sea-ice cover are ice extents (the total area enclosed by the ice/ocean edges) and the area of open water within them. The sea-ice cover limits the solar radiation absorbed in its hemisphere and alters the atmosphere-ocean exchanges of heat, moisture, and momentum. The area of open water within the ice pack, even when small compared with the ice extent, is critically important because the wintertime fluxes of heat and moisture through a given area of open water are 2 to 3 orders of magnitude greater than through the same area of sea ice.

The SMMR, which operated on board the Nimbus-7 satellite from October 1978 to August 1987, obtained sequential synoptic observations of the entire Arctic and Antarctic sea-ice covers through cloud cover, night and day, every 2 days. The Arctic and Antarctic ice extent and open-water variations were determined with all of the SMMR data, corrected for instrumental drift and variations with unequal solar heating, obtained over the polar ice covers. A band-limited regression (BLR) technique was used to obtain an offset and a trend in the SMMR data, which are serially correlated and, therefore, are not properly analyzable with standard linear regression. Briefly, the method entails smoothing the data with a multiband filter, and then determining the trend in the filtered data, from which the high-frequency fluctuations and seasonal cycle have been removed.

When the BLR is applied to the Arctic sea-ice extent data, a 2.1 ± 0.9 percent decline in the Arctic sea-ice extent is found for the 8.8-year span of SMMR data. The confidence level of the determination is 96.5 percent, obtained from the BLR and based on the ratio of the trend to the standard deviation equal to 2.2. Application of the BLR technique to Arctic open-water area within the ice cover yields a trend of -3.5 ± 2.0 percent, at a confidence level of 93.5 percent. This implies that the areal coverage of the Arctic by sea ice was decreasing more slowly than its ice extent. Application of the BLR technique to the Antarctic sea-ice extent and open-water area leads to statistically insignificant results, since the standard deviations of the trends are greater than the trends themselves. The results are illustrated in the first and second figures. In the first figure (sea-ice extents), the Arctic trend (solid line) is a 2.1-percent decline over the 8.8-year time interval under discussion and is significant to the 96-percent confidence level. The Antarctic trend (dashed line) is statistically insignificant. The extents are determined from the horizontally and vertically polarized radiances at wavelengths of 0.8 and 1.7 cm obtained by the SMMR on board the Nimbus-7 spacecraft. The radiances are corrected for instrumental long-term drift and variations and systematic variations over the course of an orbit.

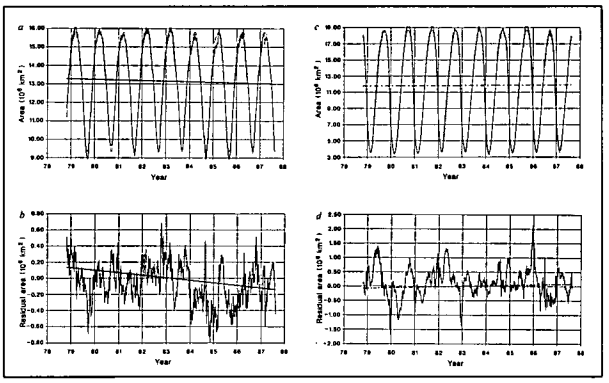

Sea-ice extents (the areas enclosed by the margin of the sea-ice covers) for the Arctic and Antarctic from October 25, 1978 to August 20, 1987 and their trends.

In the second figure (leads and polynyas), the Arctic trend (solid line) is a 3.5-percent decline over the 8.8-year time interval under discussion and is significant to the 93-percent confidence level. (Polynyas are open water within the ice margin, obtained by subtracting the sea-ice areas from the ice extents shown in the first figure.) The Antarctic trend (dashed line) is statistically insignificant.

It is interesting to note that a recent simulation at the Geophysics and Fluid Dynamics Laboratory, with a coupled ocean/atmosphere model, of the atmospheric response to a doubling of the global CO_2 level over

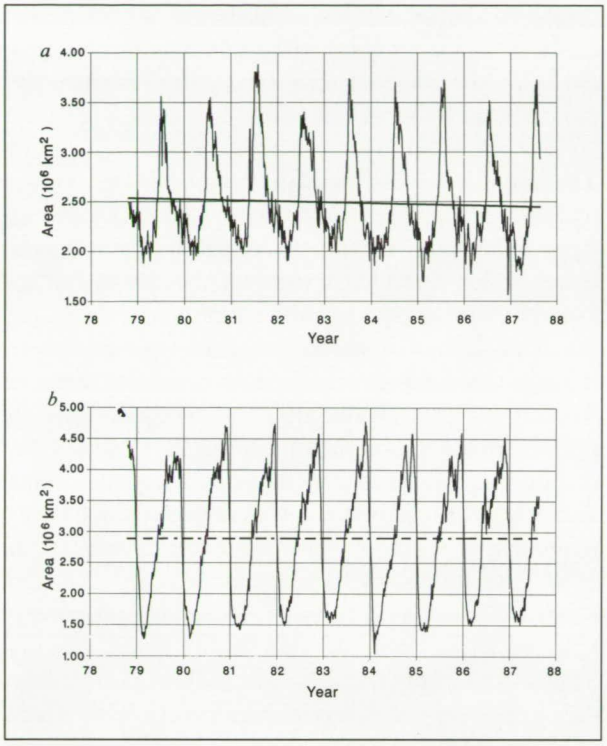

Leads and polynyas for the Arctic and Antarctic from October 25, 1978 to August 20, 1987 and their trends.

a century shows an interhemispheric asymmetry in the warming of surface air temperatures, with the Antarctic increasing very slowly and the Arctic, more quickly. A number of studies have suggested that changes in the global average air temperature might be detectable by observing changes in the extents of the polar sea-ice covers. The trend obtained by BLR analysis of the Arctic sea-ice extent may be an early signal of climate change. However, the near-decade of SMMR observations is not long enough to establish clearly a climate trend.

Contact: Per Gloersen (Code 971)
(301) 286-6362

Sponsor: Office of Space Science and Applications

Dr. Per Gloersen is a Physicist engaged in climate-related research based on analysis of data obtained from instruments on board Earth-orbiting spacecraft. Much of this research has been based on the Nimbus-7 SMMR, for which he is the Sensor Scientist and Experiment Team Leader. In collaboration with five of his colleagues, he is presently producing an atlas of the SMMR polar observations. Dr. Gloersen holds a PhD in Physics from The Johns Hopkins University and has 21 years of experience at GSFC.

SURFACE WAVE DYNAMICS EXPERIMENT

To understand both the generation of ocean waves due to winds and the fate of the waves as they dissipate, has long been a goal of oceanographers. The Surface Wave Dynamics Experiment (SWADE) was designed to provide observational data towards attaining this goal. The objectives of the experiment were to determine the evolution of the wave directional spectrum under a variety of conditions, to determine the effect of waves on air/sea fluxes of momentum, heat, and mass, and to determine wave-breaking characteristics as they depend upon sea-state, wind, and boundary layer stability. The experiment was jointly sponsored by the Office of Naval Research and the National Aeronautics and Space Administration with participation by the Army Corps of Engineers and the National Oceanic and Atmospheric Administration (NOAA). An international group of scientists was involved in planning and executing the field program and is continuing that involvement as the data are analyzed and interpreted. The Principal Investigator for the experiment was Dr. Mark Donelan of the Canada Centre for Inland Waters. He headed the SWADE steering committee. This committee consisted of Dr. Norden Huang, Dr. Erik Mollo-Christensen, and Dr. David Oberholtzer of GSFC, Dr. Owen Phillips of The Johns Hopkins University, and Dr. William Plant of the Woods Hole Oceanographic Institution.

The observational area extended for 100 miles along the Atlantic coast between Cape Hatteras, NC, and northward of the Wallops Flight Facility at Wallops Island, VA. The offshore width of the area was also ~100 miles. The site was originally instrumented

with three, 3-m discus buoys, a large spar buoy, four meteorological buoys, and several other buoys providing in-situ meteorological and wave measurements. The experiment was scheduled for the 6 months between October 1990 and March 1991. This is the period when it is most likely that storms, including cold air outbreaks and cyclogenesis, will occur in this area with the generation of interesting waves.

Several intensive data collection periods were designated, each lasting for 2 weeks. During these times, aircraft were available to provide synoptic data coverage of the SWADE area using oceanographic remote-sensing instruments. The most interesting intensive period was the third, which was during the last week in February and the first week in March. In that period, five aircraft flew out of the airfield at Wallops, and two others were staged from Navy fields at Patuxent, MD, and one near Philadelphia, PA. More than 50 data collection missions were flown.

The ocean is a harsh environment for instruments and platforms; this proved to be so for this experiment. The first casualty was the highly instrumented spar buoy. Moored at the beginning of October, it stopped its data transmission through the NOAA satellites after a series of powerful storms moved through the area toward the end of October. After a fruitless aircraft search, the buoy was located by ship through the buoy's acoustical transponder answering signals from the ship. The buoy had moved out to sea into deeper water where its anchor pulled it under. It is still on the ocean bottom, waiting to be salvaged. Several of the small meteorological buoys did not stay at their mooring locations but moved out of the SWADE area as the experiment progressed.

The loss of the spar buoy was a severe blow to the project since this buoy held many sensors for measuring atmospheric, radiative, and oceanographic parameters needed for understanding the air-sea interactions that were occurring. Two steps were taken to acquire these data, since these measurements were required. The National Data Buoy Center (NDBC) furnished another 3-m discus buoy, moored where the spar had been, to collect wind and wave data. A special ship was hurriedly outfitted with many of the same types of instruments that were on the spar. It collected data during the last intensive period along with the aircraft.

The aircraft taking part in the SWADE project included a Convair 980 from the Canada Centre for Remote Sensing; a Synthetic Aperture Radar was on board which provided images of the ocean surface. Wave fields can be measured from these images, and the Gulf Stream can be delineated as it courses through this area. A French team from the Centre de Recherches en Physique de l'Environment Terrestre et Planetaire brought over a Merlin IV in which was mounted a C-band Ocean Wave Spectrometer called RESSAC. This provided a look at ocean wave fields, particularly the larger waves. The third guest aircraft at Wallops for the intensive period was a C-130 from Ames Research Center. Several microwave scatterometers were mounted in this plane. The Jet Propulsion Laboratory's NuScat and the C-Scat from the University of Massachusetts both flew many missions during those 2 weeks. These instruments give winds at the ocean surface. Also flying out of Wallops were two of the aircraft permanently based there. The new Surface Contour Radar (SCR) was in the P-3; this instrument measures directional wave fields in the ocean. The T-39 Sabreliner flew the Radar Ocean Wave Spectrometer (ROWS); this instrument gives the ocean wave field as the RESSAC, but uses a different microwave frequency. Two P-3s from the Navy provided radar imagery. One P-3 contained a side-looking, real aperture radar; the other had synthetic aperture radars that gave registered imagery at three microwave frequencies.

Despite the problems and challenges encountered in this experiment, most of which were solved or overcome, a large dataset has been accumulated which is now undergoing analysis and interpretation.

Not only will this experiment lead to a better understanding of the interactions between the air and ocean, but through ongoing intercomparisons of the various remotely sensed data along with the in-situ data, the scientists operating the aircraft instruments will be able to improve the algorithms used to interpret the information that they collect.

Contact: J. David Oberholtzer (Code 972)
(804) 824-1241

Norden Huang (Code 971)
(301) 286-8979

Erik Mollo-Christensen (Code 900)
(301) 286-3549

Sponsor: Office of Space Science and Applications

Dr. J. David Oberholtzer holds a PhD in Physics from Florida State University, Tallahassee. He began work for NASA in 1966 at the Electronics Research Center, Cambridge, MA. In 1970 he joined what is now the Wallops Flight Facility of GSFC. Dr. Oberholtzer is in the Observational Science Branch where his interests are primarily in instrumentation and data handling for remote-sensing applications.

Dr. Norden Huang holds a PhD in Oceanography from The Johns Hopkins University, Baltimore, MD. Dr. Huang studies water waves and air-sea interactions in the ocean and in a wave tank at Wallops Flight Facility. He is a member of the Oceans and Ice Branch at GSFC where he received the NASA Exceptional Service Award in 1985.

Dr. Erik Mollo-Christensen holds a DSc in Aeronautics from the Massachusetts Institute of Technology, Cambridge. Dr. Mollo-Christensen was a professor at MIT until 1984, when he came to GSFC. His scientific interests are in geophysical fluid mechanics and turbulence. He retired from GSFC in 1991.

AIRBORNE EXPERIMENT AIDS IN ELECTROMAGNETIC BIAS DETERMINATION FOR TOPEX/POSEIDON

A main goal of the satellite radar altimeters in the Ocean Topography Experiment (TOPEX/Poseidon), scheduled for launch in 1992, is the measurement of mean sea level to an accuracy of a few centimeters. Because the troughs of ocean waves are generally better reflectors than the crests, the centroid of the return pulse is shifted away from mean sea level toward the troughs to produce an electromagnetic (EM) bias in the range measurement. The magnitude of the bias is generally quoted as a percent of the significant wave height (SWH). In general, EM bias varies with radar wavelength.

A cooperative experiment was developed between GSFC and the University of Massachusetts to provide the first airborne open-ocean measurements at the 13.6- and 5.3-GHz operating frequencies of the NASA altimeter on the TOPEX/Poseidon satellite. The GSFC P-3 research aircraft was equipped with the GSFC Surface Contour Radar operating at 36 GHz, the Airborne Oceanographic Lidar operating in the UV at 337.1 nm, and a nadir-looking scatterometer provided by the University of Massachusetts that interleaved transmissions at the TOPEX/Poseidon operating frequencies. The dots in the figure show the mean values of EM bias observed on each day of the experiment for the three radar frequencies used in the study. The large circles show the overall averages of EM bias for the experiment with a least-squares-fit solid line. The dashed straight line and the squares indicate the averages of historic EM bias data which concentrated on high winds and sea states. The radar frequency dependence of EM bias indicated by the experiment data was:

$$\text{EM bias (\% SWH)} = (3.0 - 0.0617F) \cdot (1 \pm 0.5)$$

where: F is the radar frequency in GHz.

The dashed line is drawn through the squares that indicate the averages of historic EM bias data taken by the Naval Research Laboratory at 10 GHz and by GSFC at 36 GHz; they are consistent with the recent data. The slopes of the dashed and solid lines are approximately the same. The historic data are biased high relative to the dots in the figure because of the tendency for experimenters to seek high wind and sea states in planning flights. The dots from the recent experiment represent both high and low wind speeds, and they show a strong increase at all radar frequencies with increasing wind speed. Analysis indicates that parameterizing EM bias using wind

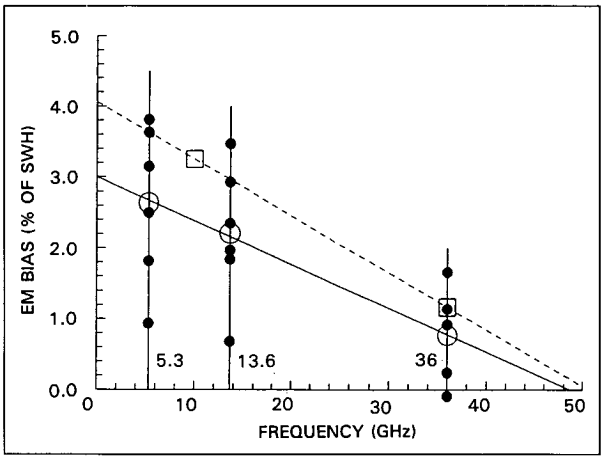

Mean values of EM bias (small filled circles) for each observation day for three radar frequencies.

speed, which can be determined from the altimeter returned signal strength, will permit the residual uncertainty to be reduced below 1 percent of SWH and allow the NASA altimeter to meet its specification.

Contact: Edward J. Walsh (Code 972)
(303) 497-6357

Sponsor: Office of Space Science and Applications

Dr. Edward J. Walsh has been with NASA since receiving his PhD from Northeastern University in 1967. He received the NASA Outstanding Scientific Achievement Award in 1975 and has served at GSFC since 1981.

Hydrology

TROPICAL RAINFALL MEASURING MISSION WILL IMPROVE GLOBAL CHANGE ASSESSMENT

Water in all three phases is the dominant active constituent of the atmosphere. It modulates both incoming and outgoing radiation, and affects global heat fluxes through condensation and evaporation. In addition, the latent heat released by tropical precipitation processes provides three-fourths of the energy the atmosphere receives. Thus, precipitation plays a key role in maintaining the wind systems of the globe and in determining their variability in space and time. The only means of acquiring spatially comprehensive precipitation data on a global scale is from satellites. This is especially true for the Southern Hemisphere, where the fraction of ocean is much larger than in the Northern Hemisphere, and where there are fewer industrially developed countries to undertake sophisticated observational programs.

The Tropical Rainfall Measuring Mission (TRMM) satellite is planned as a joint project between the U.S. and Japan to measure precipitation between latitudes 35°N and 35°S. The orbit elevation will be 350 km to ensure good resolution and an orbit inclination of 35° has been chosen to document the diurnal and semidiurnal rain variability, which are known to be significant. The rainfall package is to consist of a precipitation radar (PR) being built by Japan, a multichannel passive microwave radiometer called the TRMM Microwave Imager (TMI), and the Visible Infrared Scanner (VIRS) being built in the U.S.

The PR will be the first of its kind to fly in space. The TMI will be able to improve rain remote sensing compared to its predecessor, the Special Sensor Microwave/Imager (SSM/I), by adding a channel at 10 GHz, where the sensed brightness temperatures are nearly linearly related to the rain rate, thus obviating some of the pervasive beam-filling problems. The VIRS will have five channels. These include both 10.7 and 12 μm in the infrared, permitting the split window approach to be used in obtaining the surface temperature (ocean or land) and the moisture content of the low-level air. In the figure, the solar panels are viewed sideways so their large areas cannot be seen. The orange antenna to the left of the TMI sends the TRMM data to the TDRSS satellite to be relayed to ground receivers.

The TRMM Science Team was selected in response to a NASA Research Announcement in July 1990 that received more than 100 proposals in response.

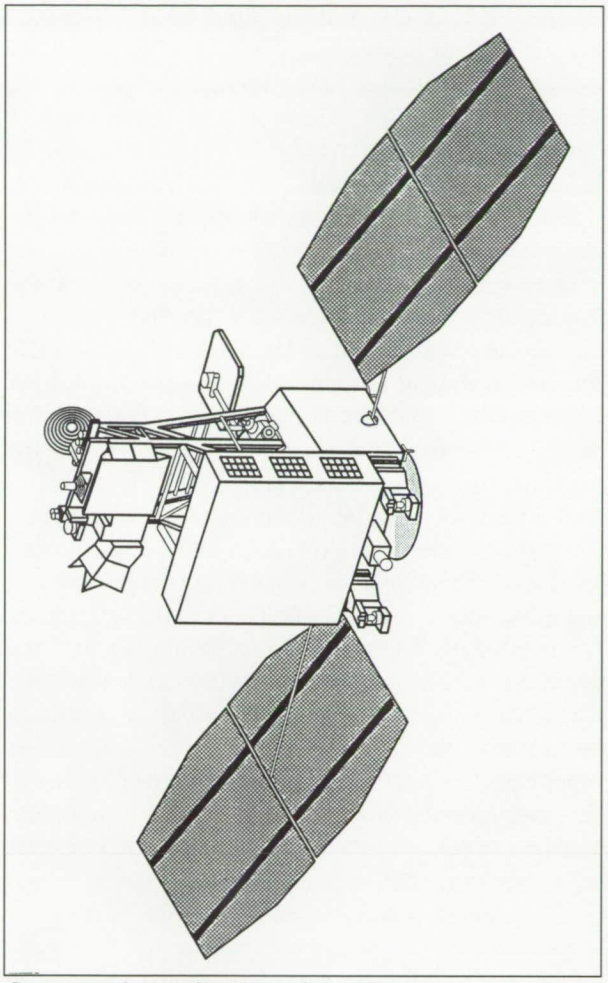

Conceptual visualization of the TRMM spacecraft and planned instruments.

The Science Team consists of 32 members and 4 associate members drawn from 5 nations. There are 13 university members and 3 from private industry. The first Science Team Meeting was held in College Park, MD on May 15-17, 1991. One outcome was a major planning document on instrument interplay, algorithms, and the data system. The data system will operate in collaboration with EOSDIS, which will be used for its first Mission to Planet Earth collection and archiving of actual space- and ground-verification data with TRMM.

An important recent finding by the TRMM Science Team is that the rain radar is essential to accurate rain data retrieval in many of the world's continental monsoon areas. A test comparison between ground radars and rain estimates based on currently orbiting satellite data was conducted over Japan by the Global Climate Research Program in the summer of 1989. The SSM/I, aboard a military satellite, greatly underestimated the rainfall over the mountainous land areas because rain clouds were produced there that topped at temperatures warmer than freezing and, therefore, failed to contain ice particles. Rain estimates over land based on passive microwave instrument data are empirically based on the scattering of radiation by ice and, therefore, fail when warm rain falls from clouds without ice. It is noteworthy that TRMM is the only satellite with rain radar planned for the EOS era. It is, therefore, extremely important that its results be available to calibrate those EOS instruments intended to document the hydrological cycle.

It has recently been decided that the U.S. will add a Clouds and the Earth's Radiant Energy System (CERES) instrument and a Lightning Imaging Sensor (LIS) to TRMM that will greatly enhance its contribution to global change assessment. This enhancement stems from the ability of CERES to measure the upwelling radiation from cloud systems. As a result, TRMM will obtain radiative cloud properties as well as their precipitation characteristics in the same location at the same time. Thus, not only will TRMM be able to provide the best tropical global rainfall dataset ever, but it will also help to resolve the controversy about whether, and under what conditions, clouds act to warm or to cool the planet, and how precipitating clouds modulate radiation differently from clouds that do not precipitate. The addition of LIS will provide additional understanding of the relationship between cloud electrification and rain processes and help to explain why these differ over land masses as compared to over oceans.

Congress voted support for TRMM in the spring of 1991 allowing it to advance to the Execution Phase. A team has been assembled at GSFC to build the spacecraft in-house and to establish a competitive industry procurement for the VIRS and TMI. The TRMM satellite will be launched by a Japanese HII rocket in August 1997.

Contact: Joanne Simpson (Code 900)
(301) 286-8569

Sponsor: Office of Space Science and Applications

Dr. Joanne Simpson came to GSFC in 1979 with a BS, MS, and PhD in Meteorology from the University of Chicago. She is currently the TRMM Project Scientist at GSFC.

CLIMATE SENSITIVITY TO TROPICAL RAINFALL VARIATION

The Earth's radiation budget, obtained from satellite observations, indicates that the atmosphere-ocean-land system radiates more energy to space than it receives from the Sun in the tropical domain, while at the high latitudes the situation is reversed. A fundamental problem in climate dynamics is to understand the processes by which heat is transported poleward by atmospheric and oceanic motions. Dynamic heat transport plays a major role in maintaining the present-day equator-to-pole difference in surface temperature of ~40°C, much smaller than what it would be if the system were in local thermal equilibrium. Paleoclimatic records suggest that 100 million years ago the equator-to-pole surface temperature may have been 2 to 3 times smaller, accompanied by a warming of a few percent in the global-mean surface temperature. The relative sensitivity between these two quantities indicates that dynamic redistribution of heat plays a key role in determining the globally averaged climate change.

A recent experiment with the GSFC Laboratory for Atmospheres (GLA) General Circulation Model (GCM) suggests that dynamic heating of the polar region is sensitive to the latitudinal position and concentration of convective heating in the tropics on time scales longer than a few weeks. In a 47-day forecast experiment, a significantly altered latitudinal distribution of ozone resulted in a shift of 5° latitude in the zonally averaged precipitation maximum (thus, the maximum cumulus heating) away from the Equator, which was accompanied by a substantial warming of the winter polar region. The result for the northern summer case is summarized in the accompanying figure. The top panel shows the July monthly-mean zonally averaged cumulus heating in °C/day in the control run. The vertical coordinate, sigma, is the ratio of atmospheric pressure to the surface pressure; its approximate relation to altitude is shown on the right. The middle panel is the July-mean difference in cumulus heating in °C/day for the case with modified ozone minus the control showing a shift of the maximum heating toward the summer pole. The bottom panel shows the warming in °C/day over the winter high latitudes for the modified ozone case minus the control. Diagnostics showed that dynamic heating is responsible for nearly all of the warming between 60°S and 90°S. Similar results were obtained for a northern winter case.

An interesting feature of these results is that the strongest warming occurs in the winter hemisphere when the maximum cumulus heating is displaced further into the summer hemisphere. This lends support to a recently proposed climate hypothesis that the intensity of the tropical Hadley circulation plays an important role in regulating wave transport in the extratropical winter hemisphere. A recent GLA study showed that concentration of tropical latent heating via redistribution can greatly increase the intensity of the Hadley circulation and enhance the baroclinicity in the extratropics (the energy source for wave amplification) in the absence of waves. Further tests are underway to determine the process by which extratropical wave transport is influenced by the tropical circulation and the extent to which variability in tropical heating distribution may affect the global climate.

The findings of this study have important implications for global data assimilation and climate simulation. It suggests that variability in tropical heating patterns may contribute significantly to global climate variability. The success of global modeling may depend critically upon our ability to simulate tropical rainfall distributions. It under-scores the importance of obtaining high-quality data of tropical rainfall with improved spatial and temporal resolutions. It also suggests that the winter polar

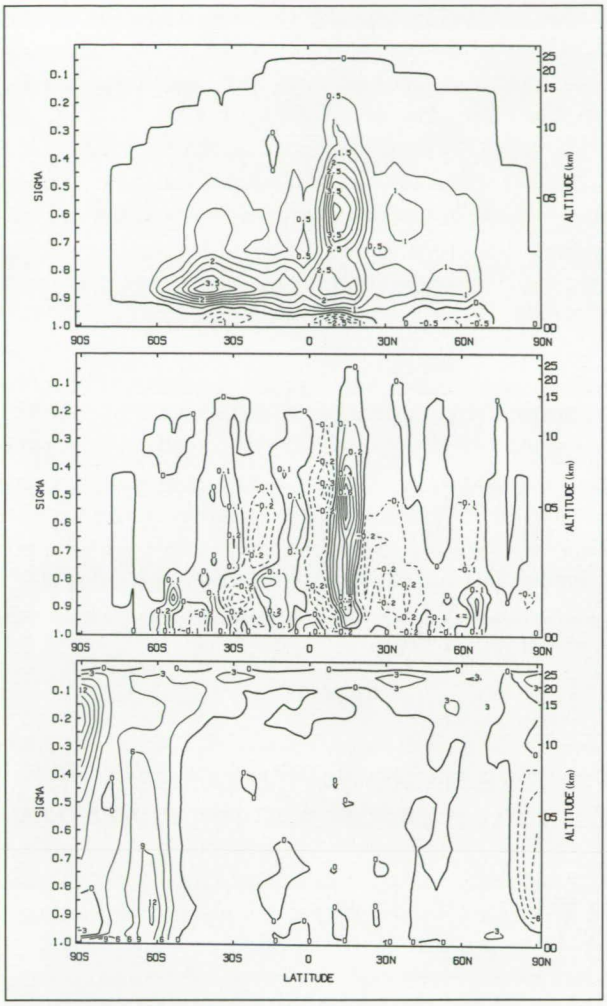

The results of a 47-day GCM forecast experiment for the northern summer case.

cold bias common in GCMs may be reduced by improving the simulation of convective heating patterns in the tropics.

Contact: Arthur Y. Hou (Code 911)
(301) 286-3594

Sponsor: Office of Space Science and Applications

Dr. Arthur Y. Hou holds a BS from the Massachusetts Institute of Technology and a PhD in Applied Physics from Harvard University. Dr. Hou is currently an Atmospheric Scientist in the Global Modeling and Simulation Branch, investigating the role of atmospheric processes in climate dynamics. His interests include the theory and modeling of the tropical circulation, tropical-extratropical, interaction, assimilation of tropical rainfall data, climate sensitivity to CO_2 perturbation, and the atmospheric superrotation on Venus.

HEATING AND WATER BUDGETS IN THE CONVECTIVE AND STRATIFORM REGIONS OF TROPICAL AND MID-LATITUDE SQUALL LINES—THEIR SENSITIVITY TO LONGWAVE RADIATION

It has been estimated that widespread stratiform rain accounts for 30 to 50 percent of the total rainfall from a squall line. Distinguishing the roles of stratiform and convective regions of tropical and mid-latitude squall lines will lead to a greater understanding of heat and water budgets in these storms. It can also provide the basis for elucidating important mechanisms for large-scale vertical redistribution of momentum, trace gases, and sensible and latent heat, as a squall line can produce significant precipitation. Furthermore, separation of returns from convective and stratiform clouds is required for successful surface rain retrieval from remote sensors.

The heating and water budgets in the convective and stratiform regions for an oceanic (tropical) and a mid-latitude squall line have been studied by using the Goddard Cumulus Ensemble (GCE) model. The GCE model results show that longwave radiative cooling can enhance the total surface precipitation ~14 to 31 percent over a 16-hour period between these two cases. The model results also indicate that radiative cooling had the biggest effect for the tropical case which has a higher percentage of stratiform rainfall and a higher moisture content. The cooling of the cloud top and warming of the cloud base by the longwave radiation can destabilize the stratiform cloud layer. Also, different cooling in cloudy and clear regions can induce weak, low convergence into the cloudy region and can enhance cloud activity as a whole.

In the convective region, significant heating was caused by latent heat released by condensation and deposition. On the other hand, the condensation/deposition was almost balanced by evaporation/sublimation in the stratiform and the nonraining regions. The total amount of melted ice, as well as freezing-water hydrometeors, is comparable to the amount of evaporated rain. The contribution of freezing/melting processes to the heating budget is small, because the latent heat of fusion is an order of magnitude smaller than the latent heat of evaporation. Longwave radiative transfer processes change individual components quantitatively in the heating budgets; however, they do not change the relative importance of each component in the heating budgets.

This study also suggests that there are many common features in the heating profiles among these two squall lines even though these systems occurred in different geographic locations. For example, convective heating is at a maximum in the lower and middle troposphere, whereas stratiform (anvil) heating is maximized in the upper troposphere. Cooling is taking place in the stratiform region beneath the melting layer. However, a moist environment for a tropical case caused much weaker cooling at low levels in the stratiform region than in the mid-latitude cases.

The horizontal transfer of the hydrometeors from the convective to the stratiform regions occurs mostly in the middle troposphere for the tropical case. By contrast, two-thirds of the horizontal transfer of hydrometeors takes place in the upper troposphere for the mid-latitude case. The contribution of stratiform rain from the convective region can be approximated by a ratio; the ratio associated with the mid-latitude squall case is 1.74. This implies a very important role for the convective region in the generation of stratiform rainfall. By contrast, the tropical case has more stratiform rainfall; the ratio is only 0.56. Both cases also show less horizontal transport of hydrometeors from the convective region into the stratiform region during their mature stages.

Longwave radiative transfer processes can increase net condensation at upper layers in the convective, stratiform, and nonraining regions. These processes result in a decrease of the ratio when longwave radiative transfer processes are included. This implies that the longwave radiative cooling is responsible for significant generation of hydrometeors (through condensation/deposition) in the upper troposphere in the stratiform region which then fall to form stratiform rain.

Contact: Wei-Kuo Tao (Code 912)
(301) 286-4035

Sponsor: Office of Space Science and Applications

Dr. Wei-Kuo Tao studies numerical modeling of clouds and precipitation processes to improve our understanding of their relationship to weather and climate. Dr. Tao has 9 years of experience at GSFC. He earned his PhD in Atmospheric Sciences at the University of Illinois.

PASSIVE MICROWAVE MEASUREMENTS OF WATER VAPOR AND PRECIPITATION

We have used airborne microwave radiometers in the 10- to 183-GHz frequency range to make measurements of water vapor and precipitation. The measurements were conducted on a NASA DC-8 aircraft, using the Advanced Microwave Moisture Sounder (AMMS) near 90 and 183 GHz, the Electronically Scanned Microwave Radiometer (ESMR) at 19.35 GHz, and the fixed-beam Airborne Multichannel Microwave Radiometer (AMMR) at 10, 18, 21, 37, and 90 GHz.

Two experiments have been performed. The first used AMMS in the Global Aerosol Backscatter Experiment (GLOBE) mission of November 1989. The second experiment was performed during September 1990 using AMMS, AMMR, and ESMR during flights over the western Pacific Ocean. This experiment was conducted in conjunction with Japanese X-band and Ka-band radars. A few flights were made over the rain bands associated with typhoon Flo near Okinawa, Japan. Remarkable

features were observed by radar over the eye and eyewalls of the typhoon. The variation of brightness temperatures from nadir-viewing radiometers and ESMR are shown in the figure.

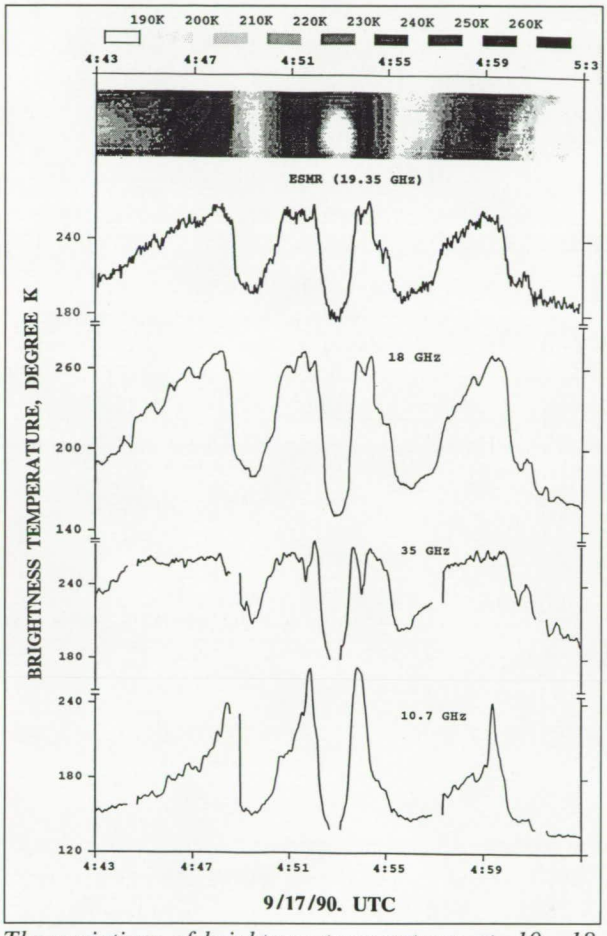

The variations of brightness temperatures at 10, 18, 19.35, and 35 GHz when NASA DC-8 aircraft flew across the strong typhoon Flo at about 11-km altitude near Okinawa, Japan on September 17.

As seen in the figure, on either side of the eye there are two rain bands that give distinct signatures in the 10- to 35-GHz frequency range. At all frequencies, rain bands are revealed by the warm brightness temperature values (T_b) due to absorption of the rain column at temperatures below freezing. In the eye of the typhoon there is no rain, and the radiometers at all frequencies respond primarily to the cold ocean surface. Also seen are differences in microwave radiometric response at 10 GHz and at frequencies ≥18 GHz. The microwave signatures of rain at high frequencies reach saturation quickly, while those at 10 GHz remain sensitive throughout the entire passage of the system. This points to the advantage of measuring rain rate at low frequencies, ~10 GHz.

Analysis of radar and radiometer data together should provide characteristic signatures of many precipitation systems. A millimeter-wave imaging radiometer airborne microwave imager, designed to operate at frequencies of 90, 150, 183.3 ± 1, 183.3 ± 3, 183.3 ± 7, and 220 GHz, is currently being built in the laboratory. This state-of-the-art instrument will provide precision measurements of water-vapor profiles, clouds and precipitation.

Contact: James R. Wang (Code 975)
(301) 286-8949

Sponsor: Office of Space Science and Applications

Dr. James R. Wang is with the Microwave Sensors and Data Communication Branch (Code 975), Laboratory for Hydrospheric Processes at GSFC. His research interest is in the application of passive and active microwave techniques for remote sensing of geophysical parameters such as soil moisture, vegetation, water vapor, and precipitation.

HYDROLOGIC CYCLE DERIVED FROM THE GODDARD LABORATORY FOR ATMOSPHERES INTERACTIVE FORECAST-RETRIEVAL-ANALYSIS SYSTEM

The hydrologic cycle is an integral component of the Earth's climate. To understand and describe those hydrologic processes that constitute the global hydrologic cycle, one must analyze satellite data together with GCM assimilation, and conventional data. The GLA has developed an interactive forecast-retrieval-analysis (IFRA) system for analyzing satellite sounding data and incorporating them into numerical weather forecasts.

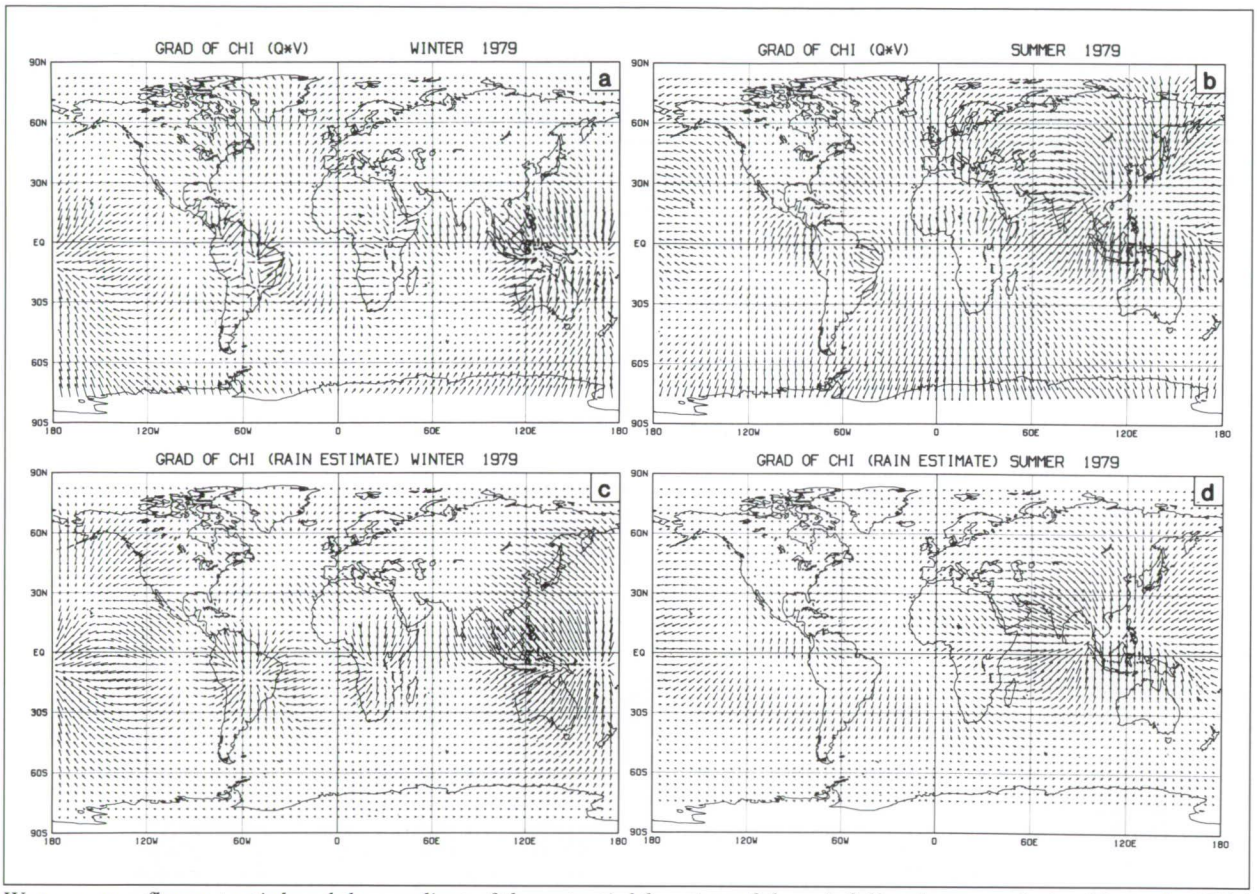

Water-vapor flux potential and the gradient of the potential function of the rainfall estimate as derived from the IFRA system analyses.

The IFRA system produces two types of datasets. The first is comprised of satellite retrievals obtained from analyses of the High Resolution Infrared Sounder 2/Microwave Sounding Unit (HIRS2/MSU) sounding data (HIRS2-based data); the second has atmospheric fields generated by assimilating conventional data together with satellite retrievals into the GLA 4th-order GCM data assimilation (GLA GCM-based data). The HIRS2-based data used for the current studies include temperature profiles, humidity profiles, surface skin temperatures, cloud-top altitudes, and effective cloud fraction. The GLA GCM-based data include wind fields at mandatory levels.

Three interrelated hydrologic parameters are derived from the above datasets: (1) vertically integrated water-vapor flux potential, which yields the divergence of water-vapor transport; (2) rainfall estimate, which is obtained using estimates of the longwave cloud radiative forcing including diurnal effects; and (3) evaporation at the sea surface, which is derived using an algorithm developed based on a bulk aerodynamic drag formulation. To derive evaporation rates, surface wind data from the comprehensive ocean-atmosphere dataset are used together with the IFRA data.

Results of the analysis are shown in the figure. Panels *a* and *b* show the gradient of the vertically integrated water-vapor flux potential for northern winter and summer, respectively, which reveal centers of major water-vapor content. Panels *c* and *d* show, for the same seasons, the gradient of potential function of the rainfall estimate, which reveals estimates of centers of major rainfall. For

example, the major water-vapor sources during northern winter occur over the equatorial western Pacific basin (Australian winter monsoon regions), the northern part of South America, and central part of South Africa. The major water-vapor centers for summer occur over Central America, equatorial Africa, and Indian summer monsoon areas. Those areas are also centers of heavy rainfall estimates.

Zonal and meridional transport of water vapor have been studied together with the above potential fields. The results reveal that water vapor converges toward three centers of high water content in the tropics, indicating that local Hadley circulation and the longitudinal Walker circulation perform the water-vapor transport necessary to maintain the high water-vapor content over these three preferred tropical centers. The water vapor in those regions is then transported upward by the Hadley and Walker circulations, increasing the overall moisture content of the atmosphere, and thereby enhancing total rainfall.

Several principal modes of oscillation have been identified through the use of empirical orthogonal function analysis of the 10-day mean rainfall estimates: a seasonal cycle over land associated with solar heating over land; a seasonal cycle largely over the ocean associated with sea surface temperature over the trade-wind areas; a tropical mode of low-frequency oscillations with a period of 30 to 60 days; and an extratropical mode of low-frequency oscillation. Our studies show that all of these rainfall variations are highly correlated with other hydrologic parameters such as total precipitable water and a potential field of vertically integrated water-vapor flux potential.

A qualitatively consistent atmospheric branch of the hydrological cycle has been derived based on a mix of satellite-retrieved geophysical parameters and a general circulation model with assimilated wind fields. The results described here establish a benchmark for the application of a mixed dataset (satellite retrievals and general circulation model data assimilation) produced from the interactive forecast-retrieval-analysis system for the study of the atmospheric branch of the hydrologic cycle.

Contact: Man-Li C. Wu (Code 911)
(301) 286-4087

Sponsor: Office of Space Science and Applications

Dr. Man-Li C. Wu's interests include the Earth's radiation budget, precipitation estimates from satellite data, seasonal and interannual variability of climate associated with rainfall, and remote sensing of cloud physical parameters using visible, near-visible, thermal IR, and microwave radiometries. She holds a PhD from the University of Chicago.

Global

ATLAS OF SATELLITE OBSERVATIONS RELATED TO GLOBAL CHANGE

An atlas of remote-sensing data depicting regional and global-scale observations of the Earth's atmosphere, oceans, and land surface is being prepared for publication by Cambridge University Press. The editors are Robert Gurney (Reading University, formerly of Code 974), James Foster (Code 974), and Claire Parkinson (Code 971). The atlas contains 28 chapters, most of which concentrate on an individual variable for which remote-sensing datasets are available or are becoming available from the investment in Earth-orbiting satellites. Many of these datasets provide time series of geophysical data that can be used for analysis of global change or quantitatively in numerical computer models. This is a marked advance from the early days of remote sensing when data were poorly calibrated and only used qualitatively. The book demonstrates the tremendous wealth of satellite data now available about the Earth system and the different degrees of sophistication reached by different disciplines in their use of remotely sensed data.

The intended audience for this atlas ranges from scientists in the remote-sensing field to nonscientists interested in knowledge being obtained about the Earth from satellite observations. In view of this

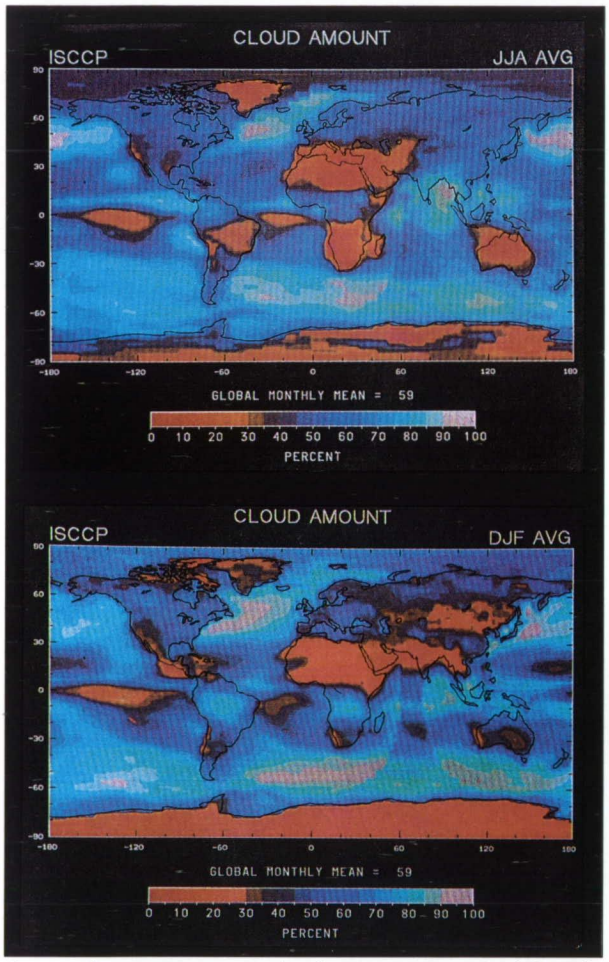

Sea surface temperature in the eastern tropical Pacific during December 1982 (top), an El Niño year, and December 1984 (bottom), a non-El Niño year.

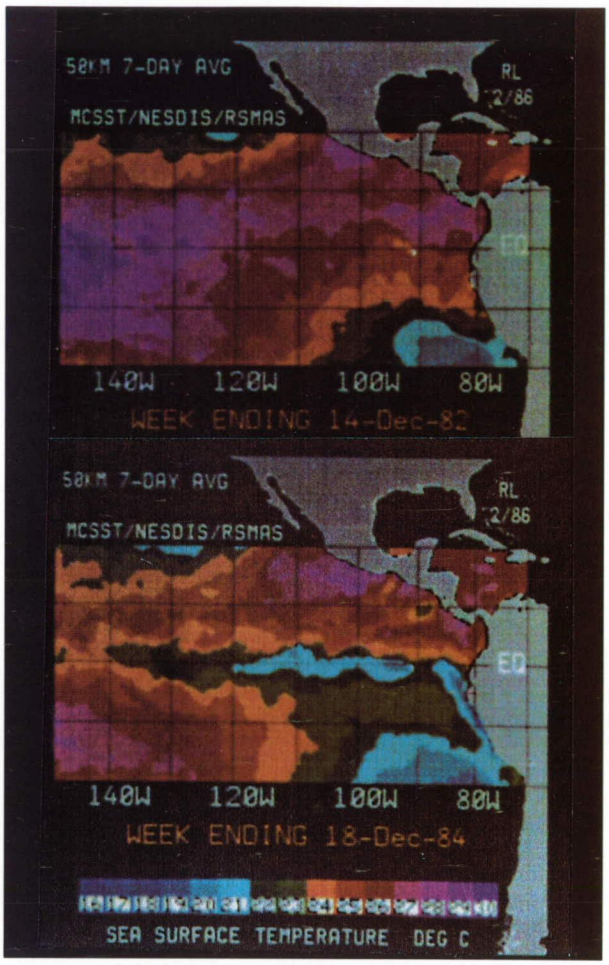

Average global cloud amount for June, July, and August (top) and December, January, and February (bottom).

varied audience, the text is written to provide informative descriptions of relevant datasets without being overly technical. It is also designed to illustrate the information contained in the datasets with examples, thereby providing a feel for seasonal and interannual variabilities. The chapters are written by individual discipline authorities and include details on how to obtain the numerical data. Since most of the datasets were derived from NASA payloads, many of the chapter authors are NASA scientists. Each laboratory of the Earth Sciences Directorate at GSFC is represented by at least one author.

The book demonstrates the applicability of different instruments for different purposes and reflects both the individual and joint value of the current suite of active and passive instruments, of imagers and sounders, and of the diverse set of wavelengths being examined, including ultraviolet, visible, infrared, and microwave. Descriptions are given not only of past and current instrumentation and data, but also of some of the expected developments over the next decade and the anticipated improvements in the respective datasets.

The individual chapters in the book illustrate the increased knowledge of the Earth system made possible through satellite technology. Strong seasonal cycles are mapped and analyzed for numerous variables, including global sea-ice

coverage, Northern Hemisphere snow cover, atmospheric temperature and water vapor, and ocean biological productivity. Lesser, but still noticeable, seasonal cycles are shown for variables such as cloud cover. In most cases, the brevity of the satellite record prevents strong conclusions about long-term trends, which are often obscured by interannual variability. However, where notable changes have occurred, these are depicted and analyzed. One such case is the stratospheric ozone depletion over the Antarctic continent, where minimum October total ozone decreased from ~280 Dobson units in 1979 to ~150 Dobson units in 1990. Even where no trends are apparent, these datasets can serve an important purpose in the study of global change, as they can be used as baselines for comparisons against future data. As the datasets increase in length, it will become more obvious which variables are undergoing significant long-term changes and for which variables apparent trends are evanescent. The book also illustrates the value of satellite measurements in recording the impacts of various individual events, such as the increased stratospheric aerosol loading resulting from the eruptions of the El Chichón volcano in 1982 and the Ruiz volcano in 1985.

Examples of the types of figures in the atlas are shown here. The first figure shows sea surface temperatures in the tropical Pacific to illustrate prominent interannual differences. The second figure shows seasonal differences in global cloud cover. The expected publication date for the volume is June 1992 with an estimated price of ~$30 per copy.

Contact: James Foster (Code 974)
(301) 286-7096

Claire Parkinson (Code 971)
(301) 286-6507

Sponsor: Office of Space Science and Applications

Mr. James Foster utilizes remote-sensing observations of snow and ice to study hydrologic and climatic processes. He has worked at GSFC for 18 years and has been a member of the Hydrological Sciences Branch since 1978. He received his BS and MA in Geography at the University of Maryland.

Dr. Claire Parkinson has been a Climatologist at GSFC for 13 years, with most of her research concentrating on polar sea ice and its climate connections. She has coauthored books on Arctic and Antarctic sea ice, the history of science, and climate modeling. Her undergraduate work was done at Wellesley College and her graduate work, at Ohio State University.

KUREX-91—A U.S.S.R./U.S. STUDY FOR GLOBAL CLIMATE PROCESSES

The growth in human populations and their impact on the environment, through both sheer numbers and technological capability to effect alterations, has made it imperative that we understand the functioning of the systems that generate the physical and biotic environment of our planet Earth. Efforts to understand these global systems involve local- to global-scale studies that must utilize large-scale, computer-based meteorological, ecosystem, and biome models that simulate the dynamics of these systems. The development, verification, and operation of these models requires collecting relevant meteorological and biological measurements of micro and local variables over grids that cover regional and global areas. The vast areal extent over which the relevant meteorological and biological interactions take place make it impossible to use only ground-based point sampling for measuring these variables. Therefore, researchers are seeking ways to use satellite remote sensing of the Earth's reflected and emitted radiation as correlated indices of the variables they would measure on the ground or within the atmosphere.

One study, the First ISLSCP Field Experiment (FIFE), was conducted in the U.S. in Kansas in 1987 and 1989 to understand how the Earth's land-surface vegetation and atmospheric boundary layer interact to affect weather and climate. The analyses have shown that the hypotheses linking energy balance components to surface biology and remote sensing are reasonable at the point level for the prairie grassland ecosystem studied, and that satellite remote

sensing can potentially provide useful estimates of the surface energy budget. Further development and testing of these hypotheses in a different part of the world is the intent of a Soviet-led study called the Kursk 1991 Experiment, or KUREX-91, involving U.S. scientists and their instruments on the Kursk Biospheric Reserve, which is located ~500 km south of Moscow in Russia.

An intensive field campaign was successfully conducted in the U.S.S.R. throughout the month of July by the 11 scientists of the U.S. delegation. The international team included 134 scientific specialists from eight countries (U.S.S.R., U.S., China, Japan, Czechoslovakia, Poland, Belgium, and Cuba), and six Soviet republics (Russia, Ukraine, Byelorussia, Lithuania, Azerbaijan, and Estonia), plus an additional 31 Moscow State University students, who provided technical support to the scientists. The experiment facilitated scientific interactions between the international participants, whose intensive ground measurements were coordinated with helicopter, aircraft, and satellite data acquisitions by both the U.S. and U.S.S.R. The lead agency in the U.S. is NASA; the lead agency in the U.S.S.R. is the U.S.S.R. Academy of Sciences. The focus of the U.S. component of the study was to examine the steppe vegetation type, wherein different levels of vegetation productivity are being evaluated for their influences on the climate-related variables and the ability to measure them from an international array of satellites, including the U.S. Landsat and AVHRR, Soviet Cosmos-1939 and Almaz, and French SPOT satellites.

In general, the U.S. component included collecting data on energy balance by two teams—one looking at latent and sensible heat fluxes at the surface, and a second looking at surface radiation balance. This was related to the work of two other teams working on biological and productivity characterization who measured biophysical characteristics, including stomatal conductance and ecosystem productivity variables. Two teams worked on soil moisture characterization, one taking direct measures of soil moisture and the other using a helicopter-mounted radar to infer soil moisture. Three teams were involved in taking measurements that will ultimately relate the land surface variables to aircraft and satellite data through the measurement of atmospheric optical properties and bidirectional surface reflectances, and through the evaluation site scaling effects.

An important aspect of the study for global experiments is the capability to intercompare datasets of the same physical and biological variables as acquired by different instruments from the international contingent of scientists. Congruity of the results will give confidence to the global scientific community that the measurements made by the different scientists at different times and places will yield reliable results. The ground, aircraft, and satellite data acquired during the July KUREX-91 study are currently being processed and analyzed. The results will not only help to develop better models of the biological, boundary layer, and climatic phenomena, but will also contribute to the design of more useful aircraft and satellite sensor systems for studying and monitoring global change events.

Contact: Donald W. Deering (Code 923)
(301) 286-9186

Sponsor: Office of Space Science and Applications

Dr. Donald W. Deering works in the Biospheric Sciences Branch and conducts research on fundamental characterizations of the bidirectional reflectance of Earth surface cover types. He has managed the Remote Sensing Science Program for NASA Headquarters, and is currently the team leader for the U.S. study in the Kursk region of Russia. He has worked at GSFC for 13 years and holds a PhD from Texas A&M University.

POSITIVE WATER-VAPOR FEEDBACK IN CLIMATE MODELS CONFIRMED BY SATELLITE DATA

Increasing amounts of anthropogenically produced greenhouse gases (in particular CO_2) are expected

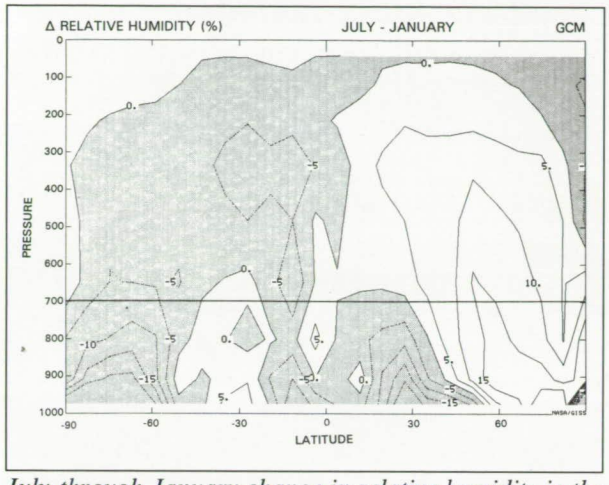

July-through-January change in relative humidity in the GISS general circulation model.

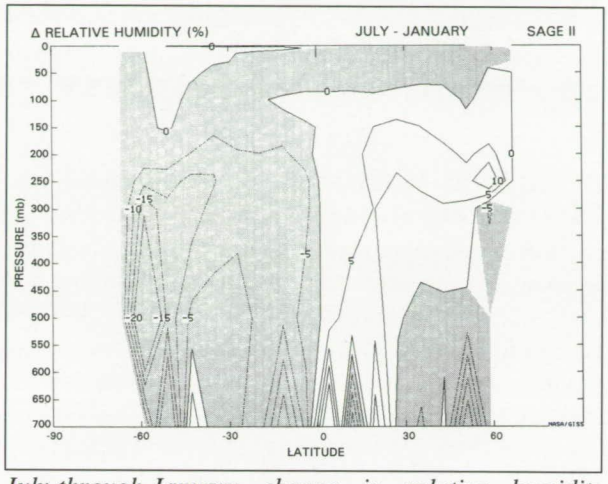

July-through-January change in relative humidity observed with the SAGE II instrument.

to warm the climate in the next century. However, the magnitude of this warming is still uncertain. The prime factor amplifying the warming, in models, is increased water vapor. As the climate warms, more moisture evaporates from the oceans; convection and other processes can then act to transport this moisture to high altitudes, where it acts as an additional greenhouse gas.

Will this feedback really occur? Some controversy has arisen about this subject, and the best way to test the hypothesis, and models, is to observe regions that are currently warm and that experience substantial convection. Examination of this issue has been retarded by limitations in the methods for retrieving water vapor above 5-km altitude. A new satellite-derived water-vapor dataset (SAGE II) has recently become available that could help solve this problem.

To assess whether modeling of this water-vapor feedback is accurate, a comparison was made between observations and model simulations of water vapor for two situations of warming and increased convection: the summer hemisphere versus the winter hemisphere, and the warmer west Pacific compared to the east Pacific.

The results are shown in the two figures. Both the model and observations show slight increases in during the respective summers (July through January relative humidity in the middle and upper troposphere, representing summer in the Northern Hemisphere). Given that temperatures are much warmer during summer, this translates into a substantial increase in specific humidity or the absolute amount of water vapor in the atmosphere during the warmer season.

The same results were obtained in the western versus eastern Pacific comparison. We conclude, therefore, that warmer conditions do lead to increased water vapor at high altitudes in the troposphere, and that the model assessments of water-vapor feedback for the future are not overestimated. This result should help us to quantify our prediction of the future global warming.

Contact: David Rind (Code 940)
(212) 678-5593

Sponsor: Office of Space Science and Applications

Dr. David Rind directs the development of three-dimensional climate and stratospheric models at GISS. He is also responsible for leading the Institute's upper atmospheric research program. Dr. Rind has a PhD from Columbia University and has been with NASA since 1980.

EXPANDED INTERNATIONAL COOPERATION IN SPACE GEODESY

The Crustal Dynamics Project (CDP) was created in 1979 to measure—with unprecedented accuracies—several phenomena including: (1) global tectonic plate motion, (2) regional crustal motion and deformation at or near the plate boundaries, (3) Earth orientation and rate of rotation, and (4) the Earth's gravitational field. The project sought to exploit the Agency's unique capabilities in two high-precision space geodetic techniques: Satellite Laser Ranging (SLR) and Very Long Baseline Interferometry (VLBI). In SLR, the round-trip transit time of an ultrashort laser pulse between the ground station and a satellite equipped with special reflectors is measured with an accuracy measured in trillionths of a second. The ranging data from a global network of stations are input to a data processor containing accurate models of the Earth's gravitational field and other geophysical phenomena to obtain a measurement of the intersite baselines. In the VLBI technique, radio emissions from distant quasars are observed simultaneously by a network of large radio telescopes, accurately timetagged via on-site hydrogen masers, and recorded on magnetic tape. The tapes are then sent to a central processor, or correlator, which determines the differential times of arrival of the quasar signals between sites. The differential arrival times are proportional to the intersite vector component along the quasar line of sight. The two techniques are illustrated in the first figure.

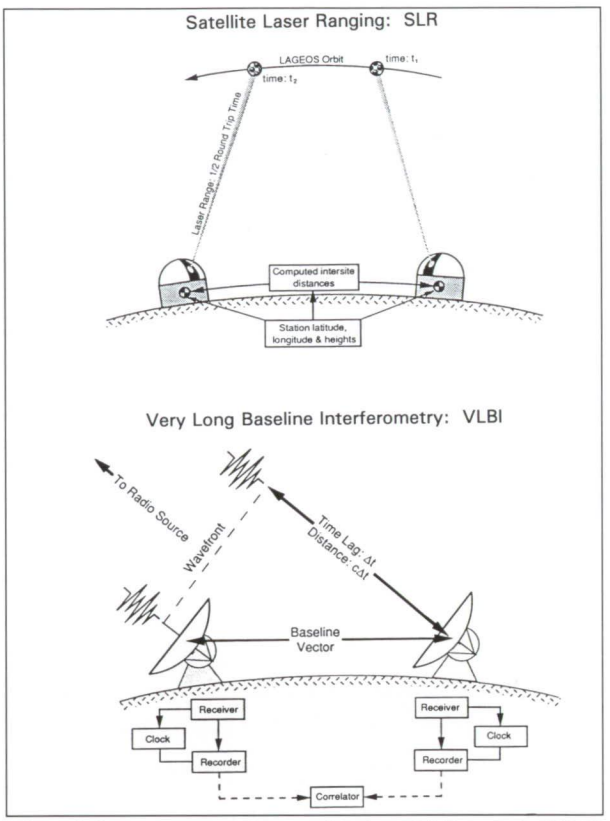

Pictorial representation of the SLR and VLBI measurement techniques.

Because of the global nature of its science mission, the Project naturally fostered close international ties with a number of foreign government agencies and universities. Although the CDP is officially scheduled to end on December 31, 1991, NASA-sponsored spaced geodetic measurements will continue under the joint auspices of the Dynamics of the Solid Earth (DOSE) Program, recently inaugurated by the Solid Earth Sciences Branch at NASA Headquarters, and the TOPEX/Poseidon oceanographic mission. Over the next decade, the SLR and VLBI geodetic networks will be augmented by a greatly expanded Global Positioning System (GPS) component. During its final year, the CDP has worked hard to promote further international cooperation and involvement in space geodesy on all seven continents as outlined in subsequent paragraphs.

Recently, the National Radio Astronomy Observatory (NRAO), with funding support from the National Science Foundation (NSF), has been establishing a Very Long Baseline Array (VLBA) of nine radio telescopes for radio astronomical measurements that will eventually stretch from Hawaii to St. Croix. The CDP and its interagency partners have worked closely with NRAO in the evaluation of station performance and its integration into the global VLBI measurement program.

FY91 also saw a significant increase in joint U.S./Canadian activities in space geodesy. The

9-meter MV-1 VLBI radio antenna was transferred to the Canadians on a long-term loan to serve as a permanent VLBI site at Yellowknife in the Northwest Territories. With Canadian funding, the CDP built and delivered Mark III VLBI S/X-band receivers for two new permanent Canadian VLBI sites at Yellowknife and Algonquin, Ontario. The new sites are part of a long-term science program to measure uplift rates in the Canadian Shield and have already participated in several successful VLBI measurements with U.S. and European stations.

Although there has been strong, active participation in the SLR and VLBI programs by the European geodetic community for a number of years, several partners have recently expressed an interest in initiating, or expanding, their level of participation via responses to the DOSE NASA Research Announcement (NRA). European nations proposing to DOSE include Great Britain, France, Germany, the Netherlands, Italy, Austria, Switzerland, Poland, Czechoslovakia, Spain, Sweden, Israel, Finland, Norway, Iceland, Portugal, Greece, Hungary, and Turkey. In addition to free exchanges of space geodetic data from permanent stations and technological advances, the U.S. and Europe have cooperated in joint regional measurement campaigns, using mobile SLR and VLBI units in both North America and Europe.

In early FY91, at the invitation of the U.S.S.R. Academy of Sciences, the Crustal Dynamics Satellite Laser Ranging (CDSLR) Network was a major participant in an international campaign to track two new Soviet geodetic satellites—ETALON I and II. As a result of this cooperative campaign, the CDP received data, for the first time, from three new SLR sites within the U.S.S.R. which are located at Majdanak, Dunaevy, and Evpatoria and are operated by GLAVCOSMOS. The technology issues and scientific results of the campaign were discussed at an international symposium held in Moscow in June 1991.

Over the past 2 years, the CDP had the opportunity to meet with the various science and engineering groups within the U.S.S.R. that have an interest in space geodesy. These include the Physical Institute of the U.S.S.R. Academy of Sciences (FIAN), GLAVCOSMOS in Moscow, and also the Institute for Applied Astronomy (IAA) in St. Petersburg. The IAA is developing a network of six VLBI stations called QUASAR. In addition to the six QUASAR sites, the Soviet GLAVCOSMOS group—who control two large radio telescopes at Odessa, in the Ukraine and at Ussurijsk in the far east near Vladivostok—have proposed joint VLBI experiments. Based on joint discussions with the Soviets, the CDP, in cooperation with JPL and NASA Headquarters, drafted and forwarded a set of proposals, outlining increased cooperation in all three space geodetic techniques (i.e., SLR, VLBI, and GPS), which were approved at the U.S./U.S.S.R. Joint Working Group on Earth Sciences Meeting in September 1991. The resulting Memorandum of Understanding (MOU) provides for expanded cooperation in space geodesy which includes exchanges of data, hardware and personnel.

Until now, space geodetic data from Africa have been limited to periodic SLR measurements from a Czech-built station in Helwan, Egypt and a VLBI facility in Hartebeestoek, South Africa. During FY91, the CDP, working closely with Nigerian scientists, selected a site on the Jos Plateau for a future occupation by a NASA transportable SLR system and a NOAA-supplied GPS receiver. The CDP has also provided engineering and analysis support to the development of an SLR station destined for Riyadh, Saudi Arabia. In cooperation with our European colleagues, the CDP has been planning expansions of the European SLR and GPS regional campaigns into the African continent by early 1993. Very recently, NASA began to explore a possible transfer of the decommissioned MOBLAS-6 SLR system to the Hartebeestoek site. These steps would provide much-needed SLR tracking coverage in Africa in support of several important solid-Earth, oceanographic, and gravity-field studies.

Japan has supported CDP measurement programs for several years at its permanent SLR site at Simosato and permanent VLBI site at Kashima. A second permanent SLR site has recently been established in Tokyo, and Japan operates a mobile SLR system as well. During FY91, Japan provided the first mobile

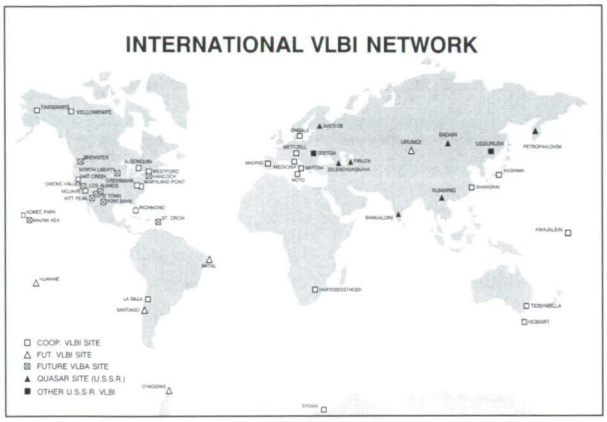

Geographic distribution of VLBI sites as they exist presently and in the near future (by 1995).

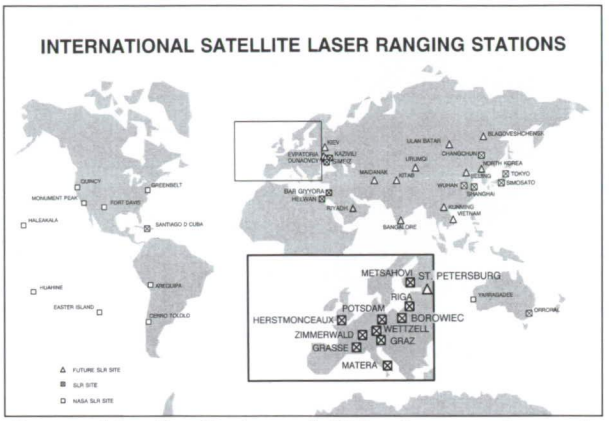

Geographic distribution of SLR sites as they exist presently and in the near future (by 1995).

VLBI data to the CDP. The mobile VLBI data were successfully analyzed by the CDP and were included in the VLBI Terrestrial Reference Frame report.

The Peoples' Republic of China (PRC) has responded to the recent NRA for DOSE and has offered to provide SLR tracking for the TOPEX/Poseidon mission and the constellation of geodetic satellites from five sites within the PRC located near the cities of Shanghai, Wuhan, Beijing, Kunming, and Changchun. VLBI stations at Shanghai (existing), Kunming and Urumqui are also contemplated. During the summer of 1991, the CDP performed an onsite technical evaluation of the Chinese SLR sites (except Changchun) during which many programmatic and technical topics were discussed with Chinese scientists and engineers.

The CDP has also been supporting efforts of the Indian Space Agency to establish a VLBI site in Bangalore, India. Preliminary discussions have also been held regarding a possible cooperative effort between the U.S., Russia, and India to establish an SLR station at the same site.

Colleagues from the Australian Land Information Group (AUSLIG) operate an SLR station at the Orroral Geodetic Observatory near Canberra, and for several years, NASA has operated the MOBLAS-5 SLR station at Yarragadee on the West Coast of Australia. In addition, radio telescopes at the Tidbinbilla Station of the Deep Space Network (also near Canberra) and at Hobart, Tasmania have participated in global VLBI measurements conducted by both NASA and NOAA. The NASA/NOAA team provided scheduling, engineering, and maintenance support to the two Australian VLBI stations.

During FY91 and at the invitation of AUSLIG, NASA SLR experts provided on-site technical consultation and off-site data analysis support during system upgrades at Orroral and also participated in technical reviews of a new SLR system being built by an Australian contractor for Saudi Arabia. Also during FY91, the second-generation SAO-2 system was replaced by the third-generation TLRS-3 highly transportable SLR system in South America. The all-Peruvian crew from the University of San Augustin (UNSA) completed a very successful collocation and transition at Arequipa. Using Arequipa as a home base, TLRS-3 will provide temporary occupations at Cerro Tololo, Chile.

In a similar fashion, the NASA TLRS-2 SLR system, operated by staff from the University of Chile, alternates between sites on Easter Island (Chile) and Huahine, French Polynesia. The latter group also operates a radio telescope complex for NASA in Santiago, and during FY91, the CDP reached an agreement with Germany to fund the first VLBI operations in Santiago.

The CDP has been working with scientists from Chile and with the German Institute for Applied

Geodesy to establish a permanent VLBI site in Antarctica (Chile's base at O'Higgins on the Palmer Peninsula). The radio antenna and VLBI receiver terminal for Antarctica were successfully integrated and tested in Germany with CDP hardware fabrication and data analysis support. An Antarctic VLBI site at Syowa is operated by the Japanese, and NASA has begun negotiations for a VLBI facility at the proposed Synthetic Aperture Radar (SAR) facility within the U.S. McMurdo Station.

Presently, there are ~35 SLR and 30 VLBI stations in the interagency/international networks that routinely provide data to the CDP. This does not include the many additional sites occupied by mobile SLR and VLBI systems during regional campaigns. The number of permanent SLR/VLBI stations are expected to grow significantly (by at least 30 percent) by 1995. This growth is due entirely to the efforts of our interagency and international partners and reflects their growing interest in, and commitment to, the science goals of the CDP. The remaining figures show the distribution of permanent SLR and VLBI stations, respectively, expected within the next few years. As NASA makes the transition from the earlier CDP to the new DOSE Program, these high-precision SLR/VLBI networks will form the backbone of a major, new international fiducial network of ~200 sites, most of which will be occupied by high-precision NASA-designed GPS receivers. Space geodetic data from these sites will play an important supporting role in a host of future scientific studies. These include global plate tectonics, regional crustal deformation and strain, gravity fields, relativity, land topography, oceanography, ice-sheet mass balance, and global sea level.

Contact: John J. Degnan (Code 901)
(301) 286-8470

Sponsor: Office of Space Science and Applications

Dr. John J. Degnan is presently Deputy Manager of the Crustal Dynamics Project and a member of the Geoscience Laser Ranging System Engineering Team. During his 27-year career at GSFC, he has published extensively on lasers and their applications to satellite ranging, intersatellite communications, remote sensing, and medicine. Dr. Degnan received his BS from Drexel University and his MS and PhD from the University of Maryland, all in physics.

IMPROVED MODEL OF THE EARTH'S GRAVITATIONAL FIELD

Precise knowledge of the gravity field of the Earth is important for studying the internal structure of the Earth, for computing the precise positions of artificial Earth satellites, and for computing the circulation of the ocean using satellite altimetry. The gravitational field of the Earth is determined by the distribution of mass within the Earth. If the Earth were a perfect homogeneous sphere, the gravitational attraction on an object at the Earth's surface would be the same regardless of the geographic location. However, the distribution of mass within the Earth varies considerably, and the gravitational attraction at the Earth's surface varies with geographic location. For this reason, models of the Earth's gravity field are often used for studying the internal structure of the Earth, especially in combination with measurements of the Earth's topography. Over the ocean, the water tends to conform to the geoid. The geoid is a surface on which the acceleration of gravity is the same at all locations on the surface. Therefore, if the height of the ocean surface can be measured, the gravity field over the ocean can be estimated. Variations in the gravity field cause the sea surface to deviate from a sphere by roughly ±100 m. The ocean currents cause slight deviations (±1 m) of the sea surface from the geoid, referred to as the dynamic topography. Therefore, these effects must be removed if a precise measurement of the gravity field is needed.

Oceanographers hope to use a precise model of the Earth's gravity field and measurements of the sea surface height using data from the TOPEX/Poseidon satellite altimeter mission, a joint mission with the French scheduled for launch in 1992, to estimate the dynamic topography and infer the ocean circulation. However, in order to achieve accurate results using

this technique, the position of the TOPEX/Poseidon satellite must be precisely known. Because the position of the satellite is affected considerably by the gravity field of the Earth, an accurate model of the gravity field is needed to compute the precise position of the spacecraft. Therefore, the use of satellite altimetry for determining the ocean circulation requires a precise gravity-field model for two reasons: (1) the gravity field must be known accurately so that deviations of the sea surface from the geoid may be determined, and (2) the computation of the precise position of the satellite requires accurate knowledge of the gravity field.

The gravity field of the Earth can be determined using three different methods: (1) by analyzing the variations in the positions of Earth-orbiting satellites using observations from satellite tracking stations, (2) by directly measuring the gravity field using land- and ship-based gravimeters, or (3) by analyzing the variations in the height of the sea surface using satellite altimeter measurements. Recently, GSFC Space Geodesy Branch scientists have developed a new model of the Earth's gravitational field by combining information from each of these techniques. This model, denoted Goddard Earth Model T3 (GEM-T3), was determined using tracking data collected from 31 different satellites, surface gravity measurements processed by Ohio State University, and satellite altimeter measurements collected during the GEOS-3, Seasat, and Geosat missions.

Variations in the altimeter measurements caused by the gravity field, due to both changes in the position of the satellite as well as variations in the height of the sea surface, were analyzed simultaneously in the gravity model solution. This required simultaneously estimating a model for the dynamic topography with a model for the gravity field of the Earth to remove the major effects of the ocean circulation from the altimeter measurements. The first figure shows an image of the resulting GEM-T3 gravity model. The complexity of the mass distribution of the Earth is apparent. The second figure shows a model of the dynamic topography computed in the solution using Geosat altimeter data collected between November 1986 and January 1987. The ocean currents flow in a direction parallel to the contour lines on the image (clockwise in the Northern Hemisphere and counterclockwise in the Southern Hemisphere). This model compares well with similar models computed from data taken by ships at sea. The model shows somewhat higher dynamic topography in the equatorial Pacific due to the El Niño Southern Oscillation, which was at its peak in late 1986.

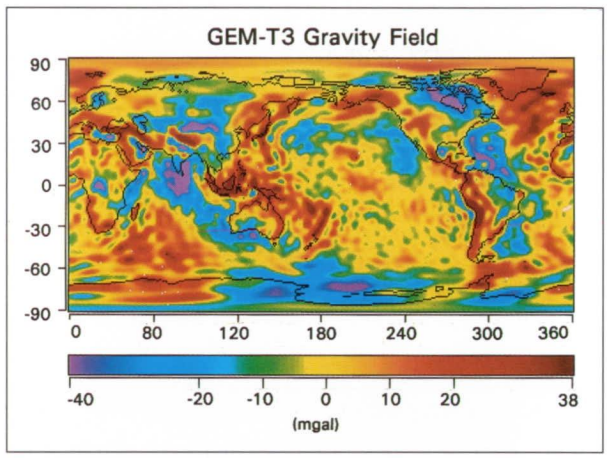

Variations in the gravitational field of the Earth computed using the GEM-T3 gravity model (units are in mgals where 1 gal = 1 cm/s^2).

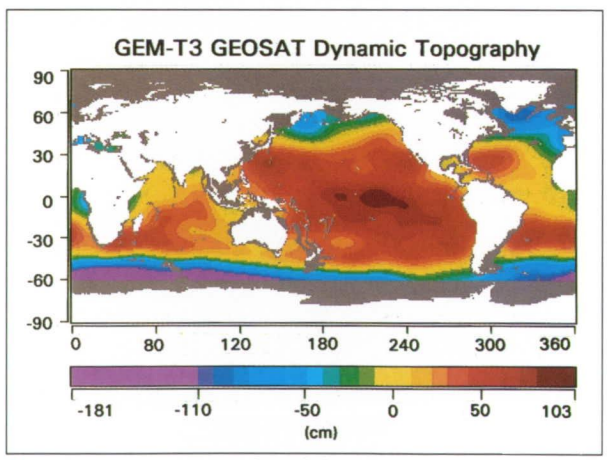

The dynamic topography of the oceans computed using GEOSAT altimeter data in the GEM-T3 gravity solution (units are in centimeters).

One reason this new model has been developed is to support the determination of a precise orbit for the TOPEX/Poseidon satellite, which will be computed at GSFC. The TOPEX mission requires that the

position of the satellite be known to a vertical accuracy of <13 cm, with 10 cm of this total error allocated to gravity-field mismodeling. Tests computed with the GEM-T3 gravity model indicate that errors in the model should contribute <10-cm error in the vertical direction to the determination of the orbit of the TOPEX/Poseidon satellite. The model also represents a considerable improvement in the knowledge of the gravity field over the oceans, which is necessary for satellite altimeter studies of the ocean currents. This model, when used in combination with measurements from the TOPEX/ Poseidon mission and combined with other oceanographic measurements, will help determine the ocean circulation with unprecedented accuracy.

Contact: R. Steven Nerem (Code 926)
(301) 286-3220

Sponsor: Office of Space Science and Applications

Dr. R. Steven Nerem, a specialist in space geodesy and satellite orbit determination, studies methods for determining the gravity field of the Earth and the planets using satellite tracking data and satellite altimeter data. He also uses satellite altimetry to study the circulation of the ocean and its variability. He has a PhD in Aerospace Engineering from the University of Texas at Austin.

DEVELOPMENT OF A UNIFORM GEOGRAPHICAL DATABASE SYSTEM IN SUPPORT OF EARTH REMOTE SENSING

We are developing a uniform global environmental data-gathering and distribution system to support the calibration and validation of remotely sensed data for global change studies. This Spatial Analysis and Modeling System (SAMS) is based on an enhanced version of the Federal Emergency Management Agency's (FEMA's) Integrated Emergency Management Information System and the U.S. Department of Defense's Air-Land Battlefield Environmental Software system. SAMS will consist of state-of-the-art graphics and visualization techniques, simulation models, database management capabilities, and expert systems for conducting environmental and disaster preparedness studies. The software will be integrated into various Landsat and United Nations Environmental Program-Global Resource Information Distribution stations which will become direct readout stations during the era of the Earth Observing System (EOS) (c. 1995 to 2010). The system will be implemented as a pilot program to support the NASA TRMM, a joint U.S./Japanese mission planned for 1996. Large, worldwide databases already exist; they will grow as satellite monitoring missions such as TRMM and direct broadcast data from SeaStar and EOS become available. SAMS will provide a framework to integrate and utilize the new datasets from these future NASA satellite missions.

Most systems for enviromental data gathering, monitoring, modeling, and information distributing exist independently of each other and not much effort has been devoted to integrating them into uniform systems. Such lack of uniformity poses a barrier to users who often have to gather *ad hoc* hardware and software to obtain real-time environmental information. A unified system is required by Earth resource scientists and managers to make informed decisions. The uniqueness of the proposed system is that it integrates several existing worldwide databases, environmental monitoring systems, and models into one computing environment.

The primary purpose of this project is to develop software to integrate data, models, and hardware/ software systems, and to provide a smart user interface. A comprehensive Reformat Compiler (RC) is needed to reformat and input the numerous varied datasets. A librarian is needed to keep track of the location of various types of data (e.g., imagery, maps, and text) of specific areas in the system's many databases. System integration tools such as X-windows, Network File Systems (NFS), and Unix-favorable systems will be evaluated and implemented as appropriate.

The system will have data input from a number of sources. Hence, data management software is needed for reformatting data inputs and outputs and data transactions between processes. The environmental

and emergency management/planning models must rely on extensive geographic information. Several existing geographic databases must be integrated to form a seamless geographic information system to support these models.

The SAMS geographic database will remain open-ended for ease of updating when future datasets become available. The user will interface with a number of software modules. Thus an innovative multitask user interface based on graphics and visualization is needed.

We envision developing a seamless database where the numerous datasets are integrated into one worldwide, accessible information system. Once developed, this seamless database would be used to feed environmental models and data analysis algorithms.

We would like to acknowledge John Hill, Paul Chan, and Robert Jaske who were contributing authors.

Contact: Fran Stetina (Code 970)
(301) 286-5717

Charles Vermillion (Code 970)
(301) 286-5111

Sponsor: Office of Space Science and Applications

Mr. Fran Stetina, a Technical Resources Manager, earned his degrees in Physics and Math from DePaul University and his MEA from George Washington University. His area of experience includes technical management of remote ocean sensor projects, instruments, communication and data acquisition systems, data processing, and archiving systems.

Mr. Charles Vermillion has been a developer/ implementer of Direct Readout Systems Technology for the last 27 years. His research area of experience includes remote sensing IR/oceans, sea ice, bathymetry, hydrology, computer systems, RF technology, interactive data processing, direct readout, and data collection systems. He is the Head of the Ocean Data Systems Office.

SPATIAL AND TEMPORAL VARIABILITY OF GLOBAL SURFACE SOLAR IRRADIANCE USING INTERNATIONAL SATELLITE CLOUD CLIMATOLOGY PROJECT (ISCCP) DATA

Incident shortwave solar radiation at the Earth's surface is the prime energy source for terrestrial and marine photosynthesis and is a major term in the global surface heat budget. Solar irradiance is also important to geochemical cycling because both biological and photochemical processes strongly perturb distributions of chemical species on land and in the ocean. Because clouds modulate surface solar irradiance, there is a need to understand the spatial and temporal variability of cloudiness on a global scale and how this variability impacts the biosphere, geochemical cycling, and climate. Such information is particularly needed for the ocean. The photosynthetic fixation of inorganic carbon into organic matter is the dominant source of energy for the biosphere. However, there are fundamental differences in the way variability of solar irradiance affects photosynthesis on land and in the ocean.

Unlike plants on land, which are large and attached to the surface, marine plants are microscopic and are distributed vertically within a euphotic zone that extends from the surface to depths as great as 150 m. The vertical distribution of plant biomass on a day-to-day basis and the supply of nutrients to this sunlit zone are determined by water-column stratification, vertical convective motions, and large-scale advection. The physical attributes of the euphotic zone are intimately connected to the daily fluctuations in air-sea heat balance, of which solar irradiance is a major component. Unlike continental systems, where plant growth time scales are seasonal, marine plant populations can double in a single day. Thus, the much smaller mass and shorter growth time scales for marine plants compared with land plants suggest that the day-to-day variability of solar irradiance has the potential to influence more strongly the distributions and production of biomass in the ocean than on land. From a physiological point of view, the impact of the high-frequency

variability of incident solar irradiance on the global distribution and species composition of phytoplankton has yet to be investigated, although it is well-known that different plankton species differ in their growth response to light. A better knowledge of the global spatial and temporal variability of surface solar irradiance can significantly improve our understanding of and ability to model the oceanic and terrestrial biospheres. We have recently developed a fast scheme for computing surface solar irradiance using cloud data from the International Satellite Cloud Climatology Project (ISCCP).

Briefly, ISCCP combines geostationary and polar-orbiting satellite data to survey clouds and their optical properties over most of the Earth's surface eight times per day on an equal-area grid 280 km in size. We found that daily mean solar irradiances from the fast scheme reproduce the detailed global results from full radiative transfer model calculations to within 6 and 10 W/m^2 over the ocean and land, respectively, but in only 1/100th of the computer time. In particular, the fast scheme reproduces the same dependence of surface irradiance on solar zenith angle which is critical for proper calculation of daily, seasonal, and latitudinal variability.

Validation of both model results is limited because globally distributed datasets of high quality are lacking, particularly over the oceans. However, comparison of calculated monthly mean results using 5 months of ISCCP data (July 1983 to July 1984) with 1970s climatology at six temperate-latitude ocean weather stations shows agreement within published estimates of interannual variability of monthly means at the individual stations.

A further test against a 17-day time series at a continental site (43°N 90°W, October through November 1986; 13 to 170 W/m^2 range of irradiance), where ground and satellite data were spatially and temporally coincident, showed an accuracy of better than 9 W/m^2 on a daily basis and <4-percent bias in the 17-day mean. Data from July (1983 and 1984) and January (1984 and 1985) were used to examine the spatial and temporal variability of surface irradiance and its potential impact on biospheric processes.

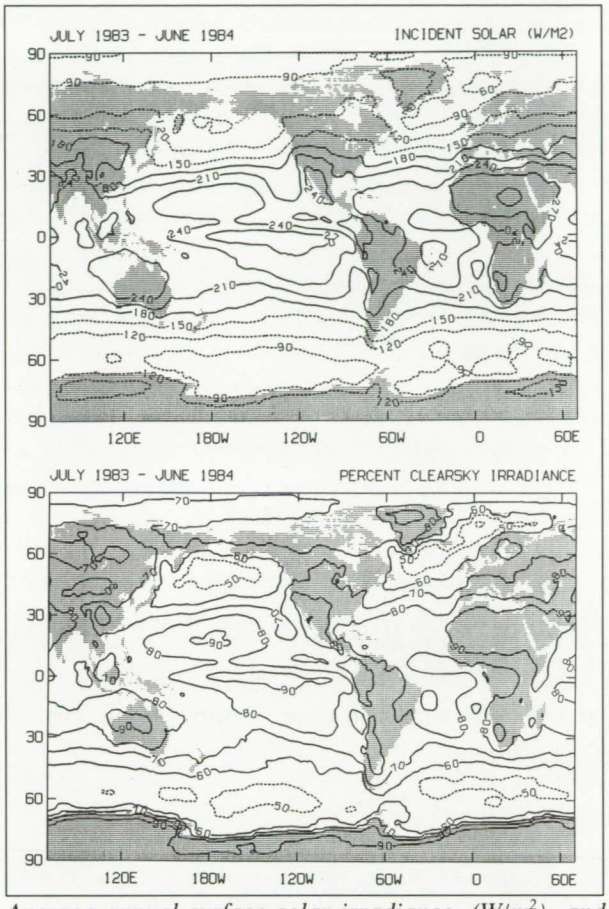

Average annual surface solar irradiance (W/m^2) and percentage of surface clear-sky irradiance for July 1983-June 1984 using the fast scheme.

Results show that the oceans and land experience fundamentally different light regimes, with continents receiving significantly greater irradiance. In summer, major interocean differences in zonally averaged irradiance are found in the Northern Hemisphere, with the Atlantic greater than the Pacific by up to 80 W/m^2.

In the Southern Hemisphere, interocean differences are small. As shown in the figure, regional interannual variability (July 1983 versus 1984) ranged between +100 and -100 W/m^2. Dashed contours are ≤150 W/m^2 and 50 percent of clear-sky irradiance. The variability, perhaps due to the 1982-1983 El Niño event, occurred mostly in the Pacific but extended beyond the tropics over the entire north Pacific basin. The nutrient-rich northern

and southern ocean waters are almost perpetually cloud-covered. However, there is a correspondence between higher-than-average surface irradiance and productivity in nutrient-rich areas of the southwest Atlantic and Weddell Sea sector of the circumpolar current. This suggests that solar irradiance must be considered as an important factor governing the productivity of these waters.

Many of the above features are evident in maps of annual mean surface irradiance and percent of clear-sky irradiance which are presented here for the first time. More ground- and sea-truth data are needed, as is a better knowledge of the global distribution of aerosols.

Contact: James K. B. Bishop
Lamont-Doherty Geological Observatory
(212) 678-5585

William B. Rossow (Code 940)
(212) 678-5567

Sponsor: Office of Space Science and Applications

Dr. James K. B. Bishop earned his ScD at the Massachusetts Institute of Technology, Woods Hole Oceanographic Institution Joint Program in Oceanography, in June 1977. He has been associated with Lamont-Doherty Geological Observatory since 1977. Dr. Bishop's research area is biogeochemical cycles in the ocean.

Dr. William B. Rossow heads the International Satellite Cloud Climatology Project (ISCCP) Global Processing Center. During his 13 years with NASA, Dr. Rossow has served on the First ISCCP Regional Experiment team, the Orbiter Cloud Photopolarimeter team for the Pioneer mission, the Photopolarimeter Radiometer team for Galileo, and the Earth Observing Scanning Polarimeter team for EOS. At GISS, Dr. Rossow performs and directs research in planetary atmospheres, atmospheric dynamics, cloud physics, radiation, remote sensing, and climate. He holds a PhD in Astronomy from Cornell University.

LEARNING CLASS DESCRIPTIONS FROM A DATABASE OF SPECTRAL REFLECTANCE WITH MULTIPLE VIEW ANGLES

The goal of this research was to develop a discrimination program to classify satellite sensor targets into user-defined ground cover and plant height classes. The program learns class descriptions from samples (both positive and negative) of spectral, directional reflectance data of natural surfaces (bare soils, natural vegetation, and agricultural vegetation). In theory, users can define any class they wish. Classes can include broad categories such as soil, vegetation, and other, more specific classes such as corn, soybeans, wheat, etc., or subclasses of continuous parameters such as sparse (0 to 30 percent ground cover), intermediate (30 to 60 percent ground cover), and dense (60 to 100 percent ground cover) of vegetation, or even structurally related classes such as homogeneous structured vegetation canopies, and nonhomogeneous vegetation canopies. Other classes could be defined that are based on species, biomass, vegetation structure, or leaf area index.

In this study, the emphasis was to capture the important common features that characterize classes in a manner similar to the way of an expert (i.e., not by using the classical statistical pattern recognition techniques but rather by using knowledge that represents relative relationships in symbolic form). The advantage of such an approach is that knowledge is explicitly represented and can be used to capture generalizations which can be insightful to the researcher.

The learning program uses Artificial Intelligence (AI) techniques that automate a very tedious process that traditionally requires an expert(s) to repeat the process for every combination of solar zenith angle, set of classes, and sensor system being used (each sensor system defines a particular set of view angles and spectral bands collected). In many cases it is known that existing relationships are subtle and

difficult to find, even for experts. Thus, the attempt is to replace the expert with an AI system.

The program is designed to be able to handle any combination of directional view angles. The program finds class descriptions that contain the most important features that distinguish each class from the others. The explicit relationships used in the class descriptions include greater-than relationships between combinations of two view angles and maximum- and minimum-value relationships. The class descriptions are used to classify an unknown target using the same directional views. The program was tested by learning class descriptions of various categories of percent ground cover and plant height. These class descriptions were then used to classify an array of target data.

The search strategy used in this study is the generate-and-test strategy. The generate-and-test strategy generates new class descriptions that are independent of the data. Furthermore, the newly generated class description is tested on the entire set of training data and then tagged as an acceptable generalization, a node to be expanded further, or a node to be pruned from the search.

The generate-and-test strategy can accommodate severe errors in the training data. An estimator function calculates a heuristic showing how well the various generated class descriptions do in characterizing the training data for a particular class. In this study, we want to try all of the generated relationships for all view-angle combinations. The best class description is the final class description used. The class descriptions that are produced can then be used to classify any unknown target(s) by testing to see which class has the most evidence that the target belongs to that class.

As a test of the system's classification performance, various runs were made as shown in the table. Various user classes were defined and the learning program was run using specific view angles, wavelengths, and solar zenith angles. Each run produced class descriptions which were then used to classify all appropriate samples (all cover types from the database that fit the solar zenith angle and wavelength intervals). The percent of correctly classified samples was then used to summarize the degree of classification accuracy achieved by the learning technique.

Run #1 used directional data similar to what the High Resolution Imaging Spectrometer (HIRIS), a proposed Earth observing instrument, could collect for an unknown target for input to the system. The classification score of Run #1 was 1.00, indicating that all samples were classified correctly. Refer to the table for various runs of the system.

Only the best three relationships of the class solution are shown. The second maximum reflectance value occurs at view angle (15 135), the (45 315) reflectance value is greater than the (60 315) value, and the (30 315) reflectance value is greater than the (60 315) value. Essentially all sparse canopies show these characteristics—peak reflectance in the solar direction that decreases continually in the direction of the extreme forward scatter direction.

The classification score of 0.67 for Run #2 was very poor. Apparently there is little structural information that is very discriminating for height. Run #3 shows the results of using a set of well-dispersed view angles with two classes of ground cover. The classification score of 0.88 was relatively good. Run #4 is the same as Run #3 except that only three poorly dispersed view angles were used. The classification score of 0.65 was relatively poor; however, it is surprising that the results are this good considering the tightly clumped view angles used as input. This example shows that relative directional-reflectance relationships can provide a significant amount of information even with extremely poorly placed view angles.

Clearly, the discrimination program works and gives valuable results. The study demonstrates that important features that characterize classes in a similar manner, as would an expert using relative directional relationships in symbolic form, can be achieved by an AI system. The approach can be applied to any combination of directional view angles, no matter what the relative placement of the view angles.

Contact: Dan S. Kimes (Code 923)
(301) 286-4927

Sponsor: Office of Space Science and Applications

Dr. Dan Kimes has 12 years of experience at GSFC. He works in the Laboratory for Terrestrial Physics in the Biospheric Sciences Branch. He develops mathematical models for radiation interactions with vegetation, and knowledge-based systems for extracting vegetation characteristics from directional reflectance. Dr. Kimes received his PhD in Earth Resources from Colorado State University.

Various runs of the system showing the identifying run number, the user-defined classes, the view angles available (zenith, azimuth) where the azimuth is relative to the Sun (0° is forward scatter and 180° is backscatter), wavelength in μm, solar zenith angle used for learning and classification, and finally, the resulting classification score of all the appropriate samples. This score is the proportion of samples correctly classified.

Run No.	User-Defined Classes	View Angles Available (Zenith Relative-Azimuth)	Wavelength (μm)	Solar Zenith Angle (°)	Score
1	Ground Cover (0-30%) (31-60%) and (61-100%)	HIRIS Example (60 35) (45 315) (30 315) (15 315) (0 0) (15 135) (30 135)	0.91	35	1.00
2	Plant Height (>10 m) and (<10 m)	HIRIS Example (60 35) (45 315) (30 315) (15 315) (0 0) (15 135) (30 135)	0.91	45	0.67
3	Ground Cover (0-30%) and (31-100%)	Well-Dispersed Data (0 0) (30 45) (60 45) (30 135) (60 135) (30 225) (60 225) (30 315) (60 315)	0.68	40	0.88
4	Ground Cover (0-30%) and (31-100%)	Poorly Dispersed Data (0 0) (10 0) (15 0)	0.68	40	0.65

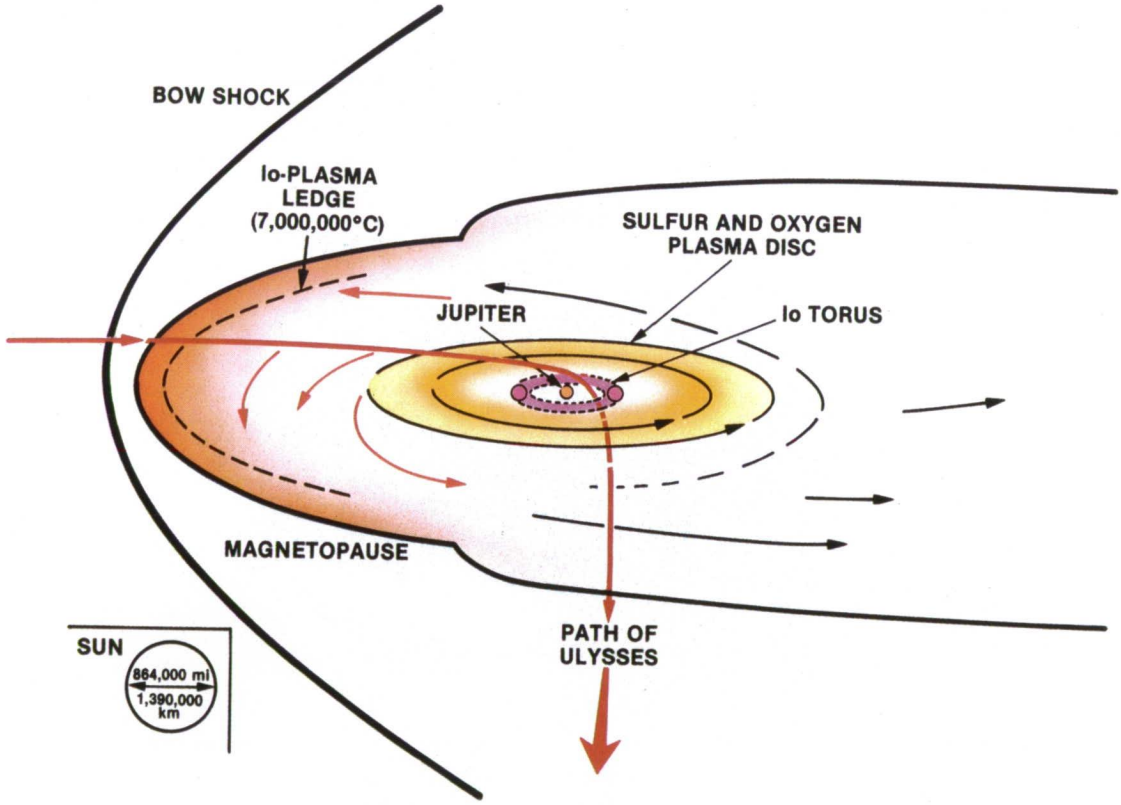

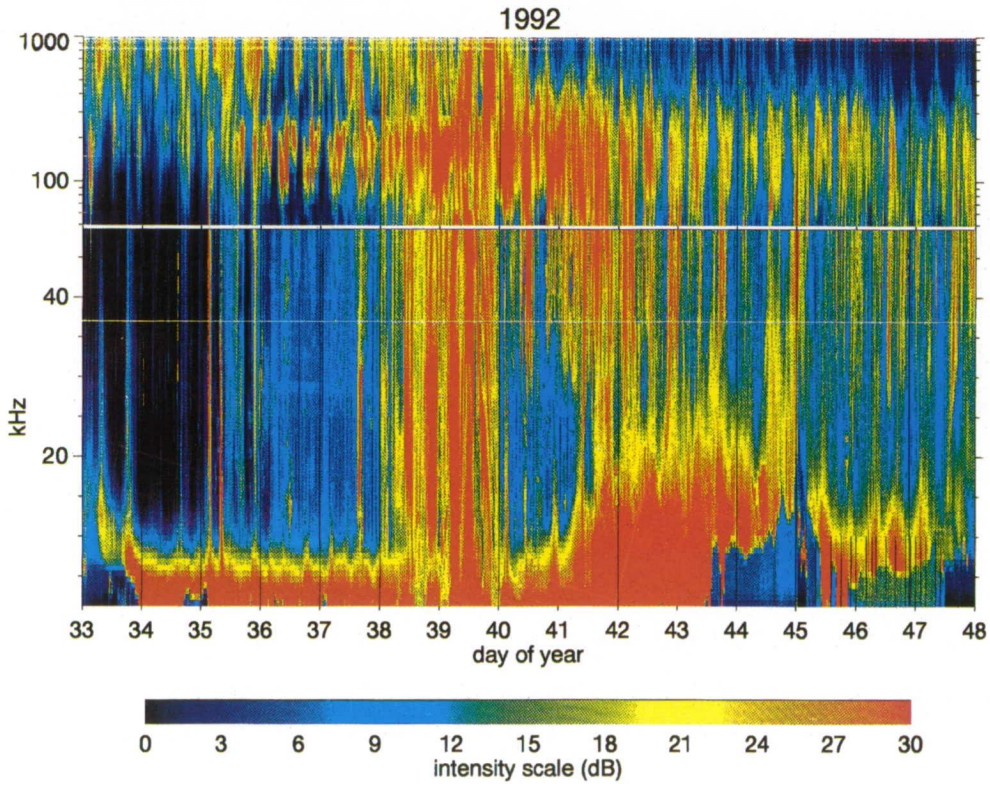

Goddard's Space Sciences program continues to unfold the mysteries of the Sun, solar system, and the universe.

SPACE SCIENCES

Solar

REALISTIC MAGNETIC FIELD LINE MAPPING THROUGHOUT THE EARTH'S MAGNETOSPHERE DURING AURORAL SUBSTORMS

A difficult problem in auroral substorm physics is accurately mapping from observed auroral features in the ionosphere to the magnetically connected regions in the equatorial magnetotail. Without such a magnetic roadmap, it is virtually impossible to deduce the nature and location of magnetotail instabilities that cause auroral substorm disturbances. Empirical magnetic modeling, as epitomized by the work of N.A. Tsyganenko in the Soviet Union, has provided a valuable framework in which to determine general magnetospheric-ionospheric connectivity. However, such models provide only an average, time-independent picture of the magnetospheric configuration. During substorms, the near-magnetotail departs drastically from this average configuration; intense, localized cross-tail currents develop during the substorm growth phase and subsequently break up at substorm onset.

Such magnetic-field changes must be incorporated into empirical models to assess their effect on mapping between the ionosphere and magnetosphere during substorm growth and early expansion phases. We have recently demonstrated a method of providing a time-dependent model of the tail magnetic field by introducing temporally varying changes into the Tsyganenko model. This gives a global growth-phase field model that compares favorably with measurements from several spacecraft in the magnetotail. Moreover, the resulting magnetic-field model can be examined to determine the times and regions where global current sheet instabilities (such as the ion-tearing mode) are most likely to occur. The model allows us to systematically map auroral features seen in remote satellite images into the near-tail region, and our results suggest that the auroral brightenings correspond to regions of thin, tearing unstable current sheets which are remarkably close to the Earth.

The 1989 version of the Tsyganenko magnetic-field model (hereafter referred to as T89) gives the magnetic field as a sum of terms representing each of the magnetospheric current systems. The ring current and the tail current are roughly in the equatorial plane, whereas other terms, such as the cross-tail closure current term, represent the currents at the magnetospheric boundaries. The field is given as a function of the dipole tilt angle between the

◂*The Ulysses spacecraft, carrying the Unified Radio and Plasma (URAP) instrument (Dr. Robert G. Stone, GSFC, PI) flew past the planet Jupiter on February 8, 1992. The top panel shows a schematic of the Ulysses trajectory including its north-south plunge through the Io plasma torus. The bottom panel shows color-coded intensity versus time from URAP for the 15-day interval centered on closest approach to Jupiter (day 39). The period when the spacecraft was inside Jupiter's magnetosphere is marked by intense (red) emissions at the very lowest frequencies. Throughout the entire frequency range, very strong emissions were observed with a very clear 10-hour modulation pattern corresponding to the Jovian rotation period.*

Sun-Earth line and the dipole equator, and an index indicating the level of geomagnetic activity. The contribution of the internal geomagnetic field is computed by using the international reference-field coefficients.

The growth-phase effects are included in the T89 model by varying the model parameters and by modifying of the functional form of the field components. The current sheet is locally thinned by modifying a function that determines the current sheet half-thickness. The minimum thickness, the location of the minimum thickness, and the size of the thinned region are free parameters. The increase of the tail flux is represented by a factor that enhances the model tail current intensity, leading to corresponding enhancement of the field. To prevent tail flaring, the currents along the magnetopause are enhanced correspondingly by a similar factor. To enhance stretching close to the Earth, a new current sheet is added to the model. The functional form of the new current sheet is chosen to be similar to the ring current, but the peak intensity, azimuthal and radial location of current maximum, and the thickness of the current sheet can be set according to the observed degree of field stretching. In all, these modifications are represented by a set of 11 parameters whose values are set by comparison with the field observations.

The figure shows the current integrated over the thickness of the current sheet in mA/m for a particular event we have studied, and the field lines in a particular meridian (close to the onset meridian) for the basic T89 model (a and c, respectively) and similarly for the modified model (b and d, respectively). Total current (solid line), ring current (dotted line), and tail current (dashed line) are shown for both cases (a and b). The added current sheet is shown by the dash-dotted line. In addition to the total current, the different current terms (the tail current, ring current, and the new current sheet added to the model) are plotted separately. The new current sheet increases the current maximum by ~120 mA/m, and shifts the current maximum slightly earthward. The strongly enhanced current in the near-tail region stretches the field lines to a more tail-like configuration, with the field almost parallel to the

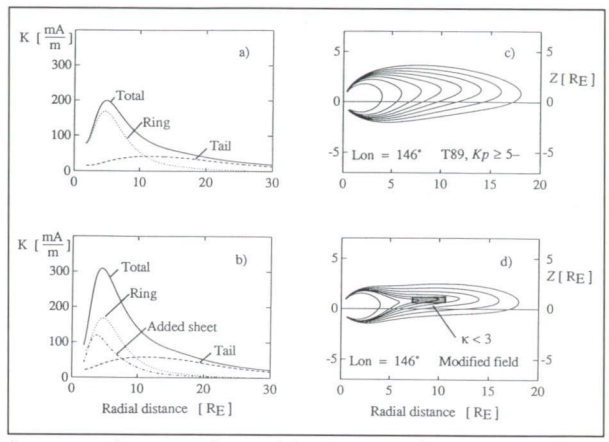

Integrated current intensities in a single meridian plane in our basic T89 (a) and modified (b) models; field-line projections to the meridian (146°) using the basic T89 (c) and modified (d) models.

current sheet at the distance of ~15 Earth radii. A region of chaotic electron motion for 1-keV electrons in this field configuration is shown hatched.

Modeling the growth phase by current systems increasing linearly with time gives insight into how the current systems could evolve in the near-Earth tail. The strong tail-like development of the field within the geostationary orbit inferred from the available measurements has been represented by several changes including an additional thin current sheet in the T89 model. The resulting cross-tail current is ~310 mA/m peaking at a geocentric distance of 4.6 Earth radii, which is in substantial agreement with earlier observational results. While the tail configuration is significantly altered as a result of adding the new currents, it is apparent that the main auroral features still map to within 10 Earth radii in this model.

The global model that we developed for the magnetic field and currents has allowed us to study the tail stability properties, thus addressing the question of the mechanism and location of the current disruption at substorm onset. Mapping of the auroral boundaries to the current sheet shows that the activity, in many cases, is located exceptionally close to the Earth, with the equatorward boundary of the auroras mapping as close to it as 4 to 5 Earth radii in the tail. We suggest that in more typical substorm

events, the regions of current sheet instability will map somewhat farther from the Earth than in these exceptional cases. In weaker events, the near-geostationary orbit spacecraft will not be monitoring the most relevant region of the current sheet development. However, we expect that a current sheet model much like that employed here, but with lower intensity and lesser earthward extent, is characteristic of the near-Earth tail during most substorm growth phases.

Contact: D. N. Baker (Code 690)
(301) 286-8112

T. I. Pulkkinen (Code 690)

Sponsor: Office of Space Science and Applications

Dr. Daniel N. Baker is the Project Scientist for the Small Explorer (SMEX) Program and the Mission Scientist for the Solar, Anomalous, and Magnetospheric Particle Explorer (SAMPEX) Project. He is Chief of the Laboratory for Extraterrestrial Physics. Dr. Baker, with over 4 years of experience at GSFC, holds a BA, an MS, and a PhD from the University of Iowa.

Dr. T. I. Pulkkinen works at the Finnish Meteorological Institute in Helsinki, Finland and recently obtained her PhD in Theoretical Physics from the University of Helsinki. The above work was performed while she visited GSFC to continue her graduate studies and is part of her PhD research.

THE ENERGETIC PARTICLE ACCELERATION, COMPOSITION, AND TRANSPORT EXPERIMENT FOR THE ISTP/WIND SPACECRAFT

Construction of the Energetic Particle Acceleration, Composition and Transport (EPACT) experiment has been a major undertaking for the Laboratory for High Energy Astrophysics during the past year. EPACT is designed to study a wide variety of energetic particle populations, including particles from solar flares, particles accelerated in interplanetary shocks, the so-called anomalous component, and the galactic cosmic rays. EPACT is intended to be a major step forward over instruments flown previously on the International Sun-Earth Explorer 3 (ISEE-3). It will reach to much lower energies and increase sensitivity by factors of as much as 50. In large solar flares, the ISEE-3 instruments were limited by the telemetry rate. By using on-board microprocessors, EPACT can increase the number of particles detected and analyzed more than a thousandfold.

One of the major goals of EPACT is to understand how particles are accelerated from thermal energies to very high energies. EPACT has been designed to observe over the broad energy range from suprathermal energies to hundreds of MeV per nucleon. In the case of interplanetary shocks, EPACT can observe acceleration occurring in situ as interplanetary shock waves go past the spacecraft. Acceleration by shock waves is also thought to produce the most common solar flare particle increases, those with large intensities of protons. By contrast, there are solar flare events in which ^{3}He is enhanced relative to ^{4}He by factors of ~2000. Heavy nuclei are also enhanced, implying a very different acceleration mechanism. It is thought, but not confirmed, that the enhancements in ^{3}He and the heavier elements are due to wave-particle interactions in the flare-heated plasma. Greatly improved measurements of abundances in these flares should help to better understand their origin. It is possible that the heavy nuclei enhancements, together with the increased sensitivity of EPACT, will permit the first observations of nuclei heavier than iron in solar flares.

The anomalous component is believed to originate as interstellar neutral atoms which are accelerated at the heliospheric shock produced where the solar wind plows into the interstellar medium. Efforts have been made to confirm this acceleration model by using the Earth's magnetic field as a magnetic spectrometer to measure the ionic-charge state. These efforts have been seriously hampered because no contemporary measurements of the anomalous component immediately outside the Earth's magnetosphere have

been available—the anomalous component fell below the threshold of detectability as a result of solar modulation. EPACT's greatly increased sensitivity is expected to overcome this difficulty and to assist the SAMPEX mission in determining the charge state.

A second goal is to measure the isotopic composition of energetic particles in solar flares, in the anomalous component, and in the galactic cosmic rays. The cause of the enhancement of ^{3}He in ^{3}He-rich events may alter other isotopic ratios as well, giving additional clues about the acceleration mechanism. The anomalous component is evidently a sample of the local interstellar medium, so its isotopic composition is also of great interest. The isotopic abundances of the galactic cosmic rays have begun to be measured, and it appears that there are significant differences relative to the solar system that can provide clues to the origin and acceleration of the galactic cosmic rays.

Finally, we are interested in the propagation of energetic particles, both those produced within the solar system and from cosmic sources. Transport processes will be studied in conjunction with data from other spacecraft such as Ulysses, the Pioneers, and the Voyagers, in addition to data from observations of local anisotropies in interplanetary shocks and for solar flare particles.

The EPACT experiment must make observations over an extremely broad range of elements, energies, and intensities. As a result, EPACT consists of multiple telescopes that also provide a level of protection against single-point failures. Solid-state detectors are used throughout for reliability and long-term gain stability. The individual telescopes include three Low Energy Matrix Telescopes (LEMTs), two Alpha-Proton-Electron Telescopes (APEs), an Isotope Telescope (IT), and a SupraThermal Energetic Particle Telescope (STEP).

The energy ranges for each are shown in the figure. All but STEP use the dE/dx by E method of particle identification. STEP, a late addition to EPACT, measures time-of-flight and energy, from which particle mass can also be obtained. STEP was originally built for the U.S. Solar Polar spacecraft by the University of Maryland. Space does not permit a detailed description of EPACT; however, some idea of its scope may be obtained by noting that it contains nine different microprocessors, more than 19,000 electronic parts, and 79 different solid-state detectors. Innovations include the on-board particle identification algorithms, the position-sensitive detectors for the IT, the time-of-flight system for STEP, the development of several general-purpose integrated circuits, and the use of memory chips to perform coincidence logic. The design, fabrication, and test of EPACT will have been accomplished in less than 3 years.

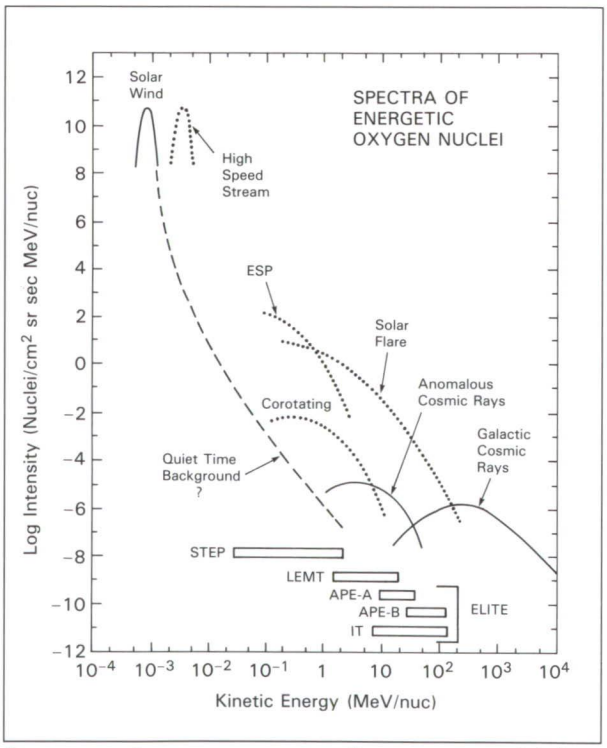

Representative energy spectra for oxygen nuclei from the different particle populations to be studied by the EPACT experiment.

Contact: Tycho von Rosenvinge (Code 661)
(301) 286-6721

Donald Reames (Code 661)
(301) 286-6454

Sponsor: Office of Space Science and Applications

Dr. Tycho von Rosenvinge is the Principal Investigator of the EPACT experiment and Head of the Low Energy Cosmic Ray Group in the Laboratory for High Energy Astrophysics. He has been pursuing studies of energetic particles at GSFC since 1969. He received his PhD from the University of Minnesota.

Dr. Donald Reames is a Co-Investigator for EPACT, with primary responsibility for the LEMT telescope system. As an astrophysicist in the Nuclear Astrophysics Branch, Dr. Reames specializes in the study of energetic-particle acceleration. He received his PhD in Physics from the University of California at Berkeley and has been at GSFC since 1964.

EVOLUTION AND STRUCTURE OF SOLAR WIND TURBULENCE

The Sun produces not only light but also a continuous, rapidly moving stream of ionized particles (a plasma) with a magnetic field imbedded in it. This plasma flow, known as the solar wind, is not steady, but rather exhibits fluctuations on a wide range of scales. We have been studying these fluctuations to understand turbulence in magnetized, conducting fluids.

One source of turbulent evolution is the variations in the wind speed that lead to shear and compression of the plasma. Recently, we found that there is an important effect due to the structure of the magnetic field. This field is an extension of a dipolar solar field, and thus one hemisphere of the heliosphere has field lines that point toward the Sun, while the other hemisphere has lines that point away from the Sun. In between the hemispheres lies a current sheet that, near the Sun, contains a very small magnetic-field component in the direction of the nearly radially directed velocity. Near the current sheet, rapid stirring of the plasma can occur due to the low fields there. Away from the current sheet, the tension in the magnetic field inhibits the development of shear-produced fluctuations.

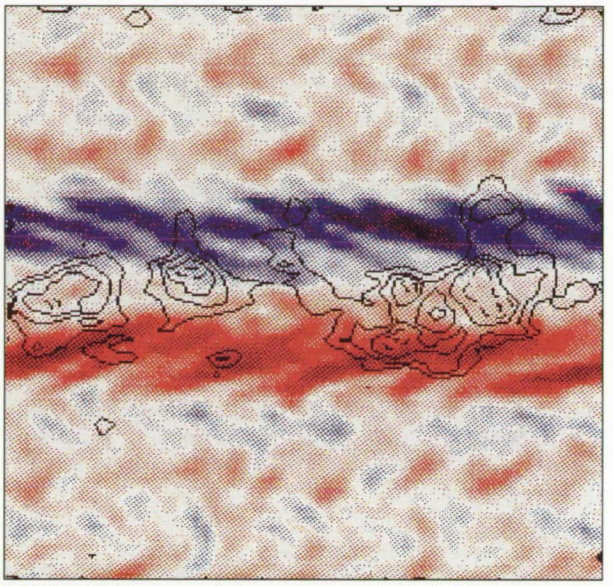

MHD simulation of the solar wind including a current sheet across the middle of the box.

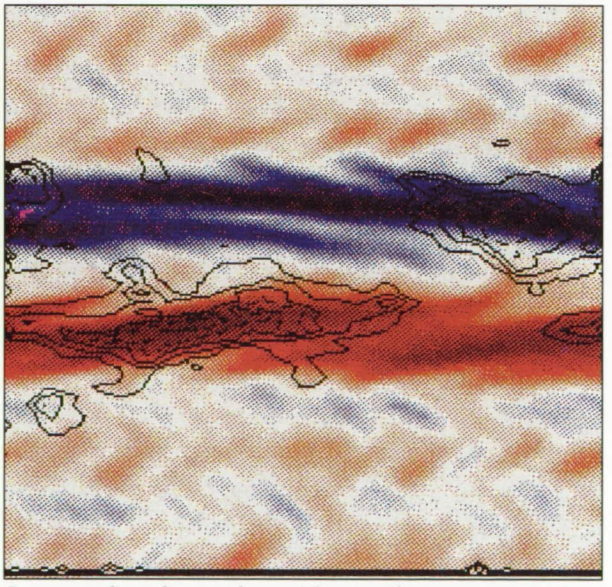

Same as first figure, but with a uniform magnetic field across the box, and thus no current sheet.

We have studied the role of the current sheet in the turbulent evolution of the solar wind using magnetohydrodynamic (MHD) computer simulations that model the behavior of a magnetized conducting fluid moving under the influence of pressure and magnetic forces. The situation we describe here

involves two fast solar-wind streams (top and bottom of the boxes in the figures) surrounding a narrow slow stream. The magnetic field changes sign in the middle of the slow stream in the first figure, representing the typical solar wind conditions at the minimum of solar activity. The colors represent the vorticity (shear) of the flow, and the contours, the degree of evolution of the turbulent fluctuations. The second figure shows the same situation without the change in sign of the field and thus no current sheet. The colors in the figure show the vorticity which represents the degree of shear in the velocity; dark blue and red show the regions of maximum shear. The contours show regions of strong evolution of the plasma from its original state. The measure of this evolution was chosen to be the degree to which an initially pure spectrum of waves propagating along the field lines is mixed with waves propagating in the opposite direction. Regions without contour lines are still very close to the original pure state. In the case with no current sheet, it is apparent that the shear produces strong evolution. By contrast, when the current sheet is present, the mild shear that exists near it is sufficient to make the central region the site of maximum activity rather than where the velocity shear is maximum. These results are precisely what is observed in the solar wind, and thus we believe that current sheets play an essential role in the turbulent evolution of magnetized plasmas.

Contact: M. L. Goldstein (Code 692)
(301) 286-7828

D. A. Roberts (Code 692)
(301) 286-5606

Sponsor: Office of Space Science and Applications

Dr. M. L. Goldstein is a Co-Principal Investigator of the GSFC Space Physics Theory Program. His research interests during 19 years have included the study of solar wind as a turbulent magnetohydrodynamic fluid, the stability of large-amplitude Alfven waves, and the processes involved in producing solar and planetary radio phenomena. He holds an AB in physics from Columbia College in New York and a PhD in physics from the University of Maryland at College Park. He received a Goddard Special Achievement Award in 1975 and NASA Exceptional Scientific Achievement Medal in 1991.

Dr. D. A. Roberts is a Co-Investigator on the Space Physics Theory Program with 5 years of experience at GSFC. His research focuses on interplanetary turbulence, solar wind acceleration, and low-dimensional descriptions of the magnetosphere. He received an SB in Earth and Planetary Sciences and a PhD in Physics from the Massachusetts Institute of Technology.

HYBRID THERMAL/NONTHERMAL MODEL OF SOLAR FLARES

During the most impulsive phase of a solar flare, a great deal of energy goes into heating the local plasma to temperatures above 10 million K and into accelerating charged particles to relativistic energies. Although some of the particles escape the flaring region and can be detected near the Earth, they are primarily observed indirectly through the x-ray and microwave radiation they emit. It is important to understand how these particles and radiation are produced, because of the impact they have upon the Earth and upon NASA activities in space, and to obtain an understanding of energy conversion processes in flares and in astrophysical plasmas in general.

The x-ray emission from flares is understood to be *bremsstrahlung* ("braking radiation") from the scattering of energetic electrons by ions. The microwave emission is gyrosynchrotron radiation emitted by the mildly relativistic electrons as they spiral around magnetic field lines in the flaring region. The spectrum of the radiation (i.e., the radiation flux as a function of wavelength) provides information about the emitting electrons and the flaring region. The spectrum of the soft x-ray emission from flares (photon energies less than a few keV) indicates that it is emitted by hot, thermal electrons which have a temperature on the order of 20 million K.

The interpretation of the hard x-ray and microwave spectra is not so clear cut, however. Because of ambiguities in determining the spectral shape, it has been possible to interpret the emission as arising from either very hot, thermal plasma (temperatures on the order of 100 million K) or accelerated, nonthermal electrons. If the hard x-ray emission is nonthermal, a high flux and total energy of electrons must be accelerated in the flaring region. The hot plasma seen in soft x-rays is presumably heated by the accelerated electrons. On the other hand, if it is thermal, it is difficult to understand all of the energetic emissions observed from many large flares. This ambiguity, and the difficulties resulting from the simple thermal or nonthermal models, have resulted in considerable controversy over the nature of the hard x-ray and microwave emissions from flares.

Recent observational advances have provided an incentive for taking a fresh look at these flare emissions and their models. New germanium crystal x-ray detectors promise much higher resolution hard x-ray spectra than were previously available. Observations of one flare with a germanium detector clearly show a thermal contribution to the hard x-ray emission at photon energies up to 40 keV. The ability to image the hard x-ray emission from flares is being developed through HEIDI (see the article by C. Crannell in this issue) and the proposed High Energy Solar Physics (HESP) mission.

The Owens Valley Radio Observatory in California is providing high-resolution spectra of the microwave emission from solar flares, and images of flare emission at several frequencies can be obtained with the Very Large Array radio telescope in New Mexico. Owens Valley observations of the microwave emission from flares have shown that the spectra of most flares are more complex than can be explained by a simple thermal or nonthermal model.

Flares are understood to result from the release of excess magnetic energy in the solar atmosphere. This magnetic energy is associated with electric currents. It is well established from laboratory studies with plasma fusion devices and from theoretical studies that these currents and their associated electric fields result in both the heating and acceleration of electrons. The resulting electron distribution consists of a thermal bulk with an attached nonthermal tail. The relative proportions of thermal and nonthermal electrons can be related to the electric field strength and other properties of the current-carrying plasma.

With this in mind, we have developed a hybrid thermal/nonthermal model for the x-ray and microwave emissions from flares. In this model, most of the released energy goes into directly heating the plasma in and around the current channels, while a smaller but significant fraction of the energy goes into accelerating electrons. Compared with the direct heating, heating of the plasma by the accelerated electrons is negligible. Because much of the hard x-ray emission is now thermal, this model relaxes the high-energy and particle fluxes required by a purely nonthermal model while maintaining the desirable features of a nonthermal model. It is also consistent with realistic theoretical expectations.

We have applied the hybrid model to existing high-resolution hard x-ray and microwave spectra. We have found that the hard x-ray spectra can be well-fit by the model, even when the presence of a thermal component is not obvious from visual inspection of the spectral shape. The combination of a hot thermal component and a nonthermal tail will often give a spectrum that is well-fit by a power law or broken power law, usually taken to be characteristic of purely nonthermal emission. We have found that a simple hybrid model provides a surprisingly good fit to the complex microwave spectra as well, while providing an explanation for several previously unexplained aspects of these spectra. The hybrid model provides a natural explanation for the presence of secondary components in the microwave spectra, for the presence of very steep, low-frequency spectral indices, and for the approximate constancy of the peak frequency of the microwave emission during the evolution of a flare. These features are not easily explained by a purely thermal or nonthermal model.

Much of this work was completed by Stephen Benka in partial fulfillment of the requirements for his Doctorate from the University of North Carolina at

Chapel Hill. This work provides a valuable formalism for the interpretation of the next generation of flare data.

Contact: Gordon D. Holman (Code 682)
(301) 286-4636

Sponsor: Office of Space Science and Applications

Dr. Gordon Holman works in the Solar Physics Branch, Laboratory for Astronomy and Solar Physics at GSFC. He obtained an MS and a PhD in Astrophysics from the University of North Carolina. He also has a BS in Physics from Florida State University. He is the recipient of two Goddard Special Achievement Awards. He has been at GSFC for 8 years.

BALLOON-BORNE HIGH-ENERGY IMAGING DEVICE FOR IMAGING HARD X-RAYS AND GAMMA RAYS FROM SOLAR FLARES

Particle acceleration and the interactions of plasmas and magnetic fields are processes that occur throughout the universe, signalling their presence by the high-energy electromagnetic radiation they emit. Solar flares, with their high fluxes at Earth and potential for multiwavelength observations, offer a unique opportunity to study these processes. High-resolution hard x-ray and gamma-ray images could reveal the basic morphology of their sources, tell us how these sources evolve on physically relevant timescales, and enable us to determine how the propagation of energetic particles depends on their spectrum and the magnetic-field structure of their sources. Despite the significance of the hard x-rays and gamma rays produced in solar flares, virtually no direct imaging of these high-energy emissions has been available to answer even the most basic observational questions.

The High-Energy Imaging Device (HEIDI) is being developed as a balloon payload to make the first imaging observations in this high-energy domain of solar physics and to develop the necessary technology for future space-flight applications. The HEIDI detectors, together with the imaging optics, are sensitive to hard x-ray and gamma-ray emission in the 20 to 700 keV energy range. This payload, scheduled for its first flight in June 1992, will provide 11-arcsec angular resolution and millisec time resolution with a whole-Sun field of view. For subsequent flights, the effective detector area can be increased by a factor of 4, and imaging optics with angular resolution as fine as 2 arcsec can be added to the existing gondola and metering structures.

Hard x-rays and gamma rays cannot be reflected or focused by lenses or mirrors. Even grazing incidence reflection, used very effectively in soft x-ray astronomy, is impossible in the photon-energy domain above a few keV. What is required is a variation on the pinhole camera consisting of material opaque to these radiations, interrupted with transparent apertures. High-resolution imaging of solar flares in this domain requires individual apertures with sizes ranging from 50 microns to 3 mm to resolve sources with angular dimensions ranging from 2 arcsec to 2 arcmin. The corresponding material thicknesses range from 3 to 60 mm to provide maximum contrast while preserving a whole-Sun field of view with high-density materials such as tungsten.

Two methods for imaging hard x-rays and gamma rays are coded-aperture cameras and Fourier-transform collimator cameras. We have chosen to pursue the Fourier-transform approach, illustrated in the first figure, because of its ability to provide high-spatial-resolution images with detectors having moderate or no spatial resolution. The technique utilizes an array of one-dimensional subcollimators, each measuring a different spatial Fourier component of the source. A subcollimator with a fixed-orientation provides measurements of only one spatial Fourier component. A rotating subcollimator, such as those employed with HEIDI, provides measurements of many Fourier components. In just half a rotation, a rotating subcollimator provides measurements of the spatial Fourier components covering a full range of angular orientations at a single spatial frequency.

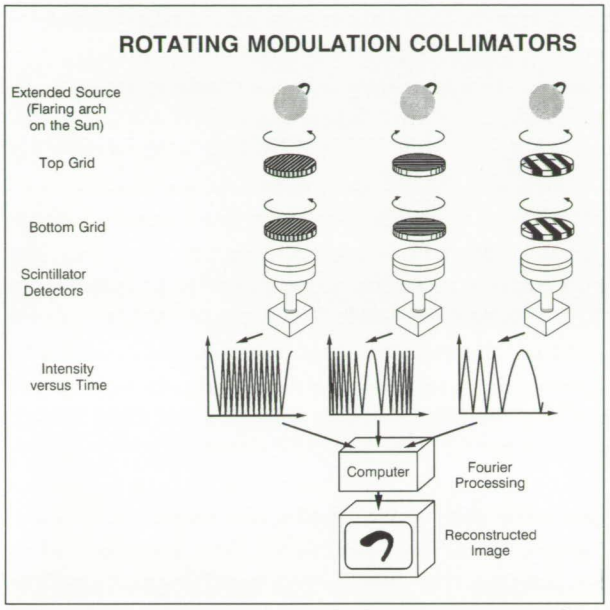

Schematic representation of the Fourier-transform technique used to obtain images of solar flares in hard x-rays and gamma rays with multiple rotating modulation subcollimators.

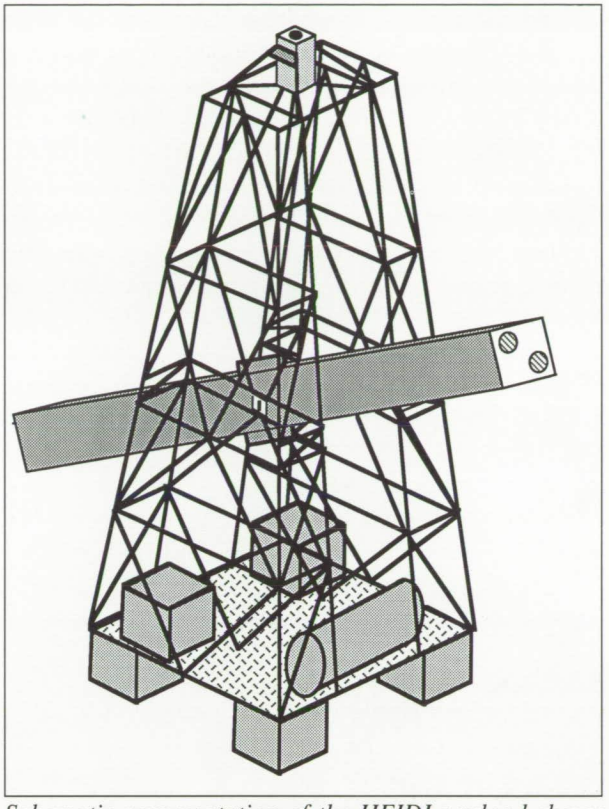

Schematic representation of the HEIDI payload shown without the rotator, crushpads, and flight-support equipment that will be provided by the National Scientific Balloon Facility.

The primary structural components of the HEIDI payload are the gondola, canister, and metering tubes illustrated schematically in the second figure. The aspect system is an integral part of the canister assembly. The purpose of the canister is to position the metering tubes with respect to aspect system components that determine the pointing axis of the telescope. The metering tubes hold the grid elements and rotate them within the canister in the careful alignment required to make x-ray imaging possible. A structural analysis of the canister/metering tube assembly indicates that deflections of the canister or the grid elements will be so small that no significant degradation of the images to be obtained during flight are expected.

The most urgent instrumental requirement for advancing hard x-ray and gamma-ray imaging of solar flares is the development of high-precision, low-cost fabrication techniques for grids used to modulate these high-energy emissions. The technique being used to fabricate the grids for the first flight of HEIDI was developed at GSFC. These grids have slit widths of 280 and 625 microns, corresponding to angular resolutions of 11 and 25 arcsec (FWHM), respectively, for a 5.2-m separation of the grids. They are being fabricated from solid pieces of tungsten alloy using conventional (die-sink) and traveling-wire Electric Discharge Machines (EDMs). The material has a density of 17.75 g/cm^3. Its composition by weight is 92.5-percent tungsten and 7.5-percent Ni/Fe. Each grid is cut from a blank which is 144 mm in diameter and 10 mm thick with a central active area 13.0 mm in diameter. A photograph of the first of the HEIDI grids to be fabricated is shown in the third figure as the slits are being cut with a traveling-wire EDM. Investigations are currently being conducted at GSFC and by our collaborators at UT Delft for grids with slit widths as fine as 50 microns.

A key objective of the first flight is to verify the imaging properties of HEIDI for a point source. This

will be accomplished with observations of the Crab nebula. Two sets of images will be made, one using data temporally phase-locked to intervals when the 33-ms Crab pulsar is on, and one when the pulsar is off. The difference in these images will represent the response to the pulsar and will be used to confirm the spatial point-response function of the system. In addition, the images themselves will provide the highest resolution maps yet obtained of the Crab nebula at hard x-ray energies.

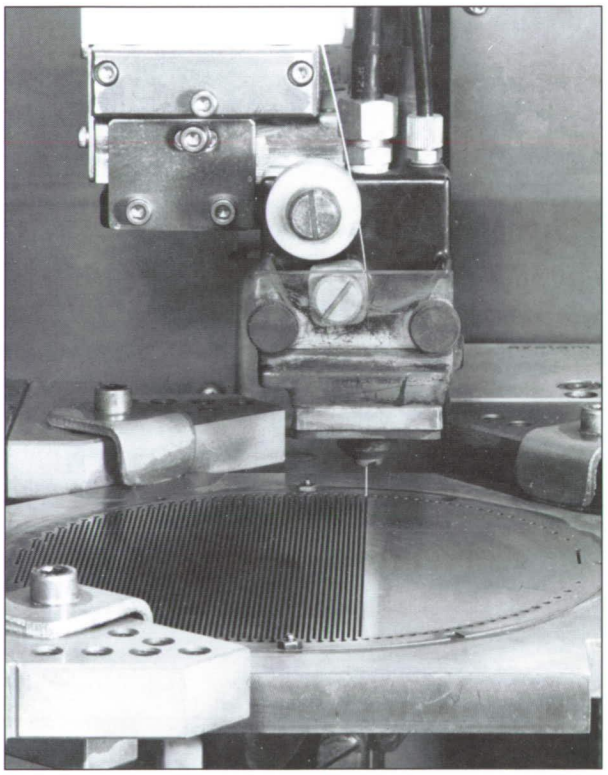

Photograph of 625-micron-wide slits being cut in a 144-mm diameter by 10-mm-thick tungsten-alloy blank with a traveling-wire Electric Discharge Machine.

An Off-Pointing Aspect System (OPAS) provides the high-resolution aspect information necessary for the Crab observations. The first component of OPAS measures the radial offset of HEIDIs optical axis with respect to Sun-center and provides the necessary real-time feedback to the pointing system. The requirements of daytime observations, arcsec precision, and modest cost-ruled-out star trackers, magnetometers, and gyros for this application. The chosen system makes use of a second lens on the front grid plate. This lens is preceded by a pair of prisms, whose orientation can be adjusted prior to launch. Because each prism deflects a beam up by 10°, their combined setting can deflect a beam to any angle within a 20° radius, as in a laser beam-steering system. For HEIDI, the prisms and the lens focus an off-axis solar image onto the solar aspect sensor. The solar aspect system then tracks the Sun while the x-ray optics view the Crab. This is possible for a 2-hour period for each day within a 40-day launch window. Notice that this system provides *relative* aspect for Crab viewing; absolute aspect is not required because the location of the pulsar is known *a priori*.

Still to be dealt with is the measurement of roll about the Earth-Sun line, which will be affected by pendulation of the suspended payload. The anticipated amplitude of pendulation is sufficiently small, ~0.1° (RMS), so that neither tracking the Crab nor the solar aspect solution will be affected adversely. Pendulation at this level, however, can seriously degrade the aspect solution for Crab observations. To remove its effects, it is necessary to monitor the roll angle of the canister about the Earth-Sun line. This is accomplished by the second component of the OPAS system, namely an off-pointing video camera which views a bright star, Sirius, whose image is recorded on a Super VHS tape recorder. Postflight analysis of the motion of the stellar image will provide a continuous record of relative roll during the 2 hours of Crab viewing. Backup transmission of the images for ground-recording will use an independent video telemetry link.

Although testing and calibration at the subsystem level will verify that critical alignment requirements have been met, a prelaunch end-to-end test of the imaging system is highly desirable. This will be accomplished by optical imaging of Sirius from the ground. For this purpose, each of the HEIDI scintillation detectors will be replaced by a photomultiplier tube, whose scaled pulse-train output will be fed into the HEIDI data system in the same manner as x-ray counts. The output of the photomultiplier tube will represent the sum of unmodulated signals from dark current and diffuse-

sky emission and the signal from the star, which will be modulated by the rotating collimators. The fixed attitude of HEIDI will be compensated for by synthetic aspect data which will account for the known sidereal drift of the star. Although the primary goal will be the recovery of the point source image of the star, analysis outputs also will include a comparison of the modulation amplitudes for the fundamental and third harmonics with the average signal enhancement as the star passes across the field of view, and the behavior of phase and amplitude response as a function of grid position angle and location of star. Additional diagnostic data can be obtained by selective masking of upper and lower grid areas.

The HEIDI team members represent a number of institutions in addition to GSFC, and bring considerable enthusiasm and expertise to this project. These include Auburn University, providing the aspect and pointing control subsystems; California Institute of Technology, providing the OPAS and image reconstruction analysis software; The Catholic University of America, providing design and analysis of gondola and canister structures; and the Naval Research Laboratory providing the detector design.

High-altitude, scientific ballooning, with its heavy-lift capability and the cost-effective approaches for the fabrication of payloads that it enables, offers unique opportunities for the development of new technologies and the pursuit of new and exciting science. Hard x-ray and gamma-ray imaging technology is now being developed with the HEIDI balloon payload. X-ray and gamma-ray spectroscopic capabilities are being developed with the High-Resolution Gamma-Ray Spectrometer (HiREGS) balloon payload that will be flown on long-duration balloon flights from Antarctica as part of NASA's Max '91 Program. Together, these technologies provide the basis for the High Energy Solar Physics (HESP) Mission that has been studied for possible space-flight opportunities during the solar maximum that will begin in approximately the year 2000.

Contact: Carol Jo Crannell (Code 682.2)
(301) 286-5007

Kenneth N. Segal (Code 752.2)
(301) 286-2895

Sponsor: Office of Space Science and Applications

Dr. Carol Jo Crannell works in the Laboratory for Astronomy and Solar Physics, Solar Physics Branch. She has 17 years of experience working at GSFC as a Civil Servant and 5 years of experience as a contractor. She received her PhD in Physics from Stanford University. She also holds a BA in Physics from Miami University.

Mr. Kenneth Segal has worked at GSFC for 6 years. He holds a BSME from the University of Maryland, College Park.

THE SUN AS A VARIABLE STAR

Twelve and one-half years of accurate measurements by the Nimbus-7 Earth Radiation Budget (ERB) experiment have demonstrated that the Sun is a low-level variable star. It has long been known that there is a solar activity cycle whose period is somewhat variable, but whose mean length is ~11 years. At the activity peak, dark sunspot groups and bright facular patches are both common; both are rare during the activity minimum. Changes in the Sun's magnetic field and far ultraviolet and x-ray radiation outputs are well-known features of the cycle. Changes in the mean total irradiance were suspected, but, due to atmospheric noise, ground-based measurements were not accurate enough to detect them. They did show, however, that any variations must be below the 1-percent level. The mean irradiance was, therefore, commonly called the "solar constant." Over the past 12 years, accurate satellite instruments demonstrated that the "solar constant" was ~0.15 to 0.2 percent larger at the peaks of solar cycles 21 and 22 than it was during the minimum activity years of 1985 and 1986.

The Nimbus-7 observations started on November 16, 1978, near the brightness peak in cycle 21. At present, we are near the peak of cycle 22. The

monthly means are shown in the first figure. March 1979 had the highest mean (1374.3 W/m^2) while the lowest (1370.9 W/m^2) occurred in January 1984. This minimum is associated with a large sunspot group that occurred near the end of the active period of cycle 21. Note that this January mean is below the normal quiet Sun measurements. The highest value shown in cycle 22 (1373.4 W/m^2) occurred for April 1991. Future measurements will tell us if this was actually the peak. General solar activity is known to vary from cycle to cycle, and it is expected that the solar irradiance cycle will show a similar variability. For comparison, the measurements made by Richard Willson of the Jet Propulsion Laboratory, with his Solar Maximum Mission (SMM) satellite experiment, are also shown for the period February 1980 through December 1988. The SMM re-entered the atmosphere and sank in the Indian Ocean on December 2, 1989, thus ending its observations. Both instruments indicate similar solar behavior. The bias between the two curves is due to uncertainties in the absolute calibration. While both sensors are stable to 0.01 to 0.02 percent, their absolute calibration is good only to a few tenths of a percent. Thus, the two sensors show good agreement within their calibration and stability limits.

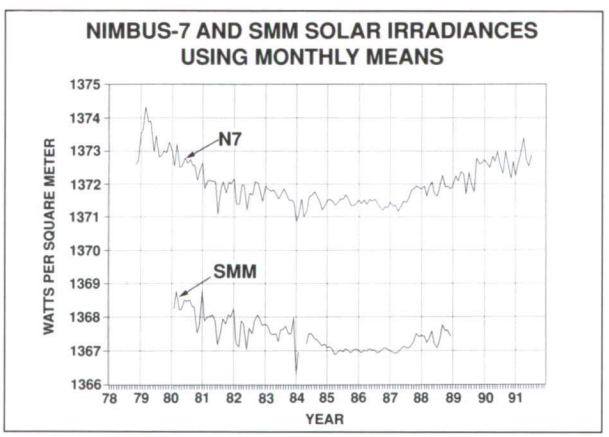

Nimbus-7 monthly means from November 1978 to July 1992 and SMM monthly means from February 1980 to December 1988.

Solar physicists, climatologists, and sensor engineers have all been very interested in the Nimbus-7 results. Solar physicists are interested in the physical causes of the variations and what this means about the Sun—its past and its future. Observations show that the Sun's brightness fluctuations are intimately connected to the general solar activity cycle. When bright faculae regions face the Earth, the received irradiance increases. When major sunspot groups face us, the irradiance decreases. In the long-term, the faculae predominate. Some investigators introduce an *X*-factor to account for brightness changes perhaps not connected with either faculae or sunspots. This *X*-factor is identified by some investigators with possible changes in the solar diameter. Spurred by the discovery of solar variability, astronomers have recently discovered similar low-level variability in a number of solar-type stars. For the moment, climatologists seem satisfied that the solar brightness range observed during the past 12 years has not greatly affected the Earth's climate. However, cyclic activity varies with time and was extremely low during the entire 17th century. Thus, past and future irradiance changes large enough and long enough to affect the climate are distinct possibilities. Both solar physicists and climatologists are anxious for the measurements to continue.

The steady degradation of the Nimbus-7 power system is expected to end that satellite's useful life sometime between 1993 and 1996. However, Richard Willson has a follow-on experiment on the Upper Atmosphere Research Satellite (UARS), launched in September 1991. A year or more of simultaneous measurements by the Nimbus-7 and UARS sensors should allow the two datasets to be accurately joined together. Thus, we can look forward to a precision solar irradiance dataset covering at least two, and hopefully many, solar cycles. Sensor scientists are anxious both to continue the measurements and to make them as accurate as possible.

Making and calibrating a fine instrument is important, but the final results depend on careful analysis of the sensor's behavior in space. The ERB Sensor Scientist, John Hickey of the Eppley Laboratory, Inc., flew a solar sensor similar to that on Nimbus-7 on the Long Duration Exposure Facility (LDEF) satellite. Recovered in 1990 after 6 years in space, it appears and tests as good as new; however,

serious problems can occur. The present ERB analyst, Douglas Hoyt, a Senior Scientist at Research and Data Systems Corporation, recently led a review of the ERB solar measurements. It was discovered that the scale measuring the angular pointing of the ERB solar telescope slipped 0.5° in July 1980 and another 0.5° in June 1986. This study resulted in the reprocessing of the data to correct this and a number of lesser problems. The old and revised results are shown in the second figure. As indicated above, the absolute value changes are rather arbitrary, but the changes in the curve shape, and the noise reduction are real and significant. In the old results, the incorrect angular information caused the irradiance to decrease too slowly in cycle 21 and to increase too rapidly in cycle 22. It also introduced arbitrary bumps in the data when the telescope was moved to track the Sun.

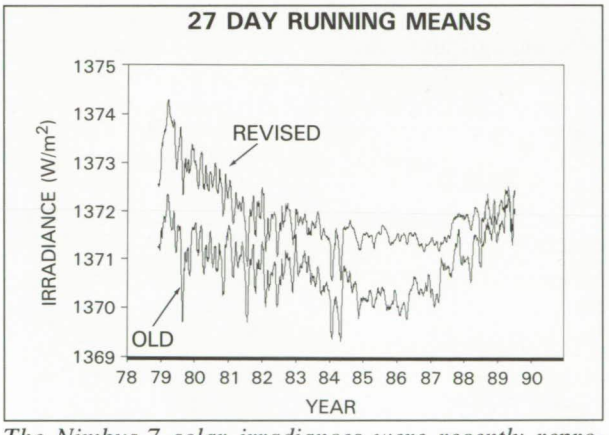

The Nimbus-7 solar irradiances were recently reprocessed because the reported pointing of the telescope was found to be in error. The old and revised values are shown here.

Careful and continuous work has given us 12½ years of excellent solar constant measurements. The new UARS experiment is expected to continue the measurements through the rest of this century. The ERB solar data are currently available at GSFC's National Earth and Space Science Data Center.

Contact: H. Lee Kyle (Code 936)
(301) 286-9415

Sponsor: Office of Space Science and Applications

Dr. H. Lee Kyle is Manager of Nimbus-7 Clouds and Earth Radiation Budget datasets preparation. Dr. Kyle, who received a PhD in Atomic Physics from the University of North Carolina, has been at GSFC for 32 years. He has received a Certificate of Outstanding Performance and a Group Achievement Award for his work.

THE 11-YEAR CYCLE OF SOLAR CONSTANT VARIATION FROM SPACECRAFT MEASUREMENTS: 1978 TO 1991

Total solar irradiance measurements from spacecraft between 1978 and 1991 show evidence of irradiance variability on several time scales, including an 11-year cycle in the solar constant of radiation (solar energy at normal incidence outside the atmosphere at the mean Sun-Earth distance).

Accurate data on the solar constant and its temporal variations are essential to solar-terrestrial research and the understanding of climate dynamics and solar physics. Changes in solar luminosity have important implications on the generation, storage, and transport of energy in the interior of the Sun and other Sun-like stars. Of more immediate importance to us, the solar constant of radiation is the primary input into the Earth's energy budget. It determines the physical state of the Earth's atmosphere and climate. To understand the Sun and its effects on the climate, the total solar irradiance has been studied extensively for over a century from ground-based measurements, and later from aircraft, balloons, rockets, and spacecraft. However, a variety of atmospheric and radiometric limitations have prevented drawing any conclusions regarding the variability in the solar irradiance. Thus, the term "solar constant" has come to mean the total solar irradiance received by the Earth-atmosphere system.

The relationship between the temporal variations in the solar constant and the Earth's climate is a much-debated topic. The cyclic variation observed since

1978 appears too small to perturb the climate system noticeably. A significant correlation between the 11-year sunspot cycle and the sea-surface temperature over the past 130 years has been reported. Accurate irradiance measurements covering several sunspot cycles are important for understanding the physical mechanisms operating on the Sun and for understanding the Sun-climate connections.

The observed solar constant cycle is positively correlated with the indices of the solar magnetic activity cycle, namely the 11-year sunspot cycle and the 2800-MHz solar flux. The amplitude of the variation in the annual mean solar constant from maximum to minimum of the solar cycle is 0.1 to 0.15 percent. The existence of solar magnetic activity-related solar constant variation has been suspected for a long time, and its observation is another connecting link in our understanding of the solar-terrestrial interactions and the energy transfer mechanisms in the solar and stellar interiors. Using data derived from three sensors on different missions (the Nimbus-7 ERB, the SMM/ACRIM, and the ERBS/ERBE), we have examined solar irradiance over an 11-year period. Differences between the three datasets include the radiometric accuracy of the sensors, the measurement frequencies, the satellite environments, and the space-flight histories.

The data from the Nimbus-7/ERB and the SMM/ACRIM have been helpful in developing models correlating the observed solar constant variations with photospheric features on the Sun. Solar constant data from Nimbus-7/ERB, SMM/ACRIM, and ERBS/ERBE measurements have been derived for the periods November 16, 1978 through May 31, 1991, February 14, 1980 through July 14, 1989, and October 20, 1984 through April 30, 1991, respectively. The three solar sensors are calibrated independently, and the values obtained from them for the solar constant are within the accuracy limits of their absolute calibrations. Examination of the monthly mean values from the three independent measurements shows similar short-term and long-term fluctuations. The ERBS/ERBE measurements do not show as many detailed variations as the Nimbus-7/ERB and the SMM/ACRIM because of the limited number of measurements obtained.

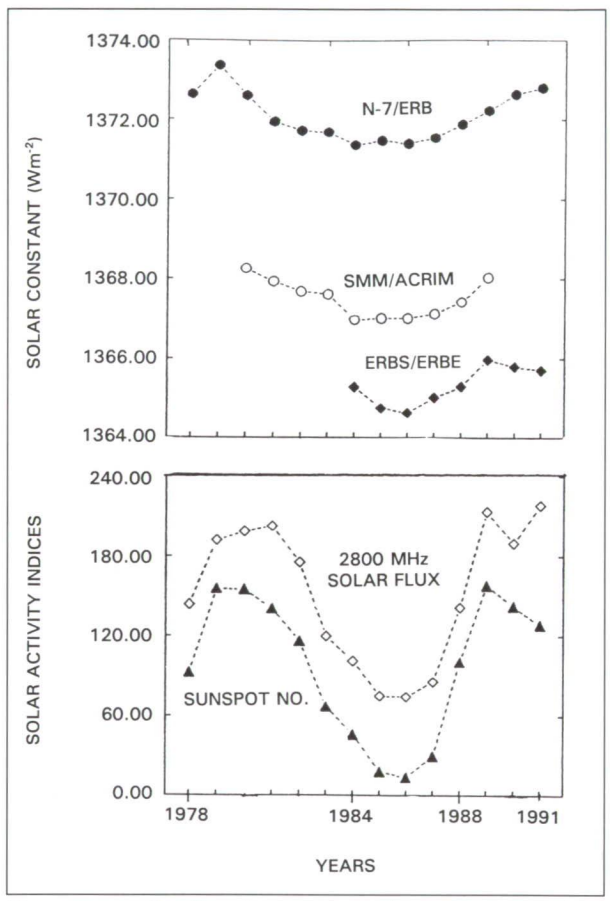

Upper panel: Yearly mean solar constant from Nimbus-7 ERB (N7), SMM/ACRIM (SMM), and ERBS/ERBE (ERBS). Lower panel: sunspot number and 2800-MHz solar flux.

During the quiet Sun period with little sunspot or faculae activity (summer of 1984 through spring of 1987), observed irradiance fluctuations were small. During the active Sun periods, variations of 0.1 to 0.3 percent occurred over periods of days and weeks. During solar cycle 21, a peak monthly mean value of 1374.31 W/m^2 was measured in March 1979; and a minimum value of 1370.85 W/m^2 was obtained in January 1984 (a difference of 0.25 percent). So far in cycle 22, a maximum monthly mean of 1373.39 W/m^2 has been observed in April 1991. The 11-year modulation is evident in the figure.

The figure shows the time series of the yearly mean solar constant, the sunspot numbers and the 2800-MHz solar flux. Annual averages of measurements for the quiet Sun period (low solar activity) of solar cycle 21 are depicted in the middle of the figure. The irradiance measurements during the active Sun periods of solar cycles 21 and 22 occupy both ends of the same graph. The effects of short-term variations are smoothed out by taking the yearly mean. The annual mean solar constants for 1978 and 1991 do not consist of 12 months of measurements. In 1978, measurements were made from November 16 to December 31, 1978. For 1991, measurements are available from January 1 through May 31, 1991.

High variabilities are observed during 1978, 1979, and 1980 in solar cycle 21, and in 1989, 1990, and 1991 in solar cycle 22. In solar cycle 21, the maximum in the yearly mean solar constant (1373.37 W/m^2) and the maximum in sunspot numbers (155.4) both occurred in 1979. The yearly maximum for the 2800-MHz solar flux occurred in 1981, 2 years later. During 1984 through 1986, a low solar constant as well as low magnetic activity levels were observed. The minimum in the sunspot numbers, 2800-MHz solar flux, and the solar constant coincided in 1986. A gradual increase in the solar constant was observed in phase with the ascending part of sunspot cycle 22. The solar constant, the yearly mean sunspot numbers, and the 2800-MHz solar flux remained high during 1989 through 1991. The sunspot maximum was observed in 1989. The maximum for the 2800-MHz flux and the solar constant appears to be approaching in 1991.

The satellite solar constant data provide important new information about the Sun. The observed 11-year solar constant cycle indicates a true luminosity change in phase with the magnetic activity cycle of the Sun. This phenomenon is also observed in older stars similar to the Sun.

Contact: Ann Mecherikunnel (Code 920.1)
(301) 286-5034

Sponsor: Office of Space Science and Applications

Dr. Ann Mecherikunnel, Principal Investigator on the ERBE Science Team, is interested in solar total and spectral irradiance, the Earth radiation budget, and the EOS calibration and data validation studies. She has 17 years of experience at GSFC, and has received two Group Achievement Awards for her work.

PUZZLE OF SOLAR/PLANETARY DIFFERENTIAL ROTATION

Everybody knows about the colorful bands seen in the atmosphere of Jupiter. Data from the Voyager spacecraft tell us that these bands delineate regions of strong winds (~100 m/s) blowing alternately in the east and west directions. Not as well-known, however, is that in the atmosphere of the Sun, similar (but fewer) strong winds also blow in the east and west directions. Traditionally, solar physicists do not refer to winds but to differential rotation, because observationally the phenomenon is manifested by different rotational periods at different latitudes, inferred from tracing sunspots or measuring Doppler shifts. Specifically, one observes that the rotational periods around the solar equator are substantially shorter (~25d) than those at high latitudes (~29d). Besides Jupiter and the Sun, Saturn and Neptune also reveal alternating winds; an important characteristic common to all these atmospheres is that they are convectively unstable due to internal heating and energy convection out of the interior.

The phenomenon of differential rotation or alternating zonal east-west winds in planetary atmospheres and in the Sun has attracted much interest, and several explanations have been put forth. One of the earliest models, and for some time the prevailing one was based on a well-known hydrodynamics theorem, proven three-quarters of a century ago by G.I. Taylor, and independently, by J. Proudman, which applies to an inviscid fluid on a rotating shell. Under this condition, the Coriolis force dominates, and the fluid along any line parallel to the rotation axis must move in unison on a

cylindrical surface, according to the theorem. This so-called Taylor-column model conceives that convection cells are arranged in arrays of north-south columns, and that differential rotation is generated as a secondary zonal flow. As a result, the surfaces tracing constant angular velocities must lie on cylinders parallel to the rotational axis. While this model has only been applied heuristically to planets, it has been applied to the Sun through elaborate numerical simulations. The numerical models more or less reproduced the differential rotation observed at the solar surface, and the computed flows inside were indeed columnar.

For a while, the problem of solar differential rotation seemed to have been settled. However, the recent results from helioseismology have changed the picture completely. Helioseismology, a powerful new technique developed during the last 2 decades, has produced some of the most important advances in solar physics. By observing the mechanical oscillations of the Sun, it is possible to make inferences about the interior, much like using terrestrial seismic data to study the interior of the Earth. Through the analysis of the symmetry-breaking effects of rotation in a large number of oscillatory modes, a discriminating picture of the angular velocity distribution inside the Sun emerged. According to these observations, surfaces of constant angular velocity tend to lie along radial directions and not in the direction of the solar rotation axis. The Taylor-column model of differential rotation in the Sun, therefore, has essentially been ruled out. Serious doubts have also been raised about similar models applied to the planets.

Why did the Taylor-column model fail? What was wrong with the numerical simulations of the solar convection region? Recent research suggests some answers and argues that the conditions for the validity of the Taylor-Proudman theorem are not satisfied in the solar and planetary atmospheres, because of the compressibility of the fluid and the significance of the buoyancy force. In fact, the buoyancy force arising from the convective instability has been shown to be extremely important in an earlier model of Jovian circulation proposed by Mayr, Harris, and Chan (hereinafter referred as MHC). The degree of convective instability determines the wind pattern. For the solar atmosphere, a numerical computation of this instability would be extremely difficult, requiring orders-of-magnitude faster computers than presently available, if indeed a brute-force approach can be applied.

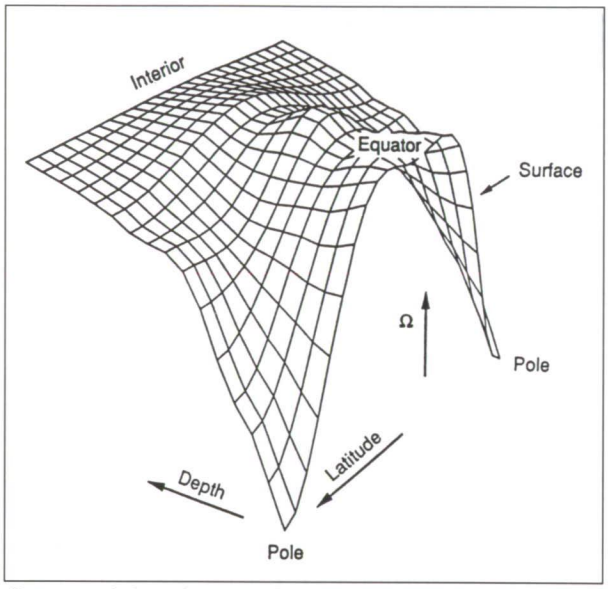

Computed distribution of angular velocity for the solar convection region, plotted versus latitude and depth.

Presently, however, it is possible to study the problem with a semianalytical model like that of MHC. Instead of computing one distribution of differential rotation for one case of convective instability (which is poorly determined), such a model can be used efficiently to explore a wide range of parameters to search for a promising solution. In contrast to the Taylor-column model where the Coriolis force completely dominates, the MHC model requires that both the buoyancy force and the Coriolis force are essential in determining the angular velocity distribution.

Applying the MHC model to the case of the Sun gives surprisingly good results. The computed surfaces of constant angular velocity are more or less radial, similar to those derived from helioseismology. For the convenience of presentation, the computed angular velocity as a function of latitude and depth is shown in the first figure as a surface plot. For

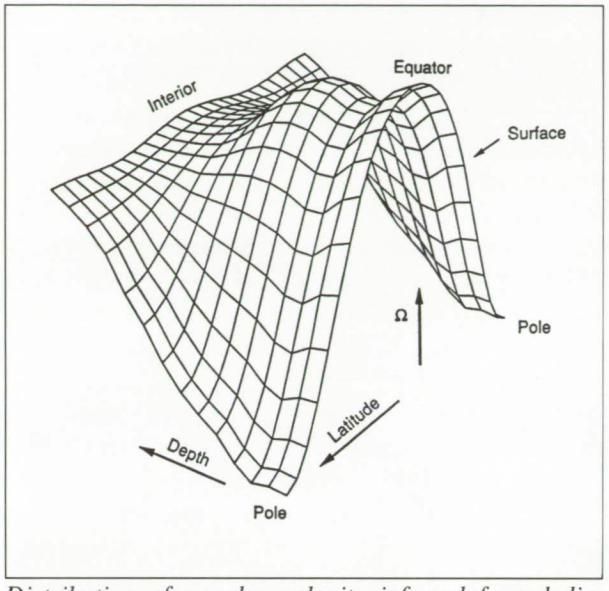

Distribution of angular velocity inferred from helioseismology.

comparison, observational data obtained by other workers are shown in the second figure. The distributions are quite similar, demonstrating the potential of this model.

Contact: Hans G. Mayr (Code 914)
(301) 286-7505

Kwing L. Chan
Applied Research Corporation
(301) 286-5216

Sponsor: Office of Space Science and Applications

Dr. Hans G. Mayr received a PhD from the University of Graz, Austria. He is an Atmospheric Scientist with the Dynamics Explorer and Pioneer Venus projects and has 23 years of experience at GSFC.

Dr. Kwing L. Chan, a Computational Astrophysicist with Applied Research Corporation, is involved in solar and planetary research. Dr. Chan received his PhD from Princeton University and has worked at GSFC for over 12 years.

Planetary

para HYDROGEN ON JUPITER

Molecular hydrogen is the primary constituent of the atmospheres of the outer planets. The collision-induced absorption of energy by hydrogen is the dominant source of thermal opacity and is of special interest in planetary modeling. Radiatively, the *ortho* and *para* hydrogen states, which form the S(0) and S(1) rotational lines of hydrogen, behave as a mixture of two separate gases with the S(0) line near 360 cm^{-1} formed by transitions between *para* levels (even rotational quantum numbers), and the S(1) line near 590 cm^{-1} originating from transitions between *ortho* levels (odd rotational quantum numbers). The diminutive feature near the center of the S(0) line at 354 cm^{-1} is due to the bound-free transitions of the hydrogen dimer. It has been common practice in planetary modeling to neglect the absorption provided by the dimer. Nevertheless, as shown in the figure, absorption by the dimer not only accounts for the characteristic features at 354 cm^{-1}, but noticeably alters the continuum in the neighboring spectral region.

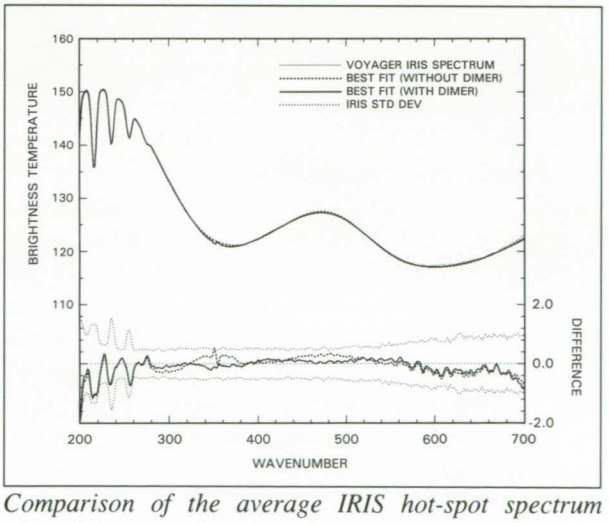

Comparison of the average IRIS hot-spot spectrum (dotted line) to best-fit synthetic spectra calculated without (dashed line) and with (solid line) the inclusion of dimer absorption.

Previous investigations of Voyager Infrared Interferometer Spectrometer (IRIS) observations have revealed that the Jovian *para* hydrogen fraction is not in thermodynamic equilibrium near the NH_3 cloud top. This implies that a vertical gradient exists between the cloud-top values measured by Voyager and the high-temperature equilibrium value of 0.25 at lower depths. Massie and Hunten have reviewed known equilibration processes and concluded that catalytic reactions between free-radical surface sites of aerosol particles and hydrogen molecules are responsible for the partial equilibration of *ortho-para* hydrogen in the Jovian atmosphere. In contrast, Conrath and Gierasch concluded, based on an apparent lack of correlation between cloud indicators (i.e., albedo and 5 μm-brightness temperatures), that catalysis of *ortho-para* conversion does not occur on cloud particles. Instead, they proposed H_2-H_2 paramagnetic interactions as the dominant equilibration process at all levels of the Jovian atmosphere. If the Massie and Hunten model is correct, then there should be a correlation between the location of the *para* hydrogen gradient and the NH_3 cloud, and a correlation between the optical depth of the NH_3 cloud and the degree of equilibration. In contrast, if the Conrath and Gierasch model is correct, then there should be no correlation between the NH_3 cloud and the *para* hydrogen gradient.

We have retrieved the height-dependence of the *para* hydrogen profile for a wide range of Jovian atmospheric conditions (spectral ensembles) using an anisotropic multiple-scattering radiative transfer model. Thermochemical equilibrium calculations were performed to determine the cloud-base locations and to ensure consistency between the clouds and the vapor profiles. At lower depths, the *para* hydrogen fraction has the high-temperature equilibrium value of 0.25. The specification of the inflection points, P_L and P_U, defines the gradient of the hydrogen *para* fraction between the deep atmosphere value below P_L and the more equilibrated value above the P_U pressure level.

As an illustrative example, we show a height-dependent *para* hydrogen profile retrieval using the IRIS measurements of the North Equatorial Belt (NEB) hot spots, which are regions of minimum cloud opacity. In hot spots, the NH_3 cloud forms near 0.5 bar with a total optical depth of 0.27 referred to visible wavelengths. The figure shows the comparison between our best-fit synthetic spectra calculated with (solid line) and without (dashed line) the inclusion of the hydrogen dimer and the average NEB hot-spot spectrum (dotted line). Inclusion of the hydrogen dimer significantly improves the fit in the region between 280 and 380 cm^{-1} as can be seen in the difference plot (synthetic - IRIS) in the lower portion of the figure. Moreover, since the noise-equivalent radiance of the average spectrum is only of order 0.1 K, (i.e., much smaller than the spatial variability of the hot-spot measurements), the improved treatment of the hydrogen absorption now allows us to model the far-infrared IRIS measurements to within the limits set by instrumental noise.

We find that for NEB hot spots, the *para* fraction increases from 0.25, at pressures greater than 0.5 bar, to 0.32 at 0.2 bar. This vertical association between the location of the *para* hydrogen gradient and the location of the NH_3 cloud layer provides support for the Massie and Hunten model. Moreover, we find, based on our analysis of colder spectral ensembles, that there is a positive correlation between the degree of equilibration and the optical depth of the NH_3 cloud. Finally, the increased height discrimination provided by the hydrogen dimer strengthens the conclusion that paramagnetic interactions on NH_3 particles, as suggested by Massie and Hunten, are the dominant equilibration mechanism in the upper troposphere of Jupiter.

Contact: Barbara E. Carlson (Code 940)
(212) 678-5538

Sponsor: Office of Space Science and Applications

Dr. Barbara E. Carlson, a scientist at the Goddard Institute for Space Studies for 5 years, specializes in radiative transfer in planetary atmospheres. She has a PhD from the State University of New York at Stony Brook.

LINE COUPLING IN RAMAN SPECTRA

Optical techniques continue to play an important role in diagnostic measurements in environments where conventional transducers cannot be utilized. In particular, Coherent Anti-Stokes Raman Spectroscopy (CARS) has been recognized as the most reliable approach to temperature measurement in a large variety of applications such as studies of internal combustion and jet engines, flames, plasmas, and industrial furnaces. These environments are high in temperature, spatially inhomogeneous, rapidly changing, chemically harsh, and susceptible to disturbance by the presence of a physical probe. Confidence in this technique requires appropriate understanding of the nonlinear processes that generate a CARS spectrum and of the performance of the optical systems used in the measurements (i.e., the instrument function for the system). It also requires a comprehensive theory to predict the temperature, pressure, and composition dependence of the third-order (CARS) susceptibility (i.e., the spectral distribution function (line shape)). It is the latter that provides the basis for analysis of the measured spectrum in terms of quantities such as temperature and density.

The CARS spectra used for thermometry have closely spaced rotational lines that are usually overlapped at pressures of interest, so collisional transfer of intensity is of particular concern. Parameters for this phenomenon, unlike line widths for isolated lines, cannot be extracted easily from experimental data. The same phenomenon is important in the transmission of radiation through planetary atmospheres, including greenhouse effects, and lack of knowledge of these parameters is currently an impediment to such studies as well.

The theory underlying spectral line formation relies on the kinetic theory of gases to simplify the many-body nature of the macroscopic sample to an understanding of microscopic interactions among a few molecules. Actual computations require a detailed knowledge of the intermolecular forces and resulting molecular collision dynamics. It is important to note that, for the weakly polar and nonpolar systems of interest in CARS diagnostics, only very recently have theory and computational capabilities progressed to the point that first-principle calculations of broadening, shifting, and collisional narrowing been made with accuracies comparable to those of state-of-the-art spectral measurements. However, results of these studies do support the basic line formation theory upon which our understanding and empirical models rest.

One of the most exciting and encouraging comparisons made to date between theory and experiment is for the system CO:He. Accurate measurements of CARS Q-branch spectra of CO in a bath of He have recently been obtained by workers at NIST. The measurements span a range of pressures from <1 atmosphere, where the spectrum is well described by a sum of noninteracting Lorentzian lines for each rotational level, to several atmospheres, where rotational structure is completely unresolved and collisional transfer of intensity is crucial for describing the line shape.

We have carried out a corresponding theoretical study. This study required the proper incorporation of three distinct branches of theoretical physics that converge in this process: molecular structure theory, to generate an accurate interaction potential; converged coupled channel solution of the quantum mechanical scattering equations, to describe binary collision dynamics; and kinetic theory, to relate line shapes to the resulting collisional scattering matrices. The theoretical interaction potential, computed for this system some time ago, had been previously used by us to calculate collisional excitation rates needed to interpret astrophysical observations in the microwave spectral region. Experimental and theoretical results are compared in the figure for two pressures, two atmospheres where rotational structure is partially resolved, and six atmospheres where lines are completely overlapped. Agreement is quite good—to within a few percent. It should be emphasized that theoretical results were obtained entirely from first principles with no adjustable parameters. To demonstrate the importance of line coupling, the spectrum predicted by a sum of appropriately broadened, but noninterfering

Lorentzian lines is also shown in the figure; the inadequacy of this approximation is clearly seen. The importance of line coupling can be seen by comparing with the sum of noninteracting Lorentzian lines which is also shown. The latter curve has been scaled downward so that it matches the full line coupling theory at high J values (low frequencies).

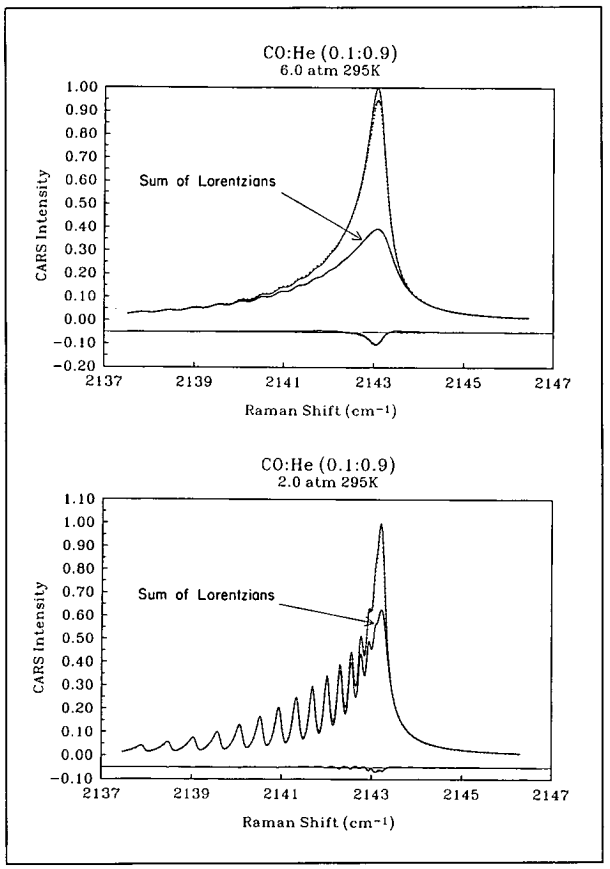

Comparison of theoretical (solid lines) and experimental (dots) Raman Q-branch spectra for CO in He at 2 and 6 atm. Deviations (theory minus experiment) are shown on the shifted lower axis.

This work is being extended to line shapes in CARS spectra of hydrogen molecules which may be useful for remote sensing of pressure as well as temperature. Recent experimental data for these show anomalous behavior which is not yet well understood and which may require extensions of the fundamental theoretical framework. It is also being extended to line shapes of terrestrial atmospheric gases.

Contact: Sheldon Green (Code 940)
(212) 678-5562

Sponsor: Office of Space Science and Applications

Dr. Sheldon Green received a PhD from Harvard University. He specializes in theoretical chemistry and molecular physics. He has been with NASA since 1978.

CASSINI/HUYGENS GAS CHROMATOGRAPH-MASS SPECTROMETER INSTRUMENT

The Cassini mission is designed to permit a detailed, second-phase exploration of the Saturn/Titan system. Cassini is a joint NASA/ESA mission for which NASA is providing the planetary orbiter, Cassini, and the European Space Agency (ESA) is contributing the Titan atmosphere entry probe, Huygens. The Cassini mission will give clues to the understanding of the processes associated with the formation and the evolution of a planetary system and of the solar system as a whole.

The analysis of the composition of Titan's atmosphere is one of the most important goals of the Cassini-Huygens Mission. Because its composition is dominated by nitrogen with a significant mole fraction of methane and a low mole fraction of hydrogen, Titan's atmosphere is one of the most favorable for the synthesis of gas-phase compounds as well as polymerized organic particulates (aerosols). The scope of this investigation is unusually large, as it includes the determination of noble gas abundances, isotopic ratios, and the identification of high-molecular-weight organic compounds in trace quantities. Despite the great success of the Pioneer and Voyager missions, even the relative abundances of major constituents of Titan's atmosphere are poorly known, while the opportunities for minor constituent formation in this evolving atmosphere are so rich that it is not possible to predict with certainty just what substances to seek.

The payload addresses this challenge with a variety of instruments on the probe and the orbiter. A versatile, sensitive gas chromatograph-mass spectrometer on the probe is essential to the success of this strategy. A gas chromatograph-mass spectrometer (GC-MS) instrument is being developed for the Huygens Probe by the Atmospheric Experiment Branch of the Laboratory for Atmospheres at GSFC; Dr. Hasso B. Niemann is the Principal Investigator. This instrument provides in situ chemical composition data, over a mass range from 2 to 146 amu, of the atmosphere along the track of the probe descent and a context for the results obtained by the remote sensing experiments. Using the best current models for the atmosphere of Titan, measurements made by the instrument will be used to determine the major isotopes of carbon, nitrogen, hydrogen, oxygen, and argon.

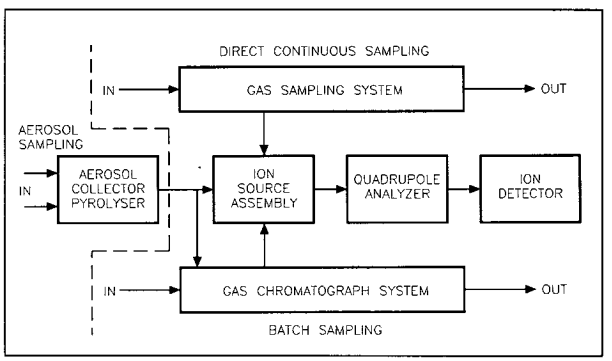

Block diagram of the Huygens Probe Gas Chromatograph-Mass Spectrometer system layout.

With a dynamic range of 1 x 10^8, the GC-MS can detect neon and the other noble gases to levels of 10 to 100 ppb. The abundance of carbon monoxide can be traced, resolving present uncertainties about possible altitude variations in the mixing ratio of this important oxygen-containing gas and the necessary data required can be gathered to determine its source(s) and sink(s). Similarly, vertical variations in mixing ratios of various organic compounds can be used to delineate the chemical processes leading to their formation. A search for new constituents (including unpredicted ones) will be conducted to a level of 10 ppb, identifying them with the aid of a computer-based library of the mass spectra of thousands of organic compounds.

The prime function of the Huygens Probe GC-MS instrument will be to perform a detailed chemical analysis of the gas-phase compounds in Titan's atmosphere. The mass spectrometer (MS) will continuously sample the ambient gases as the probe falls toward Titan, while the gas chromatograph (GC) samples are periodically collected and processed. The system operation concept is shown in the first figure. The second figure represents a more detailed schematic diagram of the key GC-MS instrument components. The view included in the third figure indicates the complexity of the instrument and includes all components except the inlet and outlet tubing, flow line interconnections, and the electronics system.

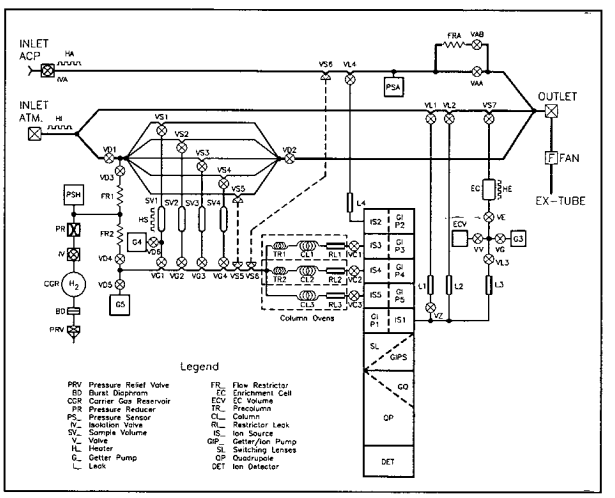

Schematic diagram indicating key elements of the Huygens Probe Gas Chromatograph-Mass Spectrometer Instrument.

A companion instrument, the Aerosol Collector and Pyrolyzer (ACP), uses the GC-MS to chemically analyze its samples; Dr. Guy Israel is the Principal Investigator. The ACP is being developed at the Service d'Aeronomie du CNRS (S.A., CNRS), Verrieres-le-Buisson, France. The companion ACP instrument uses filters to collect particulates from the aerosol-containing atmosphere. Pyrolysis breaks down the sample and the resulting gases are batch transferred to the GC-MS instrument for chemical makeup analysis. By analyzing the output of the ACP, it will be possible to study the end-products of the atmospheric chemistry of Titan.

C-2

If the probe survives the landing, the heated inlet of the GC-MS will vaporize volatile materials on the surface at the impact point, allowing the instrument to identify the resulting gases. The analysis will provide an exploration of the relative importance of aerosol deposition, vapor condensation, and endogenic processes and materials at the landing site.

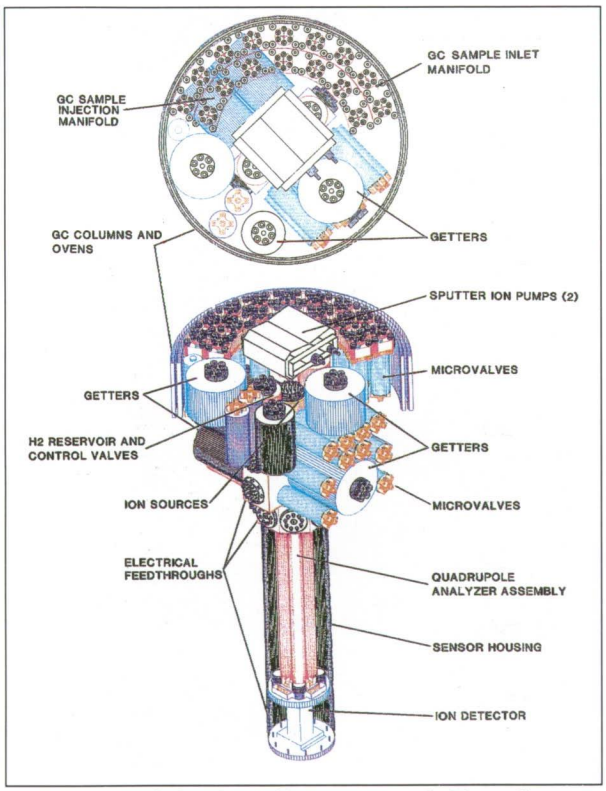

Illustration of the Gas Chromatograph-Mass Spectrometer configuration.

The GC-MS instrument has six main elements:

- The MS system that consists of multiple ion sources, a mass analyzer, and an ion detector to permit species concentration measurements to be made. Chemical (getter) and electronic (ion) pumps are used to maintain the vacuum needed for MS system operation.

- The gas sample inlet system that reduces the ambient atmospheric pressure to a lower value that is acceptable for proper operation of the MS ion source. As shown in the second and fourth

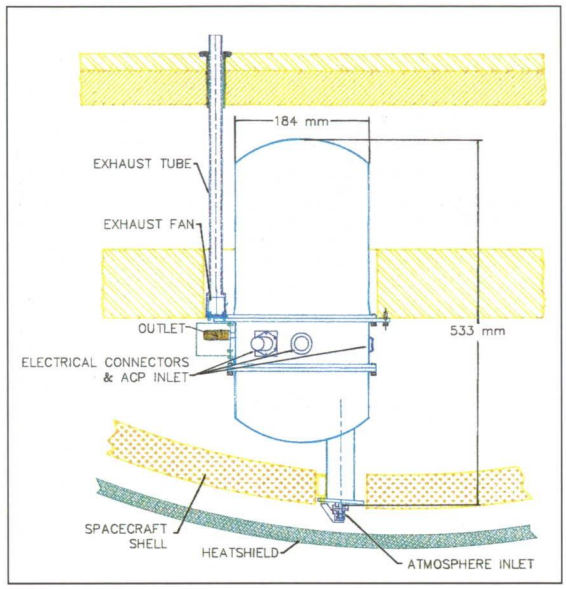

Line drawing of the GC-MS Instrument mounted in the shell of the Huygens spacecraft descent module.

figures, the ambient gases are sampled beyond the spacecraft's stagnation point, enter the instrument via metal tubing, are vented within the body of the spacecraft; a fan is used to ensure an adequate flow of gas through the inlet system. Special miniaturized valves are used throughout the instrument to control the gas flows. The sample gas inlet is positioned at the atmospheric stagnation point and the sample gas is vented directly into the spacecraft body.

- The batch sample enrichment system that increases the measurement capability of the instrument by selective physical and chemical treatment of atmospheric samples to enrich their concentration prior to their introduction into the ionization region of the ion source.

- A multicolumn GC that increases the measurement capability of the instrument by batch sampling at specific points in the atmosphere and subsequent time separation of species with different chemical properties for detection and identification and analyses by the MS. Hydrogen is used as the GC carrier gas because it can easily be removed by the getter and ion pumping system.

- The sample transfer system for the gas mixtures generated by the ACP to the GC-MS sample inlet system.

- The electronics systems, including a minicomputer, required to operate and sequence the instrument as well as to format and to output the resulting data with the probe's telemetry system.

Contact: John Haberman (Code 915)
(301) 286-4344

Sponsor: Office of Space Science and Applications
Laboratory for Atmospheres

Dr. John Haberman has been a Space Scientist in the Atmospheric Experiment Branch at GSFC for 11 years. His interests include the composition and chemical kinetics of planetary atmospheres and development of instrumentation to measure these parameters. He is currently involved with monitoring the health of the Galileo Probe Mass Spectrometer and is participating in the development of the Huygens Probe GC-MS. He earned a PhD in Physical Chemistry from the University of Wisconsin.

LONG-DURATION ANTARCTIC MARS INSTRUMENT CALIBRATION BALLOON PROJECT

An Antarctic long-duration balloon flight project has been established at GSFC for the evaluation and calibration of remote sensing Gamma-Ray Spectrometer (GRS) systems used on Planetary Science Space Exploration Missions. This is a joint effort with the Vernadsky Institute of Geochemistry, Moscow.

Remote sensing GRS systems have been used previously to determine elemental surface composition from measurements of gamma-ray and neutron spectra taken while in orbit around planetary bodies. Future space-flight missions also will include GRS instruments. GRS instruments have been flown aboard several U.S. and Soviet Lunar and Mars Missions such as the recent Soviet Phobos Mission. The next-generation GRS is presently under construction for the Mars Observer Mission scheduled for launch in 1992. Analogs of the instruments from both the U.S. and the Soviet Mars Missions will be part of a balloon instrument payload (see figure) scheduled for launch in December 1992 from Williams Field, Antarctica. Their cross-calibration should greatly facilitate both the engineering and science data analysis. Studies of charged and neutral particle backgrounds as well as detector radiation damage effects will be conducted on this flight.

The first successful planetary science balloon flight was conducted out of Palestine, Texas in May 1984 using a payload previously flown for solar flare observation. High-resolution gamma-ray spectra from a large soil sample were obtained. Approximately 4 hours of measurements were made, 3 hours with the sample in position, and 1 hour of background. Weather conditions greatly limited the measurement time during the flight. Detailed analysis was obtained only for the natural radioactive elements. It was clear from these data that an observation time of many days would be required to obtain a more complete elemental analysis. Therefore, it is desirable for the flight that is being planned to have about a week for acquisition of soil data and a comparable time for background data acquisition.

The primary science objective of the mission under discussion here is to collect gamma-ray spectra from a soil sample whose composition is a reasonable analog of the Martian surface materials, while in a somewhat Mars-like radiation environment. The soil weight will be about 1,500 pounds out of a total payload of 4,000 pounds.

The Earth's atmosphere, all materials on the payload, and especially the gondola structure, constitute a source of gamma-ray background that must be separated from the soil spectra. To accomplish this the soil will be moved out of the field of view of the instruments so that a background spectrum can be taken. The soil will not be dumped at this point so

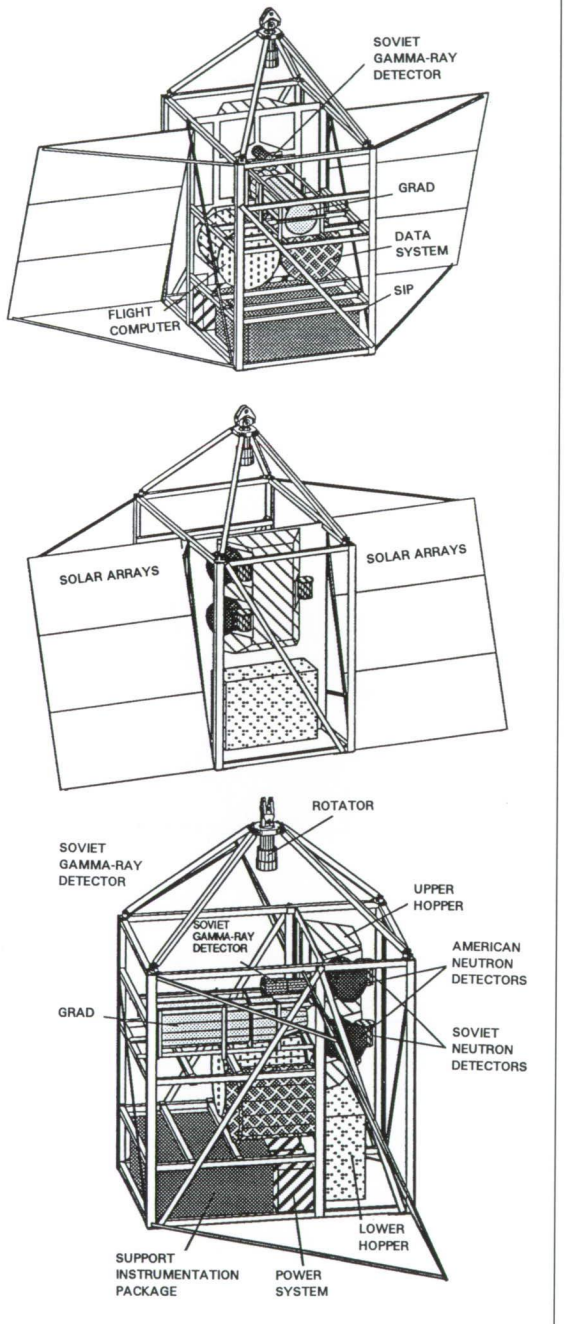

Analogs of the instruments from both the U.S. and the Soviet Mars missions.

as not to change the payload altitude. Analysis of soil together with background data will provide accurate soil composition estimates. Later, toward the end of the flight, the soil will be dumped to lighten the gondola for landing and recovery.

The suitability of Antarctic balloon flights for planetary science was amply demonstrated when a 3-day-duration balloon flight with a GRS instrument on board was successfully flown in January 1988 from Williams Field, Antarctica. The paramount purpose of this flight was for astrophysical measurements of Supernova (SN)1987A. This flight, and a 10-day circumpolar flight in December 1990, demonstrated that the Antarctic is an excellent locale for performing long-duration balloon flights. Previous international agreements and the lack of national boundaries on this large continent also make an Antarctic flight attractive from a project-management standpoint.

The severe weather conditions of the Antarctic preclude a high assurance of payload recovery. With this in mind, the payload will be designed with multiple means of recovering the science data. Primary data storage will be accomplished with a dual-redundant Write Once Read Many (WORM) optical disk system. A second means of data recovery will be the continuous, real-time data transmission to the U.S.'s McMurdo Station or any station capable of receiving them. The third data recovery system will be a high-speed data link allowing data dumps to an aircraft during occasional underflights. Once the flight has been terminated, spotting the downed payload in the vast wasteland of the Antarctic could be a considerable problem. The payload will have visual aids such as strobe lights and possibly dye markers or smoke bombs to aid in finding the payload once it is on the ground. However, complete recovery of the payload may prove extremely difficult because distance or weather conditions may limit the time the recovery team has on the ground. For this reason, the gondola will be designed with quick-release systems that will allow relatively easy retrieval of the optical disk and instrumentation even if the complete payload cannot be recovered.

Contact: J. I. Trombka (Code 691)
(301) 286-5941

L. G. Evans
Computer Sciences Corporation
(301) 286-5759

S. R. Floyd (Code 691)
(301) 286-6881

R. Starr (Code 682.2)
(301) 286-5073

Sponsor: Office of Space Science and Applications

Dr. Trombka is the Principal Investigator on the LAMB Project, and works in the Laboratory for Extraterrestrial Physics at GSFC. He received his PhD in Nuclear Science from the University of Michigan. He has 26 years of experience at GSFC.

Dr. Larry Evans has been a participant in the Apollo, Comet Rendezvous and Asteroid Flyby, and Soviet Phobos projects, and is a co-investigator on the LAMB Project. He has earned a BS and MS from Purdue University, and a PhD from Northwestern University. He has 14 years of experience at GSFC.

Mr. Samuel R. Floyd is the Project Instrument Manager and a Co-investigator on LAMB. He has earned BS and BA degrees from Minot State University, and an MS from The Johns Hopkins University. He has 11 years' experience at GSFC.

Dr. Richard Starr is the Co-Investigator on the LAMB Project in the Laboratory for Astronomy and Solar Physics. He received a PhD from the University of Illinois, and has 11 years of experience at GSFC.

PLANETARY ZONAL CIRCULATIONS

The Voyager encounter with Neptune has brought many discoveries, among which is a surprise found in Neptune's atmosphere: the observation of a strong zonal circulation in the longitudinal direction, as revealed by the imaging experiment. Storm-like features were observed circling the planet, with wind speeds ranging from 300 m/s westward (opposite to the planetary rotation) at low latitudes, to 100 m/s eastward at high latitudes. What is surprising about these velocities is that they are among the highest observed in planetary atmospheres, contrary to expectations based on energetic considerations. Neptune is known to have an internal heat source and radiates energy at a rate comparable to that received from the Sun; compared with Venus, Earth, and even Jupiter, these energies are very small, down by as much as a factor of 1000.

Across a range of different planets, zonal wind velocities observed at cloud levels are typically on the order of 100 m/s. This is perplexing considering the wide range of conditions encountered. Venus is a solid planet, close to the Sun, rotating very slowly; Jupiter is a large gaseous planet with an entirely different composition, farther away from the Sun, and rotating rapidly; and Neptune, another gas giant, has zonal winds that are relatively large although the planet is farthest away from the Sun. This behavior of atmospheric circulations may be coincidental, but we present here a heuristic argument that may provide some unifying understanding. We also present results from a numerical model that applies to a Neptune-like atmosphere.

One may view the atmosphere as a heat engine in which the circulation is driven by some source, such as solar radiation or another form of energy from the planetary interior. Presumably, the energy that drives the circulation also drives the eddies that dissipate the energy, and the resulting wind velocities then would tend to be independent of the source. The question is not so much where the energy comes from, but how that energy is dissipated.

To address this question, it is helpful to consider a simple model, in which the variables are averaged over longitude. Given a heat source, we know that it can drive a meridional circulation in the north-south direction that redistributes angular momentum. For dissipation, eddy diffusion is introduced phenomenologically. In the framework of such a model, the vertical diffusion of momentum in the zonal velocities (east-west direction) then balances

the advection of angular momentum carried by the meridional circulation (north-south direction).

On Venus, where the rotation rate of the atmosphere is much larger than that of the planet, advection by the meridional circulation and diffusion both work on the same zonal velocities. Thus, the two are related, and this can provide estimates for the eddy diffusion rates in a mixing-length formulation. Energy and momentum transports are closely tied together; our analysis indicates that the mixing length formulation for the eddy diffusion rate is also consistent with energetic considerations in general, not just for conditions that apply to Venus.

With the above mixing-length formulation for diffusion, one obtains an expression for the zonal velocity that does not depend on the heat source, the rotation rate of the planet, or its size. The zonal velocity is proportional to the speed of sound. It increases with the depth of the circulation, and with the vertical gradient of the potential temperature, and decreases with increasing importance of radiative cooling. This trend is consistent with planetary observations.

It is necessary to distinguish between two kinds of zonal circulations. In the case of Venus, the observed zonal velocities are in one direction and vary gradually with latitude. In the other case to be discussed here, that of Jupiter, Saturn and Neptune, the zonal velocities alternate direction with latitude; this phenomenon is not understood. These outer planets, unlike Venus, have an internal heat source that is important relative to the solar input. Thus, energy is transported or convected to higher altitudes where it can be radiated away. In such an environment, the upward motions, for example, in the meridional circulation, supply energy instead of removing it. This process is in the opposite direction to that of eddy diffusion and the two can cancel each other. Cancellation occurs preferentially for a particular horizontal wavelength which is characterized by alternating zonal jets, qualitatively consistent with the observations.

This effect can be described with a two-dimensional model. The figure shows a solution that applies to a Neptune-like atmosphere, with a minimum temperature of 80 K at the tropopause (3400 km). Below that level, the atmosphere is convective, which accounts for the alternating zonal winds. A heat source that peaks at the poles is used to drive the retrograde motions, and eddy diffusion rates are prescribed. At lower altitudes, we see that the zonal wind velocities are relatively large near the pole compared to the equator, and the zonal jets alternate direction. At higher altitudes, however, this effect gives way to a structure in which the winds are much larger closer to the equator, while the wind reversal near the pole is comparatively small. This is qualitatively consistent with the Voyager observations of Neptune.

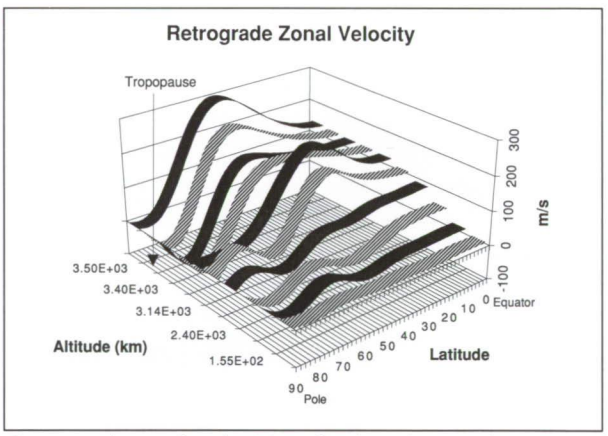

Computed zonal velocities displayed as a function of latitude and altitude.

In general, planetary atmospheres, and in particular those of Earth, Venus and Jupiter, tend to superrotate (i.e., the zonal velocities are in the direction of planetary rotation). This may be explained by preferential solar heating at low latitudes. Uranus is an exception, however, in that the observed wind velocities show a trend suggesting subrotation near the equator, but superrotation is observed in the southern hemisphere.

Among the outer planets, Uranus is the only one that does not have a strong internal heat source; solar heating dominates. Moreover, unlike all the other planets, its rotation axis lies in the orbital plane around the Sun, and the polar regions experience large seasonal variations in solar heating that can

produce large seasonal variations in the zonal velocities. Neptune's atmosphere, on average, subrotates, different from Jupiter and Saturn. But compared to these planets, Neptune has a stronger internal heat source relative to the solar input. Conditions there might be closer to those in the Sun, which also appears to subrotate when compared to the interior and averaged over the globe.

The model presented here is mainly diagnostic in nature. The proposed mixing-length formulation for the diffusion rates is incomplete; it does not provide an explicit mechanism for transferring or dissipating energy and momentum. Thus, we cannot explain why the zonal velocities have the magnitudes observed. Even if the winds are capped by the sound velocity as our analysis suggests, we still do not understand the underlying processes, which are probably strongly nonlinear.

Contact: Hans G. Mayr (Code 914)
(301) 286-7505

Isadore Harris (Code 914)
(301) 286-8560

Kwing L. Chan
Applied Research Corporation
(301) 286-5216

Sponsor: Office of Space Science and Applications

Dr. Hans G. Mayr received a PhD from the University of Graz, Austria. He is an Atmospheric Scientist with the Dynamics Explorer and Pioneer Venus Projects and has 23 years of experience at GSFC.

Dr. Isadore Harris, who received a PhD from Northwestern University, is a Planetary Aeronomist with 31 years of service at GSFC.

Dr. Kwing L. Chan, a Computational Astrophysicist with Applied Research Corporation, is involved in solar and planetary research. Dr. Chan received his PhD from Princeton University and has worked at GSFC for over 12 years.

Astro-I

PLANNING A SHUTTLE-BASED ASTRONOMY MISSION—ONE APPROACH TO MAXIMIZING SCIENCE IN A RAPIDLY CHANGING ENVIRONMENT

Astro-1 was an astronomy-dedicated space shuttle-based mission involving a payload of four telescopes: one observed x-ray emissions, and three observed in the ultraviolet (see the figure). After many delays, the mission flew on Space Shuttle Columbia beginning December 2, 1990, and over the next 9 days, produced exciting scientific data.

When the Astro Science Working Group began planning the astronomical sources that would be observed during the 9-day mission, they faced a formidable task. Because Astro-1 was a manned mission, the timeline had to be planned in detail well in advance to ensure that the shuttle and its crew would be safe at all times. Mission planning was complicated by two fundamental issues: first, astronomical sources move into and out of the night sky on an annual cycle; and second, the importance of specific scientific observations can change rapidly with time. The very low-density—but sunlit—atmosphere at shuttle altitudes glows brightly during orbital daytime, swamping weak signals from faint stars and galaxies. Distant galaxies are so faint that they can only be observed during the night portion of an orbit. If the launch date slips from the planned date by even a month, that faint galaxy is likely to have slipped from a nightside location into one on the dayside, and hence would be no longer observable. As the shuttle timeline included over 200 individual observations, a major replanning activity was required each time the launch date was delayed. Moreover, software tools were needed to allow rapid replanning during the mission itself.

In principle, an automated scheduler could have been built provided that rigid scheduling rules could have been devised along with rigid priorities for each

observation of each star. However, astronomers work by comparing one star or galaxy with unknown spectral properties with a star or galaxy with known properties, often in a different location. As the night sky changes throughout the year, the accessibility of targets changes. In addition, the scientific priorities change in unpredictable ways based on the science requirements. Unpredictability abounds, as newly discovered comets pass through the inner portion of the solar system, and novae, supernovae, and eruptive galaxies also appear with no forewarning. Late-breaking analyses may require that a key ultraviolet observation be included at the last minute to verify or validate a model or an observation. Therefore, to maximize scientific discovery requires that observing schedules remain flexible immediately before and during the mission.

After multiple attempts to build an automated scheduler, the science team worked with the shuttle planners to devise a more flexible planning process. Each of the instrument teams carefully selected a prioritized list of sources to be observed. Tools to aid interactive scheduling were developed on workstations. A centralized file management system was developed to bring together the essential information for each planned observation. Once this information was available, the science team would plan a 10-day science timeline for a given launch date, a process that required 2 days of intense interaction. Such planning had attendant risks, as planning for a specific launch date proved impossible, because the mission encountered several launch delays. By the time of the actual launch, 12 timelines had been built and discarded. A 2-month launch slip meant that over half of the selected objects had to be replaced. To provide more tolerance for potential launch delays, a science timeline was built for a date in the middle of a 2-month interval (January 1, 1991) beginning on December 1, 1990. Software tools were designed to adjust the timeline for launches up to 30 days early or late.

This approach proved successful as measured by the scientific results from the Astro-1 mission. Despite many hardware complications during the flight, nearly 400 observations of over 135 objects were recorded during the 9-day mission. Astronomical sources ranging from the newly discovered Comet Levy, to stars within our galaxy, to very distant galaxies and quasars were successfully observed. The first 12 of an estimated 100 scientific papers have already been published, and astronomers throughout the world are keenly interested in the results. Three special sessions summarizing the first results from Astro-1 have been presented at national and international scientific meetings. Additional discussions and scientific papers will continue to be generated during the next few years. Clearly, Astro-1 demonstrated that we could build a responsive planning system to meet the challenges of launch slips and hardware complications.

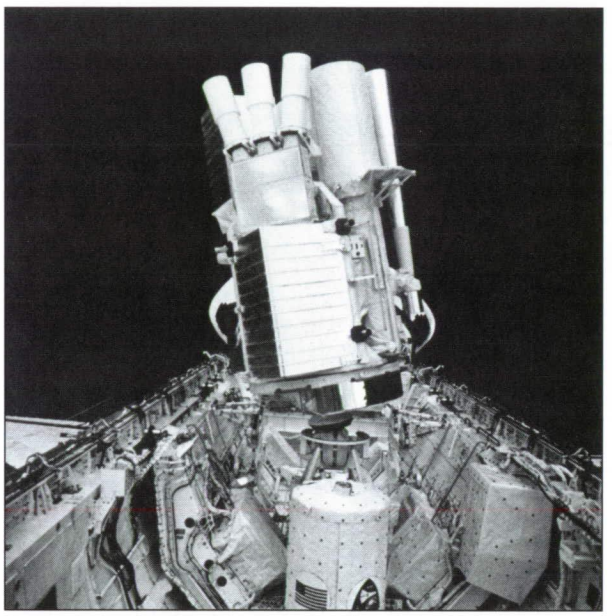

Astro-1 as depicted in the shuttle payload bay.

Contact: Theodore R. Gull (Code 680)
(301) 286-6184

Sponsor: Office of Space Science and Applications

Theodore R. Gull is Associate Chief of the Laboratory of Astronomy and Solar Physics. He served as Mission Scientist for the Astro Mission from 1982 to 1991. His scientific interests are in astronomical instrumentation, supernova remnants, interstellar bubbles, and HII regions.

BROAD BAND X-RAY TELESCOPE ON ASTRO-1

The Broad Band X-ray Telescope (BBXRT) was one of four astronomical telescopes making up the Astro-1 payload which, on December 2, 1990, flew on board the STS-35 astronomy mission. In the shuttle bay, BBXRT was operated on a dedicated pointer controlled entirely from the ground (first figure). The other three telescopes flown on Astro-1 were designed for imaging, spectroscopy, and polarimetry in the UV-band and were mounted on a separate pointer. A large effort went into coordinating and optimizing the observations of the four instruments, all of which were charting totally new areas of research. In addition to the individual observing programs, this unique instrument complement gave us the opportunity for a number of observations to be conducted simultaneously in the x-ray and the UV-bands. BBXRT was proposed more than a decade earlier as a feasible approach to conducting broadband, moderate-resolution x-ray spectroscopy of selected astronomical sources from the space shuttle. In the late 1970s, while considering options for making the transition from the coarse x-ray astronomical spectrophotometry obtainable with mechanically collimated detectors, to the higher resolution of imaging instruments, we in the GSFC X-ray Group introduced the conical foil x-ray mirror which became the centerpiece of the original BBXRT proposal.

The new concept allowed us to cover a broad spectral band (0.3 to 12 keV) using lightweight, high-throughput optics with sufficiently good resolving power to make them applicable to a wide variety of x-ray sources. By the time NASA gave us the go-ahead to develop the instrument, we had added to the package state-of-the-art, segmented Si(Li) focal-plane detectors featuring excellent energy resolution (~100 eV FWHM), and a very low background. The completed instrument uses two identical, co-aligned foil mirrors at its front-end and similar, identical five-element cooled silicon detectors at each focal site. A mirror consists of two layers of conical reflectors, each layer containing 118 confocally nested cones.

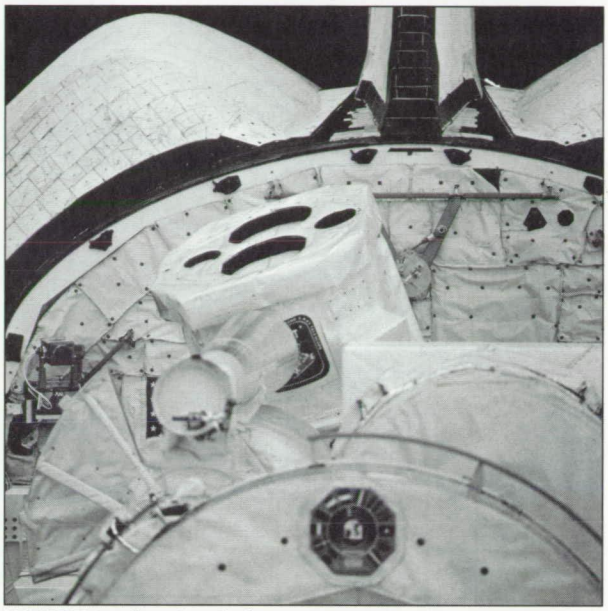

BBXRT in the shuttle bay.

The reflector substrate is 0.137-mm-thick, high-quality aluminum foil, formed into approximate cone segments which are then overcoated with ~10 μm of acrylic and ~500 Å of vacuum deposited gold, respectively. Reflectors are subsequently assembled into mirror quadrants, accurately maintained at their appropriate locations by radial grooved supports. The silicon detectors consist of five separate cylindrically symmetric detecting elements defined via grooves on a single silicon block. The second figure shows the instrument field of view defined by the mirrors and these detector elements. Each of the five segments shown includes contributions from both detectors. The type of detectors we are using only function at very low temperatures, so we housed them inside evacuated compartments (cryostats) in good thermal contact with a large supply of solid argon refrigerant carried aloft. During the flight, detector temperatures were maintained at ~105 K (-168°C).

Amplified signals corresponding to individual events in the 10 detector elements were processed on board. The information was encoded in a 32-bit word for each event. The data contain event timing to an accuracy of 62.5 μs, energy information recorded with a resolution of ~16 eV, and several data quality

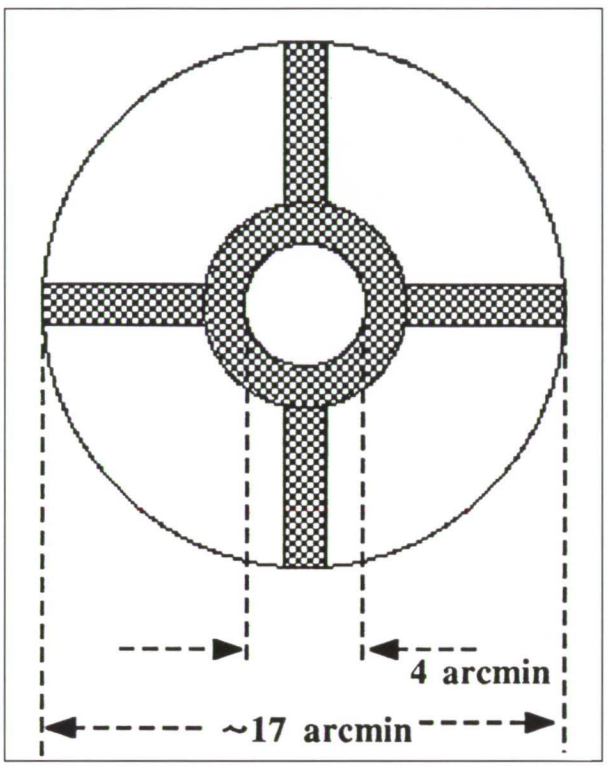

The BBXRT field of view.

flags. These prime data, along with housekeeping information, were telemetered to the ground in one of three telemetry modes, depending on TDRSS coverage. The primary telemetry mode used 65 kbps and, essentially, maintained all information from the instrument. With few exceptions, data were stored on tape whenever the instrument was out of TDRSS contact.

Because of the necessarily long focal length, BBXRT is a large instrument, a characteristic that greatly amplifies the importance of lightweight mirrors. The optical bench supporting mirrors, detectors, and all remaining instrument components are, for the most part, housed in a ~4-m-long aluminum honeycomb cylinder which, in turn, is supported in the shuttle bay on a two-axes gimbal system. Gimbal operation is effected using a star tracker and gyros. The entire system was aligned to an accuracy of ~0.5 arcmin. An observation relied on the shuttle acquiring and maintaining a desired attitude allowing a source of interest to remain within the ±17° (for each axis) gimbal operational range. This range was adequate for us to find interesting targets almost regardless of how the orbiter was oriented. The instrument was also equipped with a star camera for real-time aspect determination. Detector calibrations during the mission were frequently conducted using moveable Fe^{55} sources mounted in front of the cryostat opening. Other critical instrument components included commandable covers used throughout the mission to safeguard the instrument, a bright-object sensor in a control loop protecting against inadvertent solar exposure, and an elaborate thermal control and verification system. Pointer difficulties affecting all four instruments prevented us from achieving many of our objectives during the Astro-1 mission.

These difficulties notwithstanding, the instrument functioned largely as envisioned before the flight, giving us very exciting data on some 60 sources. We had targeted some of the most interesting sources in x-ray astrophysics and were able to obtain sample data from a variety of astrophysical settings, both galactic and extragalactic. In some cases, the intention was to improve on spectral measurements obtained with lower resolution instruments. On other occasions, we were looking for spectral features that could not have been detected before. In general, we were able to demonstrate the spectroscopic accuracy attainable with a BBXRT-type instrument, in a high-throughput mode. From the elements O through Fe, our data show large increases in observational detail and uniqueness. When our analysis is complete, we expect to have made important contributions toward the understanding of the diverse physical conditions characteristic of the many types of sources.

The BBXRT flight on Astro-1 was a pioneering mission with follow-up missions already planned. We are eagerly waiting for the flow of such information to increase in coming years, giving us a powerful tool with which to address fundamental issues in astrophysics.

Contact: Peter J. Serlemitsos (Code 666)
(301) 286-5255

Sponsor: Office of Space Science and Applications

After obtaining his PhD in 1966 from the University of Maryland, Dr. Peter Serlemitsos joined the just-forming X-ray Group at GSFC. His contributions include detector and mirror development for observations in x-ray astronomy. He served as Principal Investigator on the Group's experiment on OSO-8, on the BBXRT flight on Astro-1 (STS 35) and on GSFC's mirror development for the upcoming Japan/U.S. mission, Astro-D.

BBXRT OBSERVATIONS OF ACTIVE GALACTIC NUCLEI

The BBXRT experiment was flown as part of the Astro-1 payload on the Space Shuttle Columbia in December 1990. A major goal of the mission was to use x-ray spectroscopy to increase our understanding of the phenomena occurring in the nuclei of nearby active galaxies. It is generally believed that these nuclei are powered by the accretion of material onto a massive compact object. These enigmatic objects can produce as much energy as our entire galaxy in a region the size of our solar system. BBXRT's moderate spectral resolution (~100 eV FWHM), high sensitivity, and large effective area permitted very sensitive searches for x-ray spectral signatures due to Fe and other abundant elements that can provide clues about the workings of these objects.

Extensive observations of the bright Seyfert-1 galaxy NGC 4151 have revealed a complex x-ray spectrum. The power-law spectrum seen in hard x-rays is cut off at soft x-rays by absorption. It has been shown that the low-energy spectrum is inconsistent with absorption due to uniform, cold material, and it has been argued that the nuclear source is only partially covered by the absorbing material. A different interpretation, based on absorption by warm material, has also been proposed. An Fe line has been observed whose energy is consistent with the fluorescence of cool material. The line may be intrinsically broad, which would suggest an origin close to the central object.

Two BBXRT observations of NGC 4151 were made when the source was successfully centered on the BBXRT detectors. The spectrum for both observations can be described in terms of a power law for a source that is partially (~93 percent) covered by cooler material. There is also an unchanging softer (<1 keV) component that is presumably the extended emission seen previously with the Einstein Observatory. We clearly see a narrow Fe emission line with an equivalent width of ~150 eV and an energy that is consistent with fluorescence from cool material in NGC 4151. There is no evidence for intrinsic width in the line with a 90-percent confidence in the upper limit of 160 eV (7500 km/s) FWHM. Such a narrow line is consistent with an origin in the broad-line region (BLR) of the galaxy, but could also be produced in a nearly face-on accretion disk. Since the physical sizes of the possible regions of Fe line emission are so different, variability could provide a crucial test for the origin of the line. For a spherically symmetric gas distribution, the lack of a detectable absorption edge due to cold Fe requires that the Fe abundance is less than five times solar. While the observation of a narrow Fe line is apparently inconsistent with recent Ginga observations which showed an intrinsically broad line (38,000 km/s FWHM) with a similar equivalent width, it may be possible to reconcile these observations. The BBXRT spectrum shows additional broad features at energies just below the Fe line, and we are investigating whether these features are structure in the continuum or additional Fe line emission.

Much less is known about the x-ray spectrum of Seyfert-2 galaxies than the spectrum of Seyfert-1 galaxies. The discovery of an obscured Seyfert-1 nucleus in the archetypical Seyfert-2 galaxy NGC 1068 led to the unified view of Seyfert galaxies in which viewing angle explains many of the observed differences in Type 1 and Type 2 galaxies, including the relatively weak soft x-ray emission from Type 2s. X-ray line emission with large equivalent widths may be produced in Seyfert 2s since only a small fraction of the continuum radiation is seen, and indeed, strong Fe-K lines have been found for NGC 1068, and Mkn 3 using observations with Ginga. With such

strong lines expected, Seyfert-2 galaxies were prime targets for BBXRT.

The x-ray spectrum of NGC 1068 measured with BBXRT is complex, with a hard power-law spectrum above 3 keV and a much softer spectrum at lower energies. There are also strong emission lines in the Fe-K band and at 900 eV. The measured continuum spectrum is qualitatively similar to previous observations. The best-fit BBXRT spectrum is shown in the first figure. The broad excess at 900 eV is presumably due to many unresolved Fe-L lines, as had been predicted by others, but more detailed calculations are needed to predict individual line strengths. For descriptive purposes, we have assumed that the Fe-L blend has a Gaussian energy distribution. Best-fit parameters yield a mean energy of ~900 eV, an intrinsic width of ~120 eV (rms), and an equivalent width of ~290 eV. Emission in the Fe-K band appears to be the sum of three intrinsically narrow lines. Best-fit parameters are a line at 6.4 keV (due to the fluorescence of cold Fe) with an equivalent width of 1.08 keV, a line at 6.7 keV (due to recombination to He-like Fe) with an equivalent width of 0.88 keV, and a line at 6.9 keV (due to recombination to H-like Fe) with an equivalent width of 0.51 keV.

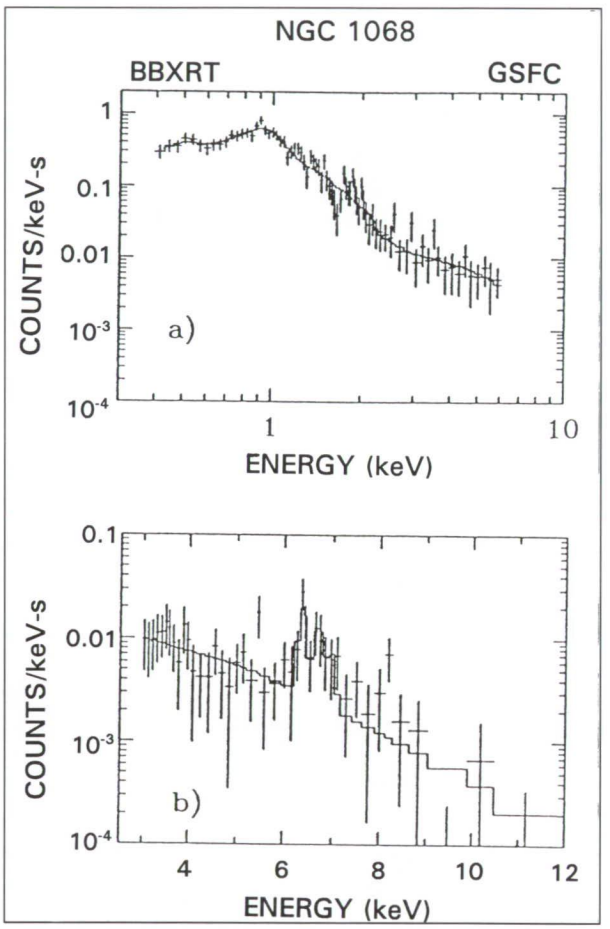

The spectrum of NGC 1068 as seen with BBXRT shown separately at (a) low energies and (b) high energies. The solid line represents the best-fit model folded through the BBXRT response.

We interpret these observations in terms of the model of Antonucci and Miller in which the direct line of sight to the Seyfert-1 nucleus at the center of NGC 1068 is obscured by a thick torus of material, but a small fraction of the light from the nucleus is scattered toward us by a gas of warm electrons. The temperature of the gas must be $<1 \times 10^6$, and the column density of the gas is estimated to be $\sim 10^{23}$. The strong Fe, L, and K emissions support such a model. The existence of highly ionized Fe ions clearly indicates that the ionization state of the gas is driven by photoionization. Comparable amounts of emission from H-like and He-like Fe requires a large ionization parameter. However, such a highly ionized gas will not produce the strong fluorescence Fe-K line seen at 6.4 keV. There must be a substantial amount of material with a much lower ionization parameter that has a direct line-of-sight to the observer. The location of this material is uncertain, but it could be in dense blobs in the scattering gas or it could be part of the obscuring torus itself.

Given NGC 1068's column density of $\sim 10^{23}$, ordinarily all the low-energy x-rays would be absorbed before leaving the source. In fact, no low-energy absorption is seen in excess of the 3×10^{20} expected from gas in our own galaxy. This lack of absorption is consistent with the idea that the gas is highly ionized. We have examined the x-ray spectrum of NGC 1068 for an absorption feature due to oxygen, which is normally the most important absorbing element for low-energy x-rays. For cold O, the optical depth due to the photo-ionization, τ_O, would be ~560 times the optical depth due to

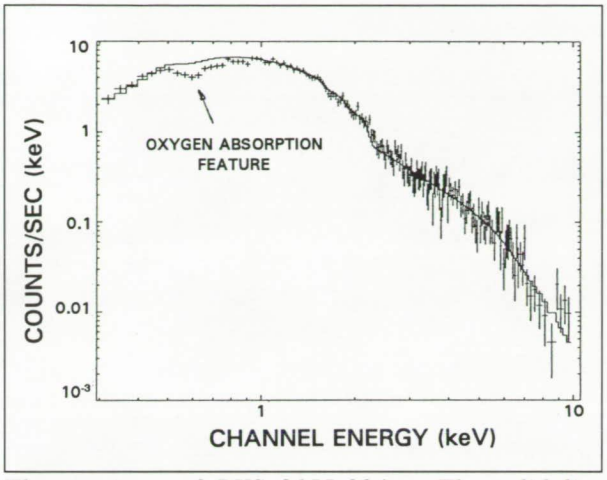

The spectrum of PKS 2155-304. The solid line represents the best-fit model to the data above 0.9 keV. The absorption feature at ~0.6 keV is apparent.

electron scattering, τ_{es}, which is expected to be about 0.05. A conservative upper limit for τ_O is 2, implying that the ratio of completely ionized O to H-like O is larger than 56 τ_{es}. For the usual estimates of τ_{es}, O must be almost entirely fully ionized, and the ionization parameter x must be more than 10^3. This lower limit is consistent with the value indicated by the Fe lines.

A major goal of BBXRT was to study absorption features in BL Lacertae-type objects (BL Lacs), such as that in the spectrum of PKS 2155-304. The feature is thought to be an absorption trough due to red-shifted resonant Ly α absorption by H-like oxygen. Determining redshifts, and thus distances, to BL Lacs has traditionally been very difficult because of the lack of strong spectral features. This x-ray absorption feature is by far the strongest feature in the spectrum of any BL Lac in any wavelength band, and could provide a new method for determining the distances to such objects. As shown in the second figure, we have confirmed with great statistical confidence the existence of the feature, thereby showing its apparent persistence for more than a decade. We have also discovered good evidence for a similar absorption feature in the spectrum of H1426+428, another BL Lac whose reported redshift is similar to that reported for PKS 2155-304.

The BBXRT experiment succeeded due to the collaborative efforts of many people led by Principal Investigator Dr. Peter Serlemitsos. The results reported herein are due in part to analysis by Dr. Greg Madejski and Ms. Kimberly Weaver.

Contact: Francis E. Marshall (Code 666)
(301) 286-5279

Sponsor: Office of Space Science and Applications

Dr. Francis E. Marshall earned a PhD in Physics at the California Institute of Technology. He has been working in the Laboratory for High Energy Astrophysics since 1977. He is currently leading an effort to prepare a new x-ray spectrometer using a quantum calorimeter for a series of sounding rocket flights.

Gamma Ray Investigations

COMPTON GAMMA RAY OBSERVATORY

The Compton Gamma Ray Observatory (CGRO) was launched from the Space Shuttle Atlantis on April 5, 1991. Deployment into a 457-km, 28.5° orbit occurred 2 days later following an unscheduled space walk by mission specialists Jay Apt and Jerry Ross to free the high-gain communications antenna. At 16,000 kg, CGRO is the heaviest payload ever launched by the shuttle system and the heaviest scientific payload ever flown. The spacecraft and instruments are in excellent health and are returning exciting results with every new observation.

CGRO is the second in NASA's series of Great Observatories, following the launch of the Hubble Space Telescope. The mission goals are to perform broadband gamma-ray observations with better angular resolution and an order of magnitude greater sensitivity than afforded by previous missions, and to perform the first full-sky gamma-ray survey. The scientific theme of CGRO is the study of physical processes taking place in the most dynamic sites in

the universe, including supernovae, novae, pulsars, black holes, active galaxies, gamma-ray bursters, and solar flares. The first 15 months of the mission are for the full-sky survey, to be followed in future years by in-depth observations of sources discovered during the survey. In addition, CGRO can be pointed at any new or transient source in the sky in less than 1 day. The primary mission goals can be successfully completed in 2 years, but the lifetime is expected to be more than 5 years. This extended mission allows the scientific involvement of a large community of observers beyond the original instrument teams. The CGRO Science Support Center has been established at GSFC to assist Guest Investigators in accessing CGRO data.

The spacecraft contains a complement of four instruments to make observations over a very broad energy range of six orders of magnitude from 30 keV to 30 GeV. The instruments and their spacecraft locations (see figure), are (1) the Burst and Transient Source Experiment (BATSE), to study gamma-ray bursters and other transient gamma-ray sources; (2) the Oriented Scintillation Spectrometer Experiment (OSSE), to perform detailed spectroscopy in the nuclear transition energy band (0.05 to 10.0 MeV); (3) the Imaging Compton Telescope (COMPTEL), to make the first full-sky survey in the difficult 1- to 30-MeV range; and (4) the Energetic Gamma Ray Experiment Telescope (EGRET), to map the full sky and in particular, our Milky Way Galaxy at high energies (20 to 30 MeV).

The gamma-ray sky has been particularly active during the first few months of the mission. We have had three targets of opportunity so far: the Sun, between June 8-15, to observe solar flares from active region 6659; Cygnus X-3, between August 8-15, in response to a large radio outburst; and GX339-4, one of the few black hole candidates in the Galaxy, between September 5-12, in response to BATSE's discovery of gamma-ray activity.

The science results from CGRO are already impressive. BATSE is seeing about one gamma-ray burst per day and finds them to be isotropically distributed on the sky; OSSE has obtained solar flare spectra with nuclear transition lines and the positron-annihilation line from active region 6659; COMPTEL has made one of the first images of a gamma-ray burst for the May 3, 1991 event; EGRET has discovered intense gamma-ray emission from quasar 3C 279, which, at a distance of 1 to 2 gigaparsecs, is the most distant and luminous gamma-ray source ever seen. All instruments are performing well and achieving sensitivities close to those predicted before launch. We expect CGRO to continue to provide significant insights into the energetic gamma-ray universe.

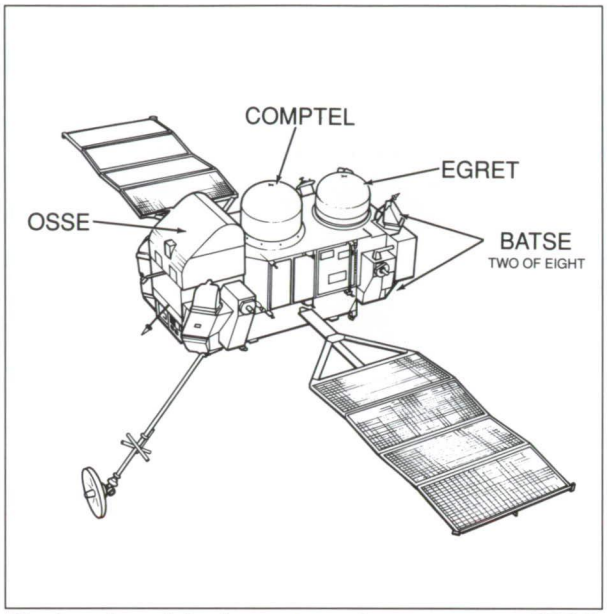

The location of the four science instruments on CGRO.

Contact: Neil Gehrels (Code 661)
(301) 286-6546

Sponsor: Office of Space Science and Applications

Dr. Neil Gehrels is an Astrophysicist in the Nuclear Astrophysics Branch, the Project Scientist for CGRO, and Co-Investigator for the balloon-borne Gamma-Ray Imaging Spectrometer (GRIS) and the Transient Gamma-Ray Spectrometer (TGRS) on Wind. Dr. Gehrels' research includes gamma-ray observations and studies of the center of our galaxy and Supernova 1987A. He has 10 years of experience at GSFC and holds a PhD in Physics from the California Institute of Technology.

ENERGETIC GAMMA RAY EXPERIMENT TELESCOPE ON THE COMPTON GAMMA RAY OBSERVATORY

CGRO, which was launched on April 5, 1991, carries four instruments that cover the gamma-ray spectrum from 0.2 MeV to 30 GeV. The upper end of this range, 20 MeV to 30 GeV, is viewed by the Energetic Gamma Ray Experiment Telescope (EGRET). The EGRET instrument consists of four main systems: the anticoincidence system, the electron-positron track imaging system, the time-of-flight coincidence system, and the energy calorimeter. The EGRET track imaging system consists of a set of 36 orthogonal wire spark chambers with digitized readout.

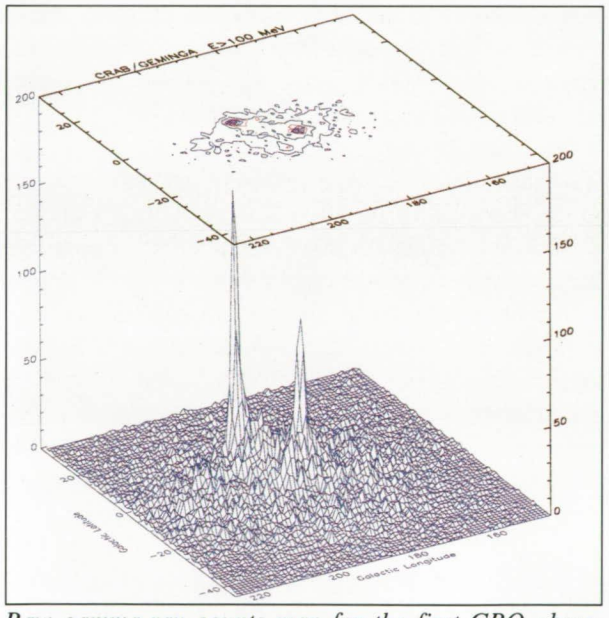

Raw gamma-ray counts map for the first GRO observation after the calibration phase, the Crab and Geminga region.

The improvements in effective area and angular resolution afforded by EGRET will allow us to survey the entire sky with an area, solid angle, and efficiency factor more than 10 times that of previous satellite gamma-ray telescopes, and to provide detailed maps of the full-sky gamma-ray emission. From these maps, the location, intensity, and spectral information can be extracted for a variety of compact objects (e.g., pulsars and neutron stars), extended objects (e.g., molecular clouds and galactic arm structure), and extragalactic objects (e.g., other active and normal galaxies and quasars).

The initial turn-on of most low-voltage systems on EGRET occurred on April 15, 1991. By April 22, the instrument was fully operational and ready for the calibration phase. After completion of the calibration and test phase, during which some scientific data were collected, EGRET was configured for Phase I, the all-sky survey, on May 16, 1991.

Through the time of writing this report, November 15, 1991, several regions of the sky have been observed, and papers on preliminary results have been presented at several conferences. These include the International Astronomical Union in July 1991, the International Cosmic Ray Conference in August 1991, and an American Physical Society Meeting. Good time profiles of pulsars are being obtained. The pointing accuracy of the spacecraft is excellent. Thus far, source locations are meeting our expectations.

The first figure shows a raw gamma-ray count map for the Crab and Geminga region, the first CGRO observation after the calibration phase. The second figure shows an early picture of the gamma rays from the direction of the Crab as a function of the pulsar phase.

The EGRET team reported in a telegram to the International Astronomical Union that a source of intense localized gamma radiation was detected between June 15 and 28. The source of this radiation has been identified with the variable quasar 3C 279, within an accuracy of better than 5 arcmin. This result is discussed further, elsewhere in this report.

Among the gamma-ray bursts, the one on May 3, 1991 is of particular interest. It is the first event seen by the COMPTEL and EGRET imaging detectors. In addition, EGRET obtained three spectra during the event covering the range from 1 to 200 MeV.

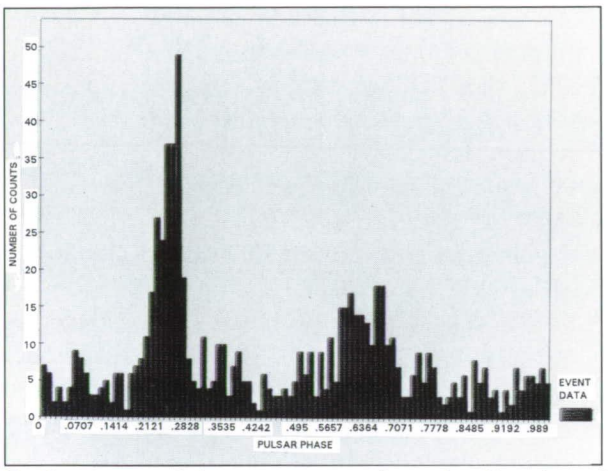

Early picture of the gamma rays from the direction of the Crab as a function of the pulsar phase.

EGRET scientists are also in the process of studying data from solar flares. The June 11, 1991 solar event is worth special note since the EGRET instrument recorded the highest energy gamma-rays yet seen from a solar event. Work is in process on other astrophysical sources, including ones that have not been seen previously.

Contact: Carl E. Fichtel (Code 662)
(301) 286-6281

Sponsor: Office of Space Science and Applications

Dr. Carl E. Fichtel is Chief Scientist at the Laboratory for High Energy Astrophysics, Acting Head of the Gamma Ray Astrophysics Branch, and a Senior Goddard Fellow. Among other awards, he has received the John C. Lindsay Memorial Award and the NASA Exceptional Scientific Achievement Medal. He holds a PhD from Washington University in St. Louis.

OPTICAL TRANSIENTS, GAMMA-RAY BURSTS, AND THE RAPIDLY MOVING TELESCOPE

Gamma-ray bursts (GRBs) were first observed 20 years ago with orbiting instruments designed to detect man-made nuclear explosions. GRBs are transient cosmic events lasting from a fraction of a second to several tens of seconds. Their detected intensities are similar to those of solar gamma-ray flares, yet their sources are at cosmic distances. Despite the implication of immense absolute intensity, the source objects have not been identified. The distribution of their source directions is consistent with isotropy, with no galactic disk clustering or other directional clue. All observations of these celestial gamma-ray events have been with balloons or spacecraft above the atmosphere, but to date, the astronomical source objects have not been identified.

Because of the lack of any GRB source identification, many theoretical models have been proposed. This multiplicity of models is further complicated by the fact that GRBs have been observed only in the gamma-ray energy band. Deep optical imaging (greater than 23rd magnitude) of the error boxes for GRBs have not yielded any source identification that is plausible and unique.

To make the first identification, our group at the GSFC Laboratory for High Energy Astrophysics has been developing a ground-based alternative approach based on the discovery of several archived optical transients from some of the smaller gamma-ray burst position error boxes. This new technique will make possible burst-source location determinations that are much more precise than can be made with detectors of gamma radiation and more timely than can be made with spacecraft systems. Using optical astronomy to study gamma-ray burst sources has several other advantages. In particular, ground instruments are cheaper than satellites and have a longer duration than balloon flights. The duty cycle is unfortunately lower, but since we need only to identify one or a few sources, rather than perform a survey, this is not a severe disadvantage.

Our instrument, the Rapidly Moving Telescope (RMT), was designed, built, and tested at GSFC. It is currently being installed at its permanent location at Kitt Peak National Observatory. The RMT works with a companion instrument being built by a group at MIT. Their instrument is a sky-survey instrument

which makes the initial observation of the optical transient counterpart to the GRB. Its imaging resolution is too coarse (a few arcmin) to make source identification possible, so it sends these rough coordinates to the GSFC RMT instrument. The RMT has the ability to slew to any point in the sky in 1 second, track that position with better than 1 arcsec accuracy, and make electronic images with 1 arcsec angular resolution.

The instrument, shown in the figure, consists of a fixed 8-inch telescope at the top of the tripod looking down at an azimuth-elevation gimballed flat mirror. It is because only the mirror moves that the RMT is capable of making such short target acquisition times. Once the target is acquired, the instrument will make a several minute series of 1.5-second CCD images. The instrument is sensitive to the 14th magnitude. While waiting for candidate transient events from the MIT instrument, the RMT will operate in stare mode on positions of interest, such as some of the smaller past GRB error boxes, with the hope of observing a GRB source object in recurrence. The RMT field of view is 9 x 11 arcmin.

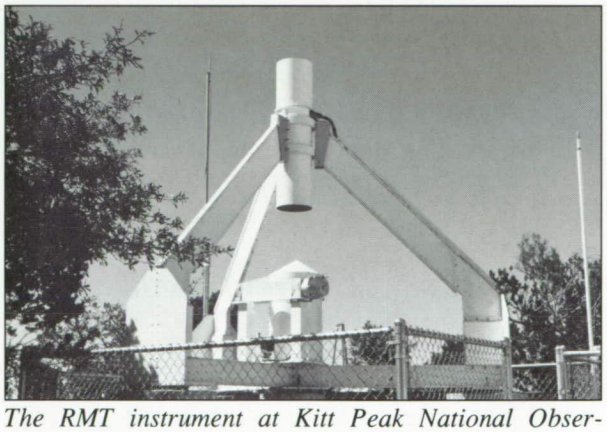

The RMT instrument at Kitt Peak National Observatory.

After observing an optical transient and making a time and position correlation with the CGRO BATSE instrument's gamma bandpass observations, the more traditional and multibandpass means of astronomy can be brought to bear on the coordinate location.

Not only will the RMT make a significant change in the study of GRBs with even a single source identification, but it will also begin an entirely new field of fast optical-transient astronomy.

Contact: Scott D. Barthelmy (Code 661)
(301) 286-3106

Sponsor: Office of Space Science and Applications

Dr. Scott D. Barthelmy has been with GSFC for 6 years, serving first under an NAS/NRC fellowship, then with the University of Maryland, and currently with the USRA organization. He received his PhD in physics from Washington University, St. Louis. He also is on the Gamma-Ray Imaging Spectrometer team.

3C 279: MOST LUMINOUS GAMMA-RAY SOURCE DETECTED SO FAR

The EGRET instrument on the Compton Gamma-Ray Observatory (CGRO) has detected strong gamma-ray emission above 50 MeV from 3C 279, an optically violent variable (OVV) quasar. Although 3C 279 was not detected by the SAS-2 and COS-B telescopes during the 1970s, it was one of the brightest high-energy gamma-ray sources in the sky during the 13-day EGRET observation during the latter half of June 1991. Comparison with upper limits obtained from SAS-2 and COS-B data indicates that 3C 279 has increased in brightness by at least an order of magnitude. For energies between 70 and 5000 MeV, the EGRET data fit a power-law photon spectrum with an index of -1.8 ± 0.07.

If 3C 279 radiates gamma rays isotropically, the intensity observed by EGRET leads to a luminosity of ~10^{48} ergs/s above 100 MeV, which would be the dominant energy output of the object. A more likely scenario is that the gamma rays are emitted within one or two narrow cones, making the gamma-ray luminosity comparable to that observed in lower frequency bands. In either case, 3C 279 is the most distant (5 to 7 billion light years) and by far the most luminous gamma-ray source identified thus far.

EGRET also detected significant intensity variations of 3C 279 within the 2-week observation. When combined with the spectral shape and high gamma-ray luminosity, this places strong constraints on possible models of the object.

Contact: Robert Hartman (Code 662)
(301) 286-7178

Sponsor: Office of Space Science and Applications

Dr. Robert Hartman received his PhD in Physics from the University of Chicago. In addition to SAS-2 gamma-ray telescope development and data analysis, he has played a major role in the EGRET development since its beginning in the early 1970s. He has directed and participated in a number of balloon investigations, including cosmic-ray electron/positron measurements as well as gamma-ray studies. Dr. Hartman has been at GSFC for 22 years.

ADVANCED GAMMA-RAY ASTRONOMY TELESCOPE EXPERIMENT (AGATE)

To continue the advancement in gamma-ray astronomy, which will be made with the EGRET instrument on CGRO, will require a next-generation gamma-ray telescope. The scientific purpose of such an instrument will be to provide detailed observations of gamma-ray sources using the EGRET full-sky survey as a guide. Clearly, increased sensitivity and angular resolution will be needed while retaining low instrumental background. Increased sensitivity can be achieved with large detectors with several square meters of active area.

AGATE is envisioned as a 2-m class telescope with 2 m x 2 m active area. To improve the angular resolution, approaching the gamma-ray pair production kinematic limit will require improvements in spatial resolution, to ~0.1 mm, and reduction of the effects of Coulomb scattering before the direction of the electron pair has been measured. Additional criteria for the design of such an instrument may also involve optimization for higher energies (20 to 100 GeV), reduced solid angle (a point-source instrument), and increased live time (reduced event-processing time). These design goals can be achieved using large-area (2 m x 2 m) drift chambers.

While drift chambers have been used as particle accelerators for many years, the power required by the high-speed amplifiers and discriminators has prevented the viable use of large-area chambers in space. An SRT research program has resulted in the design of a low-power, high-performance amplifier and discriminator, and quad, time-to-digital converter (TDC) circuits specifically suited for drift chamber applications. The amplifier has a rise-time of 6.3 ns, a gain of 10.9, and power of 40 mW. The discriminator has a 12-ns propagation time, 15-ns rise-time, 25-ns pulse width, and power of 25 mW. The quad TDC has a power of 95 mW and is capable of timing with accuracy better than 0.2 percent full scale.

Drift chambers offer another advantage for the construction of a high-energy gamma-ray telescope. Xenon gas can be used for the drift gas and, at a pressure of 2 to 3 atmospheres and a depth of 2 to 4 m, can double as the pair production medium. This configuration allows several measurements to be made of the electron and positron track directions before Coulomb scattering begins to dominate over the initial uncertainty imposed by the kinematics of pair production. Good spatial resolution is also needed to achieve angular resolution near the kinematic limit.

While these improvements affect mainly the track imaging system, all the systems of a 2-m class gamma-ray telescope will require innovative designs and careful optimization. New approaches to the coincidence, anticoincidence, and energy calorimeter systems, appropriate to the larger dimensions, using PIN photodiodes and avalanche photodiodes instead of photomultiplier tubes, are being investigated. The viable use of PIN photodiodes in conjunction with a cesium iodide scintillator for the energy measurement system has been demonstrated.

For the coincidence and anticoincidence systems, a technique using lucite strips, doped with a wavelength shifter, bonded to the edge of plastic scintillators and viewed with PIN photodiodes is being researched. The mechanical design of large-area, segmented anticoincidence domes is in progress. Additionally, the anticoincidence, time-of-flight, and coincidence systems are being considered as one interactive system. This system will require interactive computer processing to screen out potentially confusing cosmic-ray tracks. The system design will also maximize the live-time of the instrument.

Work is progressing on several engineering prototype drift chambers. The ½-m x ½-m drift chambers have been built, and the low-power amplifiers and discriminators, as described above, are being installed. These drift chambers will form the track imaging system of a complete ½-m x ½-m gamma-ray telescope, which will use sea-level muons and gamma rays to measure the angular and spatial resolution. Almost 200 quad TDC circuits are also nearing completion for this telescope.

A larger prototype instrument using ½-m x 2-m drift chambers is also being constructed. This instrument will be a mechanical and electrical prototype of the 2-m x 2-m drift chambers envisioned for the AGATE Gamma-Ray Telescope. These drift chambers are currently being fabricated.

Contact: Stanley D. Hunter (Code 662)
(301) 286-7280

Sponsor: Office of Space Science and Applications

Dr. Stanley D. Hunter, Co-Investigator on EGRET, received his PhD from Louisiana State University. During his 5 years at GSFC, he has played a major role in the EGRET hardware development and is developing a new gamma-ray telescope while also pursuing molecular cloud and cosmic-ray studies. Dr. Hunter has won a Special Achievement Award and a Certificate for Outstanding Achievement.

TRANSIENT GAMMA-RAY SPECTROMETER—A NEW INSTRUMENT FOR GAMMA-RAY BURST SPECTROSCOPY

Cosmic Gamma-Ray Bursts (GRBs) were discovered accidentally by the Vela satellites while attempting to verify the nuclear test ban treaty. Although this occurred over 2 decades ago, they have remained one of the most enigmatic and intriguing of astrophysical phenomena, despite extensive experimental and theoretical study. They are among the most violent and energetic processes known to exist in nature, characteristically emitting all of their luminosity at gamma-ray wavelengths. Typically, GRBs last from a fraction of a second to about a minute and are characterized by an impulsive rise and exponential decay. Substructure on tens-of-millisecond time scales can be discerned in most burst profiles. During the time of an outburst, the burst is usually the most luminous object in the gamma-ray sky, about 1,000 times brighter than the ambient gamma-ray background. Although ~150 such events are reported each year, it has still not been possible to identify counterparts at other wavelengths or even to find a convincing correlation with a specific class of astronomical object despite many deep searches at specific GRB locations. Presently, available GRB positions are consistent with a uniform distribution on the sky. Since there is no consensus on possible visible counterparts, it is hardly surprising that the origins of gamma-ray bursts are still unclear. The most viable models involve a neutron star origin.

The Transient Gamma-Ray Spectrometer (TGRS) is a new-generation, high-resolution gamma-ray detector, specifically designed to study GRBs. It has been selected under the International Solar-Terrestrial Physics (ISTP) Program, to fly on board the Wind spacecraft, to be launched on March 31, 1993. In addition to burst measurements, the instrument will also study solar flares and carry out a number of secondary science objectives including searching for possible diffuse background lines and monitoring the

powerful 511-keV annihilation radiation emanating from the center of the galaxy. The location of the instrument on the spacecraft is shown in the first figure. The instrument consists of four principal components: a detector/cooler assembly, a preamplifier, an Analog Processing Unit (APU), and a Digital Processing Unit (DPU). The instrument is designed around a large germanium (Ge) crystal, cooled to cryogenic temperature by a passive radiative cooler. The choice of semi-conductor rather than scintillator technology ensures a spectroscopic resolution better than 500 across the entire low-energy gamma-ray band. This is a factor of 20 times better than present-day instruments, and promises to provide new insights into the emission mechanisms and regions of GRB sources.

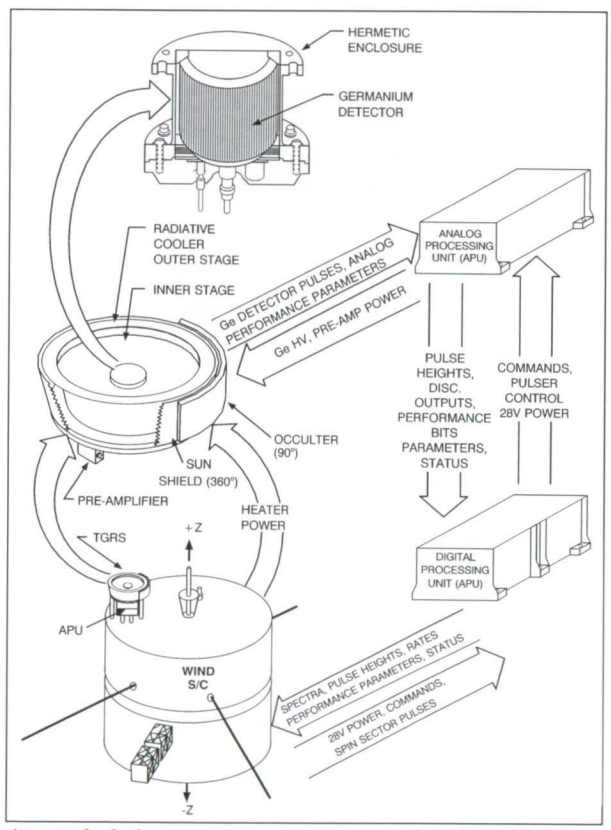

An exploded view of the TGRS and its location on the spacecraft.

A cross-sectional view of the detector/cooler assembly is shown in the second figure. The radiative cooler consists of two stages: an outer stage, and an inner stage to which the detector is attached. The two stages are coupled to each other and to the spacecraft by means of three low-thermal conduction supports of small cross-section. Physically, the entire assembly is mounted on a cylindrical tower which rises far enough above the top of the spacecraft (along the spin axis) so that the nearly hemispherical TGRS field-of-view is clear of most mechanical projections and obstructions originating from the spacecraft and the other instruments. This is particularly important in radiatively cooled systems, since such obstructions will be at significantly higher temperatures than deep space (~3 K). The spin axis of the satellite is orientated to prevent sunlight from entering the cooler field-of-view. The cooler is shielded on the sides by a thin Be/Cu alloy foil which has been included to ensure that the instrument is not continually triggered by soft solar events, such as the recently reported frequent microflare events. Surrounding a quarter of the outer diameter of the cooler is a 13.5-mm-thick passive Mo/Pb strip, which acts as an occulter for sources in the ecliptic plane. During normal operation, the occulter modulates signals originating from within ±5° of the plane of the ecliptic at the spin frequency of the spacecraft, 20 rpm. This signal will be used to study the galactic plane emission (including the center) which lies ~4° above the normal to the spin axis.

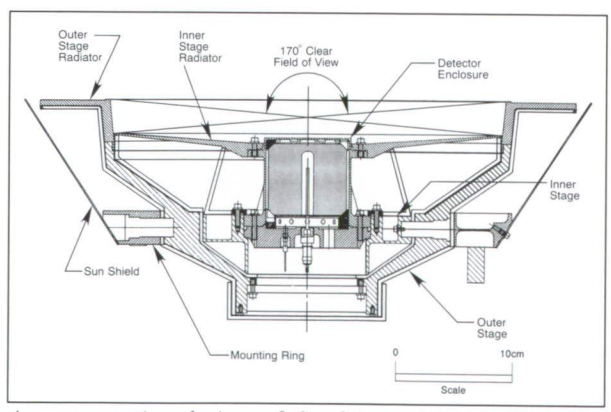

A cross-sectional view of the detector/cooler assembly.

The performance of the detector has been evaluated using Monte-Carlo techniques. It was found that the angular response is symmetric around the spin axis

and is an insensitive function of off-axis angle up to ~70°. This means that the incident source spectrum may be unfolded easily, given a crude estimate of the input source direction which can be provided by the KONUS GRB experiment, also to be flown on Wind.

For a generic burst (of size 10^5 erg/cm^2), we calculate that in 1 second the signal generated will be 30 times greater than the detector noise level. The sensitivity of the instrument to absorption and emission features has also been evaluated. It was found that the TGRS will detect nearly all previously reported line features. The third figure shows the calculated TGRS response to the nuclear line-rich April 27, 1981 solar flare which lasted 1700 s. The upper curve shows the response of an equivalently sized NaI detector, which clearly underscores the need for measurements with high spectral resolution. TGRS has over 20 times the spectral resolution of present-day instruments, including those on board the CGRO.

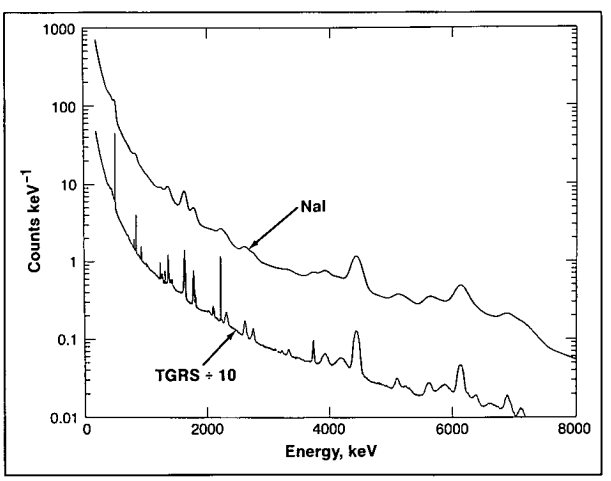

The TGRS response to the nuclear line-rich April 27, 1981 flare which lasted 1700 s.

The response of the instrument to cosmic point sources has also been estimated. It was assumed that the signal will be derived by comparing the occulted/unocculted signals, summed modulo fashion. It was found that for a spectrum representative of the powerful Galactic Center point source, the occulter attenuates the spectrum by a factor of 100 below 200 keV, and a factor of 3 at 1 MeV. Furthermore, for the important astrophysical line features reported at 511 and 1809 keV from the Galactic Center region, the signal will be modulated by a factor of ~10 and 1.8, respectively. Assuming line fluxes of 1 x 10^{-3} photons/cm^2/s and 4 x 10^{-4} photons/cm^2/s/rad, respectively, it is estimated that the time needed to detect these lines at 3 times the detector noise level is 2 days for the 511-keV line and 8 days for the 1809-keV line.

Contact: Alan Owens (Code 661)
(301) 286-4291

Sponsor: Office of Space Science and Applications

Dr. Alan Owens was a Gamma-Ray Astronomer for the Low-Energy Gamma-Ray Group in the Laboratory for High Energy Astrophysics. He is currently working at the University of Leicester in England.

Astrophysics

THE COSMIC BACKGROUND EXPLORER—2 YEARS AFTER LAUNCH

The Cosmic Background Explorer (COBE) was launched in November 1989. It was specifically designed to measure the radiation from the Big Bang, the explosion that started the present expanding Universe, and to search for the light from the first objects that formed after the explosion. With the successful COBE mission, major advances in our understanding of the very early universe have been achieved.

The COBE complement of instruments to achieve these gains in science is the Far Infrared Absolute Spectrophotometer (FIRAS), the Differential Microwave Radiometers (DMRs), and the Diffuse Infrared Background Experiment (DIRBE). Both FIRAS and DIRBE are located in a liquid-helium cryostat to operate at a temperature of 1.5 K. Essential for achieving the COBE cosmological objectives are the all-sky observing strategy, periodic

absolute calibrations of the instruments, high sensitivity, and extensive care to minimize potential systematic errors.

On September 21, 1990, the 600 liters of helium in the FIRAS and DIRBE cryostat were depleted. This date ended the operation of the FIRAS instrument which had surveyed the sky 1.6 times. The DMR continues to perform normally in all of its six channels. As the DMR continues to gather data, the noise levels in the resulting sky maps are steadily decreasing, showing that the sensitivity limits of this instrument have not yet been reached.

The DIRBE continues operating in the four near-infrared bands, even though the temperature of the dewar had warmed to about 50 K by July 1991. Continued data-taking is important to further understand any systematic errors and for gathering data on the interplanetary cloud in which we reside. This cloud must be understood well enough to model and remove its emission from the data to search for a cosmic infrared background, the light from the first galaxies that formed in the universe.

The first cosmological results from COBE were announced in January 1990, confirming the Big Bang theory with extraordinary precision by showing that the residual radiation has a nearly perfect blackbody spectrum and is almost equally bright in all directions. Since this initial release, additional data show an even greater smoothness to the universe. At the present level of data processing, there is no deviation from a perfect blackbody spectrum to 0.25 percent of the peak intensity, and any anisotropies or lumpiness on all angular scales greater than 7° must be smaller than 4×10^{-5}.

The first systematic search for cumulative light from the first objects in the universe is underway. A preliminary spectrum determined from data in one of the darkest areas of the sky shows that the faintest levels of emissions from our galaxy and solar system occur at wavelengths of 3.4 μm and longward of 240 μm. Careful modeling of these foreground emissions is now in process. The results of the model will decrease the limits on, or permit the detection of, infrared brightness of cosmic origin.

The COBE results are of major interest to the field of cosmology. One of the most important scientific questions facing astronomers today is, when in the evolution of the universe did galaxies begin to form? Cosmologists are trying to explain the fact that the COBE sensitive instruments so far have indicated that the Big Bang was a uniform, featureless explosion and there are no detectable traces of the formation of the present objects in the universe. Theorists are postulating the existence of new kinds of matter, or even the possibility that Einstein's theory of gravity is not correct. The answer to this present dilemma is not yet known, but the COBE data are having profound implications for our understanding of the early universe, laws of physics, and our perspective on our place in the cosmos. The COBE all-sky data, still at a very preliminary stage, should provide additional insights into our understanding when the data are fully processed.

In addition to the primary cosmological results, COBE data are contributing significantly to the knowledge of the Milky Way galaxy. The FIRAS instrument has made the first all-sky infrared spectral line survey and has also mapped the spectra of the galactic dust distribution at wavelengths >100 μm. Nine lines from interstellar [C I], [C II], [N II], and CO are all clearly detected, and [C II] at 158 μm and [N II] at 205.3 μm are strong enough to be mapped. These global data are important to understanding the heating and cooling mechanisms in our galaxy.

The processing and analysis of COBE data takes place at the Cosmology Data Analysis Center (CDAC) which opened in March 1991. The CDAC facility is operated by the COBE Project of GSFC, and is located off-campus in Greenbelt, MD. The massive processing of the all-sky data is underway following the pilot examination of sample data from small parts of the sky on which the preliminary results are based. Proper characterization, analysis, and removal of systematic error sources will be included in this full processing, and should result in a much improved sensitivity and accuracy of the data. The first COBE data products from all three instruments are planned for release to the scientific community in mid-1993, providing scientists with a rich set of data products covering infrared and

microwave wavelengths for further analysis. These products will enable scientists to make advances in the fields of cosmology, galactic, and solar system science that have not before been possible.

The research described in this article is the result of collaborative efforts of the COBE Science Working Group.

Contact: Nancy W. Boggess (Code 685)
(301) 286-6989

Sponsor: Office of Space Science and Applications

Dr. Nancy W. Boggess is an Astrophysicist in the Infrared Astrophysics Branch of the Laboratory for Astronomy and Solar Physics. She is a member of the COBE Science Working Group and is Deputy Project Scientist for Science Operations.

WHAT IMAGE RESTORATION CAN DO FOR THE HUBBLE SPACE TELESCOPE

The R Aquarii symbiotic system was one of the first objects observed with the Hubble Space Telescope (HST) because it is considered to be somewhat of a Rosetta Stone for many astrophysical processes. This binary star system is comprised of a hot subdwarf companion star in orbit around a cool, voluminous, red giant star which is losing mass on a continuous basis. The surface temperature of the giant is ~2,500 K which is nearly half that measured at the Sun's surface. The hot companion's temperature is ~25,000 K. The companion star's presence is inferred spectroscopically from nebular line emission, but is hidden from direct view because it is dim relative to the giant star. Moreover, the companion may be occulted by a thick accretion disk that has formed around it from material captured from the mass-losing giant. The accretion disk is very hot and beams material away from the system in the form of a collimated jet of nebular material via radiation pressure or a proton wind.

The left panel of the figure shows a three-dimensional rendering of the R Aquarii nebular jet in the light of twice-ionized oxygen atoms emitting in the optical region of the electromagnetic spectrum (wavelength ~5007 Å). The image was obtained with the HST Faint Object Camera (FOC). These data are plagued by both spherical aberration, which is responsible for the large bright, elliptical region that dominates the image, and detector saturation, which is shown as the dark, irregular central valley within the elliptical region.

Saturated data are caused by failure of the detector to accommodate very intense sources of light-information in such regions is therefore unreliable and cannot be used. However, spherical aberration causes some of the information from the intense radiation falling into the saturated regions to spread into outlying areas that are not saturated. Thus, through image restoration techniques, information concerning the saturated region can be inferred by statistical methods. Odd as it may seem, spherical aberration actually helps the restoration in this particular case.

The right panel of the figure shows the R Aquarii jet restored to the original design resolution of the HST by means of an algorithm known as Maximum Entropy. After processing, the general nebulosity is enhanced, the saturated data are restored, and three separate emission regions emerge, characteristic of the gas comprising the jet. The three restored central emission peaks are so intense that they have been scaled down to also show the restoration of the weak extended nebulosity in the same figure.

The entire binary system comprising the cool star, the hot companion, and its accretion disk are engulfed by the right-most central emission peak. The very low-level circular feature is an artifact of a noisy point-spread-function (i.e., the response of the HST-FOC combination to a point source of light) used in the restoring processing. Comparison of these HST images, with radio continuum imagery taken at nearly the same resolution, suggests that shocks account for the excitation of the jet.

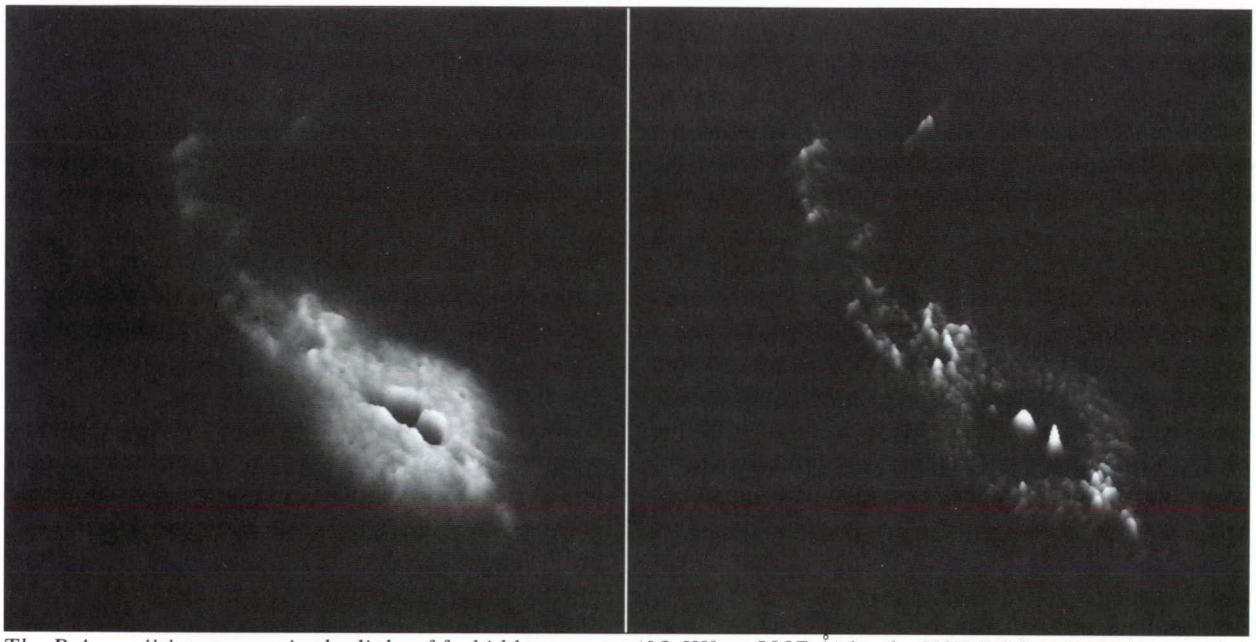

The R Aquarii jet as seen in the light of forbidden oxygen ([O III] at 5007 Å) by the HST-FOC. Both the raw (left panel) and restored HST-FOC images (right panel) are illustrated.

The restoration computations described above required 3 hours of processing on a parallel computer with 8,192 processors—the MasPar MP-1. Many image restoration techniques—such as the one used here—are not fully developed or implemented, and are areas of current computer science research, especially on parallel computer architectures. Thus, an important potential legacy of the HST may well be its advancement of restoration techniques in addition to its legacy of advancements in astronomical sciences.

Technical aspects of this work, "Comparing Restored HST and VLA Imagery of R Aquarii," by J. M. Hollis (NASA/GSFC), J.E. Dorband (NASA/GSFC), and F. Yusef-Zadeh (Northwestern University) are scheduled for publication in the February 1992 issue of the *Astrophysical Journal.*

Contact: Jan M. Hollis (Code 930)
(301) 286-7591

Sponsor: Office of Aeronautics and Space Technology

Dr. Jan M. Hollis, an Astronomer with 12 years of service with GSFC, is the Assistant Chief of the Space Data and Computing Division. Dr. Hollis, who received his PhD degree from the University of Virginia in 1976, pursues observational research on the chemical and physical conditions within interstellar clouds and nebulosity associated with binary star systems.

EARLY RESULTS FROM THE GODDARD HIGH RESOLUTION SPECTROGRAPH

The Goddard High Resolution Spectrograph (GHRS), launched aboard the Hubble Space Telescope on April 24, 1990, records the spectrum of ultraviolet light from stars, galaxies, and other objects with unprecedented detail, sensitivity, and precision of measurement. The GHRS is returning scientific information of great interest to astronomers.

Ultraviolet spectroscopy is the principal method for exploring the chemical composition and physical state of the atmospheres of stars, circumstellar

nebulae, interstellar matter, and other objects and media in the universe. GHRS has advanced this technique significantly, as shown in the accompanying figure, which compares the ultraviolet spectra of the star Chi Lupi recorded with the GHRS to one previously observed with a spectrograph mounted on the International Ultraviolet Explorer, a highly successful satellite that was launched in 1978.

Chi Lupi is a chemically peculiar star, with (for example) an enormous amount of platinum, relative to other chemical elements, in comparison to a normal star such as the Sun. The spectrum obtained with the GHRS on the Hubble Space Telescope is marked by absorption lines (dips) due to atoms of cobalt, iron, manganese, nickel, vanadium, chromium, and germanium. In contrast, a spectrum of the identical region of the same star, as obtained with an earlier satellite (upper tracing) is much harder to interpret as most of the absorption lines cannot be individually distinguished.

GHRS observations of this star have revealed that a spectral line that is normally produced by the absorption of ultraviolet light by atoms characterized by a mixture of isotopes of the element mercury is in Chi Lupi produced exclusively by a single mercury isotope. Information of this nature allows astronomers to formulate and test theories of the structure and composition of stellar atmospheres and may eventually allow them to explain how unusual concentrations of platinum and other rare elements can occur in certain stars.

This first year of the GHRS has been exciting and productive for the GHRS science team. Team members, representing GSFC and other scientific institutions across North America, with European associates, have used the spectrograph to study a diverse array of astronomical objects in our own galaxy, the Milky Way, and in other galaxies, and have also studied the ultraviolet spectrum of a quasar.

Each GHRS observation has produced new results that could not be obtained with any other existing or previously operated telescope, spectrograph, or satellite. Some examples of recent findings include the following:

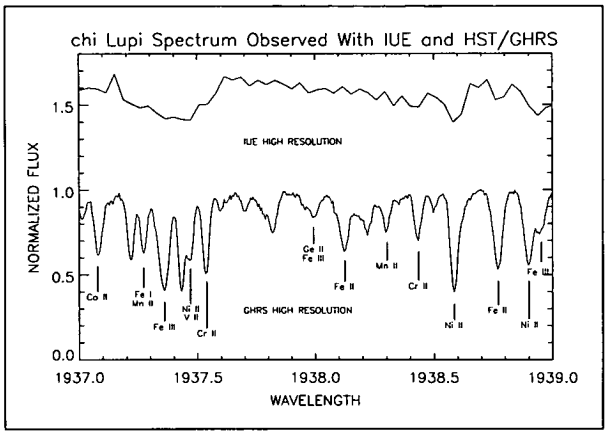

A 2-angstrom-wide region of the ultraviolet spectrum of the chemically peculiar star Chi Lupi as observed by the GHRS (lower trace) and an earlier satellite (upper trace).

- Beta Pictoris, a star that has a circumstellar disk that is widely regarded as a possible protoplanetary system, was found to be accompanied by orbiting clumps of gas that come and go as though they were falling into the star. This phenomenon may be related to the clearing phase which is thought to have occurred after the Earth and other planets formed around the Sun from a similar flattened cloud called the solar nebula.

- Previously unsuspected continuum radiation was discovered emanating from the chromospheres of red supergiant and red giant stars. Such radiation is emitted over a wide range of wavelengths, rather than in discrete parts of the spectrum. The chromosphere is a layer of a stellar atmosphere located above the visible surface of the star. It is hotter and less dense than the surface layer. Its structure is defined by magnetic fields. GHRS investigators expecting to find a spectrum of discrete *bright* lines were surprised to find the broadband glow of continuum radiation, with *dark* spectral lines superimposed.

- The presence of vertically streaming gas in the chromospheres of stars was detected and measured. The observations may provide evidence for anisotropy (change in properties with direction) in certain stellar atmospheres.

Another interpretation is the presence of separate regions in the stellar atmosphere that produce the same spectral lines at different temperatures and with different degrees of turbulence.

- Stars in galaxies beyond the Milky Way were found to be up to 100 times more massive than the Sun, and to be shedding matter at rates that are up to 300 million times greater than the corresponding mass loss in the solar wind. One of these enormous stars will shed an amount of gas equal to the mass of the Sun in only 150,000 years.

- The composition of the gas between the stars has been determined with higher accuracy than before. Such work will provide better information on the processes whereby atoms shed by stars in gaseous form condense into dust particles. Such particles may later accrete to form comets, meteoroids, and the planetary precursors.

- The unusual galaxy NGC 1068 was found to contain a cluster of very young and massive stars, with typical lifetimes of <10 million years. This cluster is unlike any formation in our own or neighboring galaxies.

- Primordial hydrogen clouds were found to be abundant in nearby extragalactic space. These clouds are believed to date to early stages in the history of the Universe and were thought to have vanished, or nearly so, by the present epoch. This discovery was made independently with the GHRS and by another science team with the Hubble Space Telescope's Faint Object Spectrograph. However, the GHRS provided the most detailed data, and detected significantly more clouds. This discovery poses a challenge to cosmologists who must explain why the clouds have persisted over cosmic time; a straightforward analysis of their detectable physical properties indicates that they should have dissipated long ago. Two of the theories advanced to explain this seeming contradiction are that the clouds may contain large amounts of so-called dark matter (invisible matter of a presently unknown type) whose gravitational attraction prevents them from dissipating, and that the Universe may be pervaded by an as-yet-undetected tenuous and hot gaseous medium which produces a gas pressure that resists the expansion of the hydrogen clouds, and thereby prevents them from dissipating.

Contact: Stephen P. Maran (Code 680)
(301) 286-8607

Sara R. Heap (Code 680)
(301 286-5359

Sponsor: Office of Space Science and Applications

Dr. Stephen Maran is a Senior Scientist in the Laboratory for Astronomy and Solar Physics with 23 years of service at GSFC. He earned a BS in Physics at Brooklyn College and an MA and a PhD in Astronomy from the University of Michigan. He received the NASA Medal for Exceptional Achievement for his contributions to the HST project. Dr. Maran's research interests include stars, nebulae, and galaxies.

Dr. Sara Heap received her PhD in Astronomy from the University of California, Los Angeles. She currently works in the Laboratory for Astronomy and Solar Physics, and has 22 years of experience at GSFC.

UV FE VII ABSORPTION AND FE II FLUORESCENCE EMISSION LINES IN CENTRAL STARS OF PLANETARY NEBULAE AND OTHER VERY HOT STARS

There have been several recent developments that have considerable significance for our understanding of stars in their late stages of evolution, such as the central stars of planetary nebulae, hot subdwarfs, white dwarfs, and hot degenerate stars. It was generally thought that these objects have stellar atmospheres that consist mainly

of hydrogen and helium without traces of heavy elements, since these should have settled out long ago. Until recently, only two central stars indicated the presence of highly ionized species of metals, such as Fe V, Fe VI, and even Fe VII in absorption lines of their ultraviolet spectra taken with the International Ultraviolet Explorer (IUE) satellite. However, a comprehensive study of the entire IUE archival database of high dispersion spectra of central stars and some hot subdwarfs showed that highly ionized species of iron are much more common than had been realized up to now.

A total of ~30 central stars showed the Fe VII absorption lines, of which only 4 are sufficiently strong to be detected in the short-wavelength region of the IUE. An example of Fe VII and Fe VI lines is shown in the first figure, a small portion of the UV spectrum of the central star of the planetary nebula Abell-36. The detection of Fe VII in the photospheres of these stars seemed counter to accepted theories of stellar evolution, but can be explained as being due to radiative levitation which raises these species to the outer layers of the stars.

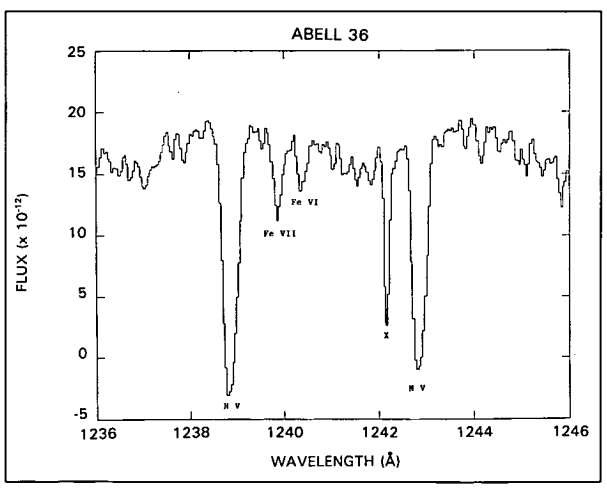

Portion of the ultraviolet spectrum of the planetary nebula Abell-36 showing Fe VII and Fe VI absorption lines between the strong N V absorption doublet.

In a related IUE archival search, Fe II fluorescence emission lines were found in a large number of the objects listed above. Although low-excitation Fe II emission lines are very common in stellar spectra, these high-excitation Fe II lines are of an entirely different nature—they are resonantly excited by O VI, C IV, or H I. Again, there are only a few of these Fe II lines observable in the IUE short-wavelength region. Of greatest interest are the Fe II lines that are excited by O VI lines (i.e., oxygen from which five electrons have been stripped) because they represent one of the highest known stages of excitation found in planetary nebulae. Of the more than 1,700 galactic planetary nebulae, <1 percent belong to a high-excitation class that is called "The O VI Sequence." Their optical spectra are characterized by a very strong pair of O VI lines near 3820 Å. The O VI double can reach such strong intensities that the amount of radiation emitted by this pair of lines alone can rival the entire output of one solar luminosity. What makes the ultraviolet Fe II lines so interesting is that they are excited by an O VI line at 1032 Å which lies beyond the spectral sensitivity range of the IUE, and that of the Hubble Space Telescope as well. By studying the resonantly excited Fe II emission lines one can estimate the intensity of the (unseen) O VI emission at 1032 Å and infer temperatures and other stellar parameters.

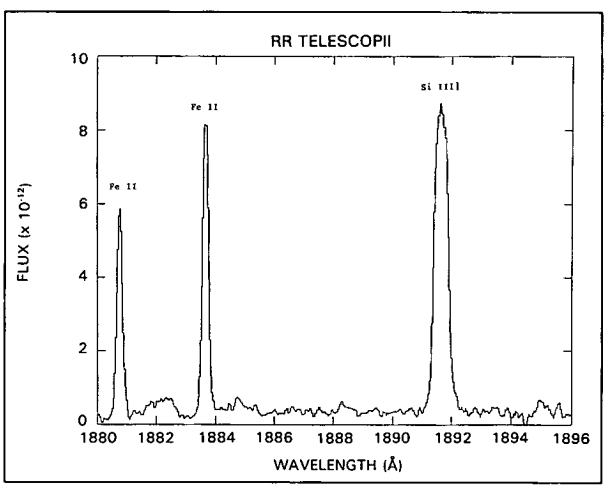

Portion of the ultraviolet spectrum of the symbiotic star RR Telescopii. The letter R denotes a reseau mark.

An example of the Fe II lines near 1880 and 1884 Å is shown in the second figure, which is from a portion of the IUE high-dispersion spectrum of the symbiotic star RR Telescopii. The other strong line

near 1892 Å is due to Si III, which has a very weak companion line between the Fe II lines near 1882 Å. The term symbiotic star refers to a binary system that simultaneously shows characteristics of a cool and a very hot component. This type of object is often referred to as a symbiotic nova in which the Fe II lines are particularly strong. Thus, it appears that there may exist a previously unrecognized symbiotic O VI sequence, analogous to the well-known but rare planetary nebulae O VI sequence.

This work was performed as a collaboration between W. A. Feibelman (GSFC), F. C. Bruhweiler (Catholic University of America), S. Johansson (Lund University, Sweden), and K.-P. Cheng (NRC Fellow, GSFC).

Contact: Walter A. Feibelman (Code 684)
(301) 286-5272

Sponsor: Office of Space Science and Applications

Mr. Walter A. Feibelman, a Physicist with 22 years of service at GSFC, has been involved with the development of the sensors for IUE and after its launch in 1978, has been Principal Investigator and Co-Investigator on more than 40 IUE observing and archival data programs.

ULTRAVIOLET IMAGING TELESCOPE OBSERVATIONS DURING THE ASTRO-1 MISSION

The Ultraviolet Imaging Telescope (UIT) is a 0.38-m (15-inch) telescope, equipped with two electronic image-intensifier cameras, a filter wheel, and diffraction gratings. The scientific objectives of the UIT include investigating regions of star formation in external galaxies, detecting and assessing populations of hot stars (e.g., white dwarfs, so-called horizontal branch stars, and others) in dense regions where they cannot be readily distinguished (if at all) with ground-based telescopes, and inferring the properties of interstellar dust in reflection nebulae and other environments through evaluation of its radiative transfer properties in ultraviolet light.

Dense regions of special interest for UIT investigations include the globular star clusters, which are spheroidal aggregations of hundreds of thousands to a million or more stars. Reflection nebulae are interstellar clouds of gas and dust that shine by the reflection (properly called scattering) of the light from adjacent stars by individual dust particles. Interstellar dust particles, microscopic in size, are thought to consist of graphite, silicates, and/or iron and other elements. The particles may be coated with water ice or with other frozen but volatile chemical compounds.

The UIT was built at GSFC and was operated by GSFC scientists, engineers, and their associates from the Payload Operations Control Center at the Marshall Space Flight Center, Huntsville, AL, during the Astro-1 mission. Members of the team alternated in 12-hour shifts throughout the flight. A member of the UIT science team, Dr. Ronald Parise of Computer Sciences Corporation, participated as a Payload Specialist on board Columbia during the mission. A total of 821 exposures (film frames) were obtained with the UIT during the Astro-1 mission.

In the UIT electronic image-intensifier camera, an ultraviolet image produced by the telescope falls on a photocathode, where it stimulates a flow of electrons that strike a phosphor, making it shine brightly in green light. This visible-light image is then readily recorded on photographic film. A special property of the UIT cameras is that they are "solar-blind," meaning that ordinary visible light, in which the Sun shines most brightly, is excluded by the judicious use of optical coatings, photocathode materials, and filters. This enables the UIT scientists to study dim ultraviolet light from white dwarf stars and other objects in environments, such as galactic bulges and globular star clusters, where the radiation consists overwhelmingly of yellow and red light from red giant stars and from main sequence stars (those which, like the Sun, derive their energy from the nuclear burning of hydrogen at their centers). The resulting photographs, which represent a total exposure time of 115,000 seconds, provide astronomers with spectacular images of such important targets as the globular cluster Omega Centauri, the spiral galaxy Messier 81, and a famous

interstellar cloud complex known as the Cygnus Loop. The Cygnus Loop is believed to consist of interstellar clouds whose appearance and physical condition has been substantially altered by the blast from an ancient supernova or exploding star.

The field of view of the UIT photographs is 40 arcmin, about 1/3 larger than the angle subtended by the full Moon. In contrast, the largest field of view that is photographed at one time with the Hubble Space Telescope is 2.7 arcmin on a side. While the HST provides images at very high spatial resolution, the UIT obtains images at lesser resolution (about 2 arcsec) but over a wide region. This makes the UIT a valuable tool for discovering objects over regions too large to survey with the HST, but which can then be studied in greater detail with HST and other ultraviolet observatories (such as the International Ultraviolet Explorer). Furthermore, the UIT can readily detect large-scale spatial changes in the properties of extended objects such as galaxies, nebulae, and star clusters over large angular distances.

The preliminary analysis of UIT photographs from the Astro-1 mission has already shown clear radial gradients (systematic variations with distance from the center) in the ultraviolet color of elliptical and spiral galaxies. Other images are providing significant information on the nature of the cooling flow (the cooling and condensation of hot intergalactic gas) in the Perseus cluster of galaxies and on the population of young stars in the stellar association NGC 206, a loosely aggregated, slowly dissipating star group located ~2 million light-years from Earth in the Andromeda galaxy.

Studies of the UIT images from Astro-1 will keep the science team busy determining the properties of the above-named objects as well as other nebulae, interacting galaxies and selected star fields in the Magellanic Clouds (the companion galaxies of the Milky Way) through the next few years as they prepare for the second flight of the UIT on the Astro-2 mission.

Contact: Theodore P. Stecher (Code 680)
(301) 286-8718

Stephen P. Maran (Code 680)
(301) 286-8607

Sponsor: Office of Space Science and Applications

Mr. Theodore Stecher is a Senior Staff Scientist in the Laboratory for Astronomy and Solar Physics and has 32 years of experience at GSFC. He obtained a BA in Philosophy and an MS in Astronomy from the University of Iowa. Mr. Stecher is the Principal Investigator for UIT.

Dr. Stephen Maran is a Senior Scientist in the Laboratory for Astronomy and Solar Physics with 23 years of service at GSFC. He earned a BS in Physics at Brooklyn College and an MA and a PhD in Astronomy from the University of Michigan. He received the NASA Medal for Exceptional Achievement for his contributions to the HST project. Dr. Maran's research interests include stars, nebulae, and galaxies.

NARROWBAND IMAGING FOR THE EARLY EVOLUTION OF GALAXIES

A program of instrument development combining new spectroscopic devices for possible future missions, and testing of detectors for missions under development is yielding interesting new results on galaxies at high redshifts, early in the evolution of the Universe.

Using the Kitt Peak 4-m telescope and our narrowband Fabry-Perot imager and charge-coupled device (CCD) detector, we have detected a galaxy in the light of the hydrogen Lyman alpha spectrum line redshifted from the UV (122 nm) into the visible (401 nm), a redshift of 2.3. It is near the line-of-sight to a quasar whose spectrum contains a strong Lyman alpha absorption line at the same redshift. At 48 arcsec (0.6 million light-years) from the quasar line-of-sight, with a velocity difference of 350 km/s from the absorber, it appears to be a star-forming galaxy in the same cluster as the absorber. It is resolved into two patches, leading us to wonder if

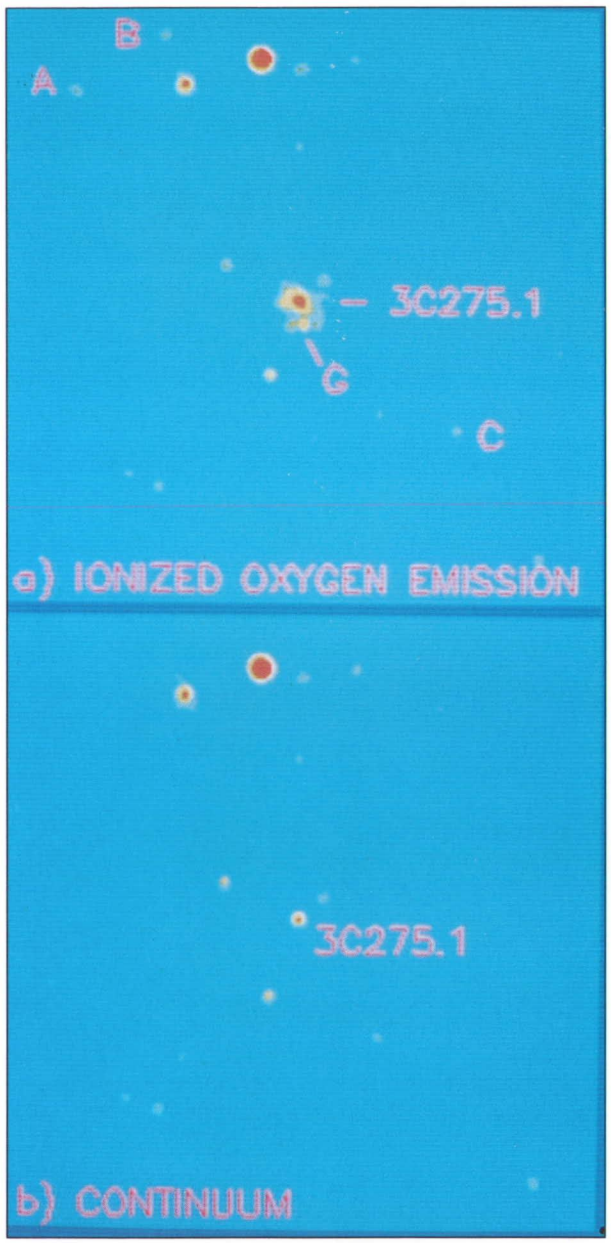

Four line-emitting galaxies within or superimposed on the core of the cluster (A, B, C, G).

this is a double-lobed structure from one galaxy, or the merger of two galaxies.

We have also detected a galaxy in a redshifted spectrum line of ionized oxygen at a redshift of 0.8, 4 arcsec away from the line-of-sight to another quasar, with the redshift corresponding to that of an absorption line of magnesium in the quasar's spectrum. This is also a strongly star-forming galaxy, possibly one of a suggested class of bright star-forming dwarf galaxies more common at these redshifts than those found at the present time.

We have also observed the quasar 3C 275.1 in its surrounding cluster of galaxies, taking narrowband images in the light of the redshifted oxygen line at the redshift of the quasar (0.55). The emission-line cloud surrounding the quasar was easily mapped.

However, we were somewhat surprised to detect four line-emitting galaxies within or superimposed on the core of the cluster, since this cluster is simultaneously rich, symmetrical, and dense (A,B,C,G in the figure). Subsequent spectroscopy of these objects revealed blue continua and confirmed strong oxygen-line emission. The active galaxies detected in this cluster have oxygen-line luminosities comparable to previously measured luminous blue galaxies, implying star formation rates of roughly 1 to 4 solar masses per year.

In addition to the current Fabry-Perot imager, which uses a 512 x 512 pixel CCD, we are building a Lyot birefringent filter to provide narrowband imaging over the field of a 2048 x 2048 pixel CCD. This capability will further extend the field of view to encompass more of the known and potential clusters of galaxies.

We would like to acknowledge the efforts of Larry Brown of Code 683, Ron Oliversen of Code 684, Paul Hintzen of Code 681, Adeline Caulet of NRC, James Lowenthal of the University of Arizona, and Richard Green of NOAO who were also authors of this article.

Contact: Bruce Woodgate (Code 681)
(301) 286-5401

Sponsor: Office of Space Science and Applications

Dr. Bruce Woodgate works in the Laboratory for Astronomy and Solar Physics at GSFC. He received his PhD in Astronomy from the University of London. He also has a BSc in Physics from the University of London. He has 16 years of experience at GSFC.

SOFTWARE CONFIGURABLE CCD CAMERA FOR SPACE-FLIGHT APPLICATIONS

The GSFC Laboratory for Astronomy and Solar Physics has developed a Charge-Coupled Device (CCD) camera (see the figure) design for space-flight use with multimission capability. The first use of this camera will be as part of a spectrographic instrument on board the Solar and Heliospheric Observatory (SOHO) spacecraft part of the ISTP mission. The SOHO spacecraft is scheduled for launch in 1995.

The multimission design philosophy allows the design of the camera electronics to be largely independent of the actual CCD selected for use as the detector. It is the CCD itself that is usually the mission-dependent part of the camera. This is of great importance to the basic camera design since CCD topologies can vary widely from one manufacturer to another. Such factors as aspect ratio, number of pixels, readout mechanisms, clock-phasing, and clocking levels are all variables that must be incorporated into the hardware design of the camera.

A typical CCD camera may use dedicated-state machine hardware (with a certain amount of programmability) to generate the various clocking and control waveforms required by a CCD. In our camera, all CCD parameters including clocking patterns are controlled by a high-performance microprocessor (an INMOS Transputer), enabling complete programmability of CCD operation. In essence, complex hardware is replaced by smart software. The only hardware change required to support different CCD styles is at the printed circuit board to which the CCD is mounted.

There are several advantages to this approach:

- It allows multimission capability;
- State machine hardware is largely eliminated, thereby usually decreasing mass/power requirements and increasing reliability;
- CCD development time is improved since iterative hardware modifications give way to on-the-fly software changes; and,
- Since the camera can be reprogrammed from the ground, it is possible to continually optimize CCD performance in orbit. This may be useful in offsetting degradation of the device due to radiation damage.

All of the analog electronics subsystems, such as the CCD phase drivers and signal processing elements, are programmable devices that reside on extensions of the transputer bus. All important voltages and currents are monitored and available for query. When configuration information is changed in software, the results immediately appear in the hardware without redesign of the electronics.

The baseline camera design uses the Tektronix 1024 x 1024 CCD. This CCD supports quadrature readout as well as the multipinned-phase mode of operation. The camera has four signal processing chains, one for each of the CCD quadrants. Enough clock drivers are provided to support this device, both in its primary readout mode (quadrature) and in any one of six alternate readout modes. These alternate readout modes require less hardware to operate and are backup mechanisms to work around hardware failures while in orbit. The software design allows for data reduction in analog form through CCD binning (pixel summing) and windowing (pixel selection) techniques. This data preprocessing reduces the workload for on-board digital processing units before transmitting the data to the ground.

Support equipment has been designed to allow this camera to be connected to virtually any computer system that has a GPIB interface. This support equipment is called the Instrument Interface Simulator (IIS). It serves as a frame buffer for the CCD camera and implements three communications interfaces: a command interface to the camera; a data interface to the camera; and, a standard GPIB (IEEE-488) interface. The first two are redundant, serial interfaces. The camera and the IIS are operated with a command list that works well over the GPIB interface.

Breadboard camera and IIS (right) with a i486-based computer, additional storage, and display equipment.

We are using Intel 386- and 486-based computers operating under the OS/2 operating system. The custom-designed control program is an OS/2 Presentation Manager application that allows us to control the camera, capture the image data and display it, and perform simple analysis tasks. We will use a Sun Sparcstation running IDL during the calibration phase of the project for data analysis with the OS/2-based machine as the camera controller.

Participating company: Advanced Technology and Research, Inc.

Contact: Leslie James Payne (Code 683)
(301) 286-8988

J. Patrick Haas (Code 683)
(301) 286-9298

Sponsor: Office of Space Science and Applications

Mr. Payne holds a BS in Electrical Engineering from Virginia Polytechnic Institute and State University. His 7 years of experience at GSFC include work on MOSAIC, a high-speed photon-counting image-intensified CCD camera, and ISTP/SOHO, an image-intensified CCD for extreme ultraviolet spectroscopy.

Mr. Haas holds a BS in Electronic Engineering Technology from Capitol College. He has 2 years of experience at GSFC, working various missions associated with the ISTP project including Wind, Polar, Geotail and currently, SOHO. His current work with SOHO involves the controller design for a large-area CCD imager used for solar EUV spectroscopy.

NEW ASTRONOMICAL DISCOVERIES WITH A 5- TO 18-μm INFRARED ARRAY CAMERA

An infrared array camera which was developed for the unusual demands of high-background astronomical imaging at 5 to 18 μm has completed nine successful observing runs at Mauna Kea Observatory in Hawaii. Eight runs used the 3-m NASA/Infrared Telescope Facility, and one used the 4-m United Kingdom Infrared Telescope. The array detector used for the observations described here is a 58 x 62 pixel hybrid Si:Ga (gallium-doped silicon) photoconductor detector, manufactured by Hughes/Santa Barbara Research Center. The array camera system was developed in the Infrared Astrophysics Branch at GSFC (Code 685).

Photometry in the thermal infrared (~10 μm) is complicated by the very large background flux radiated by room-temperature objects, such as the telescope, camera instrumentation, as well as the Earth's atmosphere. The difficulties of operating an array detector under these conditions have discouraged many potential infrared experimenters. Typical high-resolution results obtained with the array camera are illustrated by the multicolor images of the Galactic Center shown in the first figure. The striking differences in the images over this short wavelength range are due to temperature differences among the sources (the cooler dust only becomes visible at longer wavelengths) and the effects of the strong 9.8-μm spectral feature, due to silicate dust grain absorption through the disk of the Galaxy and also local to the individual Galactic Center sources. Some sources are more heavily affected than others (most noticeable in IRS3, at upper right in each image).

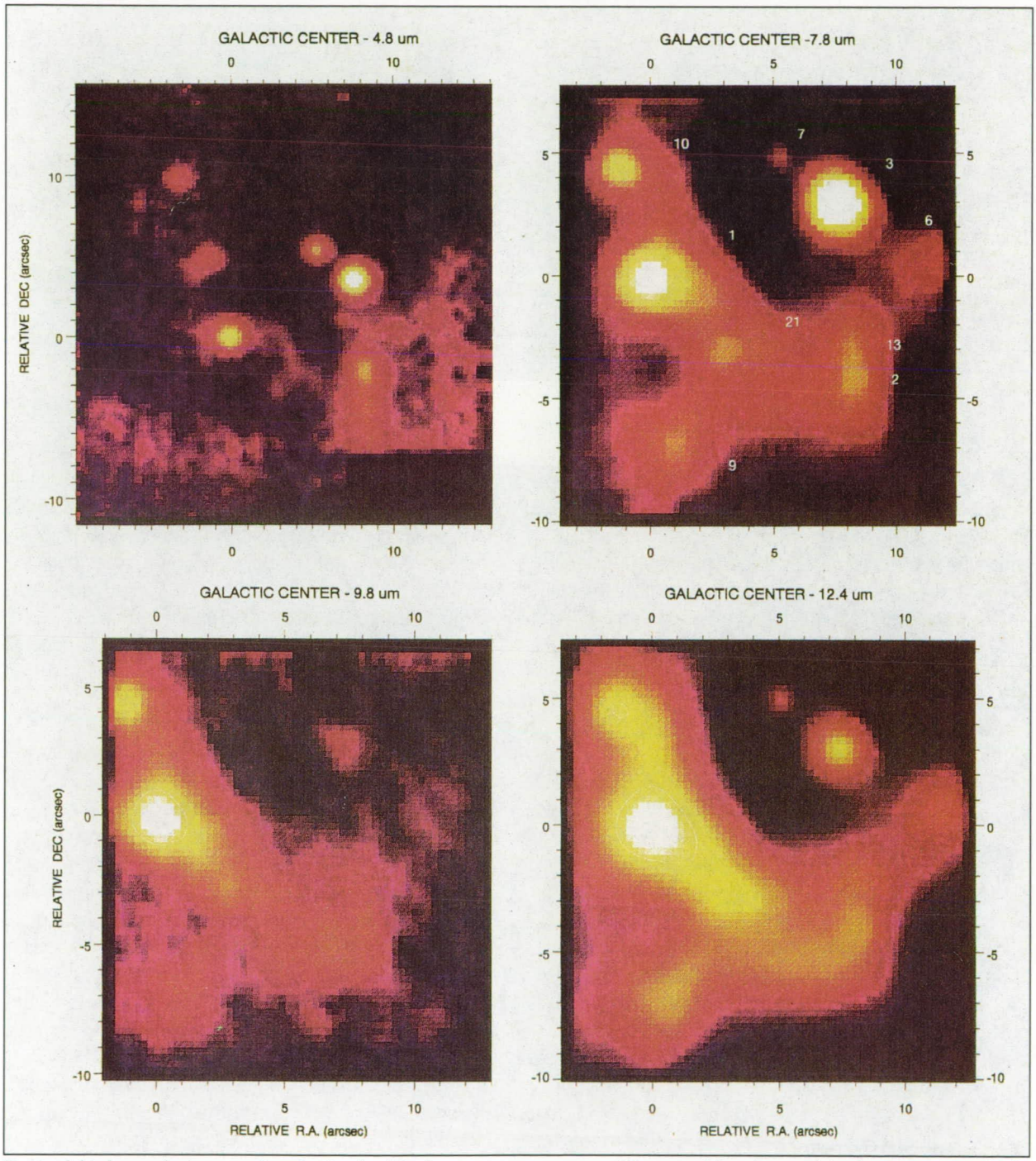

Typical high-resolution results obtained with the array camera are illustrated by the multicolor images of the Galactic Center.

A five-color infrared imaging study of the bright planetary nebula NGC 7027 has been carried out which suggests that emission from a more complex form of dust grains, polycyclic aromatic hydrocarbons (PAHs) which form from carbon ring molecules, may extend farther from the center of the nebula than common silicate dust grains. Images were obtained that show the extent of the continuum emission, the PAH grain features at 8.65 and 11.25 μm, and the 9.8-μm silicate dust emission. It appears that subtle but important differences exist in the dust distributions. The PAH emission extends ~1 arcsec (20 percent) farther out in radius than the continuum dust emission, confirming previous controversial photometric measurements.

New diffraction-limited structure has been resolved at nine wavelengths between 5 and 20 μm in the vicinity of Orion IRc2, the object widely thought of as the primary luminosity source for the entire Orion infrared complex (IRc2 is the bright, compact source seen slightly left of center in the second figure). The Orion SiO maser at IRc2 is the only example of an SiO maser identified with a star formation region rather than with a well-known late-type star, and IRc2 is the only star-formation region known to contain an SiO maser source. Thus, the Orion SiO maser is regarded as unique in the galaxy. Contrary to the prevailing view that IRc2 is extended and dominates the region, the new array images show that IRc2 and its neighbor, IRc7, are both very compact objects which are equally bright at 12.5 μm and connected by a narrow ridge of mid-infrared emission.

A new point source found in the array images has also been detected at radio wavelengths, permitting a definitive registration of the infrared and radio positional reference systems to be made. The precise astrometry shows that the Orion SiO maser is displaced 0.7 ± 0.1 arcsec from the peak of the IRc2 infrared source. Thus, the SiO maser and the IRc2 infrared source cannot arise from the same compact object. The infrared ridge seems to be eroded on the side adjacent to the maser/radio cluster, suggesting that a luminous object is present near the center of the cluster, exciting the SiO maser and contributing to the infrared luminosity observed in IRc2.

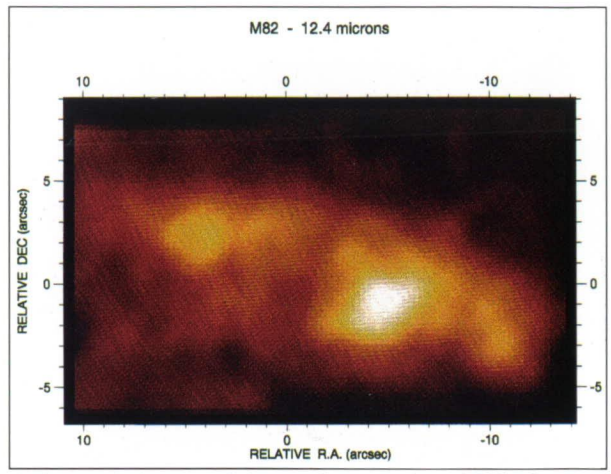

A dramatic image of the starburst galaxy M82 obtained at 12.4 μm with 1-arcsec resolution.

The first 20-μm astronomical observations using an array detector have been made in a collaboration with NASA/Ames Research Center, using an antimony-doped silicon (Si:Sb) array of the same SBRC multiplexer design as our standard array. Among the objects imaged in this first array application at 20 μm were NML Cyg, Beta Peg, NGC 7027, Epsilon Eri, Alpha Ori, Jupiter, O Ceti, and W3 IRS5. An apparently extended component to the bright nucleus of NGC 1068 was detected, which supports a similar result obtained with the array camera at 12.4 μm.

A new, large-scale structure was imaged in the Orion BN/KL complex over a 45- x 45-arcsec field with 1-arcsec resolution. Knotty detail was observed from cooler material which is not easily detected at 10 μm, suggesting that the region is more complex and contains more luminosity sources than previously thought. A dramatic image of the starburst galaxy M82 was obtained at 12.4 μm with 1-arcsec resolution (see the third figure), in a collaboration with C. Telesco of NASA/Marshall Space Flight Center. This is the highest spatial resolution infrared image of M82 yet obtained, and shows that the mid-infrared emission is very clumpy, and originates in dust heated by young stars that have formed in the nuclear region of the galaxy. Each of the brightest clumps appears to be powered by a super-star cluster of 3×10^5 solar masses and 10^8 solar luminosities. Much of the dust between these clusters has been destroyed. The ratio of gas-to-dust emission

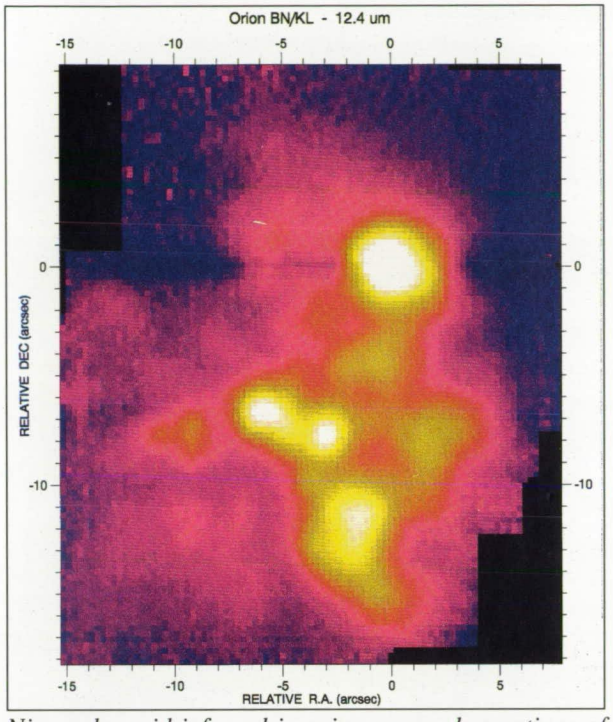

Nine-color mid-infrared imaging array observations of the Orion BN/LK infrared complex (IRc2 is the bright, compact source seen slightly left of the center).

luminosity at the infrared peaks is very high due to the expulsion of gas from the starburst. We propose that excess radio emission near the nucleus originates in supernova remnants expanding into the void left there by activity associated with the preceding, primary starburst phase. Even though young stars may be numerous in that region, the IR emission is low because most of the dust was also expelled. We see no convincing evidence that the radio and x-ray point sources (which are thought to be young supernova remnants) emit infrared radiation at a level typical of young supernova remnants observed in our own galaxy.

Contact: Daniel Gezari (Code 685)
(301) 286-3432

Sponsor: Office of Space Science and Applications

Dr. Daniel Gezari recently was awarded the NASA Exceptional Scientific Achievement Medal for his development of the Infrared Array Camera System. He received his BA in Physics from Cornell University and a PhD in Astronomy from the State University of New York at Stony Brook. He came to GSFC in 1976 as an NRC Fellow. He is a pioneer in Speckle Interferometry and submillimeter astronomy, and also is the PI for NASA's Catalog of Infrared Observations.

COMPACT DISKS OF ASTRONOMICAL CATALOGS

The objective of the Astronomical Compact Disk Project is to provide reference catalogs of data that will facilitate scientific research by astronomers worldwide. Astronomical catalogs of stars and galaxies contain a variety of tabular data, such as the position of the object, temperature, velocities or motions, variability in luminosity, distance indicators, cross-identifiers, and bibliographical references. By having these data available in one's office or observatory, an astronomer can retrieve, display, and manipulate data from a large number of catalogs whenever needed without having to request magnetic tape copies or use networks to obtain the data.

During the past several years, Compact Disk-Read Only Memory (CD-ROMs) containing astronomical data have been prepared and distributed to the scientific community primarily in the U.S. Some examples of currently available CD-ROMs include the Hubble Space Telescope (HST) Guide Star Catalog of ~20 million stars, Giacobini-Zinner and Halley cometary images, photographic images from planetary space missions to Jupiter, Saturn, Uranus and Neptune, and the NASA Astronomical Data Center's (ADC) disk of 32 frequently requested stellar and galaxy catalogs.

CD-ROMs are an attractive medium for the distribution of data because of the low cost of producing them, the ease of distribution and use, the compact size of the storage medium, and the fact that standards have been adopted which make the preparation and reading of the disks uniform across equipment. Archival data are especially suited for

distribution on CD-ROM since there is usually less need to correct or update such data than is the case with less permanent datasets.

The use of compact disks for astronomical data is especially appealing to astronomers in remote locations where networks may not be available. By installing a CD-ROM reader on a personal computer, one can examine a selected catalog. It is then possible to copy sections, sort the data, merge datasets from different catalogs and make specialized catalogs of selected objects.

A CD-ROM stores 680 MB of data, roughly equivalent to six high-density (6250-bpi) magnetic tapes. With more and more data being stored on CD-ROMs, one can obtain a number of CD-ROMs and thus have a small library at one's fingertips.

In 1990, the seven international ADCs, located in Argentina, China, France, Germany, India, U.S., and U.S.S.R, were asked to submit their recommendations for the astronomical catalogs that should be included on the first CD-ROM. From these inputs a master list was developed. Out of the approximately 650 machine-readable catalogs of stars and galaxies in the GSFC ADC, 120 of the most frequently requested catalogs were placed on a CD-ROM for international distribution.

In early 1991, the International Astronomical Union (IAU) agreed to cosponsor this project with NASA. At the 1991 meeting of the IAU, the CD-ROM project was described, and many astronomers from developing countries requested the disks.

Two thousand copies of the two-disk set have been produced. One disk is in Flexible Image Transport System (FITS) format, which has been adopted by the IAU as a standard for astronomical data; the other is in standard ASCII format, which can be easily read by any computer system.

The Compact Disks of Astronomical Catalogs Project has been recommended as a Proposed Science Project by the Space Agency Forum on the International Space Year (SAFISY). It is hoped that this international cooperative effort will prove useful to astronomers all over the world needing reference catalogs of data for stars and galaxies.

Contact: Jaylee M. Mead (Code 930)
(301) 286-8543

Sponsor: Office of Space Science and Applications

Displayed is a selection of CD-ROM data disks currently available from the National Space Science Data Center (NSSDC).

Dr. Jaylee M. Mead is Associate Chief of the Space Data and Computing Division. She received her PhD in astronomy from Georgetown University, Washington, D.C. She joined GSFC in 1959.

WHAT HAPPENS TO A WHITE DWARF STAR WHEN IT EXCEEDS CHANDRASEKHAR'S MASS LIMIT?

A white dwarf star is the final stage of a star with mass of up to several solar masses. A white dwarf is formed through a noncataclysmic process, where an evolved red giant star that has exhausted the hydrogen fuel in its core through nuclear fusion sheds its extended atmospheres, leaving in its wake its electron-degenerate core, which has a density of ~1 ton per cubic centimeter. Since its formation is nonviolent, a white dwarf can exist in a binary system.

There exists an upper bound for the mass of a white dwarf. In honor of Chandrasekhar, who first computed that limit, it is known as Chandrasekhar's mass limit and its value is 1.44 solar masses. If the mass is greater than this value, an electron-degenerate

core cannot support its own weight. Since a white dwarf is born with a mass less than that limit, we need not speculate about a single white dwarf star exceeding Chandrasekhar's mass limit.

However, in a binary star, a white-dwarf component can receive additional mass from its companion star through an accretion process. If the white dwarf is close to the 1.44 solar mass limit, we must ask what will happen to it when its mass exceeds that boundary. There are two possible consequences: (1) the added mass will increase the temperature and pressure inside the white dwarf, leading to global thermonuclear runaway, giving rise to a Type IA supernova, and leaving nothing after the explosion. (It should be noted that the mass of the white dwarf that becomes a Type IA supernova need not be at Chandrasekhar's mass limit); (2) the additional mass will cause an accretion-induced collapse, causing the white dwarf to become a nuclear-degenerate neutron star with a density of several billion tons per cubic centimeter.

Recent work in collaboration with K. Nomoto of the University of Tokyo, published this year in the *Astrophysical Journal*, shows that under the circumstances likely to prevail in such a binary, the white dwarf will probably become a neutron star rather than explode as a Type IA supernova. According to current theory, a neutron star is normally formed in the collapsing core of a supergiant star as the star becomes a Type II supernova. Since a supernova is the most violent cosmic phenomenon known, a binary system, where a supernova occurs and in which the nonexploding component is a low-mass star, is likely to be disrupted.

On the other hand, this accretion-induced collapse of a white dwarf in a binary will quite probably leave the binary intact. This process could be responsible for the production of low-mass binary pulsars.

Contact: Yoji Kondo (Code 684)
(301) 286-6247

Sponsor: Office of Space Science and Applications

Dr. Yoji Kondo received his PhD in Astronomy from the University of Pennsylvania. After 3 years at GSFC in the mid-1960s, he was at the Johnson Space Center for nearly a decade at the time of the Apollo Missions; he returned to GSFC in 1978. He serves as NASA Project Scientist for the Internationl Ultraviolet Explorer (IUE), which has been operating successfully since its launch in 1978, and is also Project Scientist for the Extreme Ultraviolet Explorer (EUVE) to be launched in 1992. He has an adjunct appointment as professor in physics at George Mason University. He is the recipient of several NASA, JSC, and GSFC awards, including the NASA Medal for Exceptional Scientific Achievement.

Flight Projects

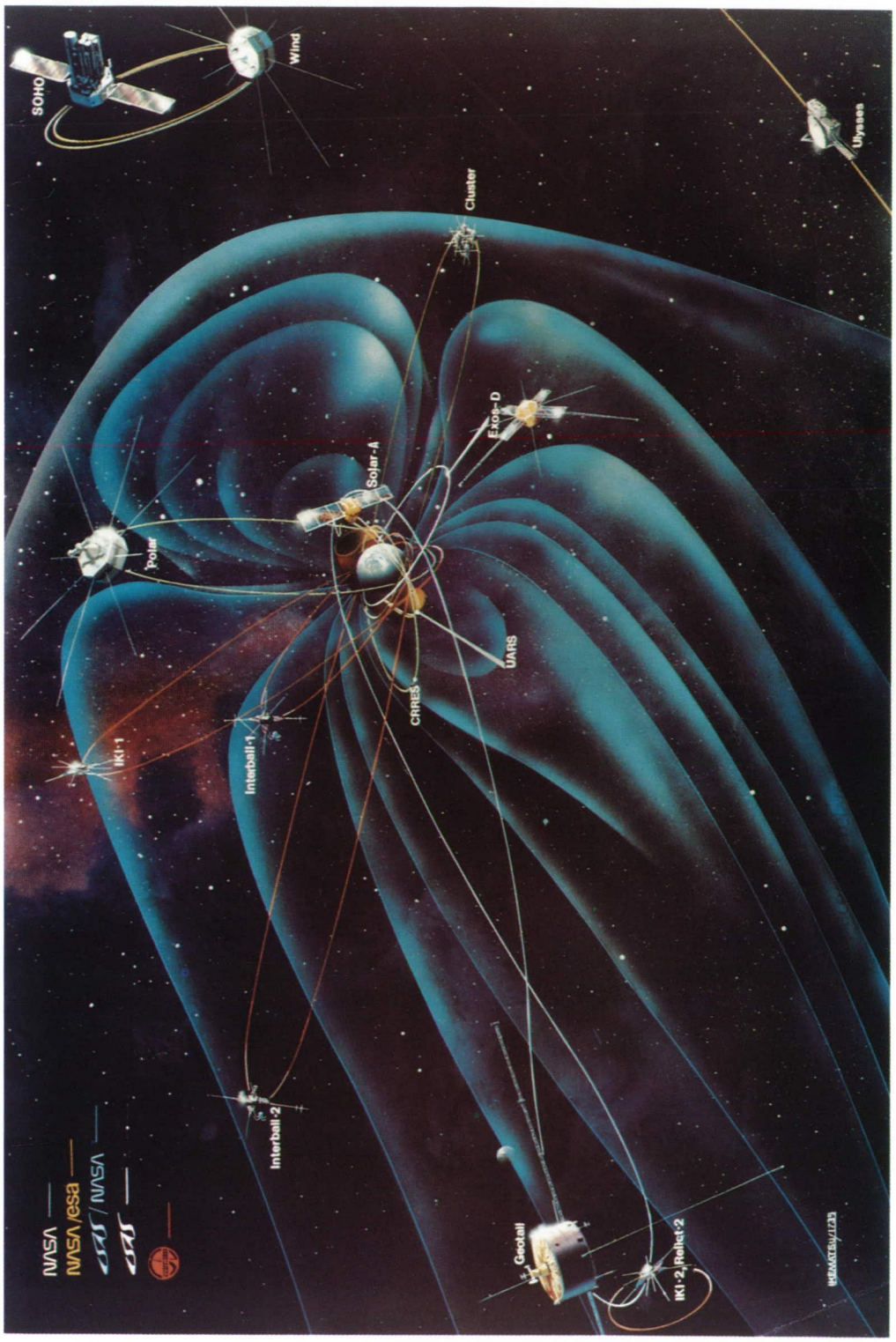

In the Flight Projects Directorate, research and technology developments reach fruition as they are translated into successful flight projects and NASA missions.

FLIGHT PROJECTS

GEOTAIL

The magnetosphere is the region around the Earth defined by the Earth's magnetic field. The field lines of the magnetic sphere are somewhat distorted by the Sun and stretch out from the Earth on the side opposite the Sun in the region known as the magnetotail. NASA is sponsoring four sets of experiment hardware to be delivered to Japan for the Geotail mission in 1991. The Geotail spacecraft is one of the International Solar Terrestrial Physics (ISTP) program observatories that is designed to explore the magnetosphere. It is in this geomagnetic tail region that the Geotail investigation is concentrated. The Earth's environment is one in which complex transformations of energy are constantly occurring. The purpose of the Geotail mission is to clarify the mechanisms of input, transport, storage, release and conversion of energy in the magnetotail. The information gathered during this mission will allow scientists to model and more accurately predict Sun-Earth interactions and their effects on space exploration, communications and in ground technology systems. The principal roles of the seven experiments aboard the Geotail are divided into magnetic-field measurements, electric-field measurements, plasma and plasma wave analysis, and energetic particles.

There are two NASA-sponsored investigations aboard Geotail that have U.S. Principal Investigators. They are the Comprehensive Plasma Instrumentation (CPI), headed by Dr. Louis Frank of the University of Iowa, and the Energetic Particles and Ion Composition (EPIC) Instrument, with Dr. Donald Williams as the Principal Investigator from the Johns Hopkins University/Applied Physics Laboratory. The CPI will obtain comprehensive plasma measurements and comprises a three-dimensional hot plasma analyzer, a three-dimensional solar-wind ion analyzer, and a three-dimensional ion composition analyzer. EPIC consists of a suprathermal ion composition spectrometer and an ion composition system that measures mass and energetic properties of energetic ions.

Two other investigations to be flown on the Geotail spacecraft have U.S. Co-Investigators with hardware responsibility. The first is the Magnetic Field Measurement Investigation (MGF) that will measure magnetic-field variation in the frequency below 50 Hz using fluxgate magnetometers and a search coil magnetometer. The Geotail Inboard Magnetometer (GIM) and associated analog electronics for this investigation are provided by Drs. Ronald Lepping and Mario Acuña of GSFC. The second, the Plasma Wave Investigation (PWI), is composed of three different instruments: (1) the Sweep Frequency Analyzer, (2) the Wave Form Capture, and (3) the Multichannel Analyzer. The Multichannel Analyzer (MCA) instrument is the responsibility of Dr. Roger Anderson of the University of Iowa.

The Electric Field Experiment (EFD), the High Energy Particle Experiment (HEP), and the Low Energy Particle Experiment (LEP) make up the remaining experiments in the Geotail payload. The

◂The Geotail spacecraft is one of the International Solar Terrestrial Physics program observatories, designed to explore the magnetosphere.

Principal Investigators for each of these experiments are from Japan.

The Geotail spacecraft will be launched in the summer of 1992 from the Eastern Space and Missile Center (ESMC) by a Delta II/PAM launch vehicle. During the first phase of the mission, the spacecraft will be placed in an orbit whose apogee radius varies from 80 to 200 Earth radii and a perigee radius from 5 to 10 Earth radii. The length of this phase is about 21 months. In the second phase, the spacecraft will be injected into an orbit of 8 x 30 Earth radii ellipse inclined 7.5° to the ecliptic plane for a period of 18 months.

Contact: Dario E. Galoppo (Code 407)
(301) 286-2808

Sponsor: Office of Space Science and Applications

Mr. Dario Galoppo is an Instrument Systems Manager in the International Solar Terrestrial Physics (ISTP) Project Office. He came to GSFC in 1989 with 25 years of experience in development of instruments for space flight. He holds a BS in Electrical Engineering from New York University.

ASTRO-D X-RAY ASTRONOMY SATELLITE

The Astro-D X-ray Astronomy Satellite is a joint undertaking of the Japanese Institute of Space and Astronautical Science (ISAS) and NASA. The Astro-D astronomy mission is to be launched from Japan in early 1993.

Astro-D will provide exceptional opportunities for the study of high-energy astrophysical phenomena. The goal of Astro-D is to examine a large variety of x-ray sources with moderate spatial resolution and spectral resolution covering the ~1- to 12-keV band with particular emphasis on the iron K-band. Spectroscopy in the iron band is a high-priority scientific objective because of the abundance and richness of features in the relevant spectra of many types of x-ray sources. The spectral coverage of Astro-D also includes spectral features of other elements such as Si and S, and is sufficiently broad to determine the shape of the underlying continuum. Astro-D has sufficient imaging capability to study the structure of extended sources such as clusters of galaxies and supernova remnants. The spatial resolution is adequate to isolate and study sources nearly as weak as those found in the Deep Survey of the Einstein Observatory. Still weaker sources can be characterized by examining fluctuations in the cosmic x-ray background.

The design and fabrication of the Astro-D spacecraft is being developed by ISAS of Japan. The spacecraft will carry four instruments: two x-ray telescopes with Solid-State Imaging System detectors provided by the Massachusetts Institute of Technology (MIT) and two x-ray telescopes with Imaging Gas Scintillation Proportional Counters provided by ISAS. The design of the spacecraft posed some unique challenges for ISAS. To contain the 3.5-m focal length required for the spacecraft's optics, the spacecraft must be at least 4 m in length; however, that spacecraft length is too long for the M-S3II launch-vehicle booster shroud. To overcome this limitation a unique carbon-fiber extensible optical bench will be used. This optical bench collapses to 3 m for the launch configuration and then extends to 4 m when the spacecraft is in orbit.

The x-ray telescope consists of four sets of multi-nested thin-foil conical reflectors in approximate Wolter-I optics. They are provided by GSFC. This technology enables a large throughput up to high energies. The effective area will be greater than 1000 cm^2 below 2 keV and greater than 500 cm^2 around 6 to 7 keV.

The Solid-State Imaging System (SIS) consists of two identical independent Charge-Coupled Device (CCD) camera system modules. Each module will have a hybrid CCD at the focus of a grazing incident thin-foil telescope. The detector for the SIS will be a 840 x 840 hybrid CCD. Each module will have its own signal-processing chain with a digital interface between the analog and digital electronics. Analog signal-processing electronics will be provided by

MIT; the digital processing electronics will be provided by ISAS. The SIS cameras include a thermoelectric cooler to maintain the CCD at -70°C (dark current 0.25 e^-/pixel/s).

The two Imaging Gas Scintillation Proportional Counters (IGSPC) are being developed by ISAS. The IGSPCs provide a better detection efficiency for high-energy protons and a larger coverage of the field than the CCD detectors. The energy range is expected to be 0.7 to 15 keV. The effective area is approximately 50 mm in diameter and the position resolution is 0.5-mm FWHM at 5.9 keV ($\propto 1/\sqrt{E}$).

The Astro-D will be placed in a circular near-Earth orbit of approximately 550 km with a 31° inclination by the ISAS M-S3II launch vehicle. All command and mission control of the Astro-D satellite will be provided by ISAS. NASA will provide routine S-band telemetry data acquisition and recording by appropriate Deep Space Network (DSN) stations during the initial calibration and check-out phase (approximately 8 months' duration) followed by the remaining period that the satellite remains operational.

The calibration and check-out period is for instrument check-out, calibration, software check-out, and preparation for a continuing scientific program with a well-characterized system. No guest investigator or visiting investigator program is planned for this period. The observations made and the data resulting from this period are part of a team effort involving the entire Japan-U.S. Astro-D team. All of the data from both SIS and IGSPC observations will be delivered to GSFC and will be available to Japanese and American Astro-D team scientists.

The Astro-D team members from GSFC will serve to coordinate the observing program and GSFC will serve as the U.S. data hub for the remainder of the Astro-D mission life. Determination of the observing program timeline, taking into account operational factors, will be the responsibility of the ISAS. During the operational phase, data from both SIS and IGSPC detectors may be requested. SIS or IGSPC data from these observations may be shipped to the U.S. at the discretion of the Japan/U.S. scientists involved in these observations and will be available to the scientists on both sides.

All of the first-pass processed data will be deposited in archives in the U.S. and Japan in order to provide suitable datasets for general release to the international scientific community. The goal is that these data will be deposited in the appropriate data archive 1 year after receipt of the data in usable form.

Contact: R. E. Donnelly (Code 404)
(301) 286-6701

Sponsor: Office of Space Science and Applications

Mr. Richard Donnelly is the Deputy Project Manager for the Astro-D Project. He is a 29-year veteran with GSFC and is currently assigned to the International Projects Office. Mr. Donnelly graduated from the New Jersey Institute of Technology with a degree in Electrical Engineering.

METEOROLOGICAL SATELLITE (METSAT) PROJECT, SEARCH AND RESCUE MISSION

NASA research and development has provided many benefits to the civil sector. The Search and Rescue Satellite (SARSAT) payload aboard the NOAA series of meteorological satellites has provided benefits that are widely recognized. Developed by the Search and Rescue Mission of METSAT, it has proven to be a boon to air and sea search-and-rescue forces worldwide. These instruments, along with a compatible set aboard the Soviet COSPAS satellites, now relay distress radiobeacon alerts to rescue coordination centers on a routine basis.

Recent experiments using airborne synthetic aperture radar to detect plane crashes have revealed the promise of another highly visible benefit of NASA research and development. These experiments have

shown that it is possible, using this imaging radar, to find crashed small planes under a forest canopy and in inclement weather—two severe obstacles to search and rescue when there is no operating radiobeacon.

To perform the experiments which led to these conclusions, wrecks of light planes were acquired and placed in the forest under the flight line of a NASA Ames Research Center DC-8 carrying a Jet Propulsion Laboratory (JPL) synthetic aperture radar. This was done in cooperation with forest science experimenters who had already arranged for the flights to conduct a variety of biology, ecology, and hydrology studies using the radar imagery. When the radar data were processed, the resulting images were examined to see if the aircraft could be detected. In five such experiments, in settings from North Carolina to Alaska, detections were made reliably through several different types of tree cover and during a rain storm. Long-wavelength (P-band) multi-polarization radar combined with simple image filtering algorithms proved to be most effective in identifying such "crash" scenes.

An operational system can be envisioned that would allow search-and-rescue forces to send an aircraft equipped with such a radar over an area that is to be searched for a lost plane. The aircraft would obtain strip maps of the search area using the radar, and record the data on a mass storage medium such as magnetic tape. The data would then be returned to the search command post along with a small image-viewing workstation. With the help of an operator, the local searchers would review the images of the search area and locate targets to investigate. In settled areas, the images would probably contain many returns from buildings and other non-natural objects, but most of these would be eliminated through comparison with maps and the searchers' knowledge of the area. The most likely targets determined through this method would be visually investigated by airborne or ground search teams.

Work is under way to determine the types of searches where this technique would be most useful, and to plan the demonstration of a practical system. Further field experiments will also be performed. Expectation is high that the benefits of this development to search-and-rescue forces will rival those of the COSPAS-SARSAT system. COSPAS-SARSAT will continue to be highly valuable when distress radiobeacons are involved, and synthetic aperture radar will complement the satellite system by aiding in searches where no beacon is detected.

Contact: Wayne A. Hembree (Code 480)
(301) 286-8332

Sponsor: Office of Space Science and Applications

Mr. Hembree is the Mission Manager for Search and Rescue at GSFC's METSAT Project. He joined NASA in 1963, and has served in various engineering positions supporting the TIROS, Nimbus, and AE-C satellite programs. In 1973, he became Mission Operations Manager of the TIROS-N series of satellites. He holds a BS in Electrical Engineering from the New Jersey Institute of Technology.

FLIGHT TELEROBOTIC SERVICER—DEVELOPMENT TEST FLIGHT

The Flight Telerobotic Servicer (FTS) activity at GSFC was recently cancelled because of changes in policy with respect to the National Space Program. Prior to these changes, a space shuttle mission was planned to test several aspects of the FTS system in the space environment. This article describes several aspects of the FTS and that now-cancelled mission.

"If I could just push on that antenna mechanism, this mission would be a complete success." This desire to reach out and touch hardware in space has occurred more than once in the course of space-flight history. Sometimes extravehicular activity by an astronaut, or the Orbiter remote manipulator system can be used to solve the unexpected problem. Sometimes there is no solution.

Over time, space-flight systems that provide sophisticated remote capabilities to electronically configure instruments and their supporting spacecraft

have evolved. The first small steps in this process were taken 20 years ago by such programs as the Small Scientific Satellite (S3), when the ability to reprogram the data system was used to compensate for unexpected stability problems. Now the technology to touch and manipulate space systems mechanically from remote, safe locations is being developed. Push the latch, tighten the connector, clean the mirror, change the film: these are future capabilities that will enable and enhance tomorrow's missions of space discovery.

A telerobot is a machine that can physically interact with its surroundings and is controlled from a remote location by a human being. The Flight Telerobotic Servicer (FTS)—Development Test Flight (DTF-1) mission was to have tested critical telerobotic technology elements and was to have provided the first flight-qualified, dexterous robotic manipulator system for use in space. The DTF-1 was to have been operated by an astronaut at the pressurized Orbiter workstation while viewing the task environment of the manipulator via a video system.

When the astronaut moves the hand controller or initiates control panel commands, the DTF-1 system interprets the commands and controls the manipulator accordingly. The DTF-1 system features force feedback to the operator's hand controller. This, combined with simultaneous control in 6 degrees of freedom, makes the manipulator capable of very fine, dexterous motion.

The DTF-1 flight system was to have consisted of a shuttle payload bay element and an aft flight-deck element integrated with the Orbiter as an attached payload and its control station. In addition to the telerobotic manipulator, the payload bay element would have housed the power system, main control computers, task panel, and video cameras. The figure shows the configuration of the planned DTF-1 payload bay element. The aft flight deck element workstation has a hand controller, a control and display panel, and an initialization/interface computer. Specific tasks would have tested the performance of the manipulator in zero gravity, as well as verified the human-machine interface capabilities of the workstation.

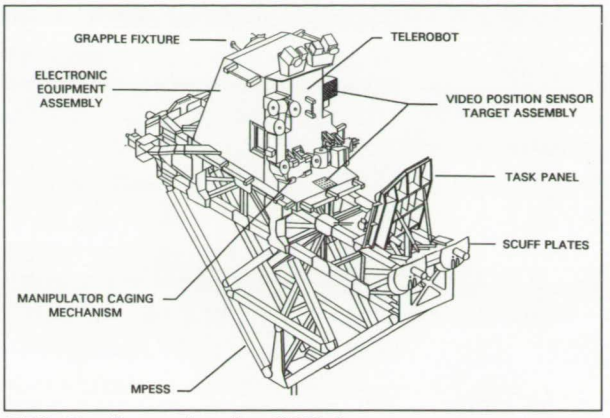

FTS Configuration for DTF-1.

Specific DTF-1 mission objectives were to have evaluated the FTS manipulator and workstation design approaches and correlated system performance in zero gravity with ground simulation and analyses. Additional DTF-1 mission objectives were to have evaluated the human-machine interface and operator fatigue, and demonstrated potential telerobot capabilities.

Performance verification tests and capabilities demonstrations were sequenced to fit into an overall mission timeline that would have taken advantage of changing Orbiter environments and would have performed the most important activities early in the mission. Twenty-four operating hours were planned for this flight, which had been scheduled for launch in late 1993.

The performance verification tests were planned to exercise the telerobot operational envelope. These tests allowed for on-orbit verification of the DTF-1 system design and performance. They provided for the full characterization of manipulator and actuator dynamics and closed-loop control performance, utilizing multiple payload masses.

The performance verification tests would have exercised the manipulator throughout the extremes of its operational envelope, and would have demonstrated the full range of manipulator dexterity. They would have measured telerobot performance by independent instrumentation such as accelerometers and proximity sensors.

Task demonstrations were designed to show the functional capabilities of the FTS. Specifically, the capabilities demonstrations included alignment and mating tasks of varying tolerances, plus elemental subtasks which would have supported future space assembly, servicing and maintenance tasks.

Several major technical challenges have confronted the DTF-1 designers. Packaging of manipulator components, including the need for a 120-volt power system, a very complex internal wiring harness, heat dissipation, and electronics volume, proved to be a significant systems engineering task. Also, compliance with Orbiter safety requirements had been an issue. Specific hazards included unplanned contact, accidental release of hardware, and excessive force to the task hardware. These safety issues will confront most space manipulators of the future. The DTF-1 with its advanced telerobotic control system would have become a pathfinder for generic space-flight telerobotic safety.

Deliveries of subcontracted systems and flight electrical components were well under way when the project was curtailed. The integration and testing of flight control software on a hydraulic manipulator testbed was the next major milestone.

Contact: John E. Oberright (Code 409)
(301) 286-2462

Sponsor: Office of Aeronautics and Space Technology

Mr. Oberright received his BME from The Catholic University of America, Washington, DC, in 1966 and took a position with GSFC upon graduation. His career at GSFC includes a wide range of engineering experience with flight projects, both in-house and contractor-provided. He transferred from the Engineering Directorate to the Flight Projects Directorate Space Station Office in 1985, as the Deputy Project Manager for the Science Laboratory Module. He was selected as Project Manager for the Flight Telerobotic Servicer Project when it was established as a flight element for Space Station in 1986. He is currently on the staff of the Advanced Missions Analysis Office.

Engineering

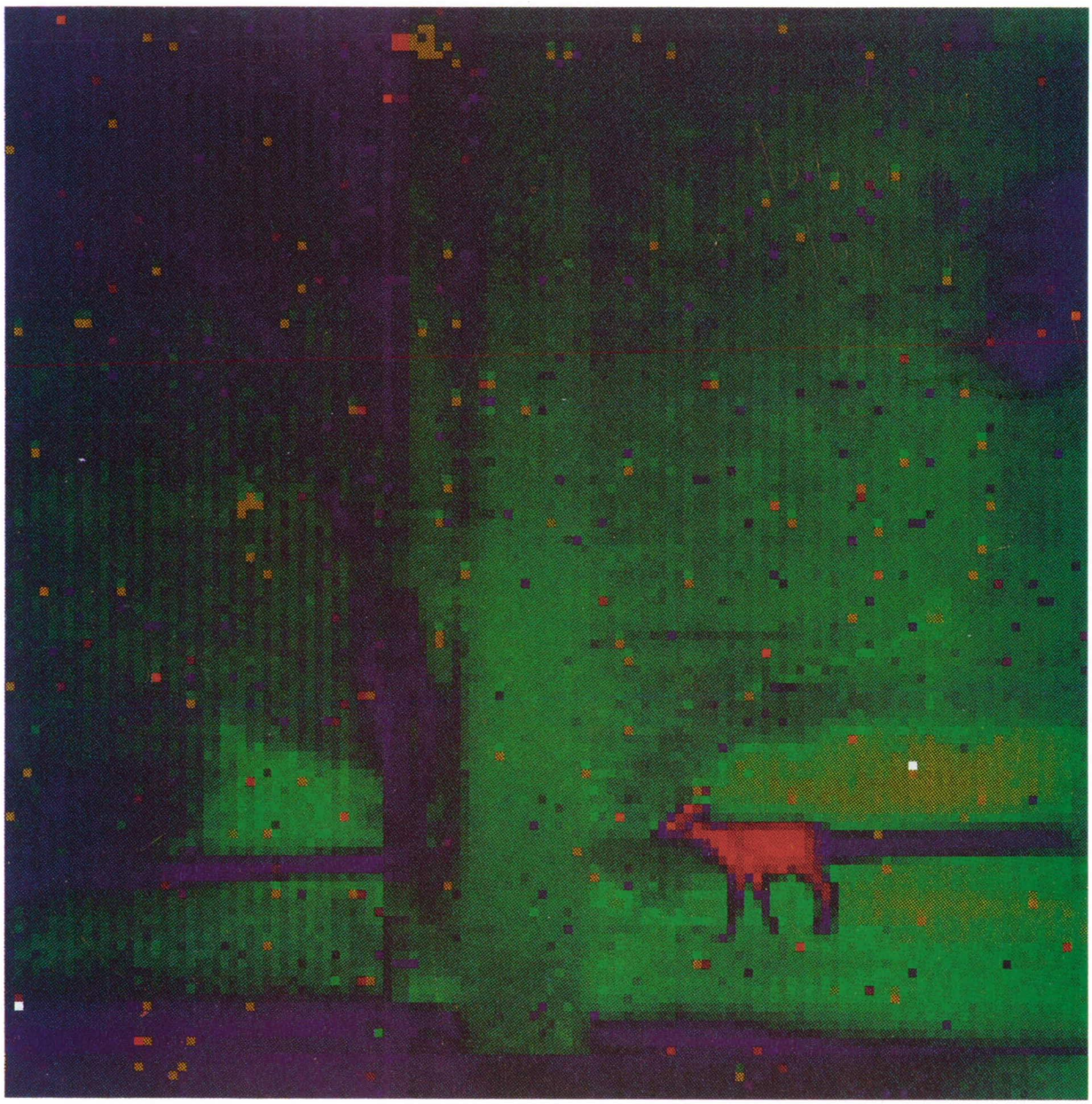

Engineering is the key to progress in more sensitive instruments, more capable spacecraft, more reliable systems, and more cost-effective research.

ENGINEERING

Robotics

TECHNOLOGY LEVERAGING AND AUTONOMOUS ROBOT OPERATION

The Data System Experiment (DSE) was a successful autonomous robotic experiment flown by GSFC on shuttle flight STS-39, one of six experiments mounted on the Hitchhiker. It included a SpaceVax computer and an erasable optical disk. The DSE was a technology experiment designed to qualify the computer and the optical disk as candidate technology for the Hitchhiker avionics and the Office of Aeronautics and Space Technology Configurable High Rate Processor System (CHRPS) testbed. The schedule at the beginning of the project, which began in June 1989, was to deliver the DSE to Kennedy Space Center in January 1990 for launch in July 1990.

An advertisement was placed in the Commerce Business Daily in June 1989 requesting responses for new technology under development for IR&D, DoD, or other government agencies in the form of breadboards or prototypes that could withstand the rigors of space and the shuttle environment. Eleven companies responded, but only two could meet the delivery schedule and the required hardware maturity. Digital Equipment Corporation responded with a MilVax that was developed for the USAF. The SpaceVax is an equivalent Model 6210 that is a 2.25-MIPS computer with 16 Mbytes of memory. Sundtrand responded with an optical disk that was developed for Rome Air Development Center and used to drive the heads-up display for the USAF F-16 fighter. The disk stores the VMS operating system and the robot operating environment in write-protected space. The optical disk has a 300-Mbyte capacity that can sustain a 10-Mbps data rate with a removable media. GSFC contracted with these two companies to repackage the military units into a space-ready configuration and to make the necessary modifications for the Hitchhiker/shuttle environment. GSFC designed the experiment, integrated the equipment into the DSE, and performed the space qualification.

The experiment consisted of using the space-based control system to control the robot, which was located on the ground. A position for the robot to move to was transmitted to the SpaceVax where the trajectory path was calculated and transmitted back to the ground to move the robot. To demonstrate the system's ability to respond to objects in the robot's path, an object was placed in the robot workspace, whose location was transmitted to the disk on the shuttle after removing the write protect. Commands to move the robot were repeated, demonstrating that the SpaceVax could move the robot around the object without collision. Any uncorrected error in the VMS operating system, the Ada trajectory software, or the robot workspace would have been obvious.

◂*Pictured is a deer grazing in the grass in front of Building 11 at GSFC. This image was acquired with FIRARI at about 9 p.m. on May 8, 1991. The color scale is red-green-blue, with blue being coldest and red being hottest. The large vertical beam in the center of the image is a street-light pole. The uncorrected image is presented.*

The DSE was successfully operated for 26 hours and 9 minutes during this mission, over a temperature range of 2°C to 41°C. During this time the DSE was in continuous operation, either controlling the ground robot or performing demanding routines that would identify any anomalies in the DSE. More than 350,000 disk blocks were correctly read and written on the optical disk. The DSE was operated through the South Atlantic Anomaly and did not experience any uncorrected errors while more than 1,500 disk blocks were correctly read and written on the optical disk. Another experiment during this mission detected and corrected 99 single event upsets. In addition, the DSE MIL-STD-1553 interface was successfully checked out on orbit. While on orbit, patches to the source code were uplinked and the Ada program was compiled; the Ada library objects were linked into executables which were used to compute the robot paths.

The DSE equipment (i.e., SpaceVax and optical disk), are examples of enabling technology receiving wide recognition within the NASA community. The experiment demonstrated that NASA can benefit from DoD technology developments and can deliver space-qualified hardware in less than 2 years.

Contact: Danny Dalton (Code 735)
(301) 286-5659

Sponsor: Office of Aeronautics and Space Technology

Mr. Danny A. Dalton, Head of the Flight Data Systems Branch was the Principal Investigator of the Data System Experiment. He received his BS in Electrical Engineering from Purdue University and has been at GSFC for 30 years.

ROBOTIC DEPLOYMENT AND SERVICING OF SCIENTIFIC PAYLOADS ON THE LUNAR SURFACE

As part of the effort to use robotics to enable or enhance Space Exploration Initiative (SEI) missions, a study was initiated to examine several novel approaches to deploying scientific payloads on the lunar surface prior to human presence. The approaches centered on the use of automation and robotics to perform the assembly, servicing, and deployment of self-contained scientific payloads. The results showed that large payloads, such as a 2.5-m Lunar Transit Telescope (LTT), could be transported to the Moon as components with supporting subsystems (i.e., power and data-handling communications) and could be assembled robotically. Various mission scenarios were examined including a fully assembled LTT, a robotically assembled and serviceable version, and a rover mission that benefitted other scientific disciplines such as surface geology and future surface systems construction. Trade-offs were studied that involved launch vehicles currently available or planned for the near-term, crew versus robot utilization, design reliability, logistics, and life-cycle costs to determine whether robotic assembly and servicing was economically viable.

To perform this study, the design of the LTT, a version of which exists at the Kitt Peak Astronomical Observatory, had to be modified and made "robot-friendly" so that it could be assembled and serviced by robotic manipulation. During this design process, the scientific requirements had to be met so as not to compromise the success of the mission. Following this activity, a task script was developed that outlined the step-by-step procedure for robotic assembly of the instrument. Task durations were then estimated (derived in part from ground laboratory tests and flight-servicing missions) and time lines were established. The results showed that the LTT could be robotically assembled—including site preparation—within 27 days of arrival at the lunar surface. If 3 crew members were used, the time for assembly would be reduced by only 9 days and bring with it the risk of extravehicular activity. A robotic graphic simulation, which kinematically represented the flight system, was used to verify the assembly sequence. For the unmanned, soft-landed scenario, the results showed that designing the instrument for robotic servicing in the event of a failure, including carrying the appropriate complement of spares, provided a lower life-cycle cost for a 15-year mission than if the LTT had been launched fully assembled with built-in redundancy.

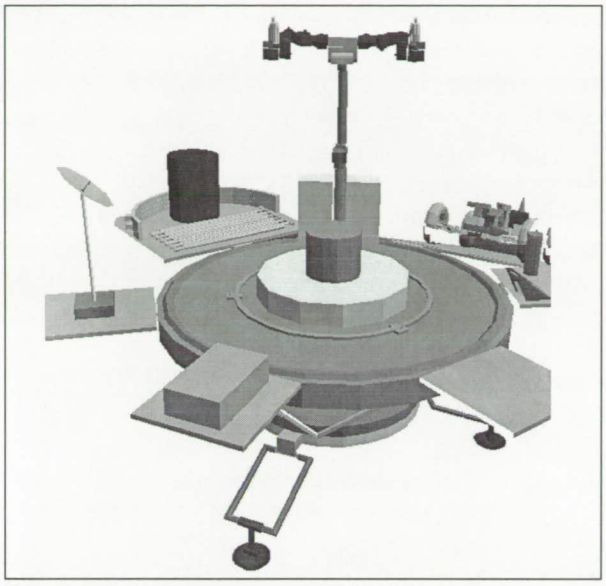

Picture of the Lunar Transit Telescope.

Contact: Stanford Ollendorf (Code 701)
(301) 286-3292

Sponsor: Planetary Surface Systems Office
Johnson Space Center

Mr. Stanford Ollendorf, an Aerospace Engineer in the Office of Technical Management, received his degree in mechanical engineering from the Rochester Institute of Technology in 1958 and did graduate work at The Catholic University of America. Currently, he is Head of the Robotics Branch, where preliminary studies of Space Robotic Applications, including the Lunar-Mars Missions are taking place.

CAPACIFLECTOR COLLISION AVOIDANCE SKIN

A collision avoidance skin has been undergoing development for telerobotic arms and for payload collision avoidance and sensory interactive docking. This skin uses a unique capacitor reflectance capaciflector technique (see the first figure) to enable simple capacitive elements to be mounted against the grounded robot arms and payloads and still produce detection ranges for humans and space station trusses in excess of 1 foot. GSFC robotics lab demonstrations of this technology have attracted Space Station project and industry interest. Project specialists in thermal, safety, and electromagnetic interference have investigated and advised that the skin can easily be adapted for space use. Accordingly, a trade study was performed which strongly endorsed the capaciflector concept. This study concluded that a skin employing capaciflectors can be used to diminish on-board computer requirements, a significant number of which are used for collision avoidance. It further stated that these sensors should be employed on the payload itself, where collision avoidance is even more critical than on the robot arms.

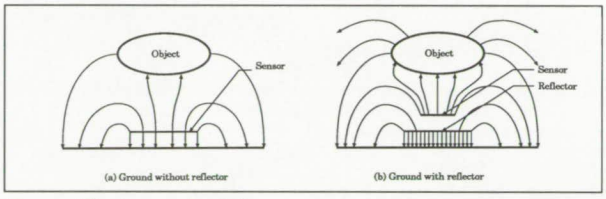

Capaciflector principle.

Recent hardware progress has taken place on several aspects of the project. An array of four sensors covering one face of a 762 Puma robot has been demonstrated (see the second figure). This array is flight qualifiable (i.e., it is made of materials that have been flown previously except for the electronics) which use military standard components; historically, these have been easy to flight qualify. The entire array is covered with Kemglaze A276 flight paint (white). Even the NASA/GSFC stickers are flight-qualified based on their use in the Spartan project. The sensors see right through the paint and stickers, and work with no discernable degradation of performance. People can now move in the previously off-limits volume of robot action with no opposition from the robot, which merely keeps 1 foot away. The technology costs the robot system very little, and its demands on computer resources are minimal. The sensors and circuitry are unobtrusive to the point of being difficult to see that they are present.

In addition to the flight-qualifiable array on the Puma arm, an array of four sensors has been mounted on a

A capaciflector sensor used by a robot in the lab. This sensor could routinely detect a human or an aluminum-truss element within 1 ft of the robot.

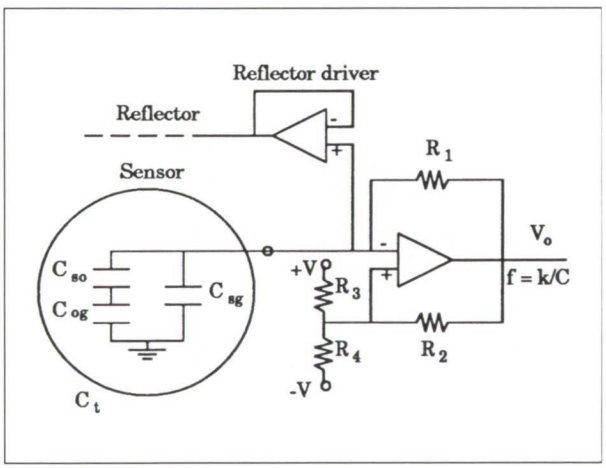

Capaciflector circuitry.

box simulating an Orbital Replacement Unit (ORU) which, in turn, has been mounted to a Cincinnati Milacron T-3 robot in the GSFC Robotics Research Laboratory. These experiments have demonstrated that capaciflector sensory-based collision avoidance can be extended to permit a payload to be easily maneuvered and docked safely, and with outstanding precision in an environment where other payloads are in close proximity.

A new phase-correcting circuit has been breadboarded and demonstrated (see the third figure). It is now undergoing optimization development. This circuit will extend the performance of the capaciflector system in several important respects. It will use a crystal-controlled oscillator, so drift will be reduced to an absolute minimum. The system will be able to perform indefinitely in space. Array cross-talk will be actively rejected, thereby allowing closely packed pixel-type imaging arrays to be used (we have already demonstrated imaging capabilities with a single capaciflector). Coarser arrays will have enhanced signal-to-noise ratios. In addition, the circuitry will be simpler and more compact than previously, and input/output connections will be minimized.

Contact: John M. Vranish (Code 714)
(301) 286-4031

Sponsor: Office of Aeronautics and Space Technology

Mr. John M. Vranish, an Aerospace Engineer in the Robotics Branch, holds several patents on robotic electromechanical systems, mechanisms, and tactile/proximity sensors. He received his MS in Electrical Engineering from George Washington University.

Mechanical

SPLINE-LOCKING SCREW-FASTENING STRATEGY

A basic fastener has been developed at GSFC for efficiently performing assembly, robot walking, equipment maintenance, and replacement functions in space for use either by a robot or an astronaut. This fastener is easily extendable to be the basis for a family of devices, one member of which has been developed and tested at GSFC. The device, called a spline-locking screw, will also have significant value in the commercial and defense sectors in advanced manufacturing and field maintenance.

The current NASA fastener was used in the Solar Maximum Mission repair of 1982. Screws with low-pitch machine threads had been used successfully many times in space-launch operations. But, they

would cross-thread when the astronauts tried to fasten them while wearing gloves and spacesuits. Numerous modifications have been made to these screws; however, the additions added a great deal of friction to the system. This, in turn, meant that very large and clumsy hand tools had to be used, thereby subjecting the astronauts (or robots) to dangerously large torques and forces needed to overcome the friction. Robots could not be used under these conditions because using large tools would severely limit their dexterity, and the existing robot-end effectors could only produce limited torque.

The spline-locking screw was developed by returning to the common machine screw and taking a fresh approach. A bolt was cut in two and the bottom half was left threaded. Thus, the bolt head (or driver) and the object (which is normally pinched by the screw system) are on one side of the interface and the bolt and the threaded fixture it screws into are on the other side. An interface was needed to complete the system. A spline-locking-type interface was chosen because it is a simple, direct way to spin the driver into the bolt and join the two so that the driver will turn the bolt under load and the system will withstand the considerable tensile loads that result. The preload spring was added to the bolt to ensure that the bolt would not turn until the driver spline drops into the bolt spline and seats. At this point, the driver and bolt will turn together. The locking splines are very coarse so they can be designed to seat and fit together so that cross-threading is virtually impossible. Because the bolt is never unthreaded, the result is a machine screw that cannot cross-thread. This design makes it possible to use low-pitch machine threads, so large preload forces can be generated from minimum input torques. An added benefit of the low pitch is that these bolts will not shake loose during launch. In addition, robot-end effectors and astronaut hand-power tools can now be made more modest in size and power, enhancing safety for the astronaut and safety and dexterity for the robot. The increase in size is negligible.

A proof-of-principle prototype of a foot to fasten the Flight Telerobotic Servicer (FTS) robot to the Space Station structure based on the spline-locking screw concept has already been built and tested. The results of this effort showed immediate success. This particular device, known as the Workpiece Attachment Mechanism/ Workpiece Attachment Fixture (WAM/WAF) performs electrical connections in addition to basic fastening. It will also permit a robot to walk on a space structure.

Contact: John M. Vranish (Code 714)
(301) 286-4031

Sponsor: Office of Aeronautics and Space Technology

Mr. John M. Vranish, an Aerospace Engineer in the Robotics Branch, holds several patents on robotic electromechanical systems, mechanisms, and tactile/ proximity sensors. He received his MS in Electrical Engineering from George Washington University.

LOW-COST SIMULATORS FOR DESIGNING OPERATOR-DRIVEN MECHANICAL SYSTEMS

High-cost simulators have been used as trainers in the aircraft industry for many years. These simulators are developed and used after a system is built and often contain assumptions and limitations incompatible with mechanical system design. There is a critical need for simulators to support the design of systems controlled by the intelligent physical exertions of a human operator. The development of low-cost, real-time operator-in-the-loop simulators represents an enabling technology for design engineers. This technology enables a transition from the use of trainers that adapt the operator to the machine, to simulators that help designers adapt the machine to the operator.

Space telerobotic system design requires simulators to better evaluate and understand the consequences of design alternatives concerning the dynamic interaction of the robot and operator. A real-time operator-in-the-loop simulator for the Flight Telerobotic Servicer (FTS) that includes a complete characterization of robot arm dynamics has been

developed at the University of Iowa for the FTS Project. It also has been interfaced to a variety of alternative operator hand-controllers. Visual feedback cues are developed with a low-cost, high-speed graphics workstation that displays high-quality animation at 25 to 30 frames per second. Tactile feedback cues are developed by transmitting computed reaction force data back to a force-reflecting hand-controller. Other types of feedback cues, such as motion, vibration, and sound, can be developed. The FTS simulator supports system design, with full consideration given to operator-machine interaction and associated human factors issues. Visual and tactile cues can be degraded to evaluate the need for of certain types of cuing information. For example, how much cuing degradation can be tolerated without jeopardizing the mission? How effectively can the operator process available cues? How fast can the operator adapt when deprived of selected cues? These issues and many more can now be investigated at low cost, without placing the operator in harm's way.

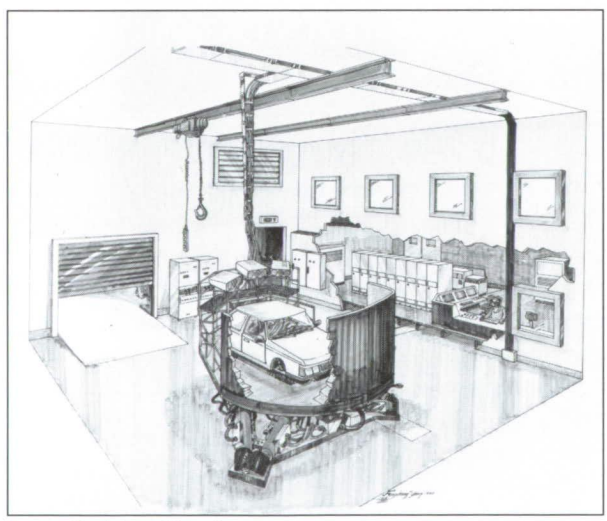

Iowa Driving Simulator.

FTS operator-in-the-loop simulator technology is also being transferred to the construction equipment industry. Simulators for a J.I. Case backhoe and a Caterpillar wheel loader have been developed with GSFC technology-transfer support. Operator consoles provided by these companies serve as interfaces between the operator and simulators for both the backhoe and wheel loader. While the characteristics of backhoes and wheel loaders differ greatly from space telerobotics, the same simulation technology and human factors challenges arise in both applications. Both J.I. Case and Caterpillar intend to use these simulators for operator-in-the-loop simulation-based design.

The National Science Foundation Industry/University Cooperative Research Center at the University of Iowa, cosponsored by GSFC and the Army Tank Automotive Command, has recently acquired an Alliant 28-processor parallel computer and an Evans & Sutherland CT-6 four-channel advanced graphics system with a 150° wraparound projection screen. This state-of-the-art computational system has enabled the development of the Iowa Driving Simulator (IDS), a $10-million facility established primarily for ground-vehicle driving simulation. The simulator technology used for the FTS, backhoes, and wheel loaders provides a technology base for the IDS.

Cooperative programs between the University of Iowa's College of Engineering, Department of Psychology, and School of Medicine are focusing on studies that will evaluate the driver's performance under the influence of drugs, alcohol, fatigue, and aging. Programs with corporate and government sponsors will also study vehicle handling problems associated with deteriorating weather, road, and vehicle conditions.

Professors K. Harry Yae, Edward J. Haug, and their students at the University of Iowa supported this research and software development effort.

Contact: Harold P. Frisch (Code 714.1)
(301) 286-8730

Sponsor: Office of Commercial Programs

Mr. Harold P. Frisch is Head of the Robotics Applied Research Section of the Robotics Branch at GSFC. In addition to his interests in robotics and the transfer of NASA-developed technology to real-world application, he is also actively supporting efforts to develop a generic man/machine interaction

design-and-analysis capability for use within a concurrent engineering environment.

NEW GENERAL-PURPOSE DETECTOR DRIVE SYSTEM

A new general-purpose detector drive system that combines the configurability and adjustability of laboratory-type equipment with a relatively compact size and a low power requirement suitable for field applications has been developed at the Detector Test Facility (Code 724).

Operation of an array detector typically requires the ability to adjust the voltage levels of a number of binary clock signals and DC biases to optimize the detector's performance. To date, this requirement has been met in the laboratory through one of two approaches: (1) a large number of small, discrete, laboratory-type DC power supplies harnessed to the drive circuitry; or (2) a large, rack-mounted commercial focal-plane test system with individually adjustable, single-channel clock drive and/or DC bias modules. Both approaches provide a high degree of flexibility of configuration and ease of voltage adjustment, but share the disadvantages of bulkiness and high power consumption; the second approach also tends to be extremely costly. Field-deployed detector drive electronics typically utilize hard-wired circuitry for driving the clocks and biases. This approach results in a very compact, low power circuit, but usually allows little or no flexibility of configuration or user adjustment of voltage levels.

The new detector drive system incorporates many of the desirable aspects of laboratory-type approaches and the hard-wired field applications approach while minimizing the disadvantages. The system is capable of generating low noise bias voltages and high-quality, electrically clean clock waveforms at frequencies in excess of 12 MHz, and has been used with great success to drive imaging detectors of many types, both in the laboratory and in the field. The new drive system has rapidly become a key component of Code 724's laboratory and field work in support of numerous projects. Laboratory applications to date include vacuum-cryogenic evaluation of high-resolution charge-coupled device imagers, charge-coupled photodiode arrays, and low-background infrared arrays, as well as wafer-level testing of new custom detector designs. It also has been utilized in the field as the airborne drive electronics for a new-technology Quantum Well Infrared Photodetector camera.

The system consists of three printed circuit cards, all developed in-house. The heart of the system is the 16-channel drive module shown in the first figure. This module consists of four major functional blocks, as shown in the second figure: (1) voltage sources; (2) configuration matrix; (3) logic input and level shifting; and (4) floating drive circuits. The drive module requires ±15-VDC power and draws approximately 600 mA from each supply. The voltage source block comprises 16 digitally controlled voltage regulators, eight of which are nominally positive, adjustable from -12 V to +4 V, and eight of which are nominally negative, adjustable from +12 V to -4 V. Each regulator is controlled by an 8-bit digital-to-analog converter (DAC), resulting in an adjustable yet stable and repeatable output voltage with a resolution of 62.5 mV.

The configuration matrix consists of a set of jumper pins which allows V_{DD} of each drive channel to be supplied by any one of the positive voltage sources, and V_{SS} by any one of the negative voltage sources, simply by changing the position of the jumper plugs. Typical applications involve grouping several related drive channels together on the same pair of voltage rails for ease of adjustment. The logic input and level shifting circuit accepts 16 differential logic signals as input and converts them to the voltage levels required by each floating drive circuit with analog switches. A floating drive circuit consists of a special-purpose high-speed CMOS-driver chip and a number of passive components. Socket mounting of several passive components allows tailoring of the clock waveform to suit the application. A floating drive circuit may be converted to a DC bias voltage by removing the driver from its socket and substituting a jumper plug that connects either the V_{DD} or V_{SS} pin to the output pin.

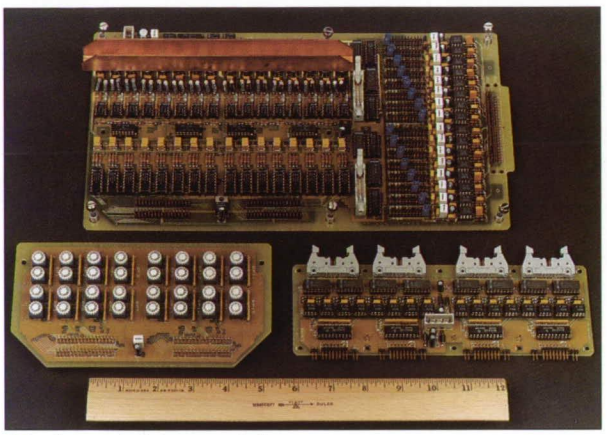

16-channel drive module.

A voltage controller module is the second component of the three-card set. This module provides digital control signals to the 16 DACs on the drive module. The signals are generated by 16 pairs of 4-bit rotary hexadecimal switches, allowing straightforward manual coarse and fine control of each voltage source. The voltage-controller module may either be piggybacked directly onto the drive module or connected via ribbon cables for remote operation. The small amount of power required for the voltage controller module is drawn from a +5 V regulator on the drive module.

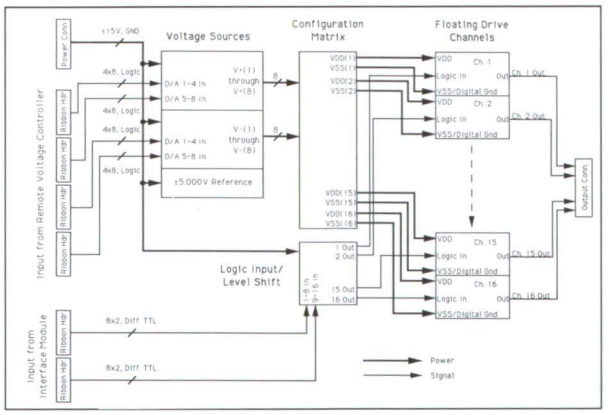

The four major functional blocks of the drive module: voltage sources, configuration matrix, logic input and level shifting, and floating drive circuits.

The third component of the three-card set is a general-purpose interface module. This module accepts 32 single-ended logic signals from any source and provides 32 differential logic outputs, enough to fully control two drive modules. The inputs are electrically isolated from the outputs using high-speed optocouplers, thus providing the drive system with total immunity to interference from the logic signal source. The module requires two isolated +5-V power supplies, and connects to the drive modules via twisted-pair ribbon cables.

Contact: Jeffrey W. Travis (Code 724)
(301) 286-7606

John T. S. Lee
Hughes STX Corporation
(703) 827-6735

Peter K. Shu (Code 724)
(301) 286-5191

Sponsor: Office of Space Science and Applications

Mr. Jeffrey W. Travis holds a BS in Electrical Engineering from the University of Michigan. He has served 4 years in the Space Science and Engineering Directorates at GSFC, and currently heads the Detector Systems Section.

Mr. John T. S. Lee holds a BS in Electrical Engineering from the George Washington University. He has over 15 years of experience in electronics design and analysis, and is currently employed by Hughes-STX Corporation.

Mr. Peter K. Shu heads the Semiconductor Device Development Branch of the GSFC Engineering Directorate. He directs the Detector Test Facility, where detectors are developed for various airborne and space-based scientific instruments.

ELECTRONIC BOLT TESTER

By meeting up-to-date specifications and quality control standards, nuts and bolts have satisfied the design requirements of many projects. Recently, however, problems have developed with the assembly

of some flight hardware. Subsequent analysis indicated that the problem was an incorrect coefficient of friction for the torque of the bolts used. The error in some cases was as high as 100 percent. Reasons for these errors are many. For example: (1) the coefficient is from an unreliable source; (2) locking mechanisms increase coefficients; (3) dry lubricants cause changes; (4) use of the wrong lubricant (or lack of lubricant) results in inconsistencies; and (5) the material of the bolt (often stainless steel or titanium) can present difficulties. Other problems have been identified in determining the coefficient of friction: joint flatness, bearing surface area, installation method, yielding 80 different factors that affect the torque/tension relationship. Tests have been performed for over 10 years with the slide-rule torque wrench and load washer. Accuracy is within ±10 percent. The main difficulty with this method is the expenditure of time. Furthermore, too little torque can lead to gaping or improper clamping, allowing nuts to back off during vibration, resulting in possible damage of other important equipment. Too much torque can break the bolt during assembly or put the bolt into the yield region, then with shuttle take-off, vibration and flight loads can force the bolt to yield further with loss of clamping force. We have developed an electronic breadboard to solve these problems in a matter of minutes.

The electronic bolt tester is a portable instrument used for measuring clamping force, torque, friction and stress on bolts. It accommodates 14 bolt sizes ranging from number 2 through 3/4 in, with national coarse or fine threads. A selection of eight different torque transducers and eight different load washers (clamping force transducers) are required to cover the wide range of bolt sizes.

By pressing the bolt size select push-button, the instrument sequentially advances through the 14 bolt sizes and displays (on a digital panel meter) the bolt size selected. It also generates voltages representative of the bolt diameter and bolt area, required for computing friction and stress. The C/F toggle switch provides compensation for area change between coarse- and fine-thread bolts.

The torque transducer signal is conditioned through an amplifier, then fed to a digital panel meter displaying torque in inch-pounds, and to the computation section for computing friction. The load-washer transducer signal is conditioned through an amplifier, then fed to a digital panel meter displaying clamping force in foot-pounds, and to the computation section for computing friction and stress.

The computation section receives the bolt-area reference signal, conditioned-torque and clamping-force signals, and then performs the computation, the output of which is displayed on a digital panel meter as the friction. The computation section also receives the bolt diameter reference signal and conditioned clamping-force signal, then calculates the stress, displayed in digital form in units of pounds per square inch.

Use of this device allows technicians to test a box of bolts where the flight hardware is assembled, and determine the proper coefficient of friction.

Contact: James Kerley (Code 754.1)
(301) 286-8115

Raymond Burkhardt/NSI
(301) 286-8186

Sponsor: Office of Aeronautics and Space Technology

Mr. James Kerley received a BA in Civil Engineering from Dartmouth in 1939. He has received several patents for cable isolation systems and compliance in robotics. He was named Inventor of the Year at GSFC in 1991. He has 27 years of experience at GSFC.

Mr. Raymond Burkhardt has 17 years of experience in structural testing of space-flight hardware, with experience in acoustics, vibration, shock, static and dynamic load testing, and in modal survey. He is employed by NSI Technical Services Corporation, involved in the design of electronic equipment, facility modifications, and space-flight instruments.

DETERMINATION OF RESIDUAL STRESS USING EDDY-CURRENT TECHNIQUES

The integrity of structural components is critical to the performance of spacecraft. The structures of spacecraft not only must support spaceborne instruments, but also must sustain related operational loads. Yield stress of material determines the maximum stress a structure can sustain before it starts plastic deformation. The total applied stress to the structure should not exceed the yield stress or the structure may fail, jeopardizing the mission. Pre-existing residual stress can significantly influence the initial stress state. Thus, it is essential to include residual stress in determining allowable loads. A material is considered to be at zero-stress state after it is annealed. It will then acquire residual stresses and change from its zero-stress state to an initial-stress state through subsequent engineering and manufacturing processes. Conventional methods using strain gauges, linear variable displacement transducers (LVDTs), ultrasonics, and other similar devices are commonly used to monitor applied stresses. However, they cannot be used to determine the initial-stress state or the zero-stress state itself. We have found that monitoring the changes of eddy-current coil resistance and reactance with respect to applied compressive and tensile load can be used to determine the residual stress in a material. The resistance and reactance of eddy-current sensing coils increase or decrease monotonically with respect to externally applied loads causing tension or compression, respectively. The cross point between the compressive stress versus signal curve and the tensile stress versus signal curve determines the point-of-zero-stress state in the material. The residual stress is the difference between the zero-stress point and the zero-applied stress point.

The block diagram of the eddy-current residual stress determination system is shown in the first figure. The system consists of an eddy-current sensing coil, an impedance measuring instrument, a mechanical push-and-pull system, and a data acquisition station. For our experiments, we used an IBM PC-compatible CompuAdd 386/25 computer as the data acquisition station. The specific impedance mea-suring instrument is a Hewlett-Packard 4284A precision LCR meter which is interfaced to the PC controller via an IEEE 488 interface bus. The eddy-current sensing coil used is a Nortec 3551 100-kHz pencil probe. The mechanical push-pull system is an in-house-designed, four-point bending fixture.

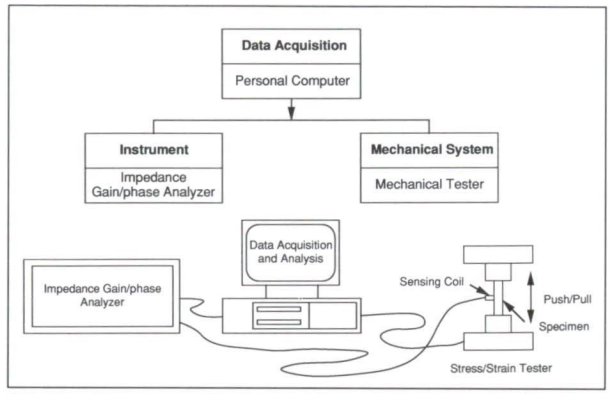

Block diagram of the eddy-current residual stress measuring system.

The resistance and reactance components of the sensing coil impedance are acquired while the specimen is subjected to compressive or tensile loads in the mechanical tester. The eddy-current signal is then plotted with respect to the applied stress/strain.

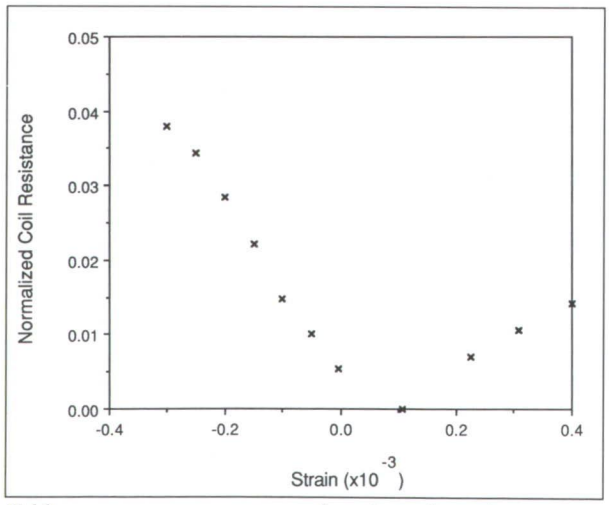

Eddy current response as a function of strain.

Typical results from a residual stress test of a nickel-200 sample are shown in the second figure.

The residual strain of the nickel-200 specimen is measured to be 0.07 x 10^{-3}. The corresponding residual stress of the nickel specimen, based on the nickel material stress-strain curve, is 13.2 MPa.

Using eddy-current techniques to determine residual stresses in a material has many practical applications in various industries, such as the aerospace and power industries, where residual stress may influence the safety and operation of structures.

Contact: E. James Chern (Code 313)
(301) 286-5836

Sponsor: Office of Flight Assurance

Dr. E. James Chern is a Materials Engineer in the Materials Branch, Assurance Technologies Division, Office of Flight Assurance. His prime responsibility is Nondestructive Evaluation (NDE) of space-flight materials and structures. Prior to joining GSFC in 1989, he worked on NDE technology for aerospace applications with various industrial laboratories.

AMSU-A2 BEARING LIFE-TEST FACILITY

The bearings that will be used to support the antenna for the Advanced Microwave Sounding Unit (AMSU), part of the TIROS-N sensor suite, must survive four years of continuous operation without failure. During this period, the bearings and lubricant must be capable of with-standing over $500x10_6$ small-angle stop-starts. Effects of operating bearings at constant angular velocity have been studied in detail, but little is known about effects of stop-start motion on bearings and lubricants.

To better understand wear processes associated with stop-start or stepping motion on bearings and lubricants, a life-test facility was constructed by the Materials Branch. This facility is being used to life-test bearings that are identical to the bearings that will be flown on the AMSU-A2 instrument. The present bearing life-test facility is divided into three subsystems: the vacuum system, the motion control system, and the monitoring system. The life tests are performed in a vacuum to simulate space conditions. The vacuum system being used for the bearing life tests is capable of supporting seven test chambers (one test station per chamber). These chambers are connected to the vacuum system using a collar that has eight ports. Each chamber has two valves used to isolate the chamber from the rest of the system if that chamber needs to be opened or if the chamber needs to be put online by first pumping on the chamber using a roughing pump. Each test chamber has a viewing port, a port for a pressure gauge, and an electrical feed-thru.

The motion control system, shown in the first figure, consists of an IBM PC-compatible computer, a motion controller, a DC brushless amplifier and motor, and an optical encoder. The computer continuously sends position commands to the motion controller, since the controller has no memory buffer to store a sequence of position commands. The controller uses these commands to generate an output voltage which is converted into motor current by the brushless amplifier. The controller uses the optical encoder output for position feedback information, and also has a built-in lead-lag compensator with programmable pole, zero, and gain. The brushless amplifier uses the three digital Hall effect sensors mounted on the brushless motor for commutation. The encoder is a quadrature incremental encoder with 1,200 lines per revolution and a home marker.

The monitoring system, shown in the second figure, uses a Macintosh computer with an analog-to-digital interface card. The computer will run a commercial program, LabVIEW 2, which was written for instrument control and monitoring applications. A capacitance meter is also part of the monitoring system. During the life test, the motor current, the bearing electrical resistance, the bearing electrical capacitance, and the encoder output will be monitored. At present, each of these quantities will be sampled at 8 kHz over several cycles of the stepping pattern three or four times a week.

The motor current will be used with angular position and velocity information derived from the encoder output to calculate bearing friction. The bearing friction and angular position data will be used to

determine whether the bearings meet the failure criteria. The bearing resistance and capacitance data will be used to determine if the bearings are lubricated and possibly the thickness of the lubricating film. Other types of analysis, such as determination of the frequency power spectrum, will also be performed on these data.

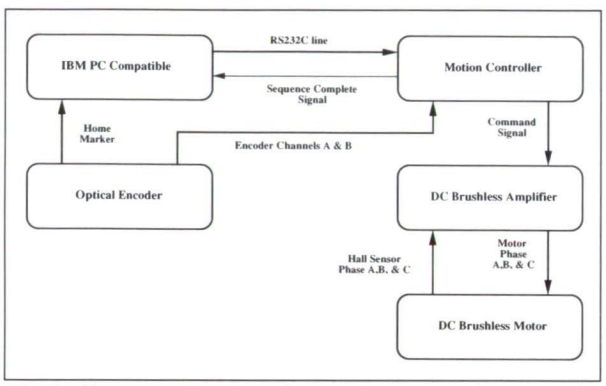

Block diagram showing the motion control system for the AMSU-A2 Bearing Life Test.

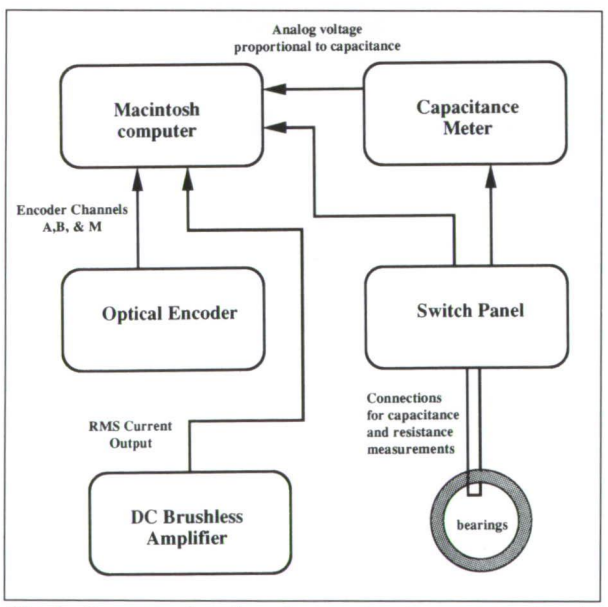

Block diagram showing the monitoring system for the AMSU-A2 Bearing Life Test.

The final figure is representative of the data measured by the monitoring system. Time is displayed on the abscissa and is found by dividing by the stated sampling frequency. These data come

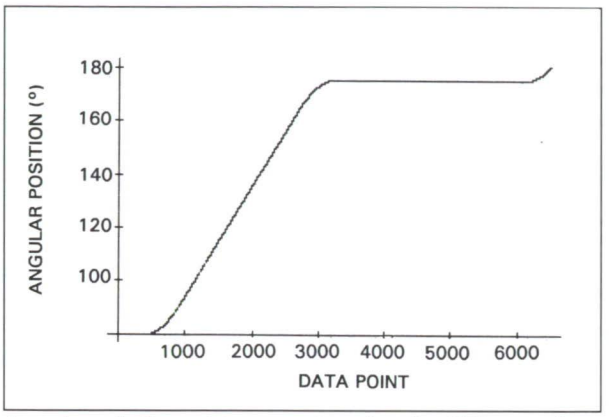

Angular shaft position vs. time for the 97° step from calibration to zenith positions (sampled at 8 kHz).

from the AMSU-A2 bearing life test which began on January 17, 1991 (from position and motor current data, the average friction in the bearings during this step was calculated to be 5.6 x 10^{-3} oz-in/rpm).

Contact: Charles E. Powers (Code 313)
(301) 286-8061

Sponsor: Office of Flight Assurance

Mr. Charles E. Powers has a BS in Engineering and an MS in Physics. He works in the Materials Branch. Mr. Powers provides support in material testing. Throughout his 8 years at GSFC, he has also been active in the use of computers for the automatic control and monitoring of experiments, as well as data reduction.

TERRIER SPIN MOTOR SYSTEM

Terrier Mark 12 Mod 1 rocket motors are currently used as boosters for three rocket vehicles in the NASA/Sounding Rocket Program. When launched as spin-stabilized unguided rockets, these vehicles are susceptible to booster thrust misalignments within the first few seconds of launch. A spin motor system was thus developed as a low-cost, low-weight approach to decreasing trajectory dispersion by inducing an initial spin rate shortly after guided rail release.

The strap-on spin motor system consists of two surplus XM37 spin motors that are attached to the existing forward Terrier launch lugs. Both spin motors burn for approximately a quarter of a second. Both are manifolded together, ensuring near-simultaneous ignition if either igniter should fail to fire its motor. The ignition deck, which accommodates the electronic timer, power, and the arming plug, is mounted to a plate that is a direct replacement of the flame deflector in the Terrier adapter. Ignition timing is provided by a Wallops-developed, 30-channel MFT electronic timer that is initiated by a vehicle first-motion switch.

Contact: David P. Kotsifakis (Code 841.2)
(804) 824-1364

Sponsor: Office of Aeronautics and Space Technology

Mr. David P. Kotsifakis is an aerospace engineer with the Flight Vehicles and Systems Section. He received his BS in Aerospace Engineering from the University of Missouri-Rolla, and has been with the Sounding Rocket Program at NASA/Wallops Flight Facility for 9 years.

Electronics

60-GHz SOLID-STATE POWER AMPLIFIER

In 1987, Raytheon Company was awarded a contract to develop a 60-GHz Solid-State Power Amplifier (SSPA). NASA's incentive for developing this technology was to support future communication programs that may utilize the V-band frequencies such as the Advanced TDRSS Program. The amplifier program goals and achieved results are summarized in the table. The primary performance goals were an RF output of 10 W with a 1-mW input, and a DC-to-RF efficiency of 10 percent. The product generated an output of 5.9 to 6.5 W across the band of interest (60.5 to 62.5 GHz) with a corresponding efficiency of 3.8 to 4.2 percent. The original goals were not achieved because of the relative inefficiency of the gallium arsenide impact avalanche transit time (IMPATT) diodes, which were the active devices used in the amplifier. Diodes with at least 17-percent efficiency are needed to achieve these goals, but such devices are very rare. The average efficiency of the diodes used in the project was only 11 percent. Nevertheless, the performance capabilities demonstrated in this effort represent the state-of-the-art with today's technology.

The architecture is based on IMPATT circuits or modules, which are one-port devices that amplify and reflect the incoming energy. The amplifier has seven stages of IMPATT module combinations. The first three stages contain single modules optimized for high gain. The last four stages begin with one module and are doubled in each stage thereafter, giving a 3-dB gain for each stage. All diodes in these later stages were optimized for maximum efficiency.

Power-combining in the multiple-diode stages is accomplished by a proprietary passive combiner plate. RF power is transferred from stage to stage through waveguide sections and isolator/circulator assemblies. Each IMPATT module has its own bias regulator circuit board, which transfers DC power from an external supply to the diode. These circuits are automatically turned on by the amplifier control logic when the input RF power (~1 mW) is detected.

This program has made a significant contribution to 60-GHz solid-state power amplifier technology. Prior to this effort, the most recent effort to build a 60-GHz SSPA was performed by TRW under a NASA contract in 1986. TRW used silicon IMPATT diodes in a parallel configuration, using a 16-way radial line combiner design. The output power of the TRW amplifier was 6 W over a 1-GHz bandwidth and a corresponding DC-to-RF efficiency of 2 percent. The Raytheon amplifier, which has a series-type configuration, improved upon this performance by doubling the bandwidth and efficiency with the same output power. In addition, the Raytheon design is ~1/3 the volume and weight of the TRW design, making the component much more suitable for future space-flight applications.

Program Goals and Achieved Results		
Parameter	Goals	Results
Center Frequency	61.5 GHz	61.5 GHz
Bandwidth	2 GHz	2 GHz
Output Power	10 Watts	5.9 to 6.5 watts
Gain	40 dB	40 dB
Efficiency	10 percent	3.8 to 4.2 percent
Spurious Output	-30 dBc (max)	-30 dBc (maximum)
Cooling	Suitable for spacecraft	Conduction through baseplate
Reliability	100,000 hours (calculation)	200,000 hours (calculation
Weight	As light as possible	5.5 pounds
Size	As small as possible	7" x 8.8" x 3" (significant further reduction feasible)

The development of this amplifier technology will play an essential role in 60-GHz communication systems of the future. While the initial purpose for developing this technology was for the Advanced TDRSS program, the Raytheon amplifier program is an important step in showing the capability of today's technology and its potential for such future applications.

Amplifier applications include high-efficiency space-to-space communications (GEO-to GEO and LEO-to-GEO) and also for proximity communications in support of programs such as the Space Exploration Initiative (SEI), where 60-GHz capabilities may be used for lunar or Mars rover communications.

Contact: Michael Powers (Code 727)
(301) 286-4820

Sponsor: Office of Space Communications

Michael Powers is an Electronics Engineer in the Communications Electronics Section. He received his BEE from the University of Delaware and has been at GSFC for 3 years. His responsibilities have included the design and testing of microwave receivers, the development of communication electronics for optical receivers, and the design of RF communications systems.

DEVELOPMENT OF Ka-BAND MICROWAVE MONOLITHIC INTEGRATED CIRCUITS

Microwave monolithic integrated circuits (MMIC) offer several advantages over conventional, hybrid microwave circuits. Their inherent small size reduces volume and weight, as well as decreasing external interconnections which may lead to fewer integration problems. NASA has recognized the need to develop such devices for passive and active RF functions. A Small Business Innovative Research (SBIR) Phase-1 contract was awarded to Hittite Microwave Corporation to study and demonstrate the feasibility of extending active circulator design to Ka-band frequencies. The following performance goals were established at the onset of the program:

Frequency:	27.5 to 30.0 GHz
Insertion Loss:	0 dB
Isolation:	< -15 dB
Power Handling:	+10 dBm

Hittite Microwave Corporation modeled and characterized several advanced GaAs (Gallium Arsenide) devices. Their findings led them to

concentrate on two devices. These devices are the GaAs/AlGaAs HEMT (Gallium Arsenide/Aluminum Gallium Arsenide High-Electron Mobility Transistor) and the AlInAs/GaInAs HBT (Aluminum Indium Arsenide/Gallium Indium Arsenide Hybrid Bipolar Transistor).

With each of these devices, two different circuit topologies for implementing the circulator function were examined. The first topology uses Wilkinson-type signal splitters in combination with amplification stages. This topological approach is a junction circulator developed by Hittite Microwave Corporation. The junction circulator method uses reactive feedback to achieve a true three-port circulator.

The performance results are summarized in the table. The results shown are from software analysis, not from actual hardware testing. We conclude that there is little difference in the performance of the HEMT versus HBT devices. Both of these devices meet the performance goals. The results also indicate that the junction circulator has less power consumption and is smaller in size than the Wilkinson-type circulator.

Hittite Microwave Corporation wishes to continue their work in this area and has submitted a proposal for a SBIR Phase-2 effort. If awarded, the Phase-2 effort will concentrate on the circuit design, layout, fabrication, and evaluation of a multifunction chip. This chip will combine the circulator with other functions (such as oscillators, amplifiers, phase modulators, and mixers) to demonstrate multifunction on-chip integration of complete transmit/receive modules.

Contact: Catherine Long (Code 727)
(301) 286-8898

Sponsor: Office of Aeronautics and Space Technology

Catherine Long received her BSEE in 1986 from the University of Maryland. Since then she has been working at GSFC in the Communications Electronics Section of the Microwave Technology Branch. Her responsibilities have included 60-GHz receiver development, state-of-the-art mixer/preamplifier development for the Differential Microwave Radiometer (DMR) instruments that were aboard the Cosmic Background Explorer (COBE) satellite, and the design and test of high-speed digital electronics utilizing Gallium Arsenide (GaAs) technology.

POWER DISTRIBUTION SYSTEM WITH MIL-STD-1773 INTERFACE

The Solar Anomalous Magnetospheric Particle Explorer (SAMPEX) spacecraft is a small satellite that will carry a complement of four particle detectors in a polar orbit to determine the dependence of solar and cosmic particles on the Earth's magnetic field. This mission is the first in a series of satellites in the Small Explorer program that utilizes new technologies and system design concepts as compared to traditional GSFC spacecraft.

The Power Distribution/Pyro Control Unit (PD/PCU) is a subsystem on SAMPEX that distributes power to the spacecraft from the battery and solar arrays. It distributes power from three power buses to spacecraft subsystems, instruments, and pyro functions via mechanical relays. The PD/PCU is controlled by the data system via a MIL-STD-1773 interface, which is a fiber-optic version of MIL-STD-1553. The PD/PCU contains an A/D converter and analog multiplexers to gather analog telemetry for the spacecraft, such as solar array deployment, current monitoring, secondary voltages, and internal temperatures.

The MIL-STD-1773 interface is designed using an off-the-shelf circuit that implements the protocol with some additional logic to tailor the design to the PD/PCU's specific requirements. It is now no longer necessary to have a processor implementing the interface.

The PD/PCU has an internal timer that controls mission-critical functions. These functions include solar array deployment/yo-yo despin, spacecraft fourth-stage separation, attitude control electronics

power-on, and data system power-on. For SAMPEX, the timer is started at third- to fourth-stage separation of the launch vehicle. It powers itself down after the last event.

The PD/PCU contains isolated DC/DC converters with the secondary grounds referenced to the chassis and the primary return grounded at a single point in the power system. The PD/PCU uses an off-the-shelf hybrid converter, which facilitates the small volume of the enclosure.

Contact: Glenn P. Rakow (Code 743)
(301) 286-5993

Sponsor: Office of Space Science and Applications

Glenn Rakow is an Electronics Engineer with the Instrumentation Branch of the Special Payloads Division. He graduated with a BSEE from the University of Maryland and has been with Goddard for 2 years working on electronics hardware for the Small Explorer and Cassini projects.

MAGNETIC EARTH-IONOSPHERE RESONANT FREQUENCY PROJECT

The Magnetic Earth-Ionosphere Resonant Frequency (MEIRF) Project at West Virginia State College (WVSC) is continuing with assistance and support from GSFC. The primary goal of this ambitious joint venture is to develop and implement an Extremely Low Frequency (ELF) monitoring system that will provide real-time data signals that exist within the cavity formed by the Earth and the upper conductive ionosphere at an altitude of ~75 km. The nominal frequency range is 3 to 30 Hz; however, recently acquired information indicates that the 0.3- to 3-Hz range may be a fruitful area of research for earthquake precursor signals. The design of existing equipment is being examined for possible extension into this lower range. Because all life on Earth exists within this cavity, the electronic pulse or condition of the cavity should be of interest to researchers of diverse technical specialties.

A team of WVSC students travelled to several locations in West Virginia and Eastern states to obtain ELF signal data with recently acquired spectrum analysis equipment. During the summer, several thousand individual spectrum measurements were taken at Huntington and Lewisburg, WV; Columbia, SC; Montgomery, AL; New Orleans, LA; Houston and Dallas, TX; Leavenworth, KS; and Indianapolis, IN. The heart of the measurement equipment is an HP 35660A fast-Fourier spectrum analyzer which was used to take base station measurements while the portable, battery-operated HP 3560A unit was used for deep penetration treks to remote locations in the bush. Reduction of the spectral data is presently in progress and should be ready for publication in December 1992.

Field reports indicated the need for a more sensitive or efficient antenna system. This requirement was anticipated early in the project since a standard half-wave dipole receiving antenna for these ELF frequencies would measure several thousand miles in length. A novel active antenna concept has been pursued by the researchers to alleviate this problem and has resulted in two patent applications as well as a journal article. The basic principle, dating back to the turn of the century, is to feed radio-frequency energy into the receiving antenna such that the effective reception area (photon capture cross-section) is significantly increased.

Contact: John F. Sutton (Code 728)
(301) 286-5454

G. Craig Spaniol
West Virginia State College
(301) 286-5454

Sponsor: Office of Aeronautics and Space Technology

Dr. John F. Sutton is a graduate of Union College, George Washington University, and American University. He designs analog electronic systems for satellite experiments and is currently designing active ULF magnetic-field antennae. He is also developing therapy equipment for the treatment of leukemia and AIDS.

Dr. G. Craig Spaniol is a graduate of West Virginia State College and Rensselaer Polytechnic Institute. He is Chairman of the Department of Industrial Technology at West Virginia State College.

IMPLEMENTATION OF THE CONSULTATIVE COMMITTEE FOR SPACE DATA-SYSTEMS TELECOMMAND PROTOCOL FOR THE GROUND SYSTEM-TELECOMMAND ENCODER CARD

GSFC's Code 743 is responsible for developing the Integration and Test Ground-Support Equipment (I&T GSE) for the Small Explorer (SMEX) Project. The I&T GSE is a ground system that determines the performance and readiness of the spacecraft and its subsystems during spacecraft integration and testing. The I&T GSE consists of two main computer systems: the front-end telemetry and command processor (FTCP), a joint development system between Code 521 and Code 743, and the test conductor workstation (TCW), a commercial Unix-based workstation. These systems communicate with each other via a local area network (LAN). The I&T GSE communicates with the spacecraft via telemetry and command hardlines or on radio frequencies, and with various spacecraft subsystem GSEs via the LAN.

The I&T GSE is one of the first ground systems that complies with telemetry and telecommand recommendations of the Consultative Committee for Space Data Systems (CCSDS). In telemetry downlink processing, the FTCP processes the simulated or actual packetized telemetry data, archives it on hard disk, and distributes the CCSDS packet to the TCW and the subsystem GSEs in real-time. The TCW processes and displays the received packets on the telemetry pages. In the spacecraft command uplink, the FTCP receives the CCSDS command transfer frame sent from the TCW, and encodes and sends multiple, 64-bit command code blocks to the spacecraft. In addition, the TCW supports various processing such as the System Test Operation Language (STOL), database, and generation of displays.

The Telecommand Encoder Card (TEC) has been developed to support the spacecraft command uplink capability in real-time during an active session. The TEC, housed in the FTCP, is to support the coding and physical layers of the CCSDS telecommand layers. The TEC contains semicustom and custom Very Large Scale Integration (VLSI) devices, microprocessor control and programmable logic. The TEC consists of several subsystems to perform the VME bus interface, test chip operation, command data and clock generation, and NASA 36-bit time decoding. The TEC is a VME card, 1/3 of which is a commercially available Mizar 8130 single-board computer that is used as the TEC Controller (TECC). The remaining 2/3 of the card contains custom specialized hardware and logic to support the TEC operations. Two cards are connected together through a side connector provided on the Mizar card. The TECC is a dedicated processor that provides the setup, hardware diagnostics, debug and control over the custom logic card. During operation, the custom logic card provides the hardware functions to perform the spacecraft command and clock generation (2 kHz), status buffering and counting, output port selection, and time decoding.

Extensive application software to support the operation of the card has been written and integrated in the FTCP, and successfully used in the SAMPEX Integration and Test Environment.

Contact: Quang H. Nguyen (Code 743)
(301) 286-5951

Sponsor: Office of Aeronautics and Space Technology

Mr. Quang H. Nguyen is an Electrical Engineer with the Instrumentation Branch, Payload Support Section. He earned an MSEE from The John Hopkins University in 1987 and a BSEE with cum laude honors from the Ottawa University, Canada in 1983. He worked for General Electric for 5 years supporting the NOAA GOES and NASA Spartan programs. Currently, he is responsible for developing and implementing the I&T GSE for the SAMPEX mission, and a command and data handling system for the SWAS mission.

THERMAL SHOCK TESTING FOR ASSURING MICROELECTRONIC PACKAGE RELIABILITY

In-service package failures can cause electrical degradation and eventual failure of microelectronic devices. Thermal shocking is one test employed for assuring reliability of hermetic packaging, such as glass-to-metal seal packages used for transistors and hybrid microcircuits. Packages are cycled between high- and low-temperature fluids to induce transient thermomechanical stresses in the glass seals; seal integrity is verified by subsequent leak testing. NASA has used the test to screen marginal packages; however, many device and package engineers regard it as destructive. The research described here was performed to determine if thermal shocking is destructive to glass-sealed microelectronic packages and to evaluate the use of thermal-shock step-stressing for comparing package reliability.

Two lots of 14-pin DIP packages, manufactured from Fe-Ni-Co alloy pins and platforms and borosilicate sealing glass, were inspected visually and fine-leak tested. Fifty packages from each lot were thermal-shocked for 15 cycles using Condition *C* (-65 to +150°C) of Method 1011 (MIL-STD-883). Subsequently, they were vacuum-baked at 80°C for 90 minutes and then fine-leak tested. This sequence was repeated five times, for a total of 90 thermal shocks. Later, packages from the lots were step-stressed by thermal shocking at temperature differentials (ΔTs) up to 646°C. These also were fine-leak tested after each 15 thermal shock cycles. The glass seals were examined under low (20X) magnification and representative pin-to-glass interfaces were examined at high (1000 to 1250X) magnification. Pin-pull tests were performed to compare seal interface strengths.

Thermal-shock step-stressing indicated no significant loss in thermal stress resistance, even at temperature differentials to 646°C (see the first table). The leak rates after thermal-shock were not significantly different from the control sample (not thermal-shocked) leak rates. Only two failures (five seals of 196 tested) occurred, at ΔTs of 415 and 515°C, and these were not statistically significant for the sample sizes used. The thermal-shock stresses were computed to be as great as 13,000 to 14,000 psi for a 596°C ΔT. Pin-pull tests also showed no significant difference in interfacial strengths between the control and thermal-shocked packages, as shown in the second table. A critical stress resistance temperature (ΔT_c) behavior was not observed, although we had expected to see a sharp decline in glass-seal thermal stress resistance at some ΔT. These results demonstrated the high reliability of this package configuration, whereas packages in other configurations or from other manufacturers may exhibit a ΔT_c behavior indicating lower reliability.

The nondestructivity evaluation yielded no hermetic failures for the 1,330 seals tested at Condition *C* for 90 cycles. Statistical evaluations showed no differences in hermeticity and pin-glass seal strength between the thermal-shocked and not-thermal-shocked packages. Based on these and the step-stressing results, we conclude that thermal-shock testing is not destructive to well-manufactured glass-to-metal packages and can be used to screen poorly manufactured packages. For glass seals with geometries other than the coaxial configuration and the Fe-Ni-Co alloy/borosilicate materials used in this study, it would be prudent to evaluate the proposed thermal-shock conditions to determine if test stresses are sufficient to screen out marginal packages.

Though not a primary objective of the research, the two package lots were compared and showed significant differences (one lot was manufactured in a cryogenic-nitrogen-based atmosphere and the other in an exothermic atmosphere). The nitrogen-atmosphere packages had lower average pin-glass failure stress, greater average oxide depth and narrower distributions (less variance) for the as-received measured leak rate, pin-glass strength, and residual oxide depth. The exothermic-atmosphere packages exhibited significant between-package variances in pin-pull failure stresses; these were bimodally distributed and related to the wider distribution of residual oxide depths. The greater package pin-glass strength was caused by chemical etching, which had roughened the pin surfaces.

Thermal Shock Test Conditions and Results								
Shock Number	Temperature (C)			Fluid		Hot Dwell Time (min)	No. Seals Fails/No. Tested	
	Cold	Hot	Difference	Cold	Hot		A	B
1-15	-65	+150	215	D-100	D-40	5	0/98	0/98
16-30	-65	+200	265	D-100	D-40	5	0/98	0/98
31-45[a,b]	-65	+350	415	D-100	Hot Air	10	0/98	1/98[c]
46-60	-65	+450	515	D-100	Hot Air	10	0/98[d]	4/98[e]
61-75	-196	+400	596	LN_2	Hot Air	10	0/98	0/98
76-90	-196	+450	646	LN_2	Hot Air	10	0/98	0/98

[a]Bake-out added after shock #31.
[b]Leak measurements retested after shock #45.
[c]SN 145 (B) failed at pin 8 after shock #45; failed after retest; replaced with SN 193.
[d]SN 52 (A) failed at 2 pins after shock #60; passed when retested.
[e]SN 192 (B) failed at four pins after shock #60; failed after retest; replaced with SN 194.

Average Pin-to-Glass Failure Stresses			
Group	Variable	Controls	T-Shocked
A	n	32	46
	x	4900	5000 psi
	s	190	130 psi
	CV	3.9	2.6%
B	n	32	52
	x	5900	6000 psi
	s	200	230 psi
	CV	3.4	3.8%

This work demonstrated that thermal-shock testing is not destructive to reliable glass-sealed microelectronic packages and that it can be used to screen marginal packages. Screening packages by visual inspections for cracks is not likely to yield a useful sorting, because identically appearing cracks were observed in packages that passed and failed thermal shock.

Acknowledgements: M. Lewis and B. Muñoz, GSFC/Unisys Systems Support Division, performed the thermal shock and hermeticity tests. Their contributions were instrumental in completing this work.

Contact: Walter B. Thomas, III (Code 311.2)
(301) 286-4125

Sponsor: Office of Aeronautics and Space Technology

Mr. Walter B. Thomas, III, a Section Head in the Parts Branch, Office of Flight Assurance, is involved with the reliability assurance of electronic parts used in space applications. He received an MS in Ceramic Engineering from the University of Illinois and had 15 years of experience in industry in

electronic materials development, manufacturing, and quality assurance prior to joining GSFC in 1986.

Imaging and Optics

FAR-INFRARED ARRAY RADIOMETRIC IMAGER (FIRARI)

The thermal infrared (TIR) region of the electromagnetic spectrum, extending from 8 to 12 μm and beyond, is a band of great interest and utility to many of NASA's remote-sensing applications. Studies of the atmosphere, ocean, biosphere, and lithosphere in this band provide vital data for energy-balance models that can shed light on the issue of global warming. Many of the instruments slated for the Earth Observing System (EOS) depend heavily on TIR for much of the information they will retrieve; one example is the Moderate Resolution Imaging Spectrometer-Nadir (MODIS-N).

There are many situations where the simplicity of a staring detector array is highly desirable; however, the technological challenge of producing high-quality IR detectors in the 8- to 12-μm waveband has made large-format, two-dimensional arrays impractical and prohibitively expensive. Until now, imaging in this band has been done mainly by mechanically scanning a scene of interest across a single-point detector (mercury cadmium telluride (HgCdTe) at 100 K, or extrinsic germanium at 4 K), or by pushbroom scanning across a linear array. Unreliability, high $1/f$ noise, and large spectral nonuniformities from pixel to pixel are among the features that make HgCdTe an unattractive prospect for large-format square arrays, whereas the very low operating temperatures of extrinsic silicon and germanium (~25 K and 4 K, respectively) make their use for long missions impractical.

The advent and development of Molecular Beam Epitaxy (MBE) and Metallorganic Chemical Vapor Deposition (MOCVD) have made possible the growth of semiconductors such as aluminum gallium arsenide (AlGaAs) in very thin layers of precisely controlled thickness. Electrons and holes in these layered structures display quantum confinement effects such as discrete subbands in the conduction and valence bands. These subbands have been exploited to make IR-sensitive devices. This is in contrast to HgCdTe, with a band-gap energy on the order of that of an IR photon (~0.1 eV) and which absorbs IR in interband transitions between valence and conduction bands. Quantum-well IR detectors can absorb in intersubband transitions as well, if the energy level spacing in the quantum wells is of the same order as the IR photon energy. Either photoconducting or photovoltaic devices can be made; to make a photovoltaic detector, the multiple quantum wells are inserted between p- and n-doped GaAs layers.

AlGaAs single-element quantum-well IR detectors have sensitivities significantly lower than for HgCdTe; however, they do not exhibit $1/f$ noise, and their response is linear over a wide range of photon flux levels. This makes calibration of large arrays a much simpler matter than for HgCdTe. The excellent quality of the GaAs substrates and high degree of process control during wafer growth result in layer thickness and compositional variations of much less than 1 percent across a 3-inch wafer. This uniformity means that large-format square arrays of AlGaAs quantum-well detectors can easily be fabricated with uncorrected pixel response and noise uniformity of 2 to 5 percent. Again, this uniformity is superior to what is attainable in HgCdTe arrays by at least a factor of 2. AlGaAs quantum-well photoconductors are high-impedance devices dissipating much less heat than HgCdTe photoconducting detectors. Because of the wider band-gap of AlGaAs, these devices are much more radiation-hard than HgCdTe.

As of May 1990, AlGaAs quantum-well detectors had not yet been made in large arrays and successfully integrated with silicon multiplexers, and no performance data existed with which performance predictions could be validated. Under the auspices of the GSFC 1991 Director's Discretionary Fund, and

with additional support from the EOS Project, we designed, built, and tested an imaging radiometer based on a 128 x 128 element AlGaAs quantum-well detector array. Since this was a Far-IR Array Radiometric Imager, the acronym FIRARI was adopted. FIRARI was test-flown in a NASA Skyvan over varied terrain near Wallops Flight Facility as part of its performance evaluation.

A schematic of FIRARI and its salient features is depicted in the figure. FIRARI consists of a 128 x 128 element AlGaAs quantum-well detector array with response peak at 9 μm, indium bump-bonded to a high-capacity silicon multiplexer. The detector pitch is 60 μm. The array is housed in a continuous-feed liquid-helium dewar with a heater and temperature controller. Custom long focal-length f/2 zinc selenide and germanium optics with diffraction-limited performance are used without a filter to image a scene onto the array; the bandpass of the optics is ~8 to 12 μm. Drive and timing electronics for the array were designed and built in-house; 12-bit digitization of the pixel signals was obtained via a standard A/D board for the Macintosh II. Macintosh II-based data acquisition, display, and analysis software was written in-house.

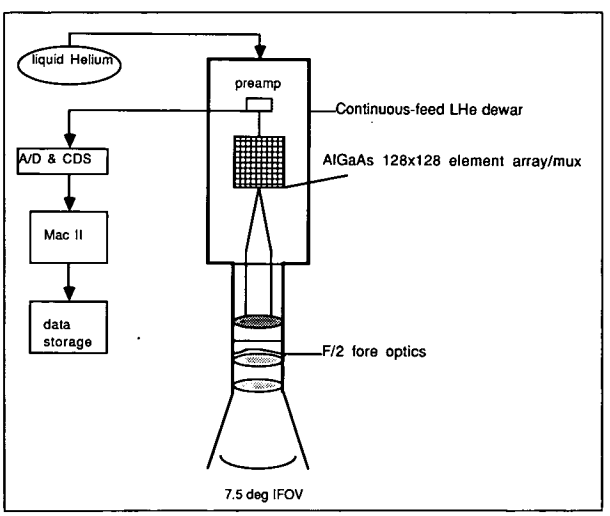

A schematic of FIRARI.

FIRARI performed very well, producing high-quality images with little need for correction other than subtraction of a reference frame at ambient temperature. Fewer than 2 percent of the pixels were bad (i.e., either hot or dark). The quantum efficiency averaged 0.1 percent, which is much lower than anticipated; single, edge-illuminated detectors of the same type have quantum efficiencies of ~25 percent. Poor coupling at normal incidence into the quantum-well structure lowers the quantum efficiency of the array. This is a weakness of this type of detector that needs to be addressed in future development. Furthermore, it is necessary to operate the array at 50 K instead of 77 K to reduce dark current to an acceptable level. Future work should be aimed at raising the operating temperature to 77 K for this detector technology to be strongly competitive with HgCdTe.

The full-page color image at the beginning of this section was acquired with FIRARI.

Contact: Kathrine Forrest (Code 726)
(301) 286-7138

Ravi Kaipa (Code 724)
(301) 286-2195

Murzy Jhabvala (Code 724)
(301) 286-5232

Sponsor: Director's Discretionary Fund

Dr. Kathrine Forrest is a Staff Scientist in the Photonics Branch. She has worked at GSFC for over 11 years, specializing in quantum electronics for NASA missions.

Mr. Ravi Kaipa works in the Solid-State Device Development Branch. He is a Physicist with 3 years of experience at GSFC, and holds an MS in Physics from the University of Maryland. He works on visible and IR detector test and evaluation.

Dr. Murzy Jhabvala works in the Solid-State Device Development Branch. In 17 years at GSFC, he has designed integrated circuits and established fabrication techniques for CMOS, PMOS, VMOS, DMOS, CCDs, JFETs, Schottky barrier devices, and far-IR detectors. Dr. Jhabvala has received awards for special achievement and for patents.

PHASE CONJUGATE MIRRORS (PCMs) FOR LASER BEAM QUALITY IMPROVEMENT

The Geoscience Laser Ranging System (GLRS) facility instrument for EOS will utilize compact, efficient, solid-state lasers requiring energy outputs of 20 to 250 millijoules in 0.1- to 50-nanosecond pulsewidths. Multistage power amplification is needed to achieve these energies, which often leads to a deterioration in wavefront quality due to thermally induced distortions, bulk crystal inhomogeneities, and optical surface finish. We are investigating Stimulated Brillouin Scattering (SBS) and photorefractive four-wave mixing to remove wavefront distortions using nonlinear techniques. Four-wave mixing can also find application in communication and fiber optic research and development.

SBS is a process that occurs when an intense, pulsed laser beam is focused into a gas or liquid sample. The beam interacts with the electrostrictive forces of the SBS material by locally heating a small volume of material and changing the index of refraction. This interaction creates a density grating traveling through the sample at the speed of sound. The laser beam is Bragg-scattered off the moving grating, resulting in a backward-going (reflected) light beam. The reverse wave has the unique property of being the phase conjugate of the input wave, which will undo any aberration acquired by the input beam as it travels back through the distorting media. This phase conjugation/wavefront reversal property can be used to compensate for amplifier-induced aberrations by placing the phase conjugate mirror (PCM) behind a double-pass amplifier instead of a conventional mirror. The figure shows the contrast between the Mach-Zehnder interferometric fringe patterns of the phase conjugate return and the return from a conventional mirror after the return beams pass back through the aberrating media.

Photorefractive, four-wave mixing accomplishes the same phase conjugate results, but entails using a continuous wave (cw) laser beam and a crystal. The beam is focused into a crystal such as barium titanate, and utilizes the photorefractive properties of the crystal to create the grating. The beam is then reflected off the grating as in the SBS process and becomes the phase conjugate of the input beam. The cross-sectional area of the phase conjugate beam was compared to the return from a conventional mirror after passing back through the aberrating media. The

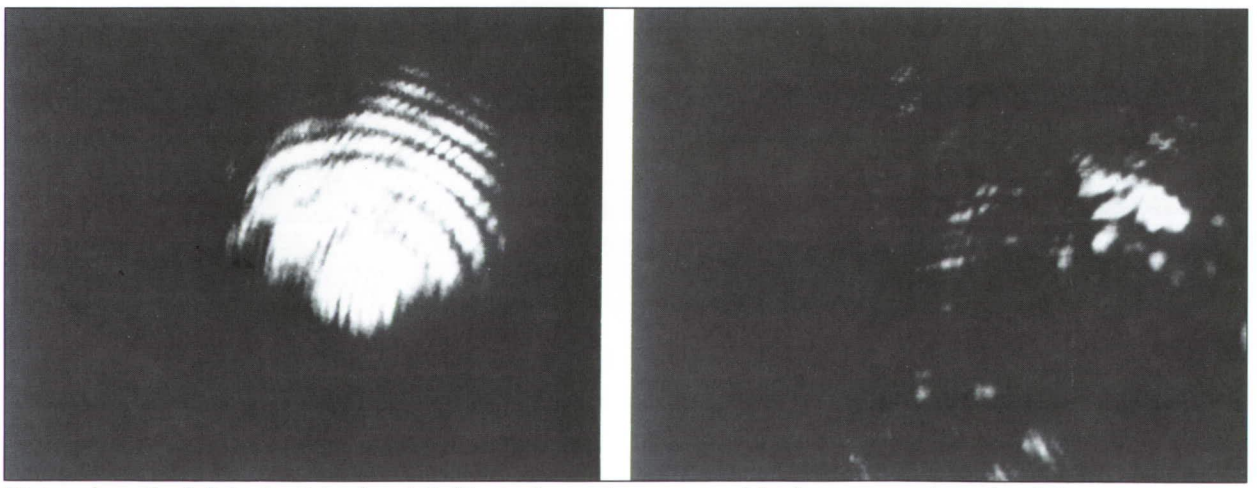

Pictured on the left is the Stimulated Brillouin Scattering return with aberrator and on the right, a retro mirror return with aberrator.

phase conjugate beam returned with a cross-sectional area equal to the unaberrated beam, but the return from the mirror became elongated.

Contact: Bernie Seery (Code 726)
(301) 286-8943

Barbara Zukowski (Code 726.1/HSTX)
(301) 286-8969

Babak Saif (Code 726.2/EER)
(301) 286-8969

Sponsor: Director's Discretionary Fund

Mr. Bernie Seery is Head of the Photonics Branch at GSFC. He obtained an MS in Optical Sciences from the University of Arizona in 1979 and he has been working in the fields of laser physics and electro-optics for 15 years.

Ms. Barbara Zukowski is a Senior Scientist working with the Laser Ranging and Altimetry Section. She graduated with a BS in Physics from Virginia Tech and has 7 years of experience working with lasers, nonlinear optics, and phase conjugation.

Dr. Babak Saif is a Senior Engineer working with the Optical Communications and Data Systems Section. He graduated with a PhD in Physics from The Catholic University of America and has been working in electro-optics research for the past 2 years.

CHARACTERIZING PERFORMANCE OF VACUUM ULTRAVIOLET OPTICS

Many of NASA's space science programs involve measuring emission of light at vacuum UV wavelengths. Performance of optics in this wavelength range is difficult to infer from conventional, visible-light, metrology data. Therefore, capabilities have been developed in the Goddard Optics Branch to predict the performance of these optics using metrology data and to experimentally verify these predictions by direct measurement in the vacuum UV wavelength region down to 100 Å using the GSFC Diffraction Grating Evaluation Facility (DGEF). Solar-blind detectors, with a variety of apertures in front, are moved about in the focal plane of the optical component under vacuum conditions using computer-controlled micropositioners. For encircled energy measurements, the detector, with an aperture as small as 2 μm, is raster-scanned throughout the image area, simulating a CCD array detector with vacuum UV sensitivity. This results in superior spatial and angular resolution since there are up to 100 pixels in the space of 1 pixel for a typical scientific CCD. For scatter measurements, extended line scans through the image peak are performed to search for light errantly scattered by the optical component outside of the image area. Scatter levels of a few parts in 10 billion have been measured.

A variety of vacuum UV optical components have been characterized experimentally and analytically for their encircled energy and scattering behavior. These include the SiC demonstration telescope mirror for the ISTP/SOHO/Solar Ultraviolet Measurements of Emitted Radiation (SUMER) instrument, diffraction gratings for the ISTP/SOHO/Coronal Diagnostic Spectrograph (CDS), a low-scatter, off-axis, parabolic mirror for solar imaging, and two Wolter Type II glancing incidence telescopes for the Solar Extreme Ultraviolet Rocket Telescope and Spectrograph (SERTS) program. For the latter, one telescope was selected over the other for a recent rocket flight based on these measurements. Analytical models of the experiments were developed using Optical Surface Analysis Code (OSAC). The models included all known aspects of the optical components from metrology (figure and roughness) and of the experimental arrangements themselves (geometry, sampling, and source extent). The significance of these achievements is the good agreement between experimental results and analytical predictions.

For optics operating in the vacuum UV wavelength range, it is crucial to have proper surface characteristics in all spatial frequency ranges: low (figure), middle (ripple), and high (microroughness). Until recently, there has been no metrology tool to directly measure mid-spatial frequency errors on

optical surfaces. To that end, a state-of-the-art instrument, developed under an SBIR contract with Bauer Associates, Inc., has been designed and built to measure this type of error. This fills the void for information about the mid-spatial frequency range important for modeling the focal plane energy distribution of vacuum UV optics.

Contact: Douglas B. Leviton (Code 717.1)
(301) 286-3670

Timo T. Saha (Code 717.4)
(301) 286-2863

Sponsor: Office of Space Science and Applications

Mr. Douglas B. Leviton earned his MS in Physics at Georgia Institute of Technology and has been in the Optical Research Section for 8 years.

Dr. Timo T. Saha earned his PhD in Physics at St. Louis University and has been in the Optical Design Section for 9 years.

REAL-WORLD IMAGE UNDERSTANDING—AN INNOVATIVE ALGEBRAIC APPROACH

The Vision Research Team in Code 735.1 at GSFC has been awarded Phase I and II Director's Discretionary Fund (DDF) Awards to pursue research on algebraic approaches to image processing and real-world image understanding.

We have developed an innovative algebraic mathematical model based on polynomial representations of two- and three-dimensional grey-level imagery, and have applied this representation by using it to develop polynomial operators on complex grey-level scenes. The advantage of this approach is that polynomials can be manipulated very easily and are readily understood, thus providing a very convenient environment for image processing. This mathematical model has proven to be highly adaptive and generic, displaying machine and language independence.

Utilizing this new algebraic polynomial structure, we have devised a unique edge-detection scheme, the Lerner Algebraic Edge Detector (LAED). A continuous, single-pixel edge, as well as inherently parallel global operations, are some of the advantages that this edge detector possesses over classical convolution-type edge detectors. We have applied the LAED to multispectral Landsat and medical imaging data, as well as to object recognition tasks in robotics.

The first figure displays a NASA Landsat image of New Orleans on the left, with the application of the LAED on the right. The second figure displays a medical image from the University of Colorado Medical School on the left with the application of the LAED on the right.

To approach the vision problem in robotics involving object recognition, we have developed a scheme based on the real-world image of an object. A three-dimensional polynomial model of the real-world object is created and stored. Then, an algebraic operator creates a shell or contour of the object, thereby providing surface information. Finally, another algebraic operator creates a wire frame or skeleton of the object, providing edge and corner information.

The algebraic edge detector has also been employed as the front end of a linear feature extraction system which is based on the Hough transform. Our primary goal is to perform feature extraction while maintaining object independence and system invariance to object rotation, translation, and scaling in the image.

Because the mathematical model is polynomial-based, it is particularly amenable to processing on parallel architectures. The Institute for Defense Analysis/Supercomputing Research Center (IDA/SRC) SPLASH processor was chosen as the target machine on which to implement several of the algebraic image operators. SPLASH incorporates electronically reconfigurable hardware yielding a performance midway between conventional software and special-purpose hardware, approximately as fast as 10 Cray processors. Dr. Neil B. Coletti, of the

A NASA Landsat image of New Orleans (left) with the application of the LAED (right).

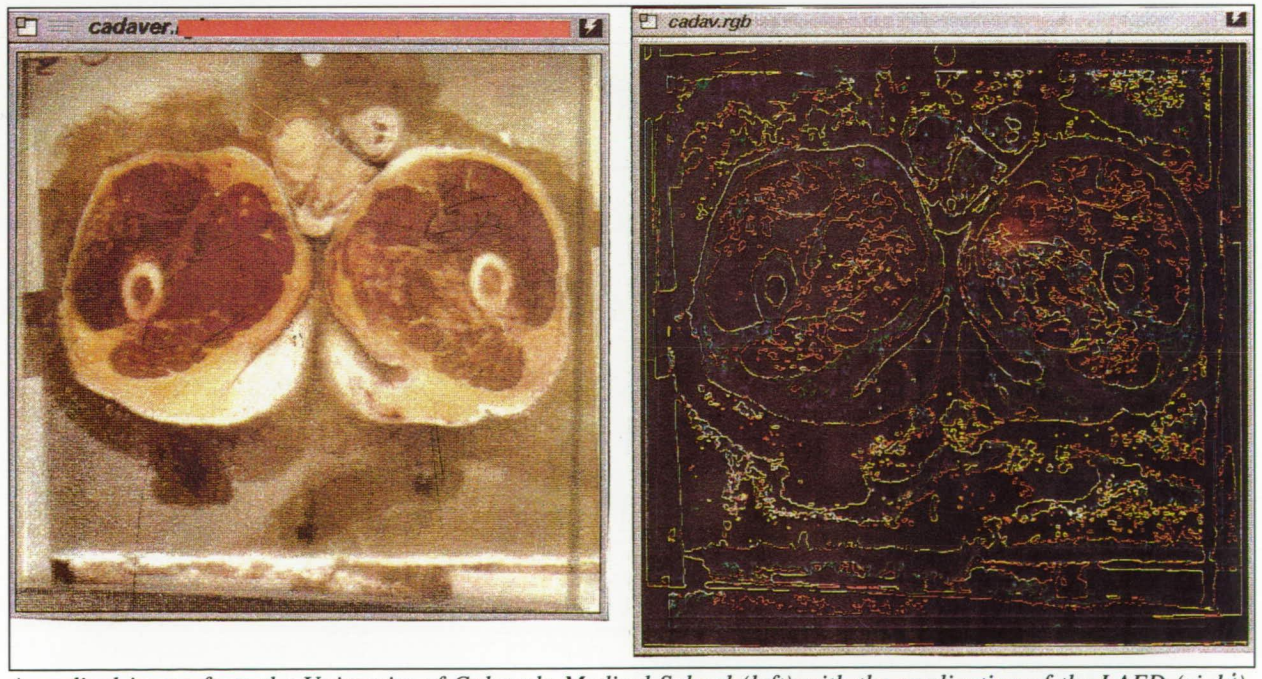

A medical image from the University of Colorado Medical School (left) with the application of the LAED (right).

IDA/SRC, has implemented the LAED, and is currently completing the mapping of the Hough transform onto SPLASH.

Future research will focus on the development of a robust method of linear feature extraction by combining the techniques of the Hough transform and a line follower. Target attributes, such as line segment lengths, intersections, angles of intersection, and endpoints will be derived by the feature extraction algorithm and employed during model matching. These activities will support our ongoing efforts to develop algebraic operators for frame-rate image enhancement.

We would like to acknowledge the expert help of Dr. Neil Coletti, IDA/Supercomputing Research Center; Dave Provost (Code 733) Head of the Electrical Engineering Branch; and Danny Dalton (Code 735), Head of the Flight Data Systems Branch.

Contact: Colleen N. Hartman (Code 735.1)
(301) 286-4666

Dr. Bao-Ting Lerner
KT-Tech., Inc.

Sponsor: Director's Discretionary Fund

Colleen N. Hartman began her NASA service at Headquarters as a Presidential Management Intern, and then served as Program Manager in the Astrophysics Division of the Office of Space Science and Applications with responsibility for the Cosmic Background Explorer (COBE), the Extreme Ultraviolet Explorer (EUVE), the X-Ray Timing Explorer (XTE), the Explorer Platform, the Infrared Astronomical Satellite (IRAS), and Gravity Probe B. In 1986, she received an Outstanding Service Award, and from 1987 to 1988 she held the Hugh L. Dryden Memorial Fellowship awarded by the National Space Club. She holds the 3-year Claire Booth Luce Fellowship in Science and Engineering to support her continuing study towards a PhD in Physics at The Catholic University of America. She joined the GSFC Robotics Data Systems and Integration Section in 1990, where she currently pursues her research interest in image processing problems in space.

Dr. Bao-Ting Lerner is President of KT-Tech., Inc. and has 9 years of experience in the research fields of mathematical modeling for machine-vision and robotics. Before forming KT-Tech., Inc., she held the position of Full Professor of Mathematics at the U.S. Naval Academy. She was an ASEE Summer Faculty Fellow in the NASA/Goddard Robotics Laboratory in 1987 and 1988. Subsequently, she became a Visiting Research Professor and consultant for GSFC from 1988 to 1991.

Thermal and Cryogenic

PROTOTYPE HEAT PIPE HEAT EXCHANGER

Two-phase thermal transport systems have a number of advantages over single-phase systems, and have become the preferred means of heat transfer for Space Station and for other long-duration space facilities. A typical two-phase thermal loop consists of an evaporator plate for absorbing heat and vaporizing the working fluid, a vapor transport line for transferring the vapor to the condenser, a condenser for rejecting heat and recondensing the fluid, a liquid return line for transferring the liquid back to the evaporator plate, and a reservoir for controlling the system operating temperature. The condenser rejects heat to space through a radiator, which must be sized to dissipate all the heat loads applied to the evaporator plate. In a direct condensation design, the condenser tubes run several passes through the radiator, and heat is rejected directly to space as the vapor condenses inside condenser tubes. In addition to a larger pressure drop and pumping requirement, this design also increases the probability of micrometeoroid attacks because of a large exposed area of condenser tubes. A single micrometeoroid puncture in condenser tubes will result in a loss of the working fluid and a total system failure. An alternative design is to distribute heat from the condenser through an interface heat exchanger to multiple heat pipes that are mounted to the radiator. Multiple heat pipes provide

redundancies and are much less susceptible to micrometeroids; only the affected segment of the radiator is lost, not the entire loop.

A prototype of the heat pipe heat exchanger (HPHX) to be used in the thermal control system in the Earth Observing System (EOS) has been designed, fabricated, and tested as part of the CAPL flight experiment (see the GSFC 1990 Research and Technology Report). The prototype HPHX consists of a heat exchanger, a header heat pipe, and a spreader heat pipe. A Capillary Pumped Loop (CPL) is used to transport heat from the evaporator plate to the heat exchanger, using ammonia as the working fluid. The objective is to demonstrate the operation of an integral design of the HPHX. In the heat exchanger section, the vapor in the CPL condenses. The heat released is used to vaporize the liquid inside the header heat pipe, which transports part of the heat directly to the radiator. Remaining heat is transferred to the radiator through the spreader heat pipe.

The design requirements imposed upon the HPHX design are: (1) the heat exchanger must accept a maximum heat load of 350 W with less than a 5°C temperature difference between the CPL and the header heat pipe; (2) the header heat pipe must have a minimum heat transport capacity of 17,000 watt-inches at 35°C with 0.25-cm adverse tilt; (3) the spreader heat pipe must have a minimum heat transport capacity of 7,000 watt-inches at 35°C with 0.25-cm adverse tilt; (4) flow regulation must be provided when multiple HPHX units are used in parallel; and (5) the HPHX must be able to collect noncondensible gas (NCG) bubbles.

The HPHX prototype employs a helical fin heat exchanger, a 2.86-cm OD header heat pipe, and a 1.91-cm OD spreader heat pipe as shown in the first figure. The header and the spreader heat pipes are rated at 24,000 watt-inches and 12,500 watt-inches, respectively, at 35°C and 0.25-cm adverse tilt. A heavy wall extrusion was used for the header heat pipe so that helical grooves could be cut into the outer surface of the heat pipe to form fluid flow passages for the heat exchanger. The helical grooves promote annular flow and enhance heat transfer under both 0-*g* and 1-*g* environments. A stand-alone flow regulator is provided for each HPHX and is plumbed downstream of the heat exchanger. The flow regulator utilizes a porous polyethylene wick structure to prevent vapor from blowing through. When the heat load to one particular HPHX exceeds its heat dissipation capability due to a hot environment, the vapor will reach the flow regulator and the porous wick will develop a higher flow resistance. As a result, any heat in excess of the heat exchanger's capacity will be diverted to other HPHXs that are still capable of dissipating heat. Flow regulation is possible as long as the pressure drop across the wick in the flow regulator does not exceed its capillary limit. The flow regulator also traps any NCG bubbles that may be present in the flow.

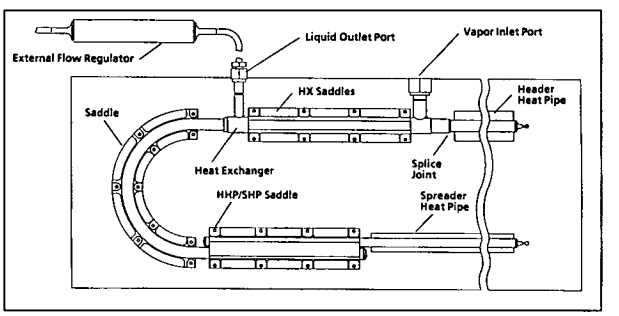

Prototype heat pipe heat exchanger design.

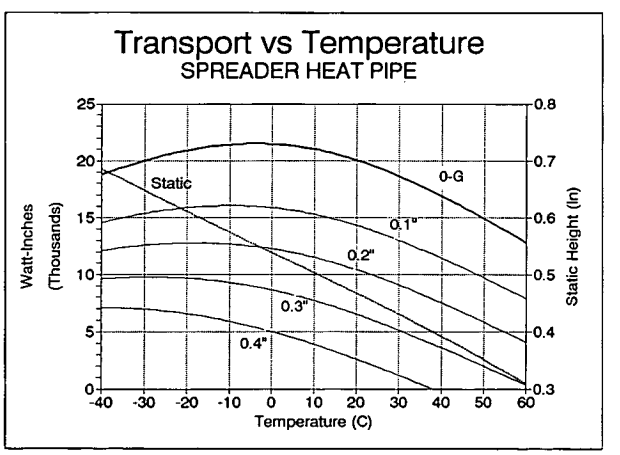

Theoretical performance of header heat pipe.

Two sets of the prototype HPHX were fabricated by the OAO Corporation for GSFC's Thermal

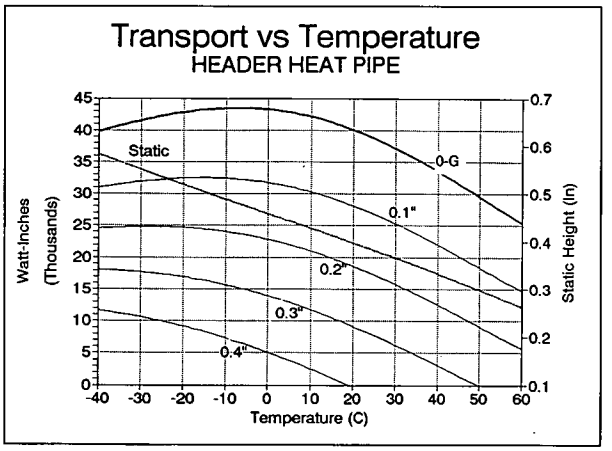

Theoretical performance of spreader heat pipe.

Engineering Branch. These HPHXs have been ground-tested in a laboratory environment. The second and third figures show theoretical predictions for the two heat pipes under various conditions. All four heat pipes were individually tested at -20°C, +20°C, and +40°C with four adverse elevations ranging from 0.25 cm to 1.04 cm. Test results showed that heat transport capabilities were within 20 percent of the rated values and far exceeded the design requirements. The heat exchangers delivered 350 W with a 3.2°C temperature difference, and 800 W with an 8°C temperature difference. Flow regulation tests were performed by installing both HPHXs in parallel. Two tests were conducted with total heat inputs of 800 W and 200 W, respectively. In either test, when the condenser heat dissipation capability in one of the HPHXs was taken away, the flow regulator directed all the heat input to the other HPHX, and the system remained operational without any problems.

Contact: Jentung Ku (Code 732)
(301) 286-3130

Dan Butler (Code 732)
(301) 286-5235

Sponsor: EOS Flight Project

Dr. Jentung Ku is responsible for the design, development, and testing of two-phase heat transfer devices and heat transport systems, and computer modeling of various thermal systems. Dr. Ku spent 11 years working on thermal sciences and two-phase systems before joining GSFC in 1991. He earned his PhD in Mechanical Engineering from Purdue University.

Mr. Dan Butler is a Research and Development Engineer in the Thermal Engineering Branch, Applied Engineering Division, with 14 years of experience at GSFC. He holds a BS in Aerospace Engineering from Virginia Polytechnic Institute and State University. Mr. Butler currently serves as Project Manager for CAPL.

TEST RESULTS OF PROTOTYPE TWO-PHASE RESERVOIRS FOR THE CAPILLARY PUMPED LOOP FLIGHT EXPERIMENT

The Capillary Pumped Loop (CPL) Flight Experiment was designed as a prototype of the EOS instrument thermal-control system, and was described in detail in the 1990 GSFC Research and Technology Report. The thermal-operating conditions of a CPL heat transport system are controlled by a two-phase reservoir. The reservoir must provide stable temperature control of the CPL, minimize discharge of vapor into the CPL during liquid inventory fluctuations, and have a small pressure drop during liquid exchange with the CPL. Heat is applied to the reservoir to control the CPL, and for microgravity use, a reservoir must be able to continuously supply liquid to the heat application region. Three prototype two-phase reservoirs designed for use in microgravity applications were built to CAPL specifications and performance-tested at GSFC using ammonia as the working fluid. Each reservoir has an internal wick structure to provide liquid to the desired locations during CPL operational control, but the wick geometry and materials of construction vary.

The Porous Plate Reservoir (PPR), an in-house design, consists of a 660-mm-long, 83-mm-diameter aluminum shell, an internal porous cylinder that

serves as the wick structure, and an internal porous disk located at the exit port to prevent vapor expulsion. The porous material used in assembly of the PPR is a high-density polyethylene with an average pore size of 50 μm. As shown in the first figure, there are 20 6.35- x 3.175-mm longitudinal grooves cut into the porous cylinder to provide a high-permeability axial flow path for liquid transport to the exit port. Strip heaters are mounted externally on the aluminum reservoir body at the end of the PPR opposite of the exit port. Axial grooves are located on the inner surface of the aluminum cylinder underneath the heaters, and four 50-mm-square windows are cut out of the transport wick to allow the vapor generated in the grooves access to the reservoir vapor space.

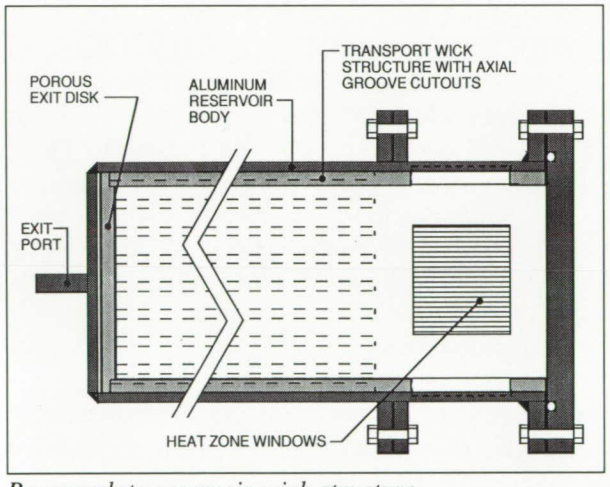

Porous plate reservoir wick structure.

The Dynatherm Reservoir (DR) is made entirely from 316L stainless steel, and was formed using an 88-mm-diameter cylinder and two hemispherical end caps for an overall length of 628 mm. The reservoir wick structure is shown in the second figure. Six internal arteries made from high-density porous polyethylene (20-μm pore size) are located at 60° intervals around the reservoir circumference and are responsible for axial transport of liquid to the exit port. The arteries are sealed at one end and empty into a void space at the exit end. To prevent vapor expulsion, the exit void is isolated from the interior of the reservoir by a 1.6-mm-thick porous stainless-steel sheet with a pore size of 5 μm. The inside surface of the reservoir is covered with five layers of 250-mesh stainless-steel screen, and the screen is spot welded to the reservoir wall. Resistance heaters are mounted longitudinally between adjacent arteries. The circumferential screen wick provides liquid to the reservoir wall underneath the heated areas. The arteries are held in place with multilayer stainless-steel screen straps that are spot-welded to the circumferential wick. The straps also allow liquid communication between the arteries and the screen wick.

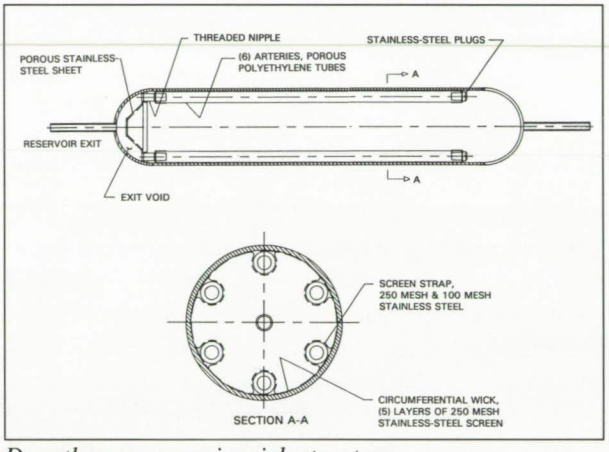

Dynatherm reservoir wick structure.

The General Electric Reservoir (GER) consists of a 168-mm-diameter 316L stainless-steel cylinder, with hemispherical end caps, and has a total length of 243 mm. The inner surface of the reservoir is lined with a thin layer of sintered stainless-steel powder metal, and capillary flow in the sintered wick is designed to keep liquid available at the heated end of the reservoir during operation. A 12.7-mm-thick sintered powder metal plug is located near the exit port of the GER to prevent vapor expulsion during liquid discharge conditions. The design pore size of the porous wick material is 20 μm. The GER also contains internal vapor bubble positioning vanes as shown in the third figure. During microgravity operation, the vanes are designed to pump all vapor bubbles larger than 31 mm in diameter to the heated end of the reservoir and away from the exit port. On Earth, the surface tension effects between the vanes and the reservoir wall are not strong enough to overcome the force of gravity, so verification of the

vane function was not possible during reservoir performance testing.

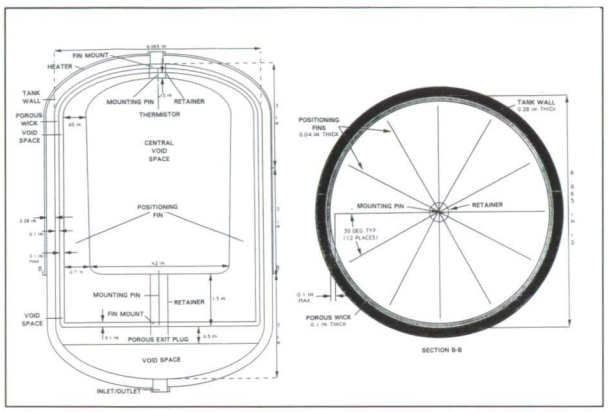

General Electric reservoir internal design.

Each reservoir was individually installed in a CPL test loop to experimentally determine the liquid discharge characteristics at various reservoir orientations, including both adverse tilt and gravity-assist modes. A sight-glass was installed between the prototype reservoirs and the CPL to visually check for vapor expulsion during discharge tests. The reservoirs were also used to control the operation of the CPL test loop at setpoints of 30 and 40°C. At each setpoint the total heat load on the CPL was varied from 200 to 3,200 W, with some instances of rapid change to verify the thermal stability of the reservoir.

Liquid discharge test results showed that each reservoir was capable of preventing vapor expulsion during normal operating conditions, although the average time necessary for complete liquid inventory discharge varied between reservoirs (100-W input). The GER consistently had the highest Mass Flow Rates (MFRs), but the MFR changed with reservoir tilt. Regardless of tilt, the DR showed a relatively constant MFR. The PPR was the poorest performer, but this was expected since the capillary pumping capability of the PPRs' 50-μm wick was the worst of the three reservoirs.

Each reservoir proved to be adequate in controlling the CPL test loop, and no operational failures occurred during any tests that were directly traceable to the reservoir. The only time differences were observed in the prototype reservoir behavior was during the CPL startup procedure. When power is applied to the CPL evaporator pumps, excess fluid is rapidly driven out of the vapor lines and condenser and into the reservoir. This rapid influx of cold liquid can cause a reservoir to cold-shock, during which the reservoir temperature quickly drops and control of the CPL is lost. The liquid flow path into any given reservoir is dependent upon the internal geometry and wick material, and some designs can tolerate the cold-shock condition better than others. The DR and PPR were highly susceptible to cold- shocking during startup, but the GER was not affected and successful startup was achieved.

In conclusion, three prototype wicked reservoirs of widely varying design were tested, and all three were shown to meet the required specifications. Based on thermal performance, structural requirements, cost, and delivery schedules, one reservoir will be selected to provide thermal control for the CPL Flight Experiment.

Contact: Matthew Buchko (Code 732.2)
(301) 286-8537

Sponsor: Earth Observing System

Mr. Matthew Buchko is an Aerospace Engineer in the Advanced Development and Flight Experiment Section. He received his BS in Physics from Millerville University and his MS in Mechanical Systems Engineering from Wright State University.

SUPERFLUID HELIUM ON-ORBIT TRANSFER CRYOGENIC COMPONENTS

The Superfluid Helium On-Orbit Transfer (SHOOT) Project objectives are to demonstrate the technology required for superfluid helium transfer in space. A side benefit of the program is the development of a number of cryogenic components that may find use in space helium dewars, other cryogenic payloads, or cryogenic systems on Earth.

Some examples of these include leak-tight, motor-operated cryogenic valves, cryogenic relief valves, cryogenic burst disks, gravity-actuated relief valves, liquid/vapor discriminators, liquid/gas phase separators for normal as well as superfluid helium, and a large-scale, simply constructed thermomechanical pump.

Stepper motor-actuated cryogenic valves in nominal 1/2- and 3/4-inch sizes were developed for SHOOT by Utah State University. These bellows-sealed valves have a Torlon™ stem in a stainless-steel seat. They have been tested by numerous thermal and mechanical cycles, and have been vibration-tested at warm, liquid-nitrogen, and liquid-helium temperatures. Throughout the testing, no degradation in performance was seen. These valves have been leak-tested with superfluid pressurized to one atmosphere on one side of the seat and superfluid surrounding the stem seal, and have been found to be leak-tight to better than 10^{-9} standard cubic centimeters per second (sccs). These valves are currently produced commercially by Space Systems Engineering, Logan Utah.

The cryogenic relief valves are actuated by differential pressure, which is adjustable from about 68 to 200 kPa (10 to 30 psid). They are meant to relieve possible trapped volumes of liquid helium. Their leak rate through the seat is ~10^{-4} to 10^{-3} sccs with 1 atmosphere pressure superfluid on the upstream side when set for a cracking pressure of 20 psid. Full flow occurred within 1 psid of the cracking pressure.

The SHOOT cryogenic burst disks were manufactured by Ketema Corporation. The major innovation over previous designs is the removable diaphragm, sealed in place with indium as opposed to being welded.

A valve has been developed for the SHOOT vent which, on the ground, serves as a relieve valve and will also serve as a relief valve. It will automatically open in a low-gravity environment without the aid of motors or electronics. When open, the valve has negligible flow impedance. To determine the position of liquid and vapor in the low-gravity environment, Liquid/Vapor Discriminators (LVDs) were developed. The LVDs are resistive devices consisting of 0.25-mm cubes of doped silicon suspended from a 0.05-mm stainless-steel wire which serves as a support and return current lead. The resistance of the LVDs rises steeply as the temperature decreases. The devices work by applying a current across them, causing self-heating. The amount of self-heating depends on whether the detector is immersed in liquid or vapor. When operating in superfluid, typical voltages across the detector are 2 V for liquid and 0.5 V for vapor for power dissipation of ~0.1 mW, so the readout electronics can be very simple. Response times in going from liquid to vapor are a few milliseconds. These devices also have been tested in liquid hydrogen and nitrogen and have been shown to be very effective, although more power is dissipated and response times are slower than for helium.

A phase separator was developed for SHOOT that allows vapor to boil off while containing the liquid within the tank for normal liquid helium (2.2 to 4.3 K) as well as superfluid ($T < 2.2$ K) at pressures up to 1.1 atmospheres. This is required for space operations where gravity is not available to position the liquid away from the vent. The phase separator captures all the cooling from the evaporating liquid and cools the liquid remaining in the dewar. This device could enable the use of liquid helium in small payloads without requiring an on-board vacuum pump, thus simplifying shuttle operations and allowing orbital operation with liquid above the superfluid transition.

SHOOT also has developed a thermomechanical pump made out of a commercially available porous ceramic and resistive heater wire. The pump, which works on the thermomechanical (or fountain) effect unique to superfluid helium, produces pressures over 63 kPa (9 psid) following the ideal London equation to within a few milliKelvin of the superfluid transition. The pump is in the shape of a cup 7.5 cm in diameter and 6.2 cm high and can pump up to 1,700 liters per hour.

Contact: Michael DiPirro (Code 713)
(301) 286-7310

Peter Shirron (Code 713)
(301) 286-7327

David Lindauer (Code 713)
(301) 286-2215

Sponsor: Office of Space Flight

Dr. Michael DiPirro has worked in the Cryogenics Technology Section for the past 11 years. He has worked on the Cosmic Background Explorer (COBE), the X-ray Spectrometer for the Advanced X-ray Astrophysics Facility (AXAF/XRS), and is Principal Investigator for the SHOOT Project.

Dr. Peter Shirron received his PhD in Low-Temperature Physics from the University of Illinois at Urbana-Champaign in 1989. He joined GSFC in 1989 and is Co-Investigator for the SHOOT program.

Mr. David Lindauer has been a member of the Fluid Systems and Hazardous Test Section for 8 years. He has worked on the Energetic Gamma Ray Experiment Telescope (EGRET) on the Compton Gamma Ray Observatory (CGRO), the COBE vent system, the Broad Band X-ray Telescope (BBXRT) cryogenic system, and is currently the SHOOT Project Manager.

HELIUM FINE-LEAK TEST IMPROVEMENTS

Open-package, helium fine-leak (hermeticity) testing is a routine quality assurance test for microelectronic packaging. It also is an endpoint measurement for other package-related tests such as thermal shock. The fine-leak test method was evaluated and its test sensitivity improved as part of a recent NASA study of microelectronic packages.

Two package lots were procured and the headers (packages) were leak-tested in accordance with MIL-STD-883, Method 1014, Condition A4, using a mass spectrometer helium leak detector (Spectron Model 3000S/3200, Edwards High Vacuum, Inc.). This machine is capable of detecting leak rates to 10^{12} atm-cc/s. Vacuum grease (Apeizon Type M) and a Viton™ gasket were used to reduce leakage between the headers and the custom-machined test fixture. Actual leak rates (not GO/NO-GO results) were recorded for all measurements. Eight headers were selected as controls; these were stored in a vacuum desiccator and their leak rates were measured immediately before and after the test headers were measured. Test headers were cleaned in ultrasonically agitated trichloro-trifluoroethane and alcohol baths before leak testing. After test number eight, all the test headers (thermal-shocked), and four of the control headers were oven-baked (200°C for 2 hours) prior to leak testing.

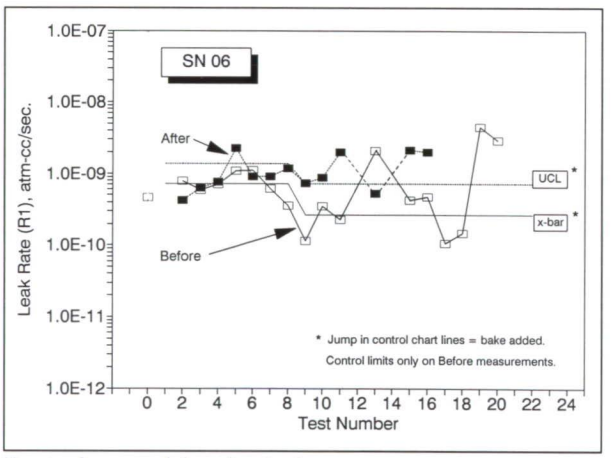

Typical control header leak measurements.

Typical control header leak measurements are shown in the first figure. Data were taken over several months during the thermal-shock test program. The leak-test measurement capability was evaluated from 3-sigma control chart statistics calculated on each control header. These are summarized in the first table. Over the test program duration, our measurements (i.e., machine, fixture, methods and headers) yielded mean leak rates of 1.7 to 15.0 x 10^{-10} atm-cc/s and yielded upper control limits (UCL) 1.9 to 3.3 times the individual mean leak rates. These exceeded the Method 1014 requirement of 1 x 10^{-9} atm-cc/s (i.e., the requirement is for a machine sensitivity of 1 x 10^{-9}).

Both the first figure and the first table show significant leak rate decreases when the bake-out was

Bake-out Effect on Leak Tests of Thermal-Shocked Headers (Mean Leak Rate x 10^{-10} atm-cc/s)			
	Test Numbers		
SN	6, 7, 8	9, 10, 11	Change (%)
01	33.5	9.7	-71.0
07	21.7	10.7	-50.8
18	16.4	10.3	-37.5
29	17.3	8.9	-48.8
44	12.5	9.1	-27.1
51	15.0	3.9	-74.2
52	14.3	4.7	-67.4
101	14.2	4.9	-65.6
102	18.7	8.0	-57.3
117	13.8	9.2	-33.2
118	15.0	10.5	-30.3
131	18.8	12.6	-33.0
145	10.7	9.9*	-8.1
192	11.5	24.7	114.5†

*SN 145 failed during #11; only #9 and #10 were used to compute average.

†Value ignored; latent defect which eventually failed at test #15.

added (e.g., 50 to 57 percent less for the control headers). These headers had not been immersed in the thermal-shock fluids. The bake-out also improved thermal-shocked header leak rates by 20 to 70 percent, as shown in the second table, which compares individual test header leak rates before and after adding the bake-out. The bake-out before leak testing removes any water or fluorocarbon plugging, which can cause erroneous hermeticity measurements. This sample conditioning (bake-out) currently is not required by Method 1011 (Thermal Shock) or Method 1014 (Seal). However, it is recommended for assuring accurate test results.

Helium Leak Test Measurement Capabilities (Control chart calculations for individuals on "before" measurements)					
			R_1, x 10^{-10} atm-cc/s		
SN	Treatment	n	x	UCL	UCL/x
00	No Bake	16	1.7	4.1	2.4
17	No Bake	16	4.2	14.1	3.3
06	Before Bake	8	7.1	13.9	2.0
	After Bake	7	2.6	7.1	2.7
90	Before Bake	7	8.6	14.4	1.7
	After Bake	7	3.7	12.1	3.2
115	No Bake	17	7.1	20.7	2.9
191	No Bake	15	6.9	14.6	2.1
116	Before Bake	7	10.9	20.9	1.9
	After Bake	6	5.5	13.8	2.5
217	Before Bake	7	15.0	34.1	2.3
	After Bake	7	7.6	15.3	2.0

The first figure also shows that the *before* leak rates (those taken before the thermal-shock test headers were measured) were less than the *after* rates (except for test number 13) and that there was a gradual increase in the *after* rates over the test program's duration (again, excepting test 13). All eight control headers exhibited both these trends and the test 13 anomaly.

The two manufacturer lots showed different leak rates for *before* measurements but not for *after* measurements. These differences were confirmed by statistical computations (t-test at 95-percent confidence). They were caused by our sniffing technique, which used a wand to effuse helium over each header tested. Continuous testing caused helium to diffuse into and accumulate in the small test room. If a period of time passed before a subsequent series of leak tests were run, the helium dissipated and its background level decreased. This helium accumulation accounted for all three observed phenomena: *before* less than *after*, different lot behavior *before* but not *after*, and gradually increasing *after* rates.

The unusual behavior at test number 13 (where *before* measurements were greater than *after* measurements) was caused when the test 13 *before* measurements were taken in the afternoon just after a previous test series was measured; the *after* measurements were completed the following morning. All these observations suggest using a closed container (cup) over the test fixture to allow helium to diffuse around the test part but to limit its diffusion into the test room and thus lower the helium background level.

Baking electronic packages before testing and limiting tracer gas (helium) diffusion during testing will improve the accuracy of helium fine-leak measurements.

Acknowledgements: M. Lewis and B. Muñoz, GSFC/Unisys Systems Support Division, performed the thermal-shock and hermeticity tests. Their contributions were instrumental in completing this work.

Contact: Walter B. Thomas, III (Code 311.2)
(301) 286-4125

Sponsor: NASA Reliability, Maintainability and Quality Assurance Division

Mr. Walter B. Thomas, III is a Section Head in the Parts Branch, Office of Flight Assurance. He received an MS in Ceramic Engineering from the University of Illinois and had 15 years of experience in industry in electronic materials development, manufacturing, and quality assurance prior to joining GSFC in 1986.

Balloons

OVERPRESSURIZED ZERO-PRESSURE BALLOON SYSTEM

Long-duration, high-altitude balloon flights using zero-pressure scientific balloons require considerable on-board ballast to maintain altitude through diurnal cycles. In turn, the use of ballasting to overcome nighttime heat loss in the lifting gas reduces the amount of payload available for science. Current efforts are directed toward reducing or eliminating the need for significant ballast mass while providing an altitude-stable flight profile through the period of diminished solar load.

The current approach stems from the recent high success rate of NASA's scientific balloon program. New developments in analytical capabilities relating to balloon structural analysis and the development of improved polyethylene films have created the opportunity to enhance the proven zero-pressure balloon. Working failure criteria have been identified for the two flight-qualified balloon films now in use. These criteria, along with finite element structural analysis, have enabled predictions of failure loadings. Initial analyses indicated that the current zero-pressure designs have been flying at float stresses well below safe working levels. In addition, vertical trajectory analyses have shown that enabling the balloons to pressurize beyond normal zero-pressure loading would allow increased performance.

The Overpressurized Zero-Pressure (OZP) balloon concept requires removal of the normal venting ducts that allow excess gas to escape while entering the float phase and when gas heating occurs due to the solar input. These ducts are designed to maintain zero differential pressure at the balloon nadir. By removing these venting ducts the balloon is allowed to pressurize. Heat gain then increases differential pressure instead of causing a loss of gas mass through venting. Similarly, nighttime heat loss results in pressure reduction rather than a reduction in balloon volume, which would result in altitude loss or ballasting. Because of structural limitations, however, a particular balloon system may not be capable of handling pressure loading high enough to completely offset the overnight heat loss. In such cases, altitude loss is postponed relative to normal zero-pressure flights and the nighttime excursion and/or ballasting is reduced.

Two flight systems were selected for studying the feasibility of the OZP application. A small, 2-

million-cubic-foot (mcf) flight system was chosen as the initial test platform. The proven, 28-mcf-class balloon was picked as the first large system to study. Performance analysis showed that for the 2-mcf balloon system, significant ballast savings could be realized with overpressure levels equivalent to apex differential pressures as small as two times the nominal apex differential pressure for the zero-pressure-flight situation. For apex differential pressures of four times the nominal, the analysis showed that nighttime flights without altitude loss would be possible using no ballast. For the 28-mcf class balloon, the initial trajectory analysis indicates that overpressure ratios of as little as three may completely overcome the nighttime heat loss. Finite-element structural analysis of the two balloons, coupled with the temperature-dependent failure criteria, predict failure loading levels that correspond to overpressure ratios of 9 and 5.5 for the 2-mcf balloon and the 28-mcf balloon, respectively. These results suggested that these two OZP designs could be flown with reasonable factors of safety and large performance improvements.

In August of 1990, a test flight of the 2-mcf balloon was flown from Palestine, Texas. An apex valve was employed to vent excess lifting gas during float acquisition and the balloon was then flown for several hours at different levels of pressure, using ballasting to increase the pressure. At the flight's end, ballasting was continued until failure, which occurred at an overpressure ratio of 8.9. The flight was considered very successful and a 24- to 48-hour test flight is planned for fall 1991.

Contact: Joel M. Simpson (Code 842)
(804) 824-1070

Sponsor: Office of Space Science and Applications

Mr. Joel M. Simpson is an Aerospace Engineer in the Balloon Projects Branch at Wallops Flight Facility. He is currently involved in performing balloon structural and performance analysis and in the development of new balloon systems. He received his BS in Aerospace Engineering from the University of Maryland and has been working in the Balloon Branch for 5 years.

BALLOON GONDOLA TERMINATION LOADS

Concerns related to gondola loading experienced during parachute inflation led to the development of a Gondola Diagnostics Package (GDP) to quantify the magnitude and characteristics of these loads. Early data suggested that scientific gondolas were experiencing from 12 to 15 *g* during nominal terminate sequences. These findings stimulated a program to further investigate the cause of these loadings and to explore shock attenuation techniques.

Recent efforts have uncovered inherent problems with the initial instrumentation. Modifications to the GDP, including the incorporation of high-resolution accelerometers with a frequency response several orders of magnitude greater than that of the flight train, have returned measurements that indicate the load levels are approximately half those originally reported. Previous resonant accelerometer data were recovered through the use of a Fast Fourier Transform (FFT) filtering technique; those data support the current analysis.

A termination load-reduction device, the Central Load Core (CLC), has been developed as a result of this work and is schematically represented in the figure. At the onset of flight termination procedures, release of elastic energy stored in the fully deployed, yet uninflated, parachute accelerates the canopy toward the gondola. Slack in the suspension system develops as the payload free-falls and the canopy blossoms. Drag area growth slows the canopy. Slack is taken up and peak loading occurs when the gondola "snaps" the parachute and the associated air mass.

The CLC is an internally adaptive device whose primary function is to minimize the system-stored elastic energy while providing adequate rotational stiffness to prevent shroud-line fouling from twisting. It provides sufficient resistive torque for any gondola positioning requirements. With the development of minimal shroud-line slack, momentum dissipation can

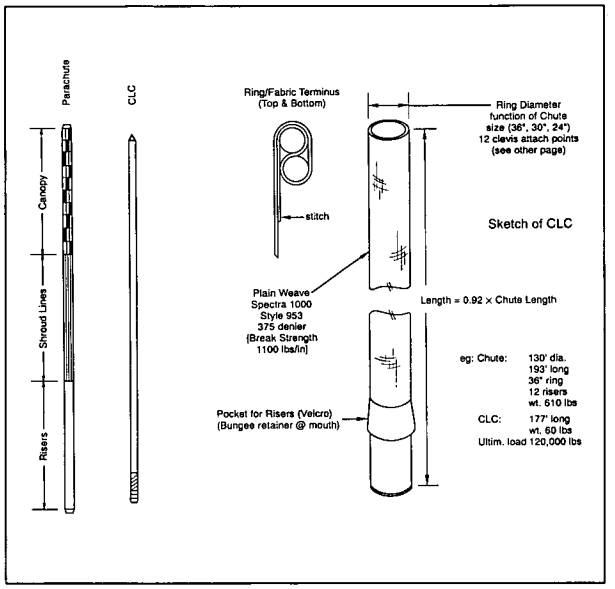

A termination load reduction device, the Central Load Core (CLC).

begin during the early stages of canopy inflation. The canopy skirt expands more rapidly and thereby reduces the total payload kinetic energy to be decelerated. Further, the pliable nylon lines remain active during peak loading since the CLC goes slack as the parachute inflates.

Small- and mid-scale sea-level drop tests show a peak load reduction of about 30 percent, with inflation times reduced to about two-thirds that of the nominal flat-circular configuration. A load reduction of greater than 50 percent is expected at float altitude.

Contact: Edward J. Robbins (Code 842)
(804) 824-1385

Sponsor: Office of Space Science and Applications

Mr. Edward J. Robbins is a BSME graduate of the University of Massachusetts with 21 years of broad mechanical and aerospace engineering experience. He is currently with the Physical Science Laboratory of New Mexico State University and has been supporting the Balloon Branch at Wallops Flight Facility for 4 years.

DRAG CHARACTERISTICS OF FREE BALLOONS

NASA's high-altitude scientific balloon vertical performance model has been enhanced with the addition of a new drag relationship incorporating a Froude number-dependent term. The Froude number is classically defined as the ratio of inertial forces to gravity forces:

$$Fr = v/gD$$

where: v = velocity, g = gravitational acceleration, and D = effective cross-section diameter. The new relationship described here has significantly improved the correlation between predicted ascent trajectories and observed flight data.

Investigations concerning the Froude number-dependency have led to surveys of work relating to buoyant processes on bubbles. These studies have shown that bubbles naturally attain equilibrium Froude numbers independent of the viscous media for Reynolds numbers greater than about 50. Energy dissipated in the wake, when balanced with the energy furnished by the buoyant force, gives an analytical relation for this equilibrium Froude number that agrees remarkably well with experimental results. A similar balance equating the potential due to the "free lift" with the energy dissipated in the turbulent wake was conducted for a typical steady-state balloon system.

The resulting expression for this theoretical equilibrium Froude number covering the balloon buoyant process is:

$$Fr = (5/3)\omega$$

$$\omega = 2 * [1 - (1 + m_s/m_g)/\xi T]$$

where: m_s = system mass (balloon + payload), m_g = lifting gas mass, ξ = air-to-lifting-gas molecular weight ratio, and T = gas-to-air temperature ratio. *Note*: $1/\xi T$ is essentially the gas-to-air density ratio.

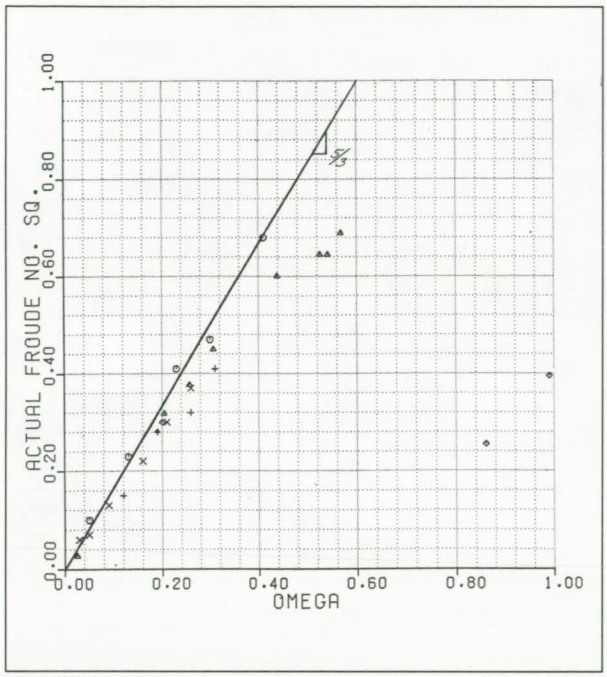

Equilibrium Froude number correlation small- and full-scale data balloon data.

The figure shows this equilibrium Froude number correlation with small- and large-scale balloon data. The deviation from theoretical becomes significant at free lifts greater than 16 percent (typical balloon flights have 10- to 12-percent free lift). At higher free lifts, flexible body oscillations become significant and exponentially dissipate additional energy from this "wave" motion.

Preliminary simulations using this relationship have shown excellent agreement with flight data when the temperature ratios above the tropopause were increased by 4 percent (suggesting possible errors with the temperature data). This relation appears to describe the buoyant process governing balloon systems performance and predicts equilibrium Froude numbers for the entire flight regime. Other retarding effects such as the skin "wave" motion, hypothesized to be related to the balloon tension field, will require additional work to reduce to a usable algorithm.

Contact: Edward J. Robbins (Code 842)
(804) 824-1385

Sponsor: Office of Space Science and Applications

Mr. Edward J. Robbins is a BSME graduate of the University of Massachusetts with 21 years of broad mechanical and aerospace engineering experience. He is currently with the Physical Science Laboratory of New Mexico State University and has been supporting the Balloon Branch at Wallops Flight Facility for 4 years.

Ground Systems, Networks, and Communications

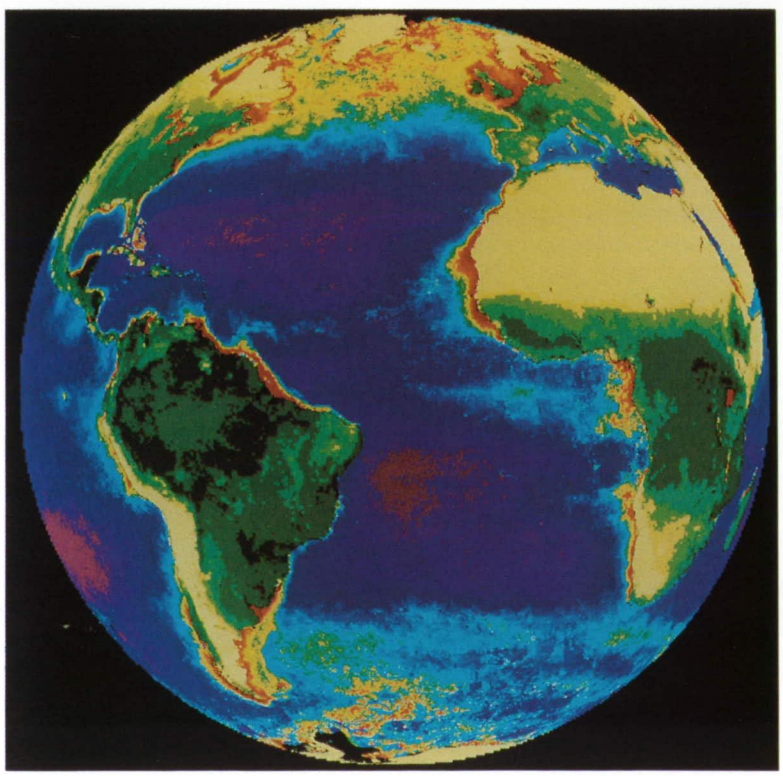

Automated information management is rapidly becoming the major hallmark of our advanced operational systems. As we continue our journey into the Information Era, the need for dealing with increasing amounts of information and the need for understanding the dynamics of information exchanges between humans and computer-based systems required for accomplishing system objectives become more critical. The utilization of advanced hypermedia and multimedia technologies in support of bidirectional information exchanges is taking on added significance.

GROUND SYSTEMS, NETWORKS, AND COMMUNICATIONS

Data and Networks

THE EOSDIS CORE SYSTEM

The Earth Observing System (EOS) includes a space-based measurement system, an Earth Science Research Program, and a Data and Information System (EOSDIS). The EOSDIS Core System (ECS) will provide the flight operations support and primary data handling within the EOSDIS. The ECS will command and control the observatories; transport, process, and store the EOS data; and provide access to the stored data. In addition, the ECS will accept, store, and distribute existing Earth science datasets and data from planned Earth probe missions. Development of the ECS is scheduled to begin in late 1992 upon contract award. Initial operational capabilities for Earth science datasets from pre-EOS sources is scheduled for late 1995. The ECS will build upon experience with Earth science data management and distribution gained from EOSDIS Version 0, a working prototype currently under development, with operational elements based on existing data systems.

Conceptually, the ECS will consist of three functional areas or segments: flight operations, science data processing, and communications and system management. These are further divided into functional elements and distributed across seven major processing sites including the Goddard, Langley and Marshall NASA centers, JPL, the EROS Data Center, the National Snow and Ice Data Center, and the University of Alaska.

The Flight Operations Segment (FOS) of the ECS will control the observatories, provide mission planning and scheduling, and monitor the health and safety of the platforms and instruments. This segment includes the EOS Operations Center (EOC) element at GSFC which will maintain the health and safety of each observatory, support planning and scheduling of platform resources, coordinate instrument observation requests, and validate commands to instruments. Instrument Control

◄ *Above is an artist's depiction of Goddard's Earth Observing System Data and Information System (EOSDIS)--the most ambitious data facility ever planned. Below, Earth-science data products such as this map of the world's ocean chlorophyll concentrations derived from satellite observations will be made available to scientists worldwide.*

Facilities (ICFs) will exist at GSFC and JPL, each comprising Instrument Control Centers (ICCs) to plan and schedule the individual instrument operations and generate appropriate commands. The JPL ICF is outside the ECS contract. The ICFs will also be responsible for instrument health and safety. The Instrument Support Terminal (IST) element is distributed to key investigator facilities to further support instrument management.

The Science Data Processing Segment (SDPS) transforms the raw instrument data into higher level scientific data, and stores and distributes these and other products. Elements within the SDPS include the Product Generation System (PGS), the Data Archive and Distribution System (DADS), and the Information Management System (IMS).

The PGS is the number-crunching element in which the scientific data processing will be performed using software developed based on algorithms provided by the EOS investigators. All instrument data will be processed on a daily production basis. Reprocessing capacity will be provided in anticipation of algorithm refinement as experience is gained with on-orbit data. Scientific data, produced by the PGS, will be stored along with the original input data and supporting information, in the DADS for archival and distribution to users. The DADS will be capable of initiating data transfers to users within minutes of a request. The DADS will also accept and store non-EOS datasets as required by the Earth science community. The IMS will provide information about all data available from the ECS, allowing users to search for and order data via a one-stop-shopping approach.

Techniques for effectively browsing and cross-referencing the vast collection of Earth science and EOS data products under ECS must evolve in accordance with user experience. The system development approach is designed to facilitate this through early prototyping, intensive user involvement in the design process, and modularity of user-related functions. The PGS, DADS, and IMS elements of the ECS will be distributed to the seven sites mentioned above, where they will be integrated into local Distributed Active Archive Centers (DAACs). The DAACs will provide additional, discipline-unique services related to the data products generated and stored at the respective sites.

The Communications and System Management Segment (CSMS) consists of two elements: the EOSDIS Science Network (ESN) which distributes data among the DAAC sites and to users over NASA-provided circuits; and the System Management Center (SMC) which provides on-line system status of all ECS elements, configuration and performance management, high-level ECS scheduling, monitoring, and accounting, security management, and user authorization and billing. The NASA Science Internet (NSI) will be used to provide connectivity between the DAACs and the Earth science user community in general.

Several key factors have influenced both the requirements and the development strategy for the ECS. The scale and complexity of the ECS, unprecedented in NASA data systems development, is driven by the sheer volume of data to be handled: input rates upward of 20 Mbps, hundreds of distinct scientific data products to be generated and regenerated daily, storage and rapid access to multiple petabytes (1000 terabytes) of data for 15 years or longer. The ECS must maximize the scientific return on this major data investment by providing efficient, uniform methods of access, synergistic approaches to searching and cross-referencing thousands of interdisciplinary datasets, and efficient, dependable distribution of the data once identified and selected. These goals will be achieved through an incremental, evolutionary approach to development that allows for continual refinement based on actual user experience.

Another factor is the anticipated life of the system. Since technology is expected to advance significantly over the next 10 to 15 years, the ECS architecture must be designed to evolve accordingly. Scientific

data-processing techniques can also be expected to evolve, thus the ECS must be expandable to accommodate processing growth and flexible enough to permit design changes in the algorithms. Because the scientific processing algorithms will be developed on Scientific Computing Facilities (SCFs) and migrated into the ECS for production operations, the ECS must provide a common, vendor-independent environment to ensure portability.

The ECS, while posing both technical and managerial challenges in data systems development, provides an unprecedented opportunity to unify and improve access to existing Earth science data, to effectively manage the tremendous influx of new data anticipated over the next decade, and to provide a coordinated systems approach in reacting to changing Earth science data needs and in infusing new technology as it becomes available.

Contact: Melvin D. Banks, Jr. (Code 502.2)
(301) 286-4237

Sponsor: Office of Space Communications

Mr. Melvin Banks, Jr. heads the EOSDIS Branch within GSFC's Mission Operations and Data Systems Directorate. He has over 20 years of experience developing spacecraft data processing and analysis systems for support of such missions as Landsat, ISEE, UARS, ISTP, and others. He holds a BS in Electrical Engineering from the University of Maryland.

GSFC INSTALLS GIGABIT NETWORK FOR CAMPUS SCIENTISTS

The NASA Center for Computational Sciences (NCCS) is currently installing the country's first gigabit-per-second, campus-wide computer network, using commercially available, off-the-shelf products. The NCCS acquired the network components from ULTRANET Technologies, Inc. by exercising an option in its contract for the CRAY YMP supercomputer. The GSFC ULTRAnet is designed to provide local scientists with high-speed network access to the resources of the NCCS. These resources consist of a supercomputer, a mini-supercomputer, IBM and DEC mainframe and mini-computers, and a massively parallel computing system. The computing complex is to be augmented with a mass data storage and delivery system that will store up to 225 terabytes of data, and a future-generation massively parallel computing system. Using the ULTRAnet, scientists at GSFC will have access to these computing facilities and a large-scale science data repository from their desktop workstations at up to gigabit-per-second data rates, which will enable them to perform the scientific modeling studies for Earth and space science on the computing platform best suited for their work. They can receive visualization displays at their workstations, thus giving them the capability for real-time interaction with computer simulations on supercomputing or massively parallel processing facilities.

The ULTRAnet consists of a set of hubs placed in the science buildings at GSFC and connected by fiber-optic cables. Science workstations, mainframes, and supercomputers are connected to these hubs by means of special electronic interface cards. The combination of special interface cards and software on the network computers allows for the maximum network data transfer rates. Actual transfer rates depend on the power and architecture of a particular workstation or computer. For example, observed data transfer rates for the CRAY YMP were over 600 Mbps, as compared to 24 Mbps for workstations. For workstations or laboratory minicomputers not directly connected to the ULTRAnet hubs, there are special network routers installed in the science buildings that can provide either dedicated Ethernet connectivity through the ULTRAnet system of up to 10 Mbps or with the emerging Fiber Data Distribution Interface (FDDI) up to 100 Mbps. User access to ULTRAnet is via the widely used TCP/IP

protocol that is available on workstations, minis, mainframes, and supercomputers. In addition to the standard TCP/IP protocol suite, there is special graphics software available for a frame buffer output device that enables a NCCS supercomputer to directly drive remotely animated displays of scientific modeling computations as they are carried out on the supercomputer.

Plans call for the expansion of the network to some of the engineering buildings on campus and a massive upgrade in the number of connected workstations. The GSFC ULTRAnet will be connected to the National Science Foundation

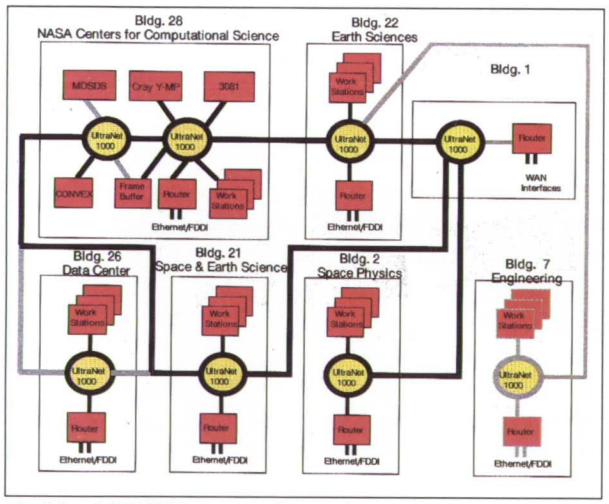

Goddard ULTRAnet configuration.

NSFNET with a 45-Mbps link in the near future, and to the National Research and Education Network (NREN) at gigabit-per-second rates when this network becomes operational. This connectivity will provide non-GSFC-resident scientists access to the NCCS at bandwidths comparable to those available to local researchers.

Contact: Herb Durbeck (Code 931)
(301) 286-8243

Sponsor: Office of Space Science and Applications

Mr. Herb Durbeck is a Systems Analyst with the NASA Center for Computational Sciences with over 25 years of experience in the area of large-scale scientific computing. His undergraduate and graduate training was in physics and computer science. He is currently the Project Manager for GSFC's ULTRAnet.

INTELLIGENT GROUND SYSTEM

The Intelligent Ground System (IGS) project examines how knowledge-based system use can achieve higher levels of autonomous activities in command and control systems for ground-based control centers. The immediate objective is to extend the state-of-the-practice of introducing single expert systems into operations to a more comprehensive system that involves many expert systems that communicate and cooperate with each other.

The technical focus of the project has been the development of a four-layer model, the Cooperating Knowledge-Based System (CKBS) model, which defines communication and cooperation mechanisms between intelligent agents. These agents represent expert systems and other AI-based systems that interact and conform to predefined communication protocols defined by the model. Because operational introduction of multiple expert systems has the potential for increasing the number of monitored items, the project examines techniques for reducing the information presented to users at any one time. The project is developing a testbed focusing on the EOS spacecraft to test these concepts.

The testbed currently consists of three expert system prototypes: the Communications Expert Assistance Resource (CLEAR), adapted from an operational COBE communications fault diagnostic system; a power expert system; and a HIRIS instrument expert system. The testbed incorporates a spacecraft simulator written in C++ and is designed to be easily

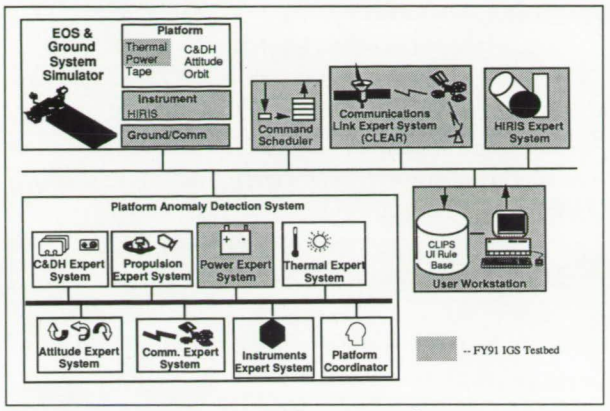

The IGS testbed in an EOS spacecraft context.

configured to simulate other spacecraft and to build new components. The current EOS spacecraft simulator includes components for simulating the power, thermal, HIRIS, and communications subsystems. The simulator feeds data to the expert systems and user interface. The expert systems monitor and diagnose problems, provide explanation and advice to the user interface, and post suggested fixes with a command scheduler. The user interface depicts a graphical hierarchy of the spacecraft and ground components. The user can zoom into lower levels of detail when a problem is detected. A rule-based front-end to the user interface filters and synthesizes related fault warnings to reduce information overload. A publication/subscription service, implemented on top of a transportable communications package called the Open System for Coordinating Autonomous Resources (OSCAR), ties each of the components together. Using the service, agents specify which data items they will receive or provide during run-time. This run-time configurability allows easy modification to agent configuration and movement of agents between host machines.

A major project objective is to develop a Platform Anomaly Detection System (PADS) for EOS. PADS is a fault-detection, isolation, and recovery system covering the various platform subsystems (power, thermal, command and data handling, communications, attitude and control, and instruments). PADS will support EOS platform integration and testing and post-launch operations. Plans call for developing an infrastructure to support multiple diagnostic subsystems with one or more in-depth knowledge bases, to be delivered for operational use. Additional subsystems may be added as resources permit.

Contact: Robert E. Dominy (Code 522.3)
(301) 286-4196

Sponsor: Office of Aeronautics and Space Technology

Mr. Robert E. Dominy of the Automation Technology Section develops technology for distributed knowledge-based systems. The technical areas that interest him most are artificial intelligence and machine learning. He earned a BA in Computer Science from the University of Tennessee and has 6 years of experience at GSFC. He has received a Goddard Group Achievement Award.

IPD DATA DISTRIBUTION FACILITY

The Information Processing Division (IPD) is developing a Data Distribution Facility (DDF) for consolidating most of its data distribution and delivery functions. The DDF will allow IPD to move from unique and mission-specific facilities and procedures to a more effective and unified method for the assembly and distribution of output products. DDF will also provide more services, such as optical and electronic distribution of data in addition to traditional magnetic-tape distribution.

The DDF is being developed in three phases. Phase I is now being completed and will provide magnetic-tape distributions for the International Solar-Terrestrial Physics (ISTP) program's Geotail mission. This work will serve as a prototype for further development. During Phase II, the DDF will be enhanced with additional operational and error handling features and support for one other

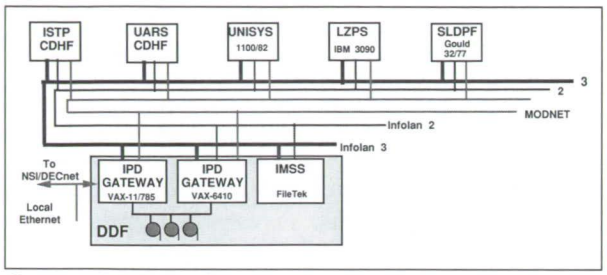

Current DDF configuration and interfaces.

distribution medium (probably CD-ROM), and its capacity will be increased to support the ISTP Wind and Polar missions. During Phase III, the DDF will incorporate the latest technologies and standards to provide an integrated and flexible system for supporting multiple missions with a range of physical and electronic distribution capabilities, while also greatly reducing the level of manual operation required. Additional missions to be supported during this phase include the Tropical Rainfall Measuring Mission (TRMM), the Fast Snapshot Explorer (FAST), ISTP's SOHO, and Small Explorer Missions (SMEX).

In developing the DDF, IPD is taking full advantage of several capabilities developed over the last few years. Data are transferred from IPD's data capture and processing facilities to the DDF over the IPD Local Area Network (InfoLAN), a HYPERchannel network with a bandwidth of 50 Mbps. The software for supporting DDF capabilities resides on the IPD Gateway Computer System. This system provides access to other networks, such as the NASA Science Internet (NSI), a wide-area network serving science users throughout the world, and has successfully supported electronic access to data for recent missions, including COBE, BBXRT, and NOAA-9. The DDF utilizes the InfoLAN Mass Storage System (IMSS) to store the data until they are needed for distribution. The current IMSS utilizes optical storage technologies to provide an efficient and compact method of storing a large volume of data so that they can easily be accessed for further processing or distribution. The major DDF accomplishments for FY91 include:

- Procured and installed a VAX 6000-410 to augment available computing power (see first figure for current DDF configuration/interfaces.)
- Procured and installed the ORACLE Relational Database Management System.
- Completed Phase I software system implementation
- Released solicitation for procuring a Phase II data recording subsystem with options for Phase III.
- Conducted feasibility studies for Phase III, documented the results in reports and presented them at an IPD Project Approval Review (see second figure for expected DDF configuration).
- Analyzed and documented expected InfoLAN load to ensure capacity to meet upcoming requirements.

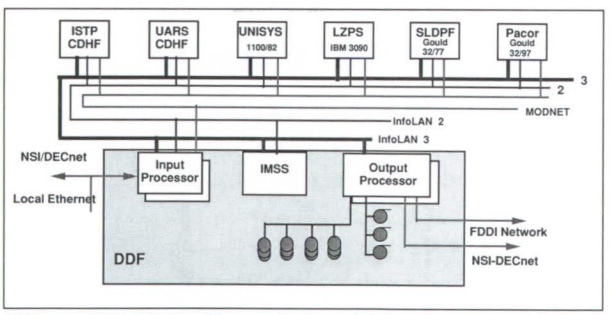

Planned DDF configuration and interfaces.

We expect that the centralization of the distribution function within the IPD will provide cost savings in terms of operations and development. The centralization of this function will also be beneficial in focusing the security problems associated with external interfaces with users into a single facility. Additional benefits will also accrue from the promotion of the use of standard output products, the

Since she came to GSFC in 1978, she has been developing systems that give scientists access to data collected by NASA.

Ed Vaughan is responsible for system engineering for the Data Distribution Facility. He received a BA in Mathematics from the University of Iowa and an MS from The Johns Hopkins University. Since he joined GSFC in 1966, he has been responsible for systems programming and other support for missions such as Atmospheric Explorer, Dynamic Explorer, HEAO-A, HCMM, Nimbus, COBE, and ISTP.

Jeannine Shirley is responsible for software development for the Data Distribution Facility. She received a BS in Mathematics from Bowie State University. Since she came to GSFC as a cooperative student in 1984, she has been developing systems for operations support of various missions used for data collection and transmission.

TRANSITION TO A STATE-OF-THE-ART SYSTEM ARCHITECTURE IN THE FLIGHT DYNAMICS ENVIRONMENT

The Flight Dynamics Division (FDD) has undertaken a project to develop a highly generalized attitude and mission planning system known as the Combined Operational Mission Planning and Attitude Support System (COMPASS). The project's primary objective is to minimize mission-specific support costs while retaining the flexibility necessary to meet the division's institutional requirements for the next 30 years.

The COMPASS approach is to completely separate the software that implements application functions from the software that provides a common computational environment. The latter software, known as the User Interface/Executive (UIX), is required to provide a standardized set of service interfaces (communications, data access, etc.) and a single, common, state-of-the-art user interface (UI) across a heterogeneous network of computers. The current FDD computer environment includes IBM 370 architecture Multiple Virtual Storage/Extended Architecture mainframes, DEC Virtual Memory System minicomputers, Silicon Graphics Unix workstations, and IBM Personal Computer (PC)-compatible Disk Operating System (DOS) microcomputers. To meet these requirements while still satisfying the overall COMPASS goals, the UIX has been designed to achieve the following primary objectives:

- Provide a networked computational environment with a standard set of platform services across all FDD platforms.
- Incorporate state-of-the-art user-interface technology in a standardized, consistent manner to reduce complexity of application system use.
- Produce reconfigurable UIX software that can be reused for all missions without source code modifications.
- Allow for transition to future hardware and software technology with minimal impact to COMPASS software.

The first objective stipulates a computer environment whereby application software can be platform-independent and can access data from or communicate with other application software that resides on any other FDD platform. To achieve this objective, a networked computer environment based on industry standard protocols has been specified (see the first figure). These standard protocols provide an open systems architecture. Additional customized application programming interfaces (APIs) are included. These APIs provide both higher level access to industry standard protocols and additional functionality specific to the FDD environment.

The second objective requires the transition from current FDD user interface technology, based primarily on device-dependent alphanumeric systems, to device-independent, state-of-the-art windowing capabilities. Currently, the FDD provides only general-purpose text and x-y plot packages that are embedded into an application program and must be

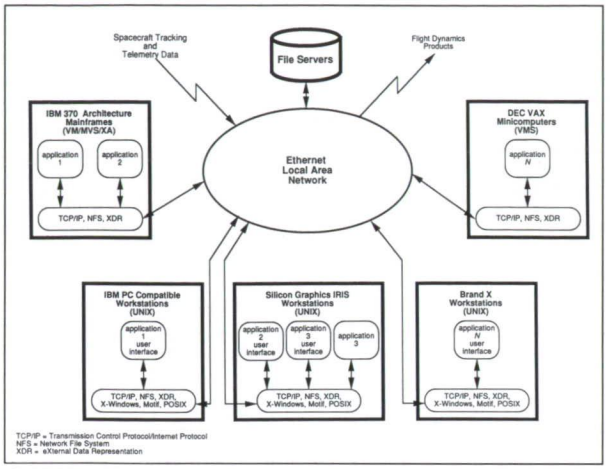

COMPASS UIX system architecture.

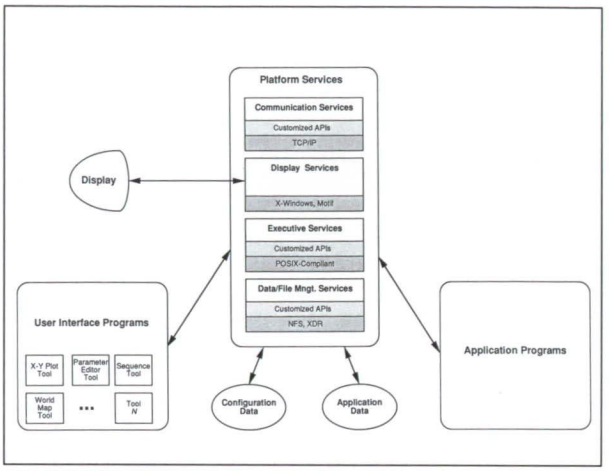

COMPASS UIX software architecture.

developed for a particular look and feel. These packages differ with each FDD computer platform due to limitations of that platform's environment, and the idiosyncrasies of its operating system. Therefore, the look and feel of user interfaces can and do vary for each application. To incorporate the latest in UI technology, and to do so in a consistent manner for all applications across all platforms, the UIX design requires that all user interfaces must reside in processes separate from the application programs, and that these processes must execute on workstations (see the second figure). A set of user interface tools, specific to the FDD environment, are provided in these processes. Each tool performs a specific function such as x-y plotting, parameter editing, and display sequencing among others. The tools can be configured to meet the specific needs of each application, but in a manner that does not change the overall look and feel.

The third objective requires the ability to reconfigure the user interface, without software modifications, to meet the requirements of different missions. The design of the UIX tools is based on a three-step configuration process. The first step requires the specification of data tokens that define the data stream by which application data are transmitted between the application process and the user interface process. The second step requires the association of the data tokens to a specific tool and the configuration of the tool itself to support that data. The final configuration mechanism requires the association of these configured tools with each interactive point in the application program. All of these configuration steps are achieved through user-modified parameter files.

The final objective of the UIX system is to allow the incorporation of future technology, in the area of new workstations, high-speed file servers, upgraded graphics adapters, etc. with minimal or no software modifications to any user interface or application software. The design approach of using an open systems architecture, combined with using commercial-off-the-shelf software whenever feasible and producing standardized higher level FDD APIs, is expected to allow such a goal to be achievable. In addition, the placement of all UI processes on workstations permits the use of current FDD resources, specifically IBM-compatible PCs, to be upgraded to POSIX-compliant workstations that can still execute all existing DOS applications. Therefore, the initial transition to this overall architecture will not impact current operations.

Over the past year, a prototyping effort has been conducted to verify that this architecture can achieve the goals and requirements of COMPASS and its UIX software. The effort has been focused on developing a mini-UIX system to provide platform

services and a reusable user interface that will be reconfigured to support sample attitude and mission planning applications. Specifically, a Coarse and Fine Attitude Determination System (CFADS) and a station-contact prediction system are being modified and created, respectively, to test this architecture. The selection of these two applications provides the means to verify both a distributed and nondistributed user interface. In the case of CFADS, the application process resides on a mainframe and the user interface process resides on a workstation demonstrating a distributed user interface. In the case of the station-contact prediction system, both processes reside on the workstation, demonstrating a nondistributed user interface. The selection of this particular mission planning application was also made for its ability to verify other COMPASS concepts, such as standardized, object-oriented specifications.

To date, an ongoing evaluation of the prototype has verified many areas of the architecture that meet all requirements (e.g., windowing technology), identified areas that require more work (e.g., specifications concepts), and has pointed out technology that is not yet mature enough to support operational software in the FDD environment (e.g., Network File System). The prototyping effort and subsequent evaluations will continue throughout the development of UIX software to verify the effectiveness of new designs and technology in meeting COMPASS requirements. The first release of the UIX system is scheduled for December 1993.

Contact: James F. Jeletic (Code 552)
(301) 286-4244

Gregory W. Shirah (Code 552)
(301) 286-7999

Sponsor: Office of Space Communications

Mr. James F. Jeletic researches, develops, manages, and analyzes the flight dynamics computer-graphics systems and other mission support software in the Advanced Technology Section. He holds a BSE in Computer Science and Engineering from the University of Pennsylvania and has 7 years of experience at GSFC.

Mr. Gregory W. Shirah holds BS degrees in both Computer Science and Mathematics from the University of Georgia. He researches, develops and analyzes flight dynamics computer-graphics systems and has 7 years of experience at GSFC.

GROUND OPERATIONS TECHNOLOGY TESTBED

The number of new technologies that can be applied to ground systems has grown steadily over the last few years. Deciding which of these technologies best meet the needs of future ground systems is a difficult and costly task. Furthermore, inappropriate use of technologies can jeopardize mission success and increase maintenance costs. To help address these issues, the Data Systems Technology Division (Code 520) is developing the Ground Operations Technology Testbed (GOTT).

The GOTT provides a testbed environment that supports rapid exploration and demonstration of technologies in a realistic, but nonoperational environment. For technologies that seem promising, the GOTT provides a laboratory environment where technologies can be formally analyzed in a controlled setting. As a testbed, the GOTT helps technologists quickly integrate their projects into a ground system context. It provides a means to show the effects, both internal and external, that the technology has on the ground system, and provides a means to control the technology and ground system to generate meaningful demonstrations and tests. As a laboratory, GOTT helps technologists control and monitor environment variables, and supports the unobtrusive measurement of human, software and hardware performance. GOTT also provides a means to record, order, retrieve, and analyze performance measurements from distributed, heterogeneous sources.

In 1991, GOTT project personnel established the infrastructure and tools needed to support GOTT's testbed and laboratory capabilities. The infrastructure includes Code 510's Transportable Payload Operations Control Center (TPOCC) software, system and software instrumentation tools, a performance data management system called the Event Manager (EM), and a toolbox of distributed system services. The tools include a prototype spacecraft simulator, the performance monitor workstation, the observer workstation, and the controller workstation. The figure illustrates the current architecture of GOTT.

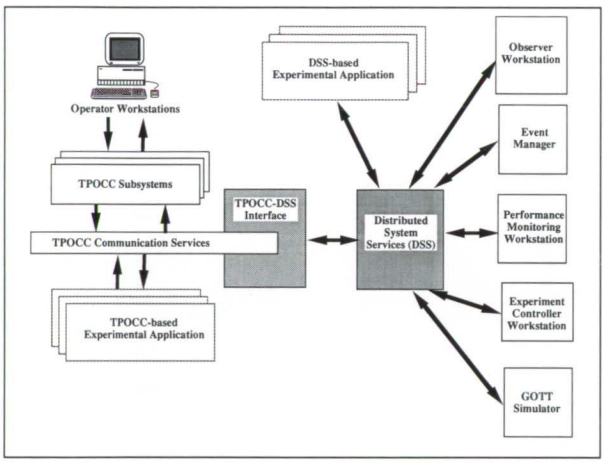

Ground Operations Technology Testbed architecture.

The TPOCC software has been and will be used for a number of NASA missions; it provides a realistic context for technology exploration. The version of TPOCC used in GOTT provides all standard TPOCC interfaces. This is critical to TPOCC-specific technologies. In addition, this version has been instrumented to support performance analysis and has been enhanced with a set of on-line documents that describe each TPOCC subsystem in terms of purpose, code structure, and interfaces. The most common TPOCC-technology interfaces have been abstracted into a set of reusable C++ classes so that technologists can quickly integrate their projects with TPOCC. The on-line documentation and reusable TPOCC interfaces permit technologists to integrate their tools without searching TPOCC code.

The EM collects, time-orders, and stores instrumentation results from TPOCC, new technology components, and GOTT measurement tools. The EM delivers these results to other GOTT tools in both real-time and off-line modes. To correctly time-order the results from multiple, distributed components, the EM provides a distributed clock-offset-determination algorithm. Results are time-stamped at their origin; subsequently, the time stamp is corrected based on the originating host's offset.

The performance monitor workstation helps visualize real-time system performance by providing information about the system from several points of view: operator, software, and hardware. The operator view shows the actions of the control center operator, including keystrokes, display manipulation, and mouse activity. The tool is based on the XTrap X-Windows extension. The software view shows the end-to-end throughput between selected subsystems and is based on the TPOCC instrumentation services. In the future, the software view will incorporate data from several Unix performance tools. The hardware view is not currently supported.

The Observer Workstation helps measure operator behavior. Many operator behaviors are difficult to measure because they occur outside the system's hardware and software (e.g., a conversation between two operators). The Observer Workstation allows a user to record these activities through free-form text and then log these notes with the EM. The EM time-orders the notes with other results, establishing the context for each note and activity.

The Controller Workstation is used to remotely control the system's components. Eventually, the Controller Workstation will support the introduction of commands and failures in system simulators, software, and hardware. At present, only simulator commands and failures are supported. Failures may be scripted before and played during an experiment or demonstration. Scripting is useful for creating interesting demonstrations and repeatable experiments.

Contact: Mike Moore (Code 522.1)
(301) 286-3192

Sponsor: Office of Space Communications

Mike Moore has been with GSFC for the past year. He is currently the technical lead and Project Manager for the GOTT project. He also is leading a study on intelligent information systems. Prior to joining GSFC, Mike worked as a contractor on several advanced ground system technology projects for GSFC.

INTELLIGENT DATA MANAGEMENT

The NASA Intelligent Data Management (IDM) Project conducts research to develop data management systems to handle the archiving and querying of data produced by Earth and space missions. Several unique challenges drive the design of these systems, including the volume of the data, the use and interpretation of the data's temporal, spatial, and spectral components, the number of users, and the desire for fast response times. The IDM group has implemented a prototype Intelligent Information Fusion System (IIFS) to test storage of and access to terabyte-sized spatial databases. Although databases such as these are common throughout NASA, the infrastructure for querying them is primitive.

Systems like IIFS will provide scientists more time to analyze their data since they can locate and retrieve data faster and more accurately than before. In previous years, the IDM research group has concentrated on advancing methods to automatically characterize features in remotely sensed satellite imagery and to use this information to construct metadatabases, which are fast-indexing schemes into the data repositories. This past year's research continued in these areas and also expanded into integrating the various modules into a fully working distributed IIFS. IDM is also investigating the design of a planning and scheduling system to ingest and

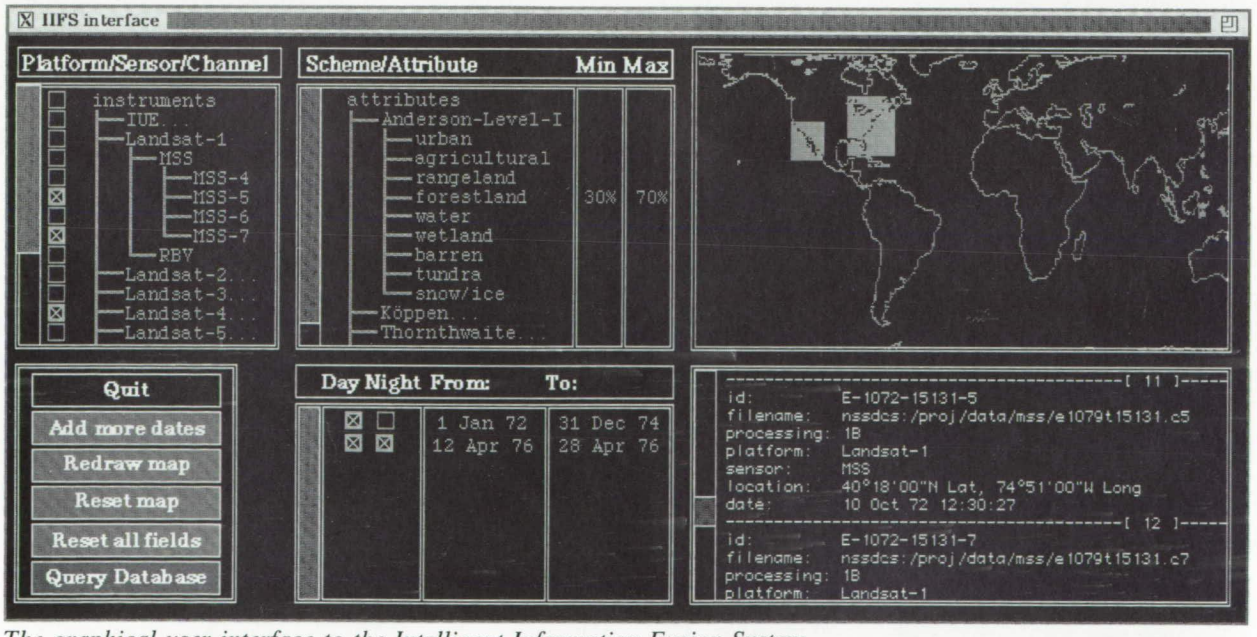

The graphical user interface to the Intelligent Information Fusion System.

characterize data as they are acquired in real-time from a mission.

The graphical user interface to the IIFS is shown in the first figure. A user is able to construct a query by choosing any combination of satellites/platforms/ sensors, features within images, times of observations, and locations around the globe. All that occurs next is transparent to the user. The query is sent to the machine where the object-oriented metadatabase resides. The metadatabase is queried, its indices are rapidly traversed, and the file names and locations in storage of the images that satisfy the query are discovered. This information is transmitted back to the user's machine and the metadata are displayed. If the user desires, choosing any of the returned file names causes the accompanying image data to be retrieved and displayed.

The overall architecture of the system is presented in the second figure. The IIFS design is novel in a number of areas. Whereas it is impossible to search the raw datasets for every query due to the mammoth size of the repositories, it is feasible to pass queries through a metadatabase which serves as a catalog to the data in these terabyte-sized spatial databases. The metadata about the underlying images that potentially satisfy the user's query are supplied to the user who can then construct a private knowledge base that contains the identified images. This smaller, spatial database can then be managed and processed at the user's site with conventional technologies and local machines. This frees the central data management facility to perform only high-level data processing requests to locate datasets. Users are responsible for using their own machinery for the more intensive data analysis computations.

A combination of neural networks and expert systems defines how metadata are extracted to build up search indices to the underlying database. Neural networks transform signal data into symbolic features, such as using sensor readings to derive a land-use category. A domain-specific expert system can verify the characterization of the network and tag it with a degree of certainty. The objective is to construct an IIFS that can keep pace with the high data rates

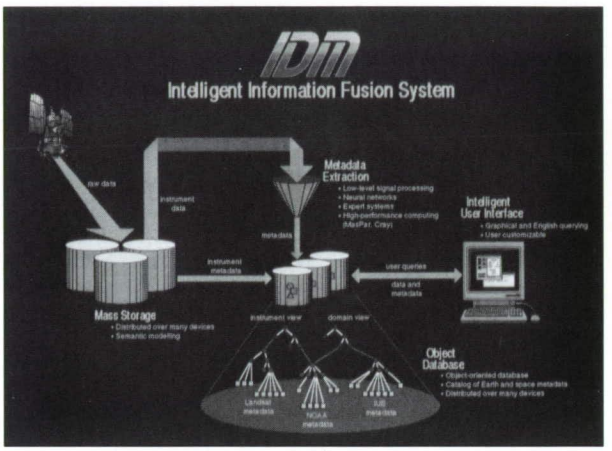

The overall architecture of a distributed Intelligent Information Fusion System.

projected for the Earth Observing System. The IDM group is exploring the feasibility of this approach in its current research on real-time planning and scheduling.

The metadata are organized in an object-oriented database that has special data structures for representing the multiple views of the data (such as temporal, spatial, spectral, project, sensor) without resorting to redundant copies of information. A spherical quadtree (a special data structure that maps directly between the Earth and a sphere) organizes the data for efficient spatial querying. Enhancements to this data structure permit searches for images of differing extents and resolutions. The user interface is configured dynamically at run-time depending on the scientist's discipline and the current knowledge in the metadatabase. As designed, the user interface is run on the user's machine with network communications necessary only for transmitting the formed query and receiving the query results. Once the query is formed, it is sent to the pertinent domain metadatabases which can be distributed throughout the scientific community. The IIFS combines the results and returns the metadata to the user's interface.

Contributors to this work include Nicholas Short (Code 934) and Samir Chettri and Erik Dorfman of Hughes-STX Corporation.

Contact: Robert F. Cromp (Code 934)
(301) 286-4351

William J. Campbell (Code 934)
(301) 286-8785

Sponsor: Office of Aeronautics and Space Technology

Dr. Robert F. Cromp is the Principal Investigator of the Intelligent Data Management project at the National Space Science Data Center. He earned his PhD in Computer Science from Arizona State University, specializing in artificial intelligence. He has 2 years of service at GSFC and has received an Outstanding Performance award and both a best paper and honorable mention award for work related to this research.

William J. Campbell was the former Principal Investigator of the Intelligent Data Management project and is currently Head of the Data Management Systems Facility. He has 12 years of service at GSFC and has received several Director's Discretionary Fund awards, three Outstanding Achievement awards, two Special Achievement awards, and several Special Service Awards. He also received a best paper award. He earned his MS in physical geography from Southern Illinois University.

ADVANCED ORBITING SYSTEMS FRONT-END SYSTEM

The Advanced Orbiting Systems Front-End System (AFES) is a prototype system that will demonstrate the front-end functions required for high-rate processing for missions based on recommendations generated by the Consultative Committee on Space Data Systems (CCSDS). Specifically, the AFES will focus on the core return- and forward-link services defined by these standards. In addition, the system will be part of a larger effort in which prototypes in a testbed environment will help determine the end-to-end functions needed to support the space-to-ground link, including space-flight systems, ground data-processing systems, and ground communications networks. The AFES will provide a realistic, low-cost environment for identifying and evaluating the technical challenges and processing bottlenecks involved in performing these front-end functions.

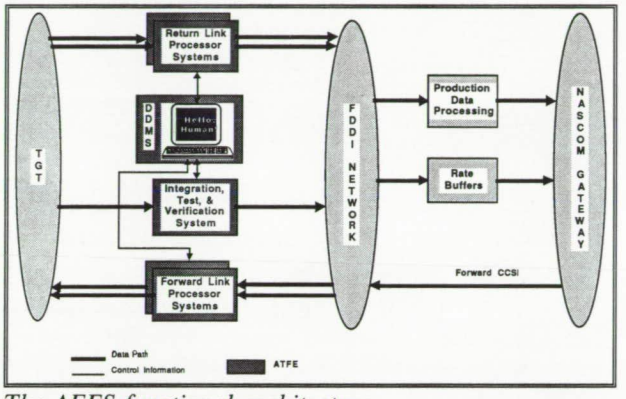

The AFES functional architecture.

The AFES will provide a generic front-end system capable of transporting return- and forward-link CCSDS-formatted data to and from the TDRSS Ground Terminal (TGT) and a commercial communications network. In the return-link direction (from the spacecraft to the ground), spacecraft data are input to the AFES after demodulation and bit-synchronization. The AFES then synchronizes with the data stream, corrects errors in the data introduced by the noisy transmission path, and extracts or demultiplexes user packages of information (packets) from the data stream. The extracted packets are then routed onto commercially available networks using standard protocols and sent to the end-user. In the forward-link direction (from the ground to the spacecraft), commands are packaged in packets (or other recommended CCSDS formats), and routed from the end-user to the AFES over the commercial network. The AFES accepts the packets, reformats the data if necessary, and transmits the data to the spacecraft via the TGT.

Current work on the AFES focuses on developing standard hardware and software modules. These

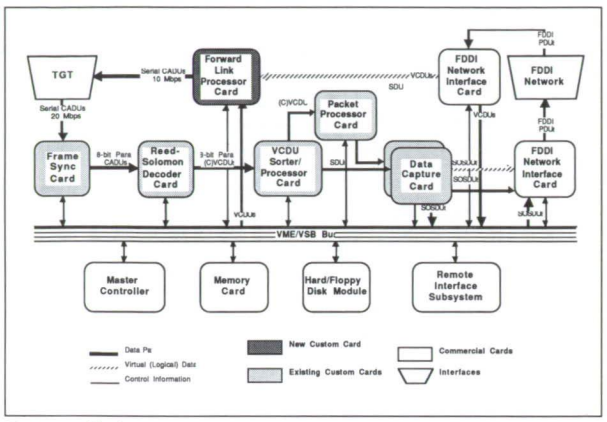

Return-link processor system.

modules can be used in a ground-processing system to perform the necessary functions recommended in the CCSDS standards. Included in the AFES are boards that provide standard frame synchronization functions, Reed-Solomon error correction, virtual channel sorting of data based on spacecraft configuration, packet extraction, and routing via either a commercially available Ethernet or FDDI network. The entire system is compact and may be housed in a single, 20-slot, VME-based card cage. The first phase of the AFES system, which will be processing, functions at rates up to 20 Mbps and is capable of performing both return- and forward-link processing. It is scheduled for completion in February 1992. The second phase of the AFES, capable of operation at rates of over 150 Mbps, is scheduled for completion in January 1993.

Contact: Nicholas Speciale (Code 521.2)
(301) 286-8704

Sarah Hand (Code 521.2)
(301) 286-3912

Sponsor: Office of Space Communications

Mr. Nicholas Speciale is head of the Systems Application Section, Code 521.2, and is responsible for taking developed technology into operational systems. He received his BS in Electrical Engineering from Manhattan College, NY and his MS in Electrical Engineering from The Johns Hopkins University.

Ms. Sarah Hand received her BS in Electrical Engineering from the University of Maryland and her MS from The Johns Hopkins University. She led the development of the Virtual Channel Sorter Multiplexer System from which the AFES derives its heritage.

NEXT-GENERATION FUNCTIONAL COMPONENTS FOR SPACE DATA COMMUNICATIONS

Currently, many NASA flight and ground data communication systems are developed uniquely on a project-by-project basis. Project duration and resource constraints often limit system development to meet only the requirements of a specific mission. These project-oriented data systems often lack the flexibility and generic capability to be reused in subsequent missions leading to very high recurring costs for telemetry data system development and maintenance. As budgets tighten and demand for space data increases, a growing number of projects are seeking lower cost alternatives to past development methodologies.

In an effort to lower data system development costs, the MO&DSD Data Systems Technology Division (DSTD) has been developing a set of generic, reusable components for space data communication systems. These components, referred to as *functional components*, rely on very large-scale integration (VLSI) microelectronics technology to create compact, low-cost implementations of commonly used space communication functions. Fourteen different standard, open-bus components are currently available for modular data system development. These include such functions as frame synchronization, Reed-Solomon error correction, and packet processing. The functional components have already been used to create low-cost ground telemetry data systems for such NASA projects as the Topographical Explorer (TOPEX), Small Explorer (SMEX), and the Deep Space Network (DSN). These new data systems are an order of magnitude

greater in performance, compactness, and cost effectiveness over previous-generation systems.

Recent advances in integrated circuit densities and design automation tools have yielded the means to achieve yet another leap in the performance, cost-reduction, and compactness of space data systems. The DSTD is currently applying state-of-the-art VLSI design and manufacturing technology to create the first in a series of next-generation functional components: a single-card return-link telemetry processor. This next-generation component integrates the functionality of three current functional components while increasing performance and decreasing manufacturing costs. The card is targeted towards system implementations based on recommendations by the CCSDS. A functional diagram of the CCSDS Return-Link Processor card showing its constituent VLSI devices is shown in the figure.

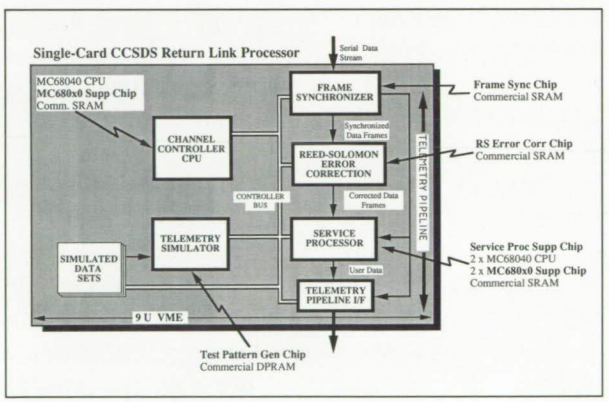

CCSDS return-link processor card.

The card is functionally separated into a controller CPU module, a telemetry simulator module, and a pipeline of telemetry processing modules. The telemetry processing modules consist of the frame synchronizer, Reed-Solomon decoder, and service processor modules. Each module affords a high degree of programmability to meet the requirements of many different missions.

The controller CPU module is used to configure and monitor the operation of each of the other processing modules. Prior to receiving downlink telemetry data, the controller CPU downloads parameters that configure each module for a particular spacecraft's data format. During processing, the controller CPU monitors each module and periodically reports status to higher level system processing elements. The telemetry simulator module is used with the controller CPU to perform diagnostic testing of the card prior to operation.

The frame synchronizer module receives space data serially (i.e., bit by bit). For the receiving system to make any sense of the incoming stream, the receiver must be synchronized to the data stream's frame structure. The frame synchronizer module determines the stream's frame boundaries and converts the data into a parallel format that is more convenient to process.

The Reed-Solomon decoder module is used to detect and correct transmission-induced errors. When data are transmitted through space, they are susceptible to random errors caused by natural and man-made phenomena. Error correction codes are often applied to data prior to space transmission to allow ground equipment to detect and correct the errors. The decoder module, based upon the CCSDS's recommended Reed-Solomon code, is one of the most powerful error-correction decoders implemented to date.

The service processor module accepts framed data units and routes embedded data to downline data users. For CCSDS-based protocols, received frame data units can contain a mix of data from any source on the spacecraft. Because different data users may only be interested in receiving data from a particular set of sources, the service processor module must separate incoming data by source and route it to its appropriate destination. The service processor module also checks the sequence of data to ensure that no data are lost.

To achieve the higher integration levels required for the CCSDS Return-Link Processor card, the telemetry processing modules will be created using very high density integrated circuits, compact CPUs, and memory elements. Current effort centers on the

C-3

development of the integrated circuits using a new software automated design technique based upon the VHSIC Hardware Description Language (VHDL).

The complexity of the integrated circuits currently being developed is much higher than of those previously used in functional components. Achieving these higher complexities with a conventional design approach would require a significant increase in staff resources and would probably be unattainable given the reality of current budget constraints. Fortunately, new computer-aided design (CAD) software tools have become available that provide an economical means for the design of very complex VLSI devices. The CAD tools offer a new design technique known as *logic synthesis*. Conventional design techniques require working with very low level logical gate constructs. As designs become more complex, the base number of low-level constructs can quickly overwhelm a single designer. Logic synthesis techniques are based on high-level hardware description languages that can abstract the functionality of hundreds or thousands of low-level constructs into a single lexical entity. With logic synthesis, hardware descriptions are transformed automatically into manufacturable gate-level representations.

Logic synthesis not only increases a designer's productivity, but it also promotes design reuse. Hardware description languages can be used to design without specifying a particular technology. Logic synthesis tools automatically perform the translation into targeted technologies. Therefore, the same design can easily be retargeted to other circuit technologies or inserted in new, higher integration designs. Logic synthesis is now available for a number of commercial and space-flight (radiation-hardened) processes. Several VLSI chips are being designed for the CCSDS Return-Link Processor card using this approach.

The Frame Synchronizer (FS) chip is a monolithic entity that synchronizes serial data streams. This chip replaces six VLSI devices used on previous functional components. The FS contains many programmable registers that allow it to be configured for a variety of spacecraft data formats. The FS design is being implemented in two different technologies, 0.7-μm CMOS and 0.6-μm GaAs, to allow system developers a choice of performance and cost solutions.

The Reed-Solomon Error Correction (RSEC) chip is a high-performance processor that provides powerful error correction. Internal Reed-Solomon decoders perform code word and/or header error correction based on the CCSDS recommendations. The RSEC also performs deinterleaving and annotation. The RSEC is being implemented in a 0.7-μm CMOS 160-K sea-of-gates gate array.

The Service Processor Support (SPS) chip is designed to automate CCSDS service processing tasks. It supports both the conventional and Advanced Orbiting Systems (AOS) recommendations. The SPS has multiple memory interfaces that allow it to perform a number of simultaneous processing tasks including data-unit buffering, frame-header validation, packet extraction, and cumulative quality accounting. The SPS is being implemented in a 0.7-μm CMOS 132-K sea-of-gates gate array.

The Test Pattern Generator (TPG) chip is designed to automate card testing and startup diagnostics. It is capable of addressing large files of simulated telemetry data which can be output at programmable rates. It can also be programmed to generate a number of simulated error conditions. Like the frame synchronizer chip, the TPG is being implemented in both CMOS and GaAs technologies.

The MC680X0 Microprocessor Support (MMS) chip enables the creation of very compact, high-performance processing modules. The MPS integrates all of the support logic associated with processor implementations based on a family of common commercial microprocessors. The MMS is being implemented in a 10-K gate, 0.7-μm complementary metal oxide semiconductor (CMOS) gate array.

Contact: Toby Bennett (Code 521)
(301) 286-5365

Kristin Looney (Code 521)
(301) 286-2586

Sponsor: Office of Space Communications

Mr. Toby Bennett coordinates VLSI circuit development activities within the Microelectronics Systems Branch of the Data Systems Technology Division. Mr. Bennett received his BS in Electrical Engineering from the University of Maryland.

Ms. Kristin Looney works in the Microelectronics Systems Branch designing and developing VLSI circuits for telemetry acquisition systems. She is chairperson of the Code 521 VLSI Design Quality Committee. Ms. Looney received her BS in Computer Science from the University of Maryland.

SMALL EXPLORER (SMEX) TELEMETRY CAPTURE AND DATA DISTRIBUTION SYSTEMS

The Small Class Explorer (SMEX) Project is a GSFC in-house project. The objective of the SMEX Project is to provide periodic, relatively low cost flight opportunities for scientific payloads and to build in-house expertise in spacecraft design and development.

The first of these missions, the SAMPEX spacecraft (the first GSFC CCSDS mission) required the development of CCSDS-based ground telemetry capture and distribution systems for spacecraft integration and testing, ground station support, and, for future missions, remote science analysis. In response to this need, the Microelectronics Systems Branch has, over the last 18 months, worked with the SMEX integration and test (I&T) team and Wallops Telemetry Branch to develop and deploy operational CCSDS telemetry data capture and distribution systems. These systems are based on standard modular hardware and software building blocks configured to give the end-user low-cost, high-performance front-end processing systems. The first of these systems, the Front-End Telemetry and Command Processing (FTCP) System, was developed by Codes 521 and 743. It provides CCSDS frame synchronization, optional Reed-Solomon decoding, CCSDS packet extraction, and distribution over standard Ethernet networks to I&T Ground Support Equipment. Additionally, the FTCP provides local data simulation capability and line-outage storage and playback data rate buffering functions. Three FTCPs have been provided to Code 743 and are being utilized in support of SAMPEX integration and testing efforts. The Wallops Front-End Processor (WFEP), provides standard ground-station NASCOM blocking and deblocking functions but also provides the necessary real-time virtual channel stripping of data for operational support of the SMEX-SAMPEX spacecraft. Additionally, the WFEP provides line-outage protection and prepass simulation data. Three WFEP Systems have been delivered and are operational in several Wallops-supported projects.

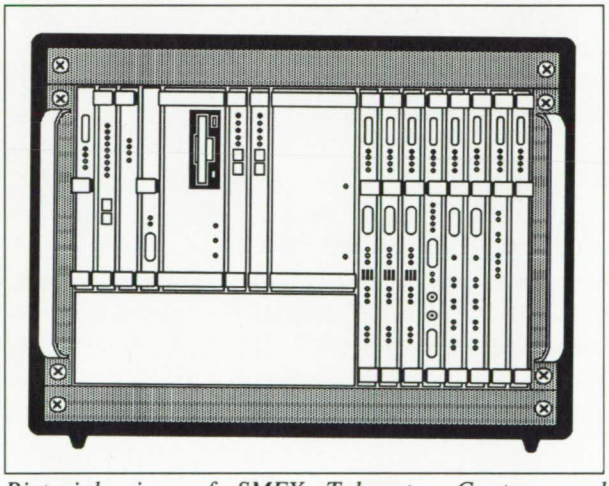

Pictorial view of SMEX Telemetry Capture and Processing Systems.

The final SMEX System delivered provides for remote CCSDS data capture and distribution functions (similar to FTCP) and for NASCOM blocking and deblocking functions (similar to WFEP). Four Wallops Front-End Telemetry and Command Processing (WFTCP) Systems will be deployed in the TOTS to provide remote CCSDS data capture and data distribution functions.

Contact: Nicholas Speciale (Code 521.2)
(301) 286-8704

Sponsor: Office of Space Communications

Mr. Nicholas Speciale is Head of the System Applications Section and is responsible for taking developed technology into operational systems. He received his BS in Electrical Engineering from Manhattan College, NY and an MS in Electrical Engineering from The Johns Hopkins University.

THE GENERIC SPACECRAFT ANALYST ASSISTANT (GenSAA)

During numerous contacts with a satellite each day, spacecraft analysts must closely monitor real-time data, watching for combinations of telemetry parameter values, trends, and other indications that may signify a problem or failure. As the number of data items increases and the satellites become more complex, this task is becoming increasingly difficult for humans to perform at acceptable performance levels. At GSFC, fault-isolation expert systems are currently in operation to support this data monitoring task. A new domain-specific expert system development tool, the Generic Spacecraft Analyst Assistant (GenSAA) introduced in last year's R&T, is now under development based on lessons learned during these initial efforts in expert system automation.

GenSAA is an advanced tool that will enable spacecraft analysts to rapidly build simple, real-time expert systems that perform spacecraft monitoring and fault-isolation functions. These systems will, in turn, assist analysts during real-time operations in satellite control centers. The GenSAA tool consists of a development environment—the GenSAA Workbench—and runtime framework. The development environment is composed of three utilities: the Data Manager, the Rule Builder, and the User-Interface Display Builder. Collectively, these utilities will be used to create or modify an instance of an expert system.

The GenSAA runtime framework is comprised of an inference engine, a display driver, and a process that manages the reception of data. The expert system developer will use the Data Manager to select the real-time spacecraft or ground-system parameters to be monitored; the Rule Builder, to define the rules which will act on the values of these telemetry parameters; and the Display Builder to lay out a graphical representation of the subsystem or process being monitored. The graphical elements of the user interface can be connected to telemetry points and/or rules for dynamic animation during operation. The components generated by the development utilities are called application-specific components. They will be integrated with the GenSAA Runtime framework to create a GenSAA Expert System which will be executed during spacecraft contacts to monitor the selected telemetry parameters and to notify the flight operations analysts of faults inferred from these data.

GenSAA expert systems are intended to be relatively simple expert systems with small rule bases that are usually developed by a single analyst. A typical GenSAA expert system might monitor and isolate faults for one subsystem on board a spacecraft. To handle more complex monitoring situations involving, for example, several spacecraft subsystems, multiple GenSAA expert systems can be built, each responsible for a discrete subsystem or function. During operation, these expert systems would execute concurrently, and would share key conclusions with one another using a publish-and-subscribe model of communicating.

GenSAA utilizes a highly graphical, point-and-select method of interaction to insulate the spacecraft analysts from the complicated, programming details of the systems with which the expert system will have to interface. Perhaps more importantly, this tool will promote the utilization of previously developed rule bases and system components, thus facilitating software reuse and further reducing development time and effort.

GenSAA is well-suited for use on projects that involve a series of similar but nonidentical missions. The Small Explorer (SMEX) and International Solar Terrestrial Physics (ISTP) Program families of missions are ideal, based on the appropriate time frame of these programs, the low-cost nature of the missions, the emphasis on system reuse, and the rapid turnaround between missions. Hence, GenSAA is being applied to support these classes of missions. GenSAA is designed to be used by spacecraft analysts in a satellite Payload Operations Control Center (POCC). The expert systems created with GenSAA will greatly assist the analysts with the tedious task of data monitoring thereby allowing them to focus on other, higher level responsibilities during the real-time contacts with the satellite. By facilitating the reuse of expert system elements from mission to mission, GenSAA will reduce development costs, serve as a training tool, preserve expertise between missions and during periods of personnel turnover, and provide reliable and accurate monitoring capabilities of our rapidly advancing satellites.

Contact: Peter M. Hughes (Code 522.3)
(301) 286-3120

Sponsor: Office of Space Communications

Mr. Peter M. Hughes works in the Automation Technology Section. He received his BS in Computer Science from the College of William and Mary and an MS in Computer Science at The Johns Hopkins University.

TDRSS

LOW-COST TDRSS COMMUNICATIONS FOR NASA'S LONG-DURATION BALLOON PROJECT

NASA's geosynchronous Tracking and Data Relay Satellite System (TDRSS) provides forward- and return-link communications for spacecraft over 85 percent of the orbit for unparalleled flexibility in conducting spacecraft mission operations. However, the complexity and expense of using TDRSS has limited its benefits primarily to projects such as the space shuttle, the Great Observatories, and several other mainline NASA spacecraft projects. With the development of a low-cost TDRSS user transponder, the benefits of the extensive TDRSS infrastructure are now becoming available to new classes of users, opening vistas of flexible and imaginative flight operations for low-budget scientific investigations. Wallops Flight Facility's Long-Duration Balloon Project (LDBP) will be the first user of the new hardware for TDRSS communications during their around-the-world scientific balloon flight campaigns.

The key to providing low-cost TDRSS communications is the Balloon-Class TDRSS User Transponder (see figure), being developed for GSFC by Stanford Telecom of Santa Clara, CA. By taking advantage of previous developments in integrated receivers utilizing Lincoln Labs' programmable charge coupled device (CCD) correlator chips, the cost of transponder production units is now less than 1/10 that of current-generation, space-qualified TDRSS user transponders. Despite the dramatically lower cost, the balloon-class transponder has a number of advanced features resulting, in part, from the use of CCD correlator technology.

For example, PN-matched filter acquisition of the TDRSS forward-link short code using the CCD (4-ABC) correlator chip is <2 seconds; the Fast Fourier Transform (FFT) acquisition of the carrier is <1 second for a total acquisition time of the command receiver of <3 seconds. The maximum forward-link command rates have been increased from 1 to 24 Kbps and can be extended to the full TDRSS S-Band capability of 300 Kbps, if the new Lincoln Labs 2-ATC CCD chip is incorporated into the design in the future. A statistical pseudo bit error rate (BER) data-quality monitor of user command data has been added as a telemetry parameter. Power consumption of the receiver has been reduced from 17.5 to 12 W; the weight of the transponder has been reduced from 16 lbs to 13 lbs.

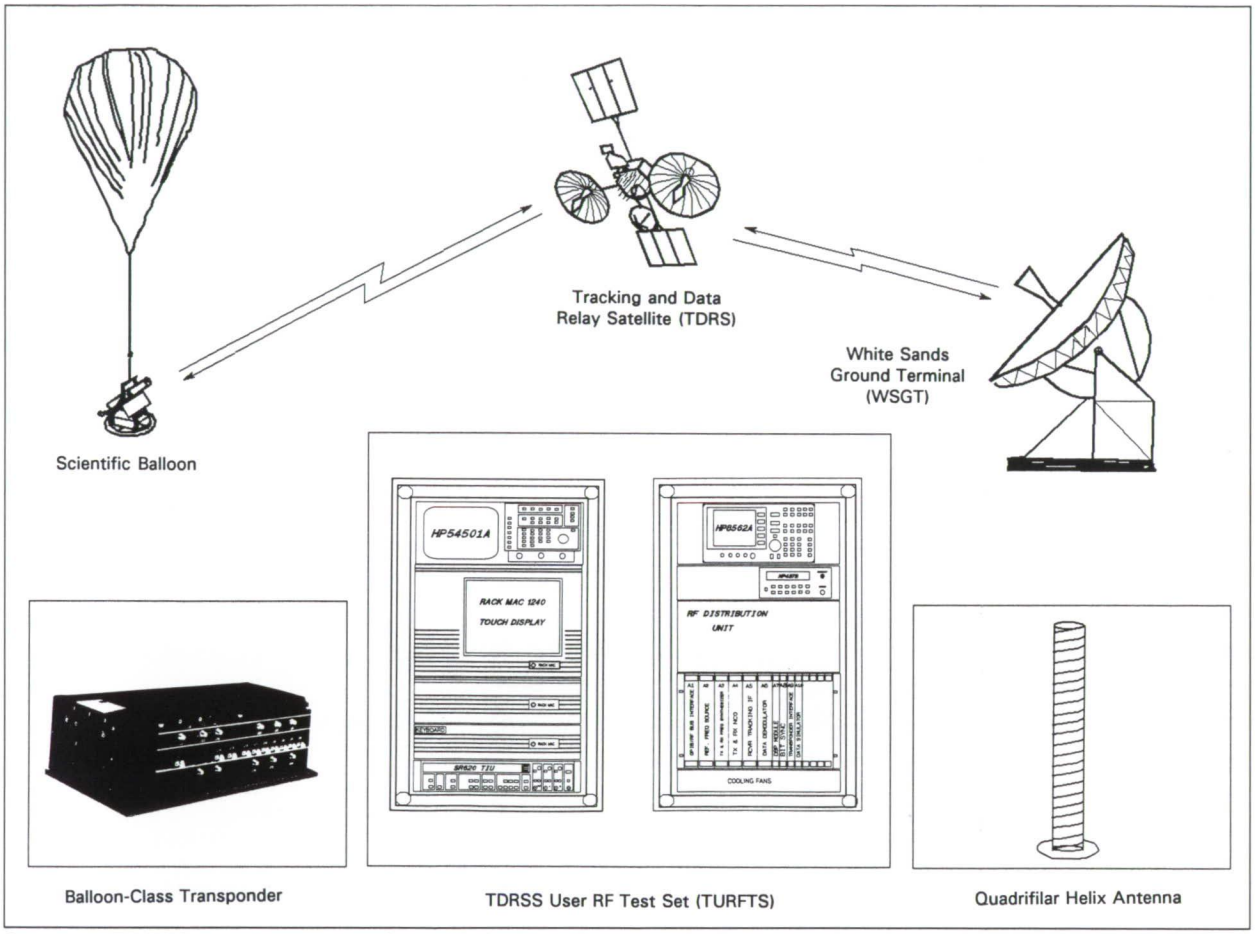

Low-cost TDRSS communications for NASA's Long-Duration Balloon Project.

The balloon-class transponder has been designed to survive balloon deployments and parachute landings and operate at 150,000 ft over a temperature range of -40° to +65°C. Although not radiation-hardened, it has been designed to detect and recover from single-event upsets, such as may occur during flights in the Antarctic.

Another essential component required for long-term operations with TDRSS is RF test equipment. This equipment is necessary to characterize flight hardware performance and to emulate TDRSS communication functions linking the user's ground command and telemetry data systems with the flight payload during all phases of preflight testing. Code 530's RF Systems and Embedded Systems Sections have joined forces to develop a TDRSS User RF Test Set (TURFTS) as a GSFC in-house project to leverage a decade of TDRSS testing experience into an automated, user-friendly, state-of-the-art set of transportable hardware for the new class of TDRSS users. TURFTS is being designed under the leadership of John R. Badger by Jeff Drake, Dave Israel, Frank McCluer and Carlos Taveras of Code 530 and Steve Leslie of Bendix Field Engineering Corporation. The benefit to the LDBP of using GSFC engineers for the development of TURFTS is the ability to obtain an advanced, custom hardware set at greatly reduced cost, estimated at 1/3 to 1/2 that of commercially available TDRSS test hardware.

A novel TDRSS S-Band antenna design for flights originating in Antarctica and meeting the LDBP requirements of low-cost, omnidirectionality in the

azimuth plane and mechanically passive operations was developed by Armen Caroglanian and Fernando Pellerano of the RF Systems Section. The design allows for the varying rotation rate of the free-floating balloon and takes advantage of the limited elevation variation of TDRS in the Antarctic sky, as the balloon circumnavigates, to maximize supportable data rates without requiring active antenna pointing.

The first articles of all major components will be complete by early 1992. A test flight in North America is planned for the spring of 1992; the first LDBP mission flight using TDRSS communications will take place during the December 1992/January 1993 Antarctic campaign. Other programs that may benefit from a low-cost TDRSS communications capability are the NASA/Ames ER-2 aircraft for Earth resources studies, and the Dryden SR-71 aircraft for National Aerospace Plane (NASP) flight experiments.

Contact: David J. Zillig (Code 531.2)
(301) 286-8003

Sponsor: Office of Space Communications

Mr. David J. Zillig, Head of the RF Systems Section, is involved in developing and applying advanced technology in the RF systems of the Telecommunication Systems Branch, including developing a TDRSS communications capability for the Wallops Flight Facility's Long Duration Balloon Project. Mr. Zillig has a degree in Electrical Engineering from the Pennsylvania State University and has 25 years of experience in engineering telecommunications and tracking systems for GSFC's Ground and Space Networks.

TDRSS USER RF TEST SET (TURFTS)—TRANSPORTABLE TDRSS GROUND SUPPORT EQUIPMENT

The Networks Division (Code 530) and the Balloon Projects Branch (Code 842) have combined efforts for the development of new, state-of-the-art transportable test equipment to support the entry of the LDBP into the community of TDRSS users.

TURFTS is RF test equipment that simulates the TDRS RF interface linking the user's ground and flight command and data systems, and provides the functionality to characterize the performance of the user's TDRSS communication transponders. The operations concept that drives the TURFTS design is to provide both two-way TDRSS communications capability and test capability for performance characterization and assessment of TDRSS compatibility (refer to the figure in the previous article entitled, *Low-Cost TDRSS Communications for NASA's Long-Duration Balloon Project*).

TURFTS is packaged in two, 4½-foot-tall transportable racks: one contains the system controller, a time interval counter, and a digital oscilloscope; the other rack contains a spectrum analyzer, an RF power meter, a custom-designed S-Band RF chassis, and a VME chassis housing the majority of TURFTS' custom-designed modules. Integration in shock-mounted packing cases provides TURFTS the flexibility of exercising the TDRS/user interface for testing during integration of the payload, at the launch site, or wherever transponder or RF system communications testing are required.

TURFTS' design incorporates many new technologies that have greatly reduced the space requirements of the test set. The TDRSS PN Code Generator, which generates all 85 TDRSS user codes for the forward and return links, was developed by Code 531.2 as a VLSI chip with the assistance of the GSFCs Microelectronics Systems Branch (Code 521). The frequency synthesizers use the direct digital synthesis technique using a Numerically Controlled Oscillator (NCO) VLSI chip. The NCO, bit synchronizer, and the Viterbi convolutional decoder are commercially available VLSI chips. The receiver's traditional baseband analog functions, such as PN code acquisition, PN code tracking, carrier acquisition, carrier tracking, transmitter and receiver frequency synthesizer sweeping functions, are

replaced by a high-performance, 32-bit floating point Digital Signal Processor (DSP) chip.

A Macintosh IIfx computer will be used to control TURFTS and its supporting commercial test equipment. TURFTS' operator interface is implemented using National Instruments' LabVIEW graphical user interface to allow ease of use by individuals who are not experts in the operation of the test set. The operator will be able to customize complex transponder test sequences and design unique screen displays by means of this user-friendly graphical interface.

TURFTS has three basic operating scenarios: (1) to provide RF communications with the flight vehicle by an air or cable link at the integration facility or launch site; (2) to provide RF communications and direct control and monitoring of the user transponder in a laboratory environment; and (3) to provide a means to verify TURFTS' own operational status (i.e., self-test).

TURFTS' transmitter provides a simulated TDRSS S-Band forward-link signal at a suitable power level and the receiver provides sufficient sensitivity to transmit and receive a TDRSS S-Band signal by air or cable link over moderate distances. Any one of the 85 TDRSS user codes can be selected. Computer control of forward-link power level, frequency, and frequency rate provides the ability to thoroughly characterize the user's receiver acquisition and tracking performance, including thresholds. Transponder ranging delays can also be measured with the commercial time-interval counter under control of the Mac IIfx. Commands are transmitted through the TURFTS forward-link command channel to the flight vehicle from the user's ground control system. The return-link telemetry (both the recovered data clocks and convolutionally decoded data) is available from the TURFTS' I and Q output channels.

Because the LDBP will re-fly the TDRSS user transponder many times, bench or laboratory testing between balloon flights will be required. A direct connection between the TURFTS and user transponder is used for control and monitoring of critical transponder performance parameters making it possible for the first time to easily incorporate transponder control and response indicators into automated test sequences. TURFTS has a data simulator for providing test signals for both the forward-link command channel and the return-link telemetry I and Q channels. TURFTS also includes a BER measurement capability to test the transponder's forward-link command threshold and to calibrate the new pseudo-error rate telemetry parameter generated by the balloon-class transponder's receiver. Provisions have been made for the addition of a signal analysis capability to generate multidimensional signatures indicative of transmitter user constraint/distortion assessments to establish trends throughout the lifetime of the user mission, from manufacture through operational life in flight.

Verification of the TURFTS' RF communications links are made possible by utilizing a frequency translator and identical PN coders in the transmitter and receiver. The TURFTS' receiver can acquire its transmitter signal using any of the TDRSS user PN codes for forward- and return-link modes allowing easy isolation of problems between TURFTS and the equipment under test. Provisions have been designed into the TURFTS' circuits for future inclusion of a diagnostic expert system, similar to the Ground Network's Ranging Equipment Diagnostic Expert (REDEX), to aid the operator in rapid fault isolation of failures in TURFTS.

TURFTS should serve the needs of the LDBP well in the 1990s as the project becomes a regular user of the TDRSS. In addition, the improvements realized in the TURFTS design and those planned for the future should have far-reaching implications, setting new standards for testing of TDRSS user communication systems.

Contact: John R. Badger (Code 531.2)
(301) 286-4675

Sponsor: Office of Space Communications

Mr. John R. Badger is a Senior Electronics Designer in the RF Systems Section of the Telecommunication Systems Branch. He is Project Manager and Design Team Leader for the development of the TURFTS system for the LDBP. Mr. Badger has 31 years of experience in electronic circuit and system design of telecommunications and tracking systems for GSFC's Ground and Space Networks.

DEVELOPMENT OF A QUADRIFILAR HELIX TDRSS-USER ANTENNA FOR THE LONG-DURATION BALLOON PROJECT ANTARCTIC FLIGHTS

The LDBP, managed by Wallops Flight Facility, was conceived as a way to conduct low-cost scientific investigations by means of high-altitude, around-the-world balloon missions. The program calls for balloon flights of up to 15 days in duration, launched from locations such as Antarctica, Australia, and North America. To enhance mission flexibility, reliable real-time communications are required. The TDRSS was chosen as the best means to achieve this.

A key element in providing communications through the TDRSS is the user antenna (refer to the figure in the previous article entitled, *Low-Cost TDRSS Communications for NASA's Long-Duration Balloon Project*). To maximize the capabilities of the system, a custom antenna will be used for each of the major launch areas. Of particular interest are the Antarctic flights, which present unique requirements. Given that the TDRS are in geosynchronous orbit and that the balloons fly at a nominal altitude of 120,000 ft, the minimum view angle to TDRS from the balloons will be -6.1° and the maximum view angle will be 8°. This condition will allow the use of a shaped beam antenna, increasing the gain and the return-link data rate capabilities of the science payloads.

A determining factor in selecting the antenna was that, once in flight, the balloon's position cannot be controlled from the ground and it can rotate freely. On the other hand, pointing mechanisms for a directional antenna would add more complexity to the system than was desired for the initial flights. Constraints such as these indicated the use of an omnidirectional antenna, although at the cost of some antenna gain. The quadrifilar helix antenna met all the requirements. Based upon documented empirical data, a five-turn quadrifilar helix antenna was designed by Code 531.2. The design was optimized for the return-link at a frequency of 2.2875 GHz. It uses the backfire mode; its construction is based on 0.085-in-diameter semirigid coaxial cables. The cables are wound on a 0.63-in-diameter G-10 fiberglass tube, and bonded with Hysol epoxy. The total length of the antenna is 24 in.

Several prototypes were built in-house and tested at the Code 727 anechoic chamber and at the RF Simulation Operations Center (SOC). At a return-link frequency of 2.2875 GHz, the beam peak is 1° above the balloon local horizon and the 3-dB beam covers elevation angles between 8° and -6°. The antenna provides coverage in all azimuth directions, and has a peak gain of ~4.5 dBi. This gain will allow return-link data rates >2 Kbps.

Given that the antenna design was optimized for the return-link, its performance differs at the forward-link frequency of 2.1064 GHz. At this frequency, the beam peak is pointing 6° above the horizon and the 3-dB beam covers elevation angles between 14° and -2°. The gain is ~3.5 dBi. This gain is sufficient to support a command data rate of 1 Kbps using the TDRSS multiple access system. The coverage area, however, is affected by the change in the beam shape. This must be considered during mission planning and scheduling.

Two very important design considerations were the environmental and mechanical stresses. Since the balloon gondolas are recoverable by means of a parachute, a cost-effective approach was to make the antenna strong enough to be reusable. To protect the antenna from the environment and from minor shocking stresses, a radome will be used. The radome was designed from a 5-in-inner-diameter G-10 tube with a wall thickness of 1/32 in. The top of the tube is covered with a Plexiglas plate that

helps hold the antenna and isolate it from vibration. Theoretically, the radome should introduce no more than 0.1 dB of loss.

Another challenging aspect of the antenna design for the LDBP was the presence of multipath. Due to the TDRS-to-user geometry for the Antarctic missions, a considerable portion of the antenna beam radiates towards the ground. In Antarctica, the ground could be either ice or sea water. These surfaces could cause multipath reflections and thus degrade the communications link.

One of the advantages of the TDRSS is pseudonoise (PN) coding. The PN-coded signals have the property of multipath rejection if the multipath is sufficiently time-delayed. A computer-generated analysis, considering the effects of specular and diffuse reflections from these surfaces, showed that multipath was not an insuperable problem. Only a small region of no more than 10° longitude at both sides of the TDRSS Zone of Exclusion (ZOE) would be affected by multipath. From an operational point of view, this could be regarded as an expansion of the ZOE.

The quadrifilar helix antenna allows great flexibility in design. Not only can it be shaped to meet the particular requirements of the mission, but it is relatively easy to construct. These qualities and its cost-effectiveness provided an excellent alternative to the LDBP while minimizing the impact to other onboard systems and to the science payloads.

The engineering model antenna will be passively flown in Antarctica during December 1991 and January 1992. This test flight will provide information on the structural behavior of the antenna. Fabrication of the flight model is expected to be performed in-house sometime in the spring of 1992. Its first science flight is scheduled for December 1992.

Contact: Fernando Pellerano (Code 531.2)
(301) 286-8967

Sponsor: Office of Space Communications

Mr. Fernando A. Pellerano is an Electronics Engineer in the RF Systems Section of the Telecommunication Systems Branch. Mr. Pellerano has a BS in Electrical Engineering from the University of Puerto Rico and is currently pursuing an MS in Electromagnetics at The Johns Hopkins University. He has been working at GSFC since July 1990.

DEVELOPMENT OF A PROGRAMMABLE CMOS CHARGE COUPLED DEVICE CORRELATOR OPTIMIZED FOR TDRSS/TDRSS-II SPREAD SPECTRUM RECEIVER APPLICATIONS

Since the mid-1980s, the Networks Division (Code 530) has managed the design and development of a state-of-the-art receiver by Stanford Telecom that has both near-term and future applicability to the TDRSS and its follow-on, TDRSS-II. This receiver uses programmable CCD correlator technology as the basis for novel signal processing, which encompasses extremely rapid PN acquisition as well as PN tracking and carrier/symbol synchronization.

Specific receiver implementations have included: an MA Dedicated Calibration Receiver for TDRSS Ground Terminal support, a CCD Integrated Receiver Demonstration System for both ground- and space-based applications, and an operational TDRSS user transponder for long-duration scientific balloon flights. All of these receivers used earlier generations of the CCD correlator chip which, in the TDRSS context, imposed operational and performance limitations that now have been essentially eliminated with the new 2-ATC chip. The 2-ATC chip is the newest Lincoln Labs Programmable CCD chip. The chip was developed under sponsorship of the Office of Space Communications' Advanced Systems Program (Code OP) at NASA Headquarters and Code 531 at NASA/GSFC. Unlike previous CCD chips, the 2-ATC chip has been uniquely tailored for TDRSS/TDRSS-II applications, providing enhancements of particular significance to

Space Network needs (refer to figure in the previous article entitled, *Low-Cost TDRSS Communications for NASA's Long-Duration Balloon Project*).

The CCD correlator is an MOS integrated circuit whose functional and performance capabilities have been dramatically advanced via developments at Lincoln Labs during the 1980s. The CCD correlator operates as a time-discrete tapped delay line, with no amplitude quantization. This capability is effectively achieved by sampling the signal at the CCD input and converting the analog voltage to charge, which is then transferred from one end of the CCD to the other by a string of MOS capacitors, each capacitor effectively serving as a distinct stage in a shift register. The charge transfer rate is controlled by an external clock. The charge at each capacitor may be externally accessed at each clock time, representing the tapping operation of the tapped delay line.

The 2-ATC programmable CCD analog-digital correlator is a low-power CMOS design which has 512 stages, 256 of which are tapped. The digital tap weights are externally controlled and updated in real-time. As such, this CCD correlator can be used to implement a PN Matched Filter (PNMF) that can provide an effective parallel processing capability to a degree equal to the number of stages. It is precisely this PNMF flexibility, coupled with its high-level parallel processing capability, that makes the CCD correlator approach so attractive for TDRSS applications--especially for rapid acquisition of PN-coded signals received either from power-limited, low-Earth orbiting spacecraft or from the TDRS via user low-gain spacecraft antennas. Some of the new, key-features of the 2-ATC correlator chip are highlighted below with specific attention to their particular importance to TDRSS/TDRSS-II.

- Previous CCD chips had only 128 stages (4-ABC chip) or 256 stages (2-ABC chip). For low data rates, which correspond to worst-case or threshold acquisition conditions, the number of CCD stages essentially translates into the degree of parallel processing. For example, for the TDRSS forward-link to a user spacecraft under threshold conditions of C/No=33dB-Hz, PN acquisition time for the second-generation user transponder (which does not use a PNMF) is 20 seconds; however, this time would be reduced to ~0.5 second using the 2-ATC chip in an integrated rceiver design that incorporates a PNMF approach.

- Unlike prior CCD chips, which only allowed tap weights of +1 or -1, the 2-ATC also accommodates a tap weight of 0, thereby enabling unrestricted CCD length control. This is of particular importance at higher data rates wherein a full CCD length of 512 stages may represent more than a 1/2-symbol duration which is a desirable accumulation interval to drive the symbol synchronization circuit. Thus, the 2-ATC permits integrated receiver operation over a continuum of data rates, as required in TDRSS/TDRSS-II, from 100 bps to 10 Mbps. This should be compared to the restricted subset of specific data rates imposed by the previous CCD chips arising from their inability to arbitrarily change the number of stages, especially for PN-coded operations.

- The maximum clock rate of previous CCD chips was 40 MHz or less, which significantly limited the maximum supportable data rate. The 75-MHz (or greater) clock rate of the 2-ATC chip will support all TDRSS PN-coded operations, regardless of data rate. It also supports nonspread operations to at least 10 Mbps, with a potential of 25 Mbps.

- Previous Lincoln Labs CCD correlator chips were designed for applications in which the PN code period was relatively short. As such, the CCD tap weights represented a full PN code period, yielding a nearly equal number of -1s and +1s at each correlation instance. For the much longer PN codes of TDRSS/TDRSS-II, at each time instance the CCD tap weights reflected only a partial part of the code, typically containing an unequal number of -1s and +1s. This phenomenon led to a random output bias and resulted in some signal-to-noise ratio degradation, especially during acquisition. Through judicious

circuit redesign, this bias has been eliminated for the 2-ATC chip, further enhancing the chip's performance for TDRSS/ATDRSS-II application.

The first use of the 2-ATC chip will be in the TDRSS-II Beacon Prototype Receiver, currently being developed by Stanford Telecom for NASA/GSFC, Code 531 to demonstrate key features of next-generation TDRSS/TDRSS-II space and ground receivers. Noteworthy is the ability of this receiver in a user transponder to acquire and track multiple services simultaneously. This is made feasible by the 2-ATC CCD chip which facilitates rapid PN acquisition in a low-power and compact implementation enabling flexible multichannel transponder receiver configurations. The CMOS 2-ATC chip is currently under consideration for use in several other applications as a result of its adaptability as a generic programmable transversal filter and its low power consumption compared to digital approaches.

Contact: David J. Zillig (Code 531.2)
(301) 286-8003

Sponsor: Office of Space Communications

Mr. David J. Zillig, Head of the RF Systems Section, is involved in developing and applying advanced technology in the RF systems of the Telecommunication Systems Branch, including developing a TDRSS communications capability for the Wallops Flight Facility's LDBP. Mr. Zillig has an Electrical Engineering degree from the Pennsylvania State University and 25 years of experience in engineering telecommunications and tracking systems for GSFC's Ground and Space Networks.

INTERFACE BETWEEN THE VIRTUAL CHANNEL SORTER MULTIPLEXER AND A FIBER DISTRIBUTED DATA INTERFACE NETWORK

Many future projects such as Space Station Freedom (SSF) and the Earth Observing System (EOS) will require a means of processing CCSDS formatted data, and converting it to commercial protocol data format(s). Many of the functions required in developing the space-to-ground link interface for CCSDS protocols have been prototyped in the Virtual Channel Sorter Multiplexer (VCSM). The functions required to develop ground-to-ground link interfaces have not been implemented. These functions include conversion of CCSDS structures into commercially available protocol formats. The prototyping of the gateway functions between space link protocols and industry standard protocols is essential to understanding the issues involved in performing such conversions. The Virtual Channel Sorter Multiplexer (VCSM)/Fiber Distributed Data Interface (FDDI) Integration (VFI) project was conceived by the NASA Communications (Nascom) Division, Code 540, to investigate and understand the feasibility of integrating a commercially available FDDI network with the VCSM system.

The VCSM system was a joint effort between the Data Systems Technology Division, Code 520, and the Nascom Division, Code 540. The VCSM implements some of the space-to-ground link processing functions based on SSF and EOS requirements. Each processing function prototype uses custom-designed cards installed in a Versa Module Eurocard (VME) bus chassis. Functions performed by the VCSM include: synchronization, error correction, sorting, and multiplexing.

The goal of the VFI project is to extend the custom pipeline processing architecture of the VCSM to a commercially available communication network. It will provide a means of transporting CCSDS Virtual Channel Data Units (VCDUs) using the International Standards Organization (ISO) 8473 protocol over an FDDI Local Area Network (LAN). The reason for using ISO protocols is because Government Open Systems Interconnection Profile (GOSIP) mandates the ISO standard compliance for all future NASA communication systems. The reason for choosing the FDDI LAN is because it is an example of a high-throughput communication system of the type to be used to satisfy future needs.

A block diagram of the VFI is shown in the figure. Physically, these are two VCSM racks connected by an optical fiber. Data are transmitted from the source VCSM shown on the left to the destination rack. The source VCSM consists of a master controller attached to five other VME boards. All boards connect to the VME bus and exchange control data with the master controller. The control data occupy a very small bandwidth and consist of system startup, shutdown, and status messages.

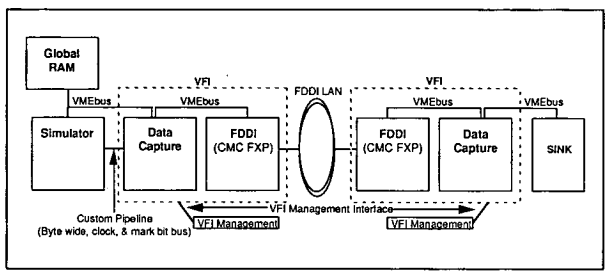

System configuration for VCSM/FDDI interface prototype system.

VCDUs are generated by the simulator card. They are transported to the data capture card through a custom pipeline. The data capture card transfers these VCDUs to the Random Access Memory (RAM) card using the VME bus. The data capture card accesses the VCDUs, converts them to ISO 8473, and then issues commands to the FDDI card causing the frames to be moved from the RAM card to the FDDI card by way of the VME bus. The FDDI card transmits the frames over the FDDI LAN to the destination rack.

In parallel to the processing described above, the destination VCSM monitors the FDDI LAN. The data capture card issues commands to the FDDI card to receive frames from the FDDI LAN and transfers them to the RAM card. The master controller then accesses the frames in the RAM, accumulates statistics, and generates reports.

The outcome of this effort will be to demonstrate that custom communications protocol processors, used in the space-to-ground link, can be interfaced to commercially available equipment to support ground-to-ground link transmissions. In addition, data rate and throughput measurements will be made utilizing the system configuration discussed above. As a follow-on, another phase of this task is currently being defined to measure optimal data rate and minimum delay between functional elements with the platform used. These performance characteristics, along with the feasibility of integrating the FDDI card with the VCSM system, will provide a better understanding of the issues and data rates involved in transporting CCSDS data in high-speed networks using standardized protocols.

Contact: Matthew D. Kirichok (Code 541.3)
(301) 286-3435

Sponsor: Office of Space Communications

Mr. Matthew D. Kirichok, an Electronics Engineer with the Advanced Development Section, holds a degree in Electrical and Computer Engineering from Northeastern University, Boston, MA. He is also currently earning his MS in Computer Engineering at The Johns Hopkins University.

Mission Planning and Scheduling

MISSION PLANNING ASSISTANT

A tool to provide mission planning service-related information to new users and to assist in the capture of user support needs is being explored. This tool is the Mission Planning Assistant (MPA). The MPA was developed to be used as a tool to capture and preserve information about Mission Operations and Data Systems Directorate (MO&DSD) institutional services and resources and make it available to a diverse user community ranging from MO&DSD managers and mission support specialists to external users. Applications targeted by the MPA include new mission support requirements capture, orientation, and training of engineers and new employees; training for Mission Operations Managers (MOMs) and for Mission Support Managers (MSMs).

MOMs are MO&DSD engineers assigned to work with mission project managers to help ensure that planning, facilities preparation, mission testing, and related operations procedures are accomplished in time for mission launch. MSMs are responsible for ensuring that required mission interfaces to lead centers external to GSFC are established and ready for mission support. Thus, MOMs and MSMs support mission planning for new users.

The MPA supports mission planning by orienting managers and engineers of other Directorates to MO&DSD services and products. A subset of the MPA has been developed that provides user support for requirements capture, evaluation, and tracking for a mission's life-cycle via the user-generated Support Instrumentation Requirements Document (SIRD) and the high-level MO&DSD institutional statement of support, the NASA Support Plan (NSP). The MPA architecture currently uses Macintosh Hypercard which will be linked to a powerful expert system shell and the Oracle RDBMS as the development and delivery platform for interactive mission planning tools, tutorials, and service descriptions. This modular approach enables information to be linked and shared among subordinate applications as desired.

The current version of the MPA is a prototype, developed to show the feasibility and utility of using Hypercard as a tool for capturing, associating, and disseminating information about MO&DSD services and resources to users and, in turn, for the users to provide information and feedback to the MO&DSD. MO&DSD managers and engineers will be able to access the MPA platform to obtain and input specialized information about MO&DSD services and resources, i.e., retrieve engineering-level information about available services and resources, and input the knowledge gained. The MPA can be used as a repository of institution-specific information.

The current prototype includes the capability to browse the instructions and page formats for the current version of the SIRD and a sample of its resulting NSP. When fully implemented, the SIRD/NSP builder will interface directly with the System and Operations Requirements Document (SORD)—the MO&DSD institutional decomposition of the users' support requirements.

The objectives of mechanizing the SIRD/NSP production are to reduce both the time and the engineering effort required to produce a signed document. The SIRD/NSP builder will also provide traceability from SIRD/NSP to users' mission and project requirements. The SIRD/NSP builder will also include interactive menus of MO&DSD institutional services that, when combined with the on-line instructions and sample completed pages of the SIRD and NSP, will enable more efficient and accurate completion of the SIRD and NSP. Once completed, the documents can be printed at the user's request.

When fully implemented, the SIRD/NSP builder will include an expert system that will be a repository for MO&DSD services and resources. The SIRD author will be prompted (on his display) with pertinent information to be included in the SIRD. The user will interact with the system through a dialogue, and the SIRD and NSP will be built in the background. The completed SIRD text will be electronically transferable to the SORD Generation System (SGS). While not totally automated, the process will be greatly streamlined, enabling the requirements engineers to focus on unresolved issues and on new technology rather than on the mechanics of producing requirements documentation.

Contact: William Macoughtry (Code 501)
(301) 286-7155

David Beyer
Bendix Field Engineering Corp.
(301) 794-3440

Sponsor: Office of Space Communications

Mr. William Macoughtry graduated from West Virginia University in 1958 with a BS in Electrical Engineering, and received an MEA from George Washington University in 1981. During his employment at NASA, he has been in charge of

ground-tracking network testing and evaluation using instrumented aircraft, has developed and utilized scheduling simulation software to produce network loading studies, and has been instrumental in utilizing expert systems to develop spacecraft user planning systems. He is now Associate Chief of the Flight Mission Support Office, in charge of spacecraft mission support planning and requirements analysis and processing.

Mr. David Beyer is a Senior Project Systems Analyst with the Bendix Field Engineering Corporation. Currently he is providing systems engineering support to Code 500. He is a co-founder of the Goddard Conference for Space Applications of Artificial Intelligence. Mr. Beyer has 22 years of experience providing engineering support to Code 500, beginning with the Apollo Project. He is a winner of an individual Silver Snoopy Award for providing HF radio propagation predictions to the Apollo Network in near-real time.

MISSION OPERATIONS MANAGER HYPERMEDIA WORKSTATION

The MOM Hypermedia Workstation is a tutoring/training program that presents mission management information via text, graphics, animation, video, and audio. The tool can be used as a general trainer, but can also be used as a searchable database of mission management, technical, and administrative information. In hypermedia, one can access and review information using numerous machine and human navigational schemes. The goals of Hypermedia are to:

- Link and present information in a manner similar to that employed by humans as part of normal cognitive processes;
- Provide a learning/information retrieval environment richer and more robust than that provided by simple text, hypertext, or multimedia; and,
- Provide the potential for a learning experience generally thought possible only through personalized instruction.

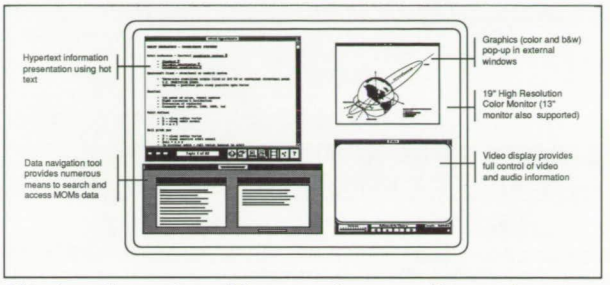

Mission Operations Manager hypermedia workstation.

The following tools and programs make up the MOM Hypermedia Workstation: the Hypertext Interface Tool is the main program in the system that presents text information to the user. From this interface, the user is presented text information and is informed whether graphics, video, or audio is associated with the topic currently presented. The user controls presentation of graphic, video, and audio information from this program. The program also provides functions to print text and figures and to search the information base. The Navigation Tool assists the user in searching and accessing data in the information base. Several search/access methods are provided, including an electronic index and a keyword search function which presents keywords in context. Direct and inferred information linking software is currently under development. The Video Program uses a video source (an addressable-frame VCR) and a video digitizer to present audio and video information on the main display. Video segments and sequences to be displayed are under the control of the main program, while the video program controls video and audio characteristics such as volume, contrast, color, and tint.

Contact: Troy Ames (Code 522.3)
(301) 286-5673

Sponsor: Office of Space Communications

Mr. Troy Ames performs research and development in advanced technologies concerning artificial

intelligence and human factors. He has been at GSFC for 7 years and currently works in the Automation Technology Section. He holds a BS in Computer Science and a BS in Mathematics from the University of Idaho.

SCHEDULING APPLICATIONS INTERFACE LANGUAGE—SUPPORT FOR GEOGRAPHICALLY DISTRIBUTED SCHEDULING

To support the distributed and complex operational scheduling required for future NASA activities, a formal, textual language, the Scheduling Applications Interface Language (SAIL), has been developed (see first figure). Increased geographic dispersion of investigators is leading to distributed instrument planning, scheduling, and operations. The growing number of sophisticated instruments that generate very high data rates and volumes is leading to a requirement for more complex and more automated planning, scheduling, and resource management. Additionally, extended mission lifetimes of 10 to 15 years are leading to hardware-independence that allows easy insertion of technology improvements into the operational environment. SAIL will support communicating scheduling information among physically dispersed applications in distributed scheduling environments.

A formal means of communication is required to support such an operational system. A language allows for expression of complex and variable requirements (e.g., flexibilities in resource usage and duration of an activity). SAIL offers a clear, concise, and unambiguous expression of scheduling information in a readable, hardware-independent format that can be processed by computer. The language concept, syntax, and semantics are described in the SAIL reference manual. SAIL incorporates language features found useful during 5 years of research, prototyping, and use of scheduling languages in physically distributed environments. SAIL allows for interoperability between the elements of a physically distributed scheduling environment. Elements with different hardware configurations running different scheduling applications can use SAIL to communicate. SAIL does not presume a specific physical topology, communications protocol, or operations scenario.

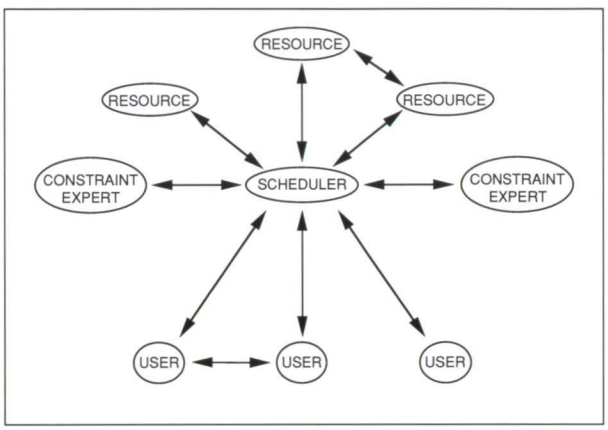

Distributed scheduling environment example.

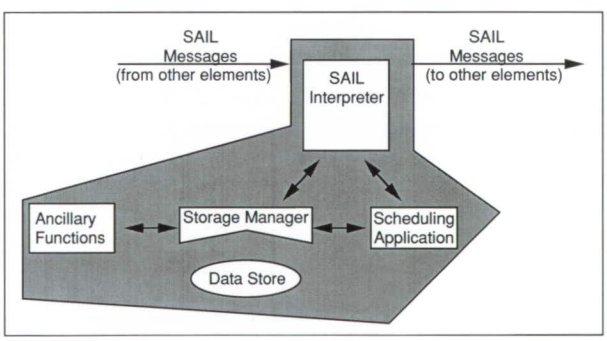

Typical scheduling element architecture.

SAIL is a representation scheme that expresses the planning knowledge and scheduling information that must be communicated in a distributed-scheduling environment. Although not intended to be a user-interface language, SAIL was deliberately designed to be readable and is readily understood by resource-providers and users. The language allows concise specification of activity plans in a format that promotes repetition and reuse. SAIL's ability to express plan flexibilities and alternatives reduces the need for schedule iterations. SAIL contains key features from languages that have been used for 10 to

30 years and is, therefore, viewed as a low-risk approach for operational implementation.

Contact: Larry G. Hull (Code 522.2)
(301) 286-3009

Sponsor: Office of Space Communications

Mr. Hull is a Senior Computer Engineer in the Data Systems Technology Division. He has over 25 years of experience in areas as diverse as real-time operational support for manned and unmanned space-flight missions, computer performance and capacity management, discrete event simulation of computer and communications systems, expert systems, activity scheduling and project management. He earned a BS in Mathematics from Worcester Polytechnic Institute, an MS in Physics from Northeastern University, and an MEA in Technical Management and a degree in Computer Science from George Washington University. He also holds a Certificate of Data Processing. He has managed the development of several operational expert systems and currently manages the Scheduling Concepts, Architectures, and Networks Testbed.

REQUEST-ORIENTED SCHEDULING ENGINE—AN ADA-BASED SCHEDULING SYSTEM

The Request-Oriented Scheduling Engine (ROSE) is the product of an investigative effort into ways of improving spacecraft operations scheduling. The ROSE software facilitates automation of planning and scheduling processes. ROSE is written in Ada, and incorporates sophisticated artificial intelligence and human/computer interaction techniques.

The ROSE scheduling system embodies significant work in three areas: knowledge representation, rescheduling, and demonstration scenarios. Knowledge representation encompasses the need to define and describe precisely the user's scheduling domain. Rescheduling involves making changes to an existing schedule, possibly moving or deleting lower priority activities to make room for higher priority activities. Demonstration scenarios address the planning and scheduling process, conflict resolution, and procedures to handle nominal and abnormal scheduling situations.

Knowledge representation outlines how information and rules are organized within an application. NASA scheduling applications are complex, often integrating information and rules from different users. In the scheduling process, users create requests that specify their resource needs. A scheduling system then processes requests from many users to produce a mission schedule. Subsequently, users conduct their flight activities based upon the mission schedule.

The knowledge representation should model the application. For example, the scheduling tool should allow users to work in terms of orbital events rather than window start and end times since the mission is really based upon orbital events, not absolute time. "Collect data over Los Angeles" is a statement tied to orbital events as opposed to an absolute time specification such as "collect data from 21:26:55 to 21:28:15 on Tuesday."

ROSE is built around a scheduling language called the Flexible Envelope Request Notation (FERN). FERN provides the knowledge representation mechanism for expressing complex user requests. The FERN language organizes the scheduling data into modular data structures that provide a general framework for scheduling.

Users tailor FERN requests to their applications. They may create user-defined time segments and constraints. FERN contains special features for spacecraft scheduling such as repetitive activities, view-period functions, pooled resources, and alternative requests. The FERN language supports many kinds of constraint relationships: activities may be related to orbital events, calendar events, or other activities.

ROSE supports a rescheduling algorithm, activity locking, what-if scheduling, and back-up requests. The rescheduling algorithm employs a classical artificial intelligence (AI) technique called a best-first search. This technique uses backtracking. In backtracking, the scheduling algorithm may move or modify activities that are already on the schedule. To prevent changes, the operator may lock activities which need to be fixed on the schedule. Locked activities are frozen and cannot be moved by the software rescheduling algorithm. What-if scheduling allows one to try different scheduling scenarios before selecting a solution. The scheduler produces many different schedules by using different combinations of input data and scheduling algorithms.

Back-up requests are tied to a relaxation-level control parameter which may be changed to select minimum resource amounts and time durations, less difficult constraints, and alternative requests. This capability permits the scheduling algorithm to reduce the resource amounts or shorten the duration of the request so that the request may fit in a limited slot on the schedule.

At the present time, ROSE supports three demonstration scenarios to show various scheduling concepts. The first scenario demonstrates an implementation of the Earth Observing System (EOS) scheduling process that includes what-if scheduling. A second scenario shows contingency scheduling for the Network Control Center (NCC) where mission support is rescheduled from TDRS East to TDRS Spare. The third scenario presents a replanning procedure for a satellite-servicing mission where a space shuttle launch slip perturbs the schedule.

The ROSE software executes on a Sun Unix-based workstation or a DEC VMS-based computer. It uses X-windows and the Transportable Applications Environment Plus (TAE Plus) user interface.

Contact: G. Michael Tong (Code 522)
(301) 286-3176

Sponsor: Office of Space Communications

Mr. G. Michael Tong received his BS degree in Engineering from Tufts University. Currently, he is working on software planning and scheduling concepts. Mr. Tong has been with GSFC for 16 years.

PROTOTYPING OF FLEXIBLE SCHEDULING OPERATIONS

Flexible scheduling operations have been proposed as the model to be used by the Space Network Control (SNC) Data System for allocating TDRSS communications services. Flexible scheduling allows service requests to be expressed in terms of single or repeated events, and allows the timing of events to be expressed either as occurring within specified time periods or relative to other events. It is more convenient to use flexible schedule requests to specify repetitive requirements than to submit separate service requests for each communications event, as is the case in current TDRSS scheduling operations. While the concept of flexible scheduling had been proposed earlier for TDRSS scheduling operations, key design issues existed regarding the format of flexible service requests and the scheduling algorithms that would process them. A prototype flexible scheduling system was implemented to explore these design issues.

Flexible scheduling operations had been expected to streamline operations by providing a more natural interface for resource requesters, and by generating fewer schedule conflicts requiring operator intervention. Our prototyping effort validated these expectations. TDRSS users met with us and verified that the proposed request features would be useful for spacecraft operations. Test runs verified that a high percentage of events could be scheduled automatically.

Databases were prepared for use with the prototype scheduling system to make the runs as realistic as possible. A request set representing an operational

week for 1997 was prepared based on meetings with TDRSS users. The request set included service requests for BRTS, COBE, ERBS, CGRO, HST, Landsat, SME, TOPEX, UARS, XTE, and shuttle missions. A data file of user antenna view (UAV) data was built that specified time periods during which user-spacecraft were able to view TDRSS-East and West spacecraft.

In the first stage of the prototype effort, alternative scheduling algorithms were tested with a request set composed of simple, repetitive requests, and view constraint data. Scheduling runs from three heuristic-based scheduling algorithms, configured with several combinations of scheduling order and scheduling placement heuristics, were compared for number of events scheduled and execution times. Each of the scheduling algorithms tested scheduled over 90 percent of the events requested. An internal expansion algorithm, which used backtracking techniques based on JPL's RALPH scheduling system, scheduled the highest number of events.

Two optimization-based scheduling algorithms, derived from mathematically optimal solutions, were tested against the same set of requests and view-constraint data. The optimization-based algorithms scheduled as many events as were scheduled by the heuristic-based algorithms. The optimization-based algorithms ran about an order of magnitude faster than their heuristic-based counterparts.

In the second stage of the prototype effort, the scheduler was refined so that one of the heuristic-based algorithms was able to process additional request features. The upgraded prototype was tested with a request set that included the equivalent of the following request expressions:

- Schedule events with either TDRSS spacecraft according to UAV periods;
- Schedule an event to occur during each of a set of time periods, such as UAV periods;
- Schedule events for the duration of each of a set of time periods, such as UAV periods;
- Calculate event durations based on minimum and maximum values; and,
- Calculate event durations as a function of time elapsed since the last such event. This is used to schedule tape dump events.

A report summarizing experiences with the TDRSS scheduling prototype has been completed. Further research into SNC scheduling functions is continuing with a new prototype. This new effort has a broader scope that incorporates science planning systems and POCC planning systems in addition to a TDRSS scheduling system.

Contact: Nancy Goodman (Code 522.2)
(301) 286-6635

Sponsor: Office of Space Communications

Ms. Nancy Goodman works in the Software and Automation Systems Branch. She has 10 years of experience at GSFC and has earned an MS in Computer Science from The Johns Hopkins University.

TRANSPORTABLE PAYLOAD OPERATIONS CONTROL CENTER ADVANCED SPACECRAFT SIMULATOR

The next generation of Payload Operations Control Centers (POCCs) that support real-time spacecraft operations are being developed using the Transportable POCC (TPOCC) architecture. This architecture is characterized by its use of distributed processing, industry standards, commercial off-the-shelf (COTS) hardware and software components, and reusable software. The key to delivering error-free software for real-time operational support is a good test environment with appropriate hardware and software.

The TPOCC Advanced Spacecraft Simulator (TASS) system has been designed to support this

development, test, and operational environment for POCC software deliveries. The purpose of TASS is to simulate spacecraft telemetry and command functions. TASS's development and implementation for POCC support is part of the TPOCC system approach to building control centers. Control-center systems are designed to eliminate single points of failure by providing prime and backup systems. TASS takes advantage of the TPOCC architecture by using the backup system configuration hardware as the simulator function. Alternatively, it can be separately hosted on a streamlined hardware version of the POCC. This eliminates the need to schedule hardware or Nascom lines during various test configurations. In essence, the user has a spacecraft simulator on call at all times. TASS also uses some of the same TPOCC reusable software that the POCC developers use, including the user interface (display and TPOCC System Test and Operations Language (TSTOL)) and the Nascom interface.

TASS's functional capabilities are based on specific spacecraft requirements and past simulator experience in CGRO, COBE, UARS, and EUVE POCCs. The TASS system resides on a commercially available workstation with a special front-end to handle the Nascom protocol. The design uses components of the TPOCC architecture; emphasis is placed on operator interface control, use of spacecraft databases, automated test procedures using the system test and operations language, and report generation. TASS has the capability to simulate the Nascom link protocols required to support satellites and generate simulated spacecraft telemetry streams using the POCC's operational database (ODB).

TASS validates spacecraft commands and will alter the real-time telemetry stream in response to those commands. The user can alter the telemetry stream either by project database mnemonic or by specifying the individual bits in the telemetry frame. Similar telemetry displays at both the simulator workstation and the POCC mission operation room aid in identifying telemetry processing irregularities. As part of the system design, simulator complexity can be added by providing various dynamic models for the telemetry-generating function.

The TASS system provides a means for saving and restoring predefined test scenarios and results, telemetry stream contents, and data structures to allow the user to repeat specific tests, retest with known data, or continue testing from a given point in the test scenario. These features allow the user to perform regression tests on new software deliverables in the shortest possible time.

TASS records all received Nascom blocks in a history file that can be viewed through the use of an off-line utility program. All system events, errors, operator input, procedure input recorded in the event log, and spacecraft memory images that are saved can be viewed by using off-line utility programs. After completing the test, the report generation subsystem is used to generate test reports and evaluate test results during the analysis process.

Unique implementations of spacecraft load and dump capabilities can be provided as well as a Network Control Center (NCC) communications protocol when TDRSS support is required. The first TASS implementation is for ISTP Wind/Polar, with SMEX SAMPEX to be supported next. Future missions using the TPOCC architecture will also be supported by TASS systems.

Contact: Jack Koslosky (Code 511)
(301) 286-8947

Barbara Hageman, Integral Systems, Inc.
(301) 497-2415

Sponsor: Office of Space Communications

Mr. Jack Koslosky is a Section Head in the Control Center System Branch, GSFC. He manages the development of real-time ground-support systems for Project Operations Control Centers. Mr. Koslosky has worked on the Transportable Payload Operations Control Center (TPOCC) project since 1985 and has 20 years of experience in control center system design and management at GSFC.

Ms. Barbara Hageman is the technical lead in the development of Code 511 simulators. She holds a BS

in Aerospace Engineering from the University of Maryland and has 9 years of experience in spacecraft simulators.

FLIGHT DYNAMICS/SPACE TRANSPORTATION SYSTEM THREE-DIMENSIONAL MONITOR SYSTEM

The Flight Dynamics/Space Transportation System Three-Dimensional Monitor System (3D-Mon) is a graphics analysis software tool developed by the Flight Dynamics Division. Originally released in 1987, the primary objective of 3D-Mon is to accurately generate three-dimensional, shaded solid models of the Shuttle, the Remote Manipulator System (RMS), and other celestial objects and spacecraft with some degree of photographic realism (see the first figure). The 3D-Mon system computes the positions and orientations of these spacecraft using spacecraft orbit and attitude data. The system then provides analysts the capability to interactively move a viewpoint to any location in the Universe that may assist in mission operation functions. These views may include a view along a spacecraft's x-axis, a view along a sensor's field of view, or a view of a spacecraft from a communications satellite.

The 3D-Mon system is designed to support any spacecraft mission. As a premission planning tool, a user can interactively manipulate the RMS joint angles to determine orientation and joint angle requirements for future payload deployment scenarios. As a mission monitoring utility, 3D-Mon provides actual spacecraft positioning and orientation information from real-time spacecraft telemetry data, with accurate solar light modeling from any viewpoint. As a mission analysis aid, 3D-Mon provides playback of previously recorded spacecraft data in slow-motion for study of mission anomalies.

Since its initial release, many new capabilities have been added to the system to increase its effectiveness as an analytical tool (see the second figure). The top left window depicts the position of a Tracking and

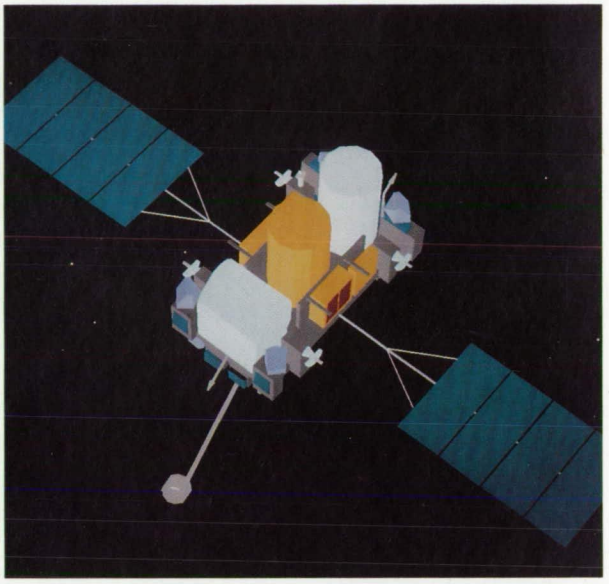

Release of the Gamma Ray Observatory as displayed in near real-time by the FD/STS 3D Monitor System.

Data Relay Satellite with respect to the field-of-view of the shuttle's Ku-band antenna. The bottom right window displays a beam angle grid used to verify gimbal angles for the TDRS Single Access antennas. The remaining windows display the deployment scenario from different user-specified perspectives. Among these new capabilities are the following major additions:

- Automation of additional shuttle appendages including cargo-bay door and Ku-band antenna configurations driven by telemetry data;
- Support and display of additional coordinate systems and associated reference frame axes;
- Display of sensor field-of-view outlines/contours;
- Simultaneous display of the Shuttle and a free-flyer based on separate telemetry sources;
- Display of TDRS beam angle grids;
- Display of the magnetic poles and magnetic field vectors;

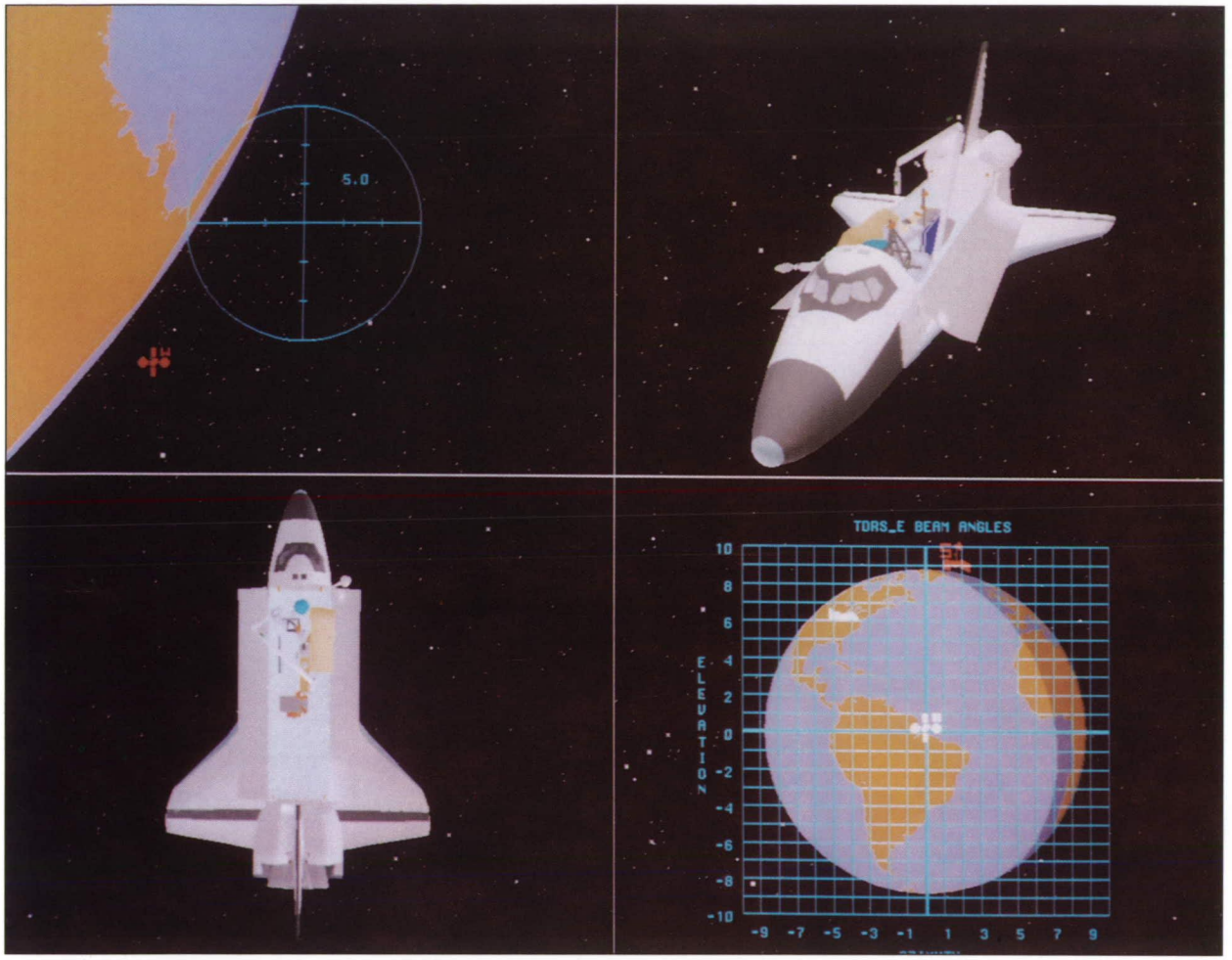

The 3D-Mon system provides the capability to present up to four different views simultaneously on the screen, as used above during the deployment of the Upper Atmosphere Research Satellite.

- Display of the position of the planet Neptune;
- Simultaneous display of different user-specified views in four separate windows.

The architecture of 3D-Mon has basically remained the same through the various releases of the software. The spacecraft and celestial object position data are collected on an Hitachi Data System 8063 (IBM 370 architecture) mainframe and transmitted to a Silicon Graphics IRIS graphics workstation for graphical display. The only architectural difference is the replacement of an asynchronous communications line and protocol with an Ethernet communications line and Transmission Control Protocol/Internet Protocol (TCP/IP). This replacement provides a faster, more reliable, and more convenient mechanism for transmitting data between the mainframe and workstation. In addition to the communications upgrade, the IRIS workstation has been upgraded to a 4D/VGX 300 class machine. This upgrade has enabled 3D-Mon to display higher resolution spacecraft and Earth polygonal databases while still achieving the required 1- to 4-second image update rate. In addition, the upgrade has provided the power and support to display these databases using shading techniques that produce a more photo-realistic picture of the object. The upgrade will also provide future releases with the ability to texture map the models (i.e., to add realistic material properties), such as tiles

to the Shuttle body and mountains to the Earth's landmasses.

Contact: James F. Jeletic (Code 552)
(301) 286-4244

Patricia A. Johnson (Code 553)
(301) 286-7952

Sponsor: Office of Space Communications

Mr. James F. Jeletic researches, develops, manages, and analyzes the flight dynamics computer-graphics systems and other mission support software in the Advanced Technology Section. He holds a BSE in Computer Science and Engineering from the University of Pennsylvania and has 7 years of experience at GSFC.

Ms. Patricia A. Johnson monitors the test and operations of three-dimensional graphics monitoring systems and the development, test and operations of other related flight-dynamics software utilities in support of the shuttle and of deployable spacecraft managed by GSFC. She holds a BA in Mathematics with Computer Science emphasis from the University of Tennessee. Space flight is a special interest for her. Ms. Johnson has served GSFC for 14 years.

SPACE NETWORK SCHEDULING TECHNOLOGY TESTBED

Towards the end of the 1990s, the TDRS-II will be operational, replacing the current space communications network. A SNC system is planned to schedule the enhanced resources and new capabilities of the TDRS-II. In support of the effort to define the SNC, the Space Network Scheduling Technology Testbed effort was started in January 1991. It builds on a key technology development that the Data Systems Technology Division has pursued for the last 5 years, that of a flexible request language for stating resource requirements and constraints to a scheduling system. The objectives of the testbed are to demonstrate and evaluate operations concepts for requesting, scheduling, and controlling space network services; to obtain scheduling operator and POCC-user feedback on the feasibility of new operations concepts; and to evaluate the effectiveness of human-computer interface and artificial intelligence technologies in the space network scheduling domain. In its first year, the testbed effort produced a demonstration illustrating the operational interface between the POCC and the SNC for the generation and processing of flexible scheduling requests. The testbed environment is composed of two main nodes, the Space Network User POCC Interface (SNUPI) prototype, and the SNC scheduling prototype.

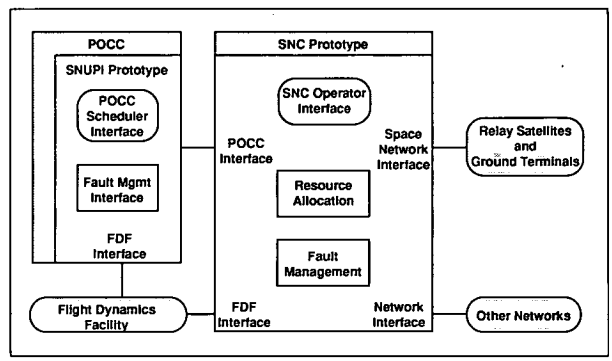

Space network control testbed environment.

The SNUPI prototype includes a flexible request editor, displays for handling messages with the SNC, and graphical representations of the POCC's scheduled items. The POCC operator interface was implemented using the NASA Transportable Applications Environment (TAE+), which provided state-of-the-art windowing and graphics tools for quickly prototyping user interface displays. Other functions, such as managing data files and communications, were implemented in the C programming language under the Unix operating system. The demonstration scenario begins with the POCC operator generating a flexible request using a form-filling user interface. First, requirements for space network services are defined, such as a forward communications link from the POCC through TDRS-II to the user's satellite. The operator determines which resources (e.g., a single-access

antenna on any TDRS-II spacecraft configured with matching data rates, polarization, etc.) that the user's satellite requires. Constraints are included, such as noting that a return-link service must start after a forward link has been established. As the operator identifies the requirements, the SNUPI request editor automatically builds the flexible scheduling language statements. After the services are defined, the space network events are created by identifying the services and time windows that comprise each event. Constraints, such as requiring that each event occurs only when the user's antenna is in view of an TDRS-II spacecraft, are identified with the accompanying data (e.g., the User Antenna View period orbital data supplied by the Flight Dynamics Facility). Finally, the POCC operator identifies repetition instructions (e.g., repeat this event once every orbit) and constraints (e.g., allow a minimum of 1 hour between each repetition). Should the prime resource be unavailable some or all of the requested time, the user may indicate backup events. For example, if the single-access antenna is prime, the multiple-access antenna could be identified as backup. Using this information, the SNUPI generates the flexible scheduling request which is transmitted to the SNC.

The scheduling engine within the SNC node was supplied by the Request-Oriented Scheduling Engine (ROSE), which receives flexible requests from several POCCs, produces a conflict-free schedule, and identifies any requests that did not get satisfied. ROSE was initially developed for NASA using a Symbolics Lisp workstation; a current effort is porting ROSE to the Ada programming language on Unix-based workstations. The SNC Operator Interface demonstrates the control available to the operator for determining request selection and expansion heuristics, as well as placement heuristics used to fill the schedule timeline. Other features include graphical representations of the timeline and resource utilization, zoom capability to focus on shorter time periods (hours to days), detailed information on the request that generated a specific scheduled item and the item itself, and the ability to determine the reasons why certain requests failed. Part of the space network operations scenario shows the ability of the operator to manually schedule items, such as a request that failed the automated scheduling process due to being overly constrained. A key benefit of this approach to space network scheduling is the shift of a significant conflict-resolution effort from humans to computers. Whereas today's scheduling approach requires POCC operators to identify specific resource and time requirements in a fixed-format, the flexible scheduling request concept allows users to describe their requirements in a readable language that accommodates flexibility. In addition, supplementary information is available directly to the automated scheduling engine for resolving resource conflicts. As a result, the time to generate a week's worth of schedules will take hours instead of days.

Contact: Karen L. Moe (Code 522)
(301) 286-5998

Sponsor: Office of Space Communications

Ms. Karen Moe is a staff member of Code 522. Her current interests include planning and scheduling, systems engineering, and user interface technology. She has 18 years of experience at GSFC in operations control center development, human factors analysis of operational systems, and technology development and transfer.

Software Development and Test

THE TRANSPORTABLE APPLICATIONS ENVIRONMENT (TAE)

Technology in the graphics user-interface domain has been in a state of evolution for several years. During this period, several *de facto* industry standards have emerged. MIT's X-Window System is recognized as an industry standard for a windowing protocol, and the Open Software Foundation's Motif has become a popular graphical user interface (GUI) software package, which many

organizations have adopted as a standard GUI. The Motif software defines a specific three-dimensional user interface style across a wide variety of different graphic workstations, and it utilizes the X-Window System technology. During FY91, in response to the numerous requests from the TAE user community, GSFC's TAE+ was upgraded to support the Motif look and feel. TAE+ is a productivity tool used for designing, building, and tailoring an application's user interface, and for controlling the designed GUI throughout the application's execution.

In April 1991, a production-quality version of this newest version, TAE+ V5.1, was delivered to COSMIC for immediate availability to the general public at a nominal distribution fee. It is available for the Unix and VMS operating system environments. Ports of the TAE+ V5.1 were completed for the Sun 3, SPARCstation, VAX (Ultrix), VAX (VMS), DECstation 3100, HP9000, Apollo, SGI Iris, and NEC EWS 4800/220 workstations. The main component of TAE+ is a user interface designer's Workbench that allows an application developer to interactively construct the look and feel of an application screen by arranging and manipulating user entry, informational, and data-driven interaction objects (e.g., radio buttons, menus, icons, help dialogue boxes, gauges, dials, etc.). This Workbench was upgraded to use the Motif interaction objects (called widgets), and new capabilities were added to support the features of the Motif widgets. The main work involved in the TAE+ upgrade was the rewrite of the runtime services, called Window Programming Tools (WPTs), which display and control the user interface during an application's operation. The application performs all its user interactions using the WPTs to access the underlying windowing software. By providing this buffer between the application software and the lower level windowing software, the TAE+ upgrade to the Motif software did not affect any existing applications written with earlier versions of TAE+. The existing applications are simply relinked to the new WPT library to become operational with the Motif user interface software. This latest version of TAE+ has many enhancements and new capabilities, such as the code generator capability of the Workbench was significantly improved to minimize the impact of user interface changes to the regeneration and recompilation of code. Also, performance optimizations were made (e.g., repairing memory leaks) in the new version, and rehearsal of the data-driven interaction objects (e.g., dials, stripchart) was added.

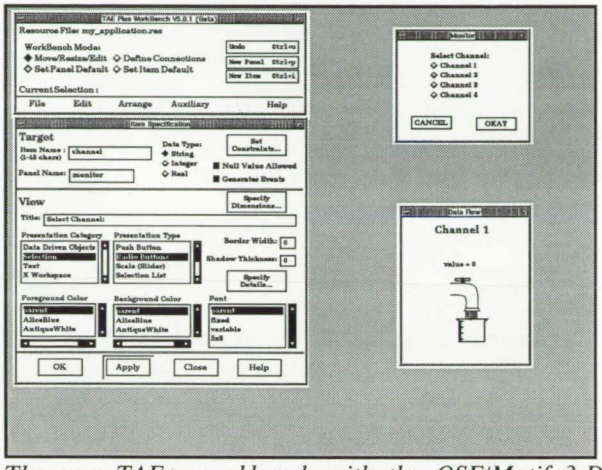

The new TAE+ workbench with the OSF/Motif 3-D "look."

TAE+ popularity continued to grow in FY91 and the user community grew to 875 user sites, a 15-percent increase from the previous year. Currently, 32 percent of the sites are NASA-sponsored, 16 percent are other government agency sites, 16 percent are university sites, and 36 percent are private industry sites. Applications cover a wide range of disciplines, such as operations, simulation, production systems, network management, real-time command and control, planning and scheduling, database management, image processing, science analysis/services, prototyping activities, and office automation. During FY92 the following TAE+ applications have been completed: an intelligent tutoring system for training GSFC satellite ground control operators (Georgia Tech), a resource scheduling system incorporating artificial intelligence (GSFC), several pilot simulation programs used for assessment and evaluation of air vehicle system designs (USAF), and the Atmospheric and Oceanic Information Processing System upgrade (GSFC).

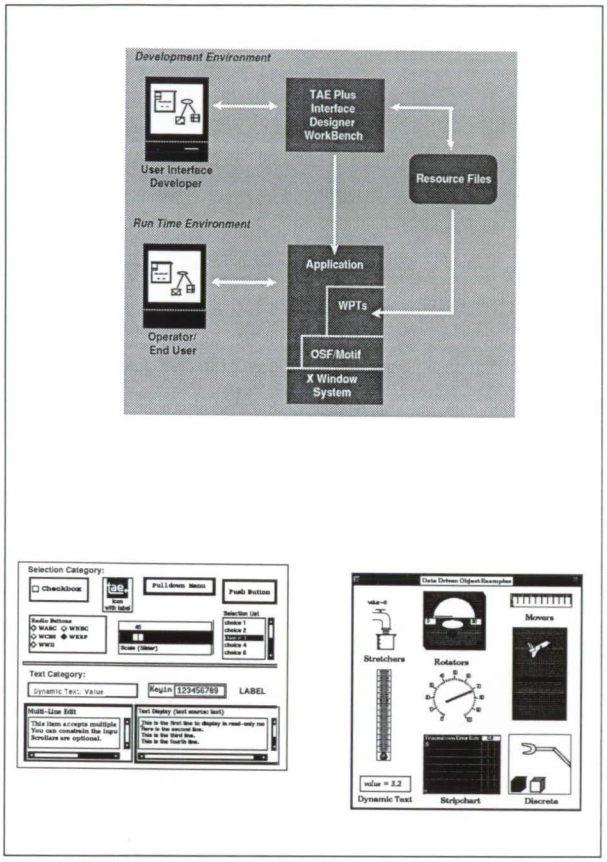

TAE+ structure.

During FY92, technical talks and papers on TAE+ were presented at the MIT X-Conference, Hounix (the Houston Unix user group,), Human Factors in Computing Systems' Annual Computer Human Interaction (CHI) Conference, Catalog Interoperability (CI) Workshop, Xhibition '91, IEEE 1201.1 Working Group, and the Space Operations and Research (SOAR) Conference. During FY91, TAE+ received a NASA Group Achievement Award and, also, received honorable mentions in two categories for the Best in Open Systems Solutions presented at the Federal Computer Conference in September 1991.

TAE+ is an evolving system and future plans for FY92 and beyond include development of a C++ code generation from the Workbench; improved connections to callback routines and data sources; introduction of hypermedia technology; integration of expert system technology to aid in making user interface design decisions; and implementation of additional user interaction objects. TAE+ continues to play a significant role in improving productivity in the development and management of application user interfaces.

Contact: Martha R. Szczur (Code 522)
(301) 286-8609

Sponsor: Office of Space Communications

Ms. Martha Szczur, Manager of the TAE Project since 1984, has over 20 years of experience in the development of GSFC software systems and holds a BS in Mathematics. Her professional interests center on graphical user interface technology, emphasizing human factors and development support tools.

COMPUTER-HUMAN INTERACTION MODELS—AN AUTOMATED AID FOR USER-INTERFACE DESIGNERS

Design of the look and feel of a user interface often occurs with little or no interaction between the designer and the end-user. Prior to usability testing, designers need feedback on various human-factors aspects of user-interface usability. To meet this need in the NASA-GSFC environment, we have been performing some research and development required to produce an automated design aid. The long-term objective is to provide advice to designers based on a human-factors assessment of visual and interactive features of user interfaces.

A method for evaluating the visual design of an individual user-interface screen is implemented in the Computer-Human Interaction Models (CHIMES) system, which exists currently as a demonstration prototype. CHIMES has the potential for aiding the user-interface designer in ensuring a usable design that complies with published guidelines.

In the original CHIMES concept, the user interface is evaluated within the context of the user's tasks. From this perspective, demands on the user's sensory, cognitive, and psychomotor resources are traced to task information requirements. The CHIMES model of demand on the operator's resources pinpoints potential operator underload and overload. The objective of modification advice to the designer is to maintain a generally moderate level of task demand for operators. Advice provided to the designer is linked to problems identified by the screen evaluation. In the existing prototype, problems are identified in the areas of visual demand and analytic assessment demand. Knowledge-base resident human-factors advice provides a rationale for at least one design modification. The designer can build a candidate interface, evaluate it, make on-line modifications, and rerun the screen evaluation until satisfied that visual and analytical demands are within recommended ranges.

Because the task-dependent approach is feasible only when detailed task information is available, a task-independent approach is under development. This approach involves evaluating a given screen design on the basis of features that are related to usability and operator performance.

In the current research-and-development phase, we are extracting visual-design requirements from the Open Software Foundation (OSF)/Motif ™ Level-One Certification Checklist (Revision 1.1). We are developing a capability to check screen designs for compliance with these requirements. We plan to use standard guidelines on color usage as the basis for evaluating multicolored designs. Because interface design is an iterative process, we recommend use of the task-independent approach early in user-interface development. The task- dependent approach is more feasible in later phases, when more detailed task information becomes available. Used in this way,

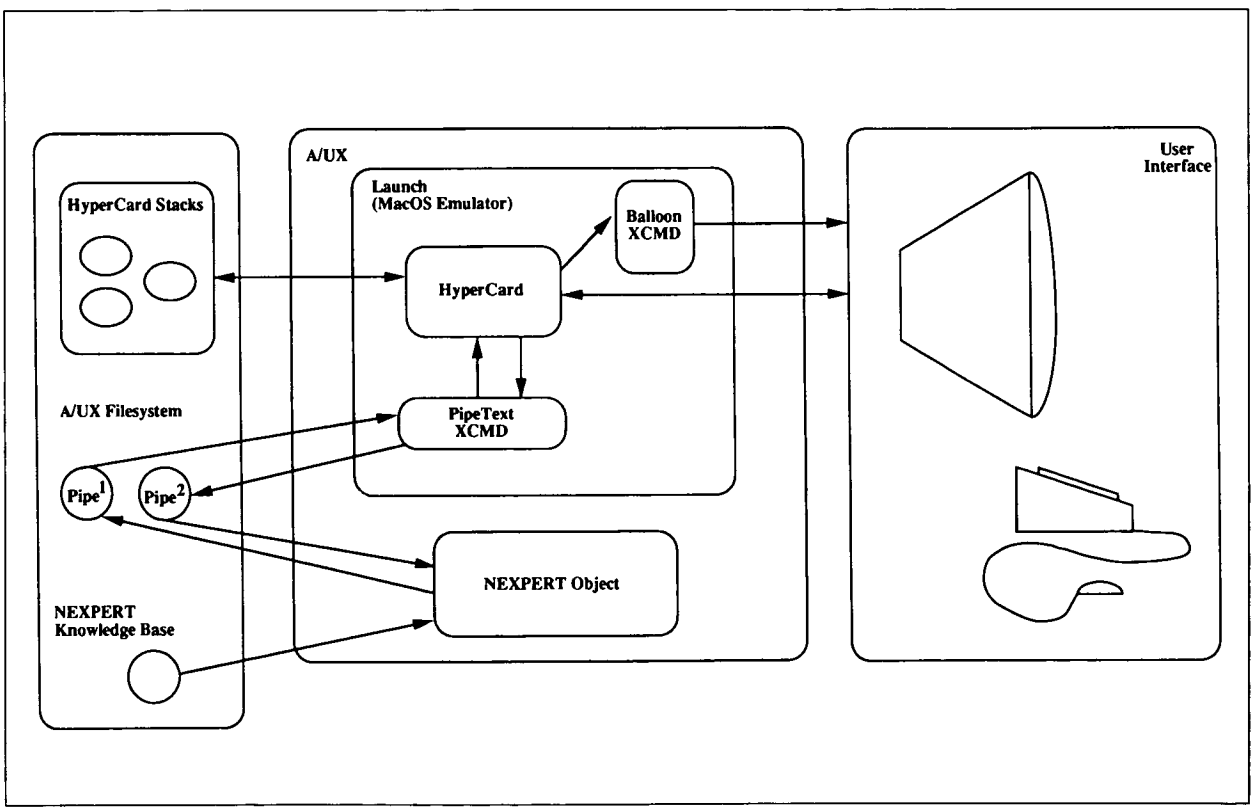

The CHIMES-2 software architecture.

CHIMES can assist the designer in building usability into user-interfaces prior to operational testing with end-users.

Working within the Macintosh environment, the CHIMES software development team chose NEXPERT Object for implementation of the expert knowledge base and HyperCard as the interface development tool. For purposes of integration, the A/UX operating system was selected (i.e., the Macintosh version of Unix). As shown in the figure, this combination of software and operating environment provided excellent functionality, availability, and flexibility. As detailed in CHIMES documentation, design issues involved file input/output, expert system operation, knowledge-based processing, and user-interface implementation. An unanticipated design issue was interprocess communication. A software bridge implemented in C permitted data and commands to be passed between HyperCard and NEXPERT.

User-interface innovations include help-clouds in which help-text can be displayed in a cloud-shaped area that seems to float in front of the HyperCard screen image. A consistent navigation aid is used to help the designer maintain a sense of placement within the network of CHIMES interface screens. Data entry in response to queries from the system is simplified through the use of check boxes and radio buttons. Initial evaluation of the prototype led to two significant improvements. Instead of requiring the user-interface designer to enter a detailed representation of the display screen to be analyzed, the upgraded prototype provides for automated input of the detailed design via an internal interface prototyping capability. Instead of providing a textual presentation of suggested modifications, apart from the interface design context, the upgraded prototype provides a rudimentary advice-in-context capability. The goal for this capability is to provide a visual linkage between an identified design problem and the displayed advice. Once we have the capability to evaluate the look of individual display screens, we plan to develop a capability to evaluate the consistency of visual design for sets of display screens. Current plans call for implementing CHIMES in NASA's Transportable Applications Environment (TAE™ Plus), a portable user-interface development environment. We also plan to develop a capability in TAE to evaluate the feel of an interface (i.e., the way it behaves in requesting and responding to user input). Long-range plans call for the integration of all the CHIMES evaluation capabilities as a TAE utility.

Contact: Walt Truszkowski (Code 522.3)
(301) 286-8821

Elizabeth D. Murphy
CTA Incorporated
(301) 816-1262

Sponsor: Office of Space Communications

Walt Truszkowski is Head of the Automation Technology Section at GSFC. He holds degrees in Mathematics and Computer Science. His professional interests include the cognitive/motor aspects of human-computer interactions, artificial intelligence, advanced knowledge-based approaches to software engineering, and approaches to information exchange among autonomous intelligent agents.

Elizabeth D. Murphy is a Human Factors Specialist, supporting and managing human factors tasks for CTA, Incorporated in Rockville, MD. Her current NASA-sponsored work focuses on the development of a knowledge-based system for user interface evaluation. Ms. Murphy holds an MA in Psychology from George Mason University. She is a member of the Human Factors Society and the Special Interest Group on Computer-Human Interaction (SIGCHI) of the Association of Computing Machinery (ACM). Her coauthored publications have appeared in scientific journals and conference proceedings.

TPOCC GRAPHICAL USER INTERFACE FOR EDITING DISPLAY PAGES

The Mission Operations Division's (MOD's) Control Center Systems Branch develops control

centers that monitor the health and safety of scientific satellites. Current development projects are using a distributed architecture that combines the latest in Unix workstation technology with reusable control center software to reduce the time and effort required to complete a POCC. The TPOCC architecture is being used for new control centers developed by the MOD (Small Explorer, Wind, Polar, and SOHO), to replace the aging control centers for the ICE and IMP satellites, and to upgrade other Code 510 institutional systems. The TPOCC systems are the first operational systems in Code 510 to employ a graphical user interface.

TPOCC builds on the X-window standard and the Open Software Foundation's Motif software to provide Flight Operations Team (FOT) members with this graphical user interface. This user environment consists of both applications written by TPOCC developers and displays defined by FOT members and stored in Motif's User Interface Language. To ensure consistency among the various graphical applications being developed for the TPOCC control centers, all developers must conform to the user interface guidelines specified in OSF's Motif Style Guide. In addition, a TPOCC User Interface Working Group has been established with a charter to develop a TPOCC graphical user environment specification based on the principles presented in the OSF document. These principles will allow TPOCC users to rapidly learn how to use new applications based on their experiences with existing programs.

In 1991, TPOCC developed an initial component of this common graphical user interface with the completion of the TPOCC page editor. This application provides a Motif graphical interface that greatly reduces the time required for FOT members to define textual display windows displaying telemetry parameters and other control center information. The page editor interface consists of two windows: the main panel and the wildcard page. The main panel window allows the user to add objects to a page and save the display definition through a point-and-click interface. It employs most of the graphical objects provided in the Motif toolkit including radio, toggle, push buttons, pulldown and option menus, dialog boxes, and text entry fields. The wildcard page window displays the current contents of the page being created. The wildcard page window is divided into cells using a tabular layout. The user may change the number of rows and columns using a menu attached to the main panel. Cells are selected by clicking them with the mouse. Once selected, a cell may be edited, cleared, or used to hold a new object. Once the page is working as desired, the user saves the page with the main panel's file menu.

The TPOCC page editor was developed using a rapid prototyping approach that involved starting with a mock-up of the final user interface. This mock-up was demonstrated to FOT members and other users to obtain their input before any coding was begun. Many of the suggestions provided at these demonstrations were incorporated into the initial version of the editor; other ideas have been slated as future enhancements. This prototyping approach is expected to increase user satisfaction with the editor by incorporating their feedback into the development cycle as early as possible. The TPOCC page editor is now being used by the ICE/IMP FOT as part of their most recent software release that is slated to support real-time operations for these spacecraft. The editor is also heavily used as the SAMPEX and Wind/Polar FOTs work to develop pages that monitor all the telemetry parameters for these spacecraft.

Current work on the common TPOCC graphical user interface centers on developing display objects that plot spacecraft telemetry values and other POCC parameters. This work includes development of an X-T graph object, which acts as a graphical stripchart recorder emulation, and an X-Y graph object that allows five parameters to be plotted against a sixth parameter or against time. Future graphical TPOCC user interface software will include a command panel and additional graphical editors. The command panel supports real-time spacecraft commanding with a palette of buttons representing sets of spacecraft commands. The graphical editors will be created to facilitate the FOT's creation of definition files (other than display pages) that are required by the POCC software.

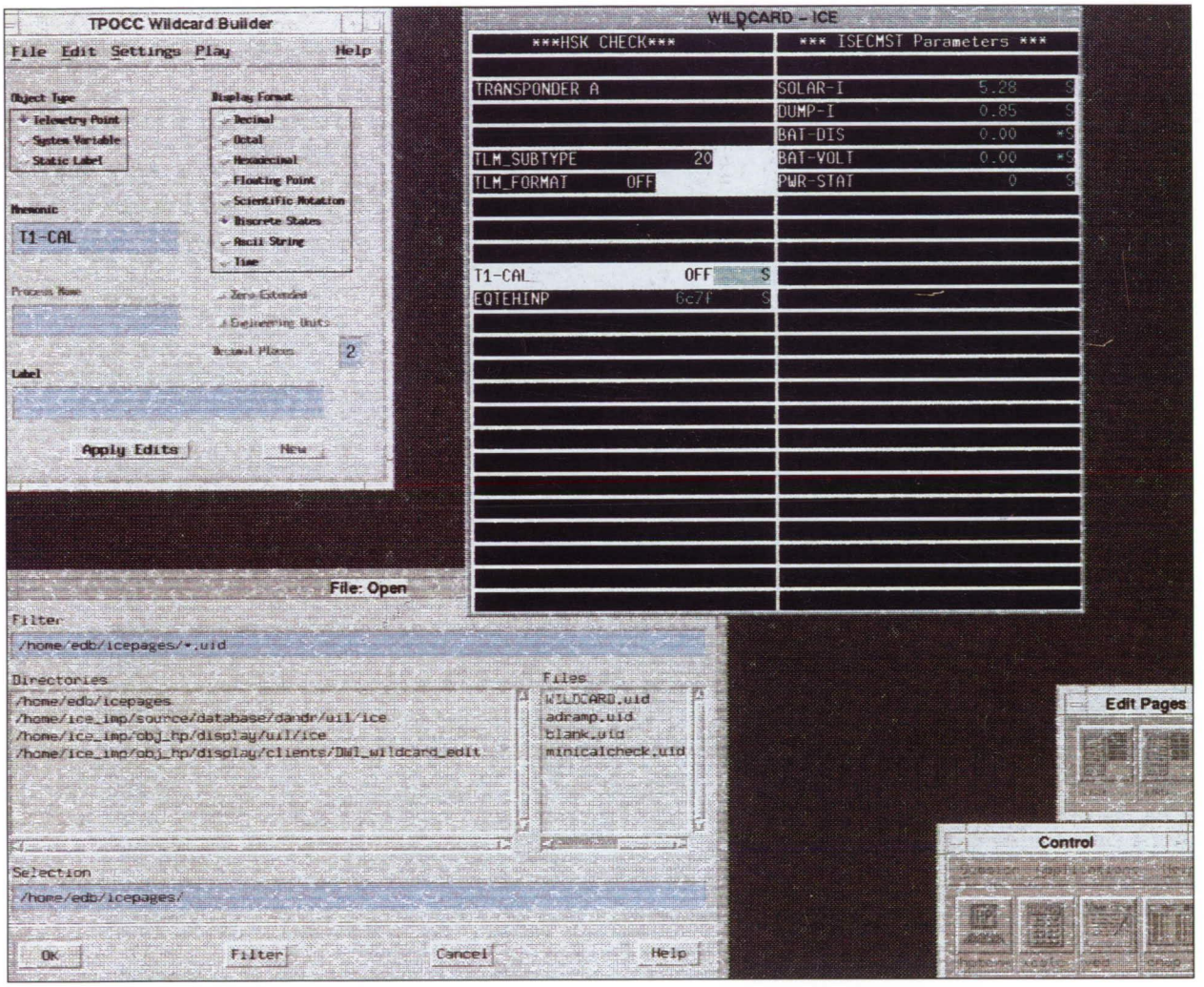

TPOCC page editor.

We would like to acknowledge the contributions made by Jack Koslosky, Barbara Schwarz, and Steven Gibson towards writing this article.

Contact: Ron Mahmot (Code 511.1)
(301) 286-8523

Edward Beach (CSC)
(301) 497-2585

Sponsor: Office of Space Communications

Mr. Ron E. Mahmot works in the Mission Operations Division's Control Center Systems Branch. He holds a BS in Computer Sciences from the University of Maryland.

Mr. Edward F. Beach is the lead developer for the TPOCC control center being built for the ICE and IMP satellites. His professional interests include graphical user interfaces such as for TPOCC. He holds a BS in Computer Sciences and Russian language from Dartmouth College.

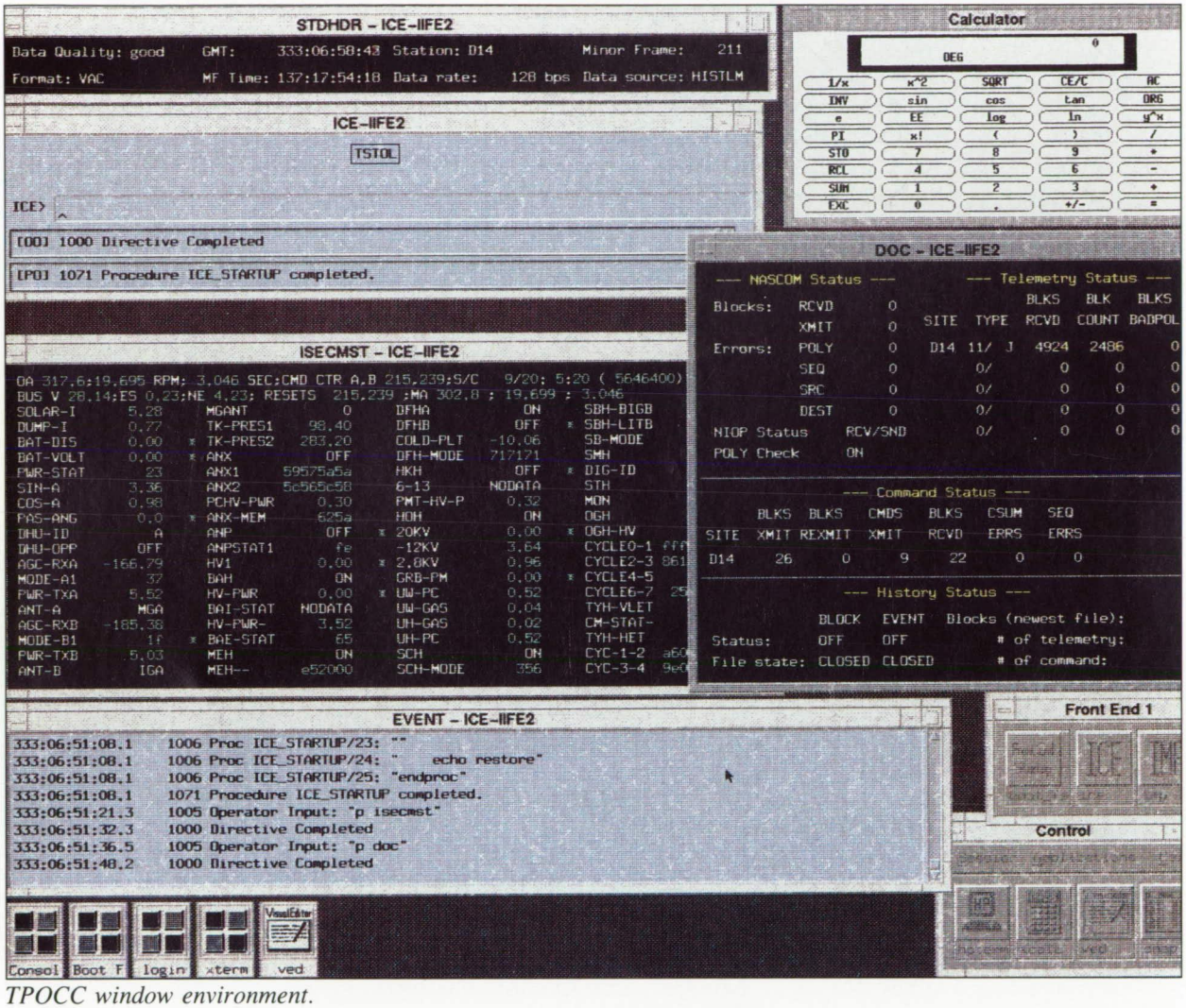

TPOCC window environment.

EXPANSION AND EVOLUTION OF THE SOFTWARE MANAGEMENT ENVIRONMENT

The Software Management Environment (SME) is a software tool designed to assist a software project manager in monitoring, analyzing, and controlling a software project. SME's major functions include the ability to track key project parameters (such as cost and schedule), to compare these parameters to past development efforts and to models of the typical project within the development environment, to predict future status of the project, to analyze the project data to determine strengths and weaknesses, and to assess the quality of the software development effort. The major components required to provide these functions are a database of metrics on both current and past software projects, a set of models and relationships that have been determined through over 15 years of software engineering research, and a rule base of knowledge of experienced software development managers.

Early research on the SME involved establishing the concept and architecture of the tool. The basic concept of the tool is to integrate software measurement, software engineering results, and a rule base into a measurement-based management tool. Without these underlying components, a tool such as the SME would not be possible. Once the concept was firmly established, the difficult task of developing an architecture for the tool became the research focus. The architecture of the tool has been stable for the last 2 to 3 years, and it includes functions providing the ability to observe, compare, and predict project measures. During the last year, we have expanded SME's functions to include analysis of project measures and assessment of project quality, and it has evolved into a tool that is currently being used by all software managers in the Flight Dynamics Division of GSFC.

The expansion of the SME includes the ability to utilize experienced software managers' knowledge within the tool. Previous research demonstrated that the experience of software managers could be captured and utilized to analyze the progress of software projects. The SME now integrates a rule base of software manager's knowledge and an expert system to utilize that rule base. This function of the SME enables the manager of an ongoing software project to call on the knowledge of other managers to analyze project problems. For example, within the SME a manager may examine the error rate of a software project. Suppose the error rate for the current project is below what is normally expected, the SME uses rules concerning this situation and examines other project parameters to provide possible explanations for why the error rate is below normal. It then provides a set of explanations that the manager can utilize as possible reasons for such a deviation. In this case, the reasons might be statements such as (1) experienced development team, or (2) not enough software testing is being performed. By providing the software manager with such explanations, the SME enables the manager to understand how the current project is different from past, similar projects. Another area of functionality that has recently expanded in the SME is the ability of the tool to assess overall project quality. This function provides the user with ratings of quality factors such as maintainability, reliability, and cost effectiveness. The figure shows an example of the quality assessment feature of the SME. The three quality factors are shown on a relative scale from below normal to above normal. The normal band is a model of where the typical project in this software development environment would rate on these measures. Each of these quality factors is determined by utilizing measurement data about the project and an established definition of the particular factor. These types of quality ratings provide the manager with an overall sense of the ongoing project and insight into future difficulties that may arise on the project.

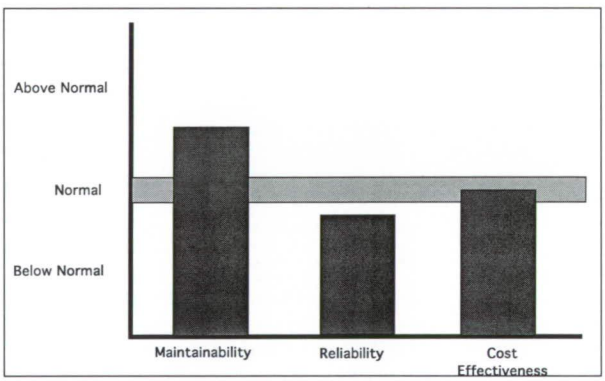

Example of the SME quality assessment capability.

The tool has reached a level of stability where project managers consult the tool regularly to determine the status of their projects. Such regular use of the tool has stimulated future research directions and has established a level of confidence in the SME that will enable the tool to be transferred to other organizations. During the next year, SME will be transferred to other organizations within NASA. Such transfer will further not only research on the SME, but also help to demonstrate how such technology should be transferred.

Contact: Jon Valett (Code 552.2)
(301) 286-6564

Sponsor: Office of Aeronautics and Space Technology

Mr. Valett is responsible for research in software engineering within the Flight Dynamics Division's Software Engineering Laboratory (SEL). His current research interests include software management tools, measuring software design and software maintenance, and the application of computer-aided software engineering (CASE) tools.

Acronyms

AAOE	Airborne Antarctic Ozone Experiment
AASE	Airborne Antarctic Stratospheric Experiment
ACP	Aerosol Collector and Pyrolyzer
ADC	Astronomical Data Center
AGATE	Advanced Gamma-Ray Astronomy Telescope Experiment
AMMR	Airborne Multichannel Microwave Radiometer
AMMS	Advanced Microwave Moisture Sounder
AMSU	Advanced Microwave Sounding Unit
APE	Alpha-Proton-Electron Telescope
APU	Analog Processing Unit
AVHRR	Advanced Very High Resolution Radiometer
BATSE	Burst and Transient Source Experiment
BBXRT	Broad Band X-Ray Telescope
BLLS	Boundary Layer Lidar System
BLR	band-limited regression
CPL	Capillary Pumped Loop
CARS	Coherent Anti-Stokes Raman Spectroscopy
CCD	charge-coupled device
CCSDS	Consultative Committee for Space Data Systems
CDAC	Cosmology Data Analysis Center
CDHF	Central Data Handling Facility
CDP	Crustal Dynamics Project
CD-ROM	Compact Disk-Read Only Memory
CDSLR	Crustal Dynamics Satellite Laser Ranging
CDS	Coronal Diagnostic Spectrograph
CERES	Clouds and the Earth's Radiant Energy System
CFC	chlorofluorocarbons
CGRO	Compton Gamma Ray Observatory
CHRPS	Configurable High Rate Processor System
CLAES	Cryogenic Limb Array Etalon Spectrometer
CLC	Central Load Core
COBE	Cosmic Background Explorer
COMPTEL	Imaging Compton Telescope
CPI	Comprehensive Plasma Instrumentation
DDF	Director's Discretionary Fund
DE-2	Dynamics Explorer-2

Acronyms

DGEF	Diffraction Grating Evaluation Facility
DIRBE	Diffuse Infrared Background Experiment
DMR	Differential Microwave Radiometer
DOSE	Dynamics of the Solid Earth
DPU	Digital Processing Unit
DSN	Deep Space Network
ECS	EOSDIS Core System
EDM	Electric Discharge Machines
EFD	Electric Field Experiment
EGRET	Energetic Gamma Ray Experiment Telescope
EIA	Equatorial Ionization Anomaly
ELF	Extremely Low Frequency
ENSO	El Niño/Southern Oscillation
EOS	Earth Observing System
EOSDIS	EOS Data and Information System
EPACT	Energetic Particle Acceleration, Composition and Transport
EPIC	Energetic Particles and Ion Composition
ERB	Earth Radiation Budget
ESA	European Space Agency
ESMC	Eastern Space and Missile Center
ESMR	Electronically Scanned Microwave Radiometer
ETWA	equatorial temperature and wind anomaly
EUVE	Extreme Ultraviolet Explorer
FFT	Fast Fourier Transform
FIFE	First ISLSCP Field Experiment
FIRARI	Far Infrared Array Radiometric Imager
FIRAS	Far Infrared Absolute Spectrophotometer
FITS	Flexible Image Transport System
FOC	Faint Object Camera
FOS	Flight Operations Segment
FTCP	front-end telemetry and command processor
FTS	Flight Telerobotic Servicer
GIM	Geotail Inboard Magnetometer
GLRS	Geoscience Laser Ranging System
GRS	Gamma-Ray Spectrometer
GCM	General Circulation Model

Acronyms

GDP	Gondola Diagnostics Package
GCMS	Gas Chromatograph-Mass Spectrometer
GHRS	Goddard High Resolution Spectrograph
GLA	Goddard Laboratory for Atmospheres
GMSB	Global Modeling and Simulation Branch
GPS	Global Positioning System
GRB	Gamma-Ray Burst
GSE	Ground Support Experiment
GSFC	Goddard Space Flight Center
HEIDI	High Energy Imaging Device
HEP	High Energy Particle Experiment
HESP	High Energy Solar Physics
HiREGS	High-Resolution Gamma-Ray Spectrometer
HPHX	heat pipe heat exchanger
HST	Hubble Space Telescope
IDS	Iowa Driving Simulator
IFRA	interactive forecast-retrieval-analysis
IIS	Instrument Interface Simulator
IAU	International Astronomical Union
IGSPC	Imaging Gas Scintillation Proportional Counter
IMPATT	impact avalanche transit time
IRIS	Infrared Interferometer Spectrometer
ISAMS	Improved Stratospheric and Mesospheric Sounder
ISAS	Institute of Space and Astronautical Science (Japan)
ISCCP	International Satellite Cloud Climatology Project
ISEE	International Sun-Earth Explorer
ISTP	International Solar Terrestrial Physics
IT	Isotope Telescope
IUE	International Ultraviolet Explorer
JPL	Jet Propulsion Laboratory
LAED	Lerner Algebraic Edge Detector
LAN	local area network
LASAL	Large Aperture Scanning Airborne Lidar
LDEF	Long-Duration Exposure Facility
LEMT	Low Energy Matrix Telescopes
LEP	Low Energy Particle Experiment

Acronyms

LIF	laser-induced fluorescence
LIS	Lightning Imaging Sensor
LP	Langmuir Probe
LTE	local thermodynamic equilibrium
LTT	Lunar Transit Telescope
LVDT	linear variable displacement transducers
MBE	Molecular Beam Epitaxy
MCA	Multichannel Analyzer
MEIRF	Magnetic Earth-Ionosphere Resonant Frequency
MIT	Massachusetts Institute of Technology
MLS	Microwave Limb Sounder
MMIC	Microwave Monolithic Integrated Circuits
MMS	Multimission Modular Spacecraft
MODIS-N	Moderate Resolution Imaging Spectrometer-Nadir
MODIS-T	Moderate Resolution Imaging Spectrometer-Tilt
MOU	Memorandum of Understanding
NASA	National Aeronautics and Space Administration
NCAR	National Center for Atmospheric Research
NDBC	National Data Buoy Center
NEB	North Equatorial Belt
NLC	noctilucent clouds
NMC	National Meteorological Center
NOAA	National Oceanic and Atmospheric Administration
NRAO	National Radio Astronomy Observatory
NSF	National Science Foundation
OI	optimum interpolation
ONR	Office of Naval Research
OPAS	Off-Pointing Aspect System
ORU	Orbital Replacement Unit
OSAC	Optical Surface Analysis Code
OSSE	Oriented Scintillation Spectrometer Experiment
OVV	optically violent variable
OZP	Overpressurized Zero Pressure
PAH	polycyclic aromatic hydrocarbons
PBL	planetary boundary layer
PCM	phase conjugate mirror
PD/PCU	Power Distribution/Pyro Control Unit

Acronyms

PEM	Particle Environment Monitor
PMC	polar mesospheric cloud
PMSE	polar mesospheric summer radar echo
PMT	photomultiplier tube
PRC	Peoples' Republic of China
PV	potential vorticity
PWI	Plasma Wave Investigation
RAC	Remote Analysis Computer
rms	root mean square
RMT	Rapidly Moving Telescope
ROWS	Radar Ocean Wave Spectrometer
rpm	revolutions per minute
rpo	revolution per orbit
RTE	radiative transfer equation
SAMPEX	Solar Anomalous Magnetospheric Particle Explorer
SAR	Synthetic Aperture Radar
SARSAT	Search and Rescue Satellite
SAFISY	Space Agency Forum on the International Space Year
SBIR	Small Business Innovative Research
SBS	Stimulated Brillouin Scattering
SCM	successive correction method
SCR	Surface Contour Radar
SEI	Space Exploration Initiative
SERTS	Solar Extreme Ultraviolet Rocket Telescope and Spectrograph
SHOOT	Superfluid Helium On-Orbit Transfer
SIR	Shuttle Imaging Radar
SLR	Satellite Laser Ranging
SMEX	Small Explorer
SMMR	Scanning Multichannel Microwave Radiometer
SOLSTICE	Solar-Stellar Irradiance Comparison Experiment
SSPA	Solid-State Power Amplifier
STEP	Solar Terrestrial Energy Program
SUMER	Solar Ultraviolet Measurements of Emitted Radiation
SWADE	Surface Wave Dynamic Experiment
TCW	test conductor workstation
TDC	time-to-digital converter
TDRSS	Tracking and Data Relay Satellite System
TEC	Telecommand Encoder Card
TGRS	Transient Gamma-Ray Spectrometer

Acronyms

TIMED	Thermosphere-Ionosphere-Mesosphere Energetics and Dynamics
TM	Thematic Mapper
TMF	Table Mountain Facility
TOMS	Total Ozone Mapping Spectrometer
TOVS	TIROS Operational Vertical Sounder
TPOCC	Transportable Payload Operations Control Center
TRMM	Tropical Rainfall Measuring Mission
TURFTS	TDRSS User RF Test Set
UARP	Upper Atmosphere Research Program
UARS	Upper Atmosphere Research Satellite
UIT	Ultraviolet Imaging Telescope
UKMO	United Kingdom Meteorological Office
UV	ultraviolet
VLBA	Very Long Baseline Array
VLBI	Very Long Baseline Interferometry
VLSI	Very Large Scale Integration
WAM/WAF	Workpiece Attachment Mechanism/ Workpiece Attachment Fixture
WATS	wind and temperature spectrometer
WORM	Write Once Read Many
WVSC	West Virginia State College
XTE	X-ray Timing Explorer

Author Index

Author Index

Author Index

Author Index

Executive Editor:
Gerald Soffen

Editors:

Howard Ottenstein
Harry Montgomery
Walter Truszkowski
Kenneth Frost
Walter Sullivan
Charles Boyle

With Special Thanks To:

Philip Sakimoto
Luann Bindschadler
Diane Teets
Emily Michaud

Technical and Scientific Editing and Production:

Brenda Vallette, Mitchell Hobish, and Philip Ardanuy

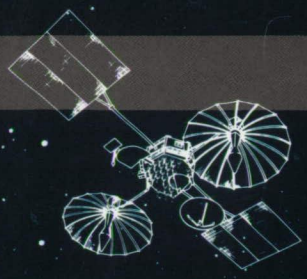

NASA

National Aeronautics and
Space Administration

Goddard Space Flight Center
Greenbelt, Maryland 20771